



Grant Agreement No.: 226479

SafeLand

Living with landslide risk in Europe: Assessment, effects of global change, and risk management strategies

7th Framework Programme
Cooperation Theme 6 Environment (including climate change)
Sub-Activity 6.1.3 Natural Hazards

Deliverable [1.3]

[Analysis of the results of laboratory experiments and of monitoring in test sites for assessment of the slope response to precipitation and validation of prediction models]

Work Package [1.2] - [Geomechanical analysis of weather induced triggering processes]

Deliverable/Work Package Leader: [ETHZ/CNRS] Revision: [No.1] – Draft/**Final**

March, 2011

Rev.	Deliverable Responsible	Controlled by	Date
0	150 pages. Some missing sections	Sarah Springman	October 2010
1	Quality Control	CNRS	January 2011
2	Final Version	ETHZ/CNRS	March 2011



Note about Contributors

The following organisations contributed to the work described in this deliverable:

Lead partners responsible for the deliverable and quality control:

[ETHZ]

Prof. Sarah Springman

Dr. Linda Seward

Dr. Francesca Casini

Amin Askerinejad

[CNRS]

Dr. Jean-Philippe Malet

Dr. Anke Spickermann

Julien Travelletti

Other Contributors:

[AMRA]: Prof. Luciano Picarelli, Dr. Emilia Damiano, Dr. Luca Comegna

[UNISA]: Prof. Giuseppe Sorbino

[EPFL]: Prof. Lyessse Laloui, Dr. Alessio Ferrari, John Eichenberger

[GIR]: Raluca-Mihaela Maftei



1	Introduction	5
2	Knowledge of slope failure mechanisms from laboratory experiments.....	6
2.1	Characterisation of material properties and failure mechanisms from hydrological and geotechnical testing.....	6
2.1.1	Coarse grained soils, typically sands – saturated and unsaturated behaviour / normally and over-consolidated (ETHZ).....	6
2.1.2	Fine-grained soils, typically silts & clays– saturated and unsaturated behaviour / normally and over-consolidated (CNRS)	7
2.1.3	The specific case of pyroclastic soils and ashes (AMRA/UNISA).....	9
	1. Soil properties	21
2.1.4	The specific case of fissured stiff clays (AMRA).....	27
2.2	Failure mechanisms observed in small-scale flume experiments	35
2.2.1	Results of flume experiments on saturated and unsaturated sands (ETHZ).....	35
2.2.2	Results of flume experiments on saturated clays (CNRS)	46
2.2.3	Results of flume experiments on pyroclastic soils (AMRA).....	51
2.3	Failure mechanisms observed in centrifuge tests.....	58
2.3.1	Results of centrifuge experiments on unsaturated sands (ETHZ).....	58
2.3.2	Results of centrifuge experiments on unsaturated clays (CNRS)	71
2.4	Synthesis	73
3	Knowledge of slope failure mechanisms from full-scale in – situ experiments.....	74
3.1	Full – scale slope failure experiments in coarse – grained soils and moraine.	74
3.2	Full-scale slope experiments in fine grained soils (cNRS).....	82
	Synthesis	92
3.3	92	
4	Knowledge of slope failure mechanisms from long-term monitoring of natural slopes	93
4.1	SYNTHESIS OF MONITORED SITES ON COARSE-GRAINED SOILS AND MORaine (BOTH SHALLOW AND DEEP-SEATED, SATURATED AND UNSATURATED) (ETHZ).....	93
	Tössegg, Canton Zürich	93



4.1.1	93
4.1.2	Gruben, Canton Wallis..... 97
	Rüdlingen, Canton Schaffhausen..... 100
4.1.3	100
	La Frasse – Large landslide in tertiary flysch (Swiss Alps)
	(EPFL)..... 103
4.1.4	103
4.2	SYNTHESIS OF MONITORED SITES ON fine-grained soils
	(overconsolidated and weathered clays, BOTH SHALLOW AND DEEP-
	SEATED)..... 112
4.2.1	Synthesis of monitored sites on reworked black marls (CNRS)
	112
4.2.2	Synthesis of monitored sites on stiff intact, jointed and highly
	fissured clays (AMRA) 135
4.3	SYNTHESIS OF MONITORED SITES ON the specific case of pyroclastic
	soils (unisa)..... 157
4.3.1	Hydrological response of instrumented slopes in pyroclastic soils
	(AMRA) 170
	181
	Synthesis 185
4.4	185
5	Conclusion (ETHZ, CNRS)..... 187
6	Bibliography 188



1 INTRODUCTION

Great efforts have been made in recent decades in predicting landslide occurrence enabling effective planning for mitigation and hazard protection measures. In the following deliverable, examples will be given and discussed to demonstrate clearly how high quality experimental data from a range of simple to advanced tests has been imperative in first understanding, and then quantifying, triggering factors for landslides. Validation and verification of prediction models have also been reviewed.

The main aim of this report is to pull together key examples of in-situ, monitored sites, case studies of past landslides, laboratory experiments and knowledge of the behaviour of certain types of soils, including sands, clays and pyroclastic deposits. This valuable knowledge can be used to predict slope response to rainfall successfully. Areas of state of the art research are presented and discussed within this report.

Basic material properties are defined within the first part of this deliverable, and knowledge of failure mechanisms obtained from laboratory experiments on small-scale soil specimens is reviewed in order to provide the reader with an adequate background for subsequent chapters. Flume and centrifuge experiments designed to test the failure behaviour in small scale slope models are described in the latter half of chapter 2.

Landslide processes reproduced at a greatly reduced scale are always influenced by scale effects. The problem of scale-dependency is overcome by full-scale experiments. Full-scale rainfall experiments in moraine, silty sand and black marls are presented in chapter 3.

Long-term monitoring of natural slopes is an indispensable tool for the analysis of landslide processes. In chapter 4, examples of monitored slopes within Europe, i.e. four field sites consisting of coarse-grained material, eleven sites consisting of fine-grained, clayey material and six site examples for the specific case of pyroclastic soils, are given.

2 KNOWLEDGE OF SLOPE FAILURE MECHANISMS FROM LABORATORY EXPERIMENTS

2.1 CHARACTERISATION OF MATERIAL PROPERTIES AND FAILURE MECHANISMS FROM HYDROLOGICAL AND GEOTECHNICAL TESTING

2.1.1 Coarse grained soils, typically sands – saturated and unsaturated behaviour / normally and over-consolidated (ETHZ)

Landslides induced by rainfall are caused by a reduction of confining stress as a result of pore water pressure rise during or following periods of intense rainfall. To characterise the material properties and failure mechanisms using hydrological and geotechnical testing, a series of tests must be performed to mimic the field stress path (Crosta & Frattini 2008).

Two categories of research programme aimed at revealing the mechanism of landslides and debris flows have been carried out worldwide through two categories of investigation: (1) in situ monitoring and measurement of the hydrological response to rainfall, and (2) laboratory characterisation of the shear strength of soil.

The determination of shear strength parameters for the stability analysis of rainfall-induced landslides requires both knowledge of the stress history and a laboratory simulation of the failure stress path of the soil. Such soils exist on steep slopes and have experienced a highly anisotropic stress action through which they have been consolidated (Zhu et al., 1998).

The following four different stress paths are likely to be relevant in the study of the response of the soil in the slope in saturated conditions, namely:

- (1) CIDC: isotropic consolidation—standard drained compression (Fig. 1a);
- (2) CIUC: isotropic consolidation—standard undrained compression (Fig. 1a);
- (3) CADCAL: anisotropic consolidation—drained shear by decreasing mean effective pressure at constant axial load (Fig. 1b);
- (4) CADCAL/U: anisotropic consolidation—drained shear by decreasing mean effective pressure at constant axial load, followed by prevention of further drainage to reproduce net undrained conditions (Fig. 1b).

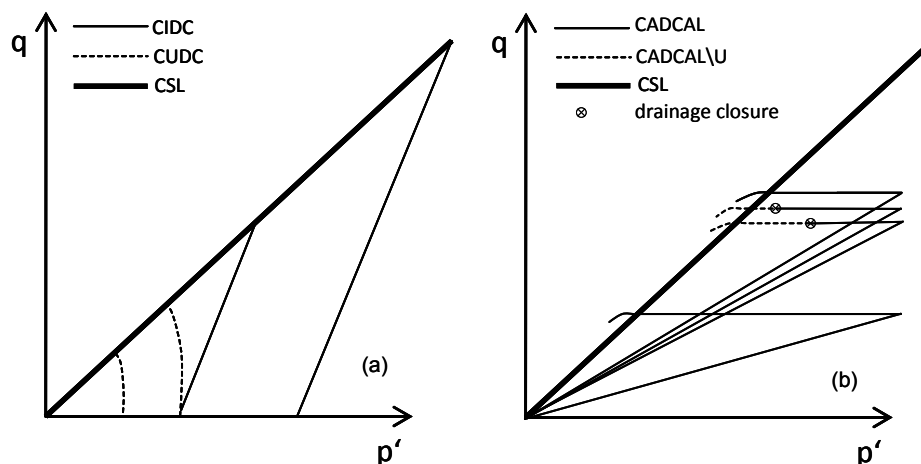


Figure 1 - Schematic diagram of the stress paths: a) CIDC and CIUC; b) CADCAL and CADCAL/U (after Casini et al., 2010).

Conventional drained and undrained compression triaxial tests are performed to study the volumetric behaviour of the soil, and to detect critical state conditions as well as peak shear strength as a function of confining pressure.

Drained shear under constant axial load and increasing water pressure, after anisotropic compression (CADCAL), was performed to simulate the stress path experienced in the field by the soil undergoing an infiltration process under its own weight. In the last type of stress path (CADCAL/U), a drained shear stage is performed at constant axial load up to a stress ratio slightly lower than the critical stress ratio. Afterwards, the drainage taps in the base and the top pedestals are closed. Pore water pressure and vertical displacement evolution were recorded to investigate better the role of drainage conditions on the mechanical response (Casini et al., 2010).

Such stress paths are typically suggested to analyse the effect of the principal stress ratio increase, eventually leading to failure of the soil following a water pressure increase in the field (Anderson & Sitar, 1995). The latter choice is rather common in the context of slope stability (see, e.g., Ng et al., 2004), together with the so called constant shear drained (CSD) stress path, performed by lowering the vertical and the lateral stress (e.g. Anderson & Sitar, 1995; Springman et al., 2003).

The two (CADCAL and CADCAL/U) stress paths are thought to replicate the range of lateral constraints to the actual stress path in the field. As the onset of failure and attainment of ultimate conditions depend on the stress path followed, together with previous stress history, imposing an initial stress state simulating the anisotropic stress state in the field seems to be more appropriate.

The same stress paths reproducing the behaviour of soils in unsaturated conditions can be followed. Following the saturation path must be achieved using one of two methods:

- imposing a controlled flow of water in the sample until it reaches saturation and measuring the pore water pressure with tensiometers or water retention curves (Thu et al., 2006; Jotisankasa et al., 2010);
- under suction controlled conditions, imposing a wetting path in terms of increasing the pore water pressure at constant air pressure until complete saturation is reached, while measuring the water inflow into the sample (Olivares & Picarelli, 2003a).

Shear tests can be performed to evaluate the friction angle of the soils in saturated (Lings et al., 2004) and unsaturated conditions (Caruso et al., 2004; Melinda et al., 2004; Casini et al., 2010b). Mobilisation of shear strength in shallow translational slips occurs at very low effective stress. Accordingly, a series of direct shear box tests must be performed to characterise the strength of soils, under drained and undrained conditions, at low vertical stresses (Fannin et al., 2005).

2.1.2 Fine-grained soils, typically silts & clays– saturated and unsaturated behaviour / normally and over-consolidated (CNRS)

In accordance with section 2.3.1 of the deliverable D1.1 (work package WP1.1), “Fine grained materials” which are typically silts and clays are summarised under the term “clays”. Section 2.3.1 contains a detailed literature review of the properties and the behaviour of saturated clay material. In case of homogeneous, continuous (intact, not fissured) material, a distinction is made between naturally cemented clays (CA), mechanically overconsolidated

clays with or without cementation (CB), normally consolidated clays with or without cementation (CO). Mechanisms that trigger failure are dependent on the type of clays.

1. Shear strength

Corresponding to the critical state concept (Roscoe et al., (1963); Roscoe & Poorooshasb (1963); Roscoe & Burland (1968)) the behaviour of normally consolidated clay is frictional in nature, i.e. cohesion is zero. The strength of overconsolidated and cemented clays is determined by the OCR, overconsolidation ratio and type or degree of bonding.

To replicate stress conditions in slopes subjected to pore water pressure increase, standard geotechnical tests (triaxial tests) are modified to investigate landslide material behaviour. The stress paths followed are at an essentially constant shear stress (constant total stress) with decreasing effective stresses (mean effective stress in particular). Petley et al. (2005) have designed a pore-pressure reinflation test, where the deviatoric stress is held constant and effective stress is reduced through pore pressure inflation until the sample fails, in order to simulate the conditions within a hydrologically triggered landslide, which has approximately constant shear stresses but variable effective normal stresses. Tests on Gault Clay samples showed a linear trend in $1/\text{velocity} - \text{time}$ space. A model of progressive failure, initialised by pore water pressure fluctuation, is proposed on the basis that the observed linearity in $1/\text{velocity} - \text{time}$ space results from a stress transfer process during crack growth, in which the fractured material loses cohesion, leading to increased stress, and hence further deformation, in the remaining unfractured mass.

2. Bonding and destruction of bonds

In CA clays, destruction processes lead to shrinkage of the Limit State Surface. As mentioned in section 2.3.1, the destruction processes under undrained conditions may lead to development of high excess pore water pressures and to a substantial reduction of undrained shear strength from peak to remoulded conditions. In their study of marly hillslopes, Maquaire et al. (2003) analysed the effect of bonding by comparing data from undisturbed and remoulded specimens, sheared by applying low and moderate normal stresses (31 and 300 kPa). In this particular material (Callovo-Oxfordian black marls), bonding effects only exist when low normal stresses are applied (<200 kPa). The destruction of the bonds between the clay particles is dependent on the stress state, but might also depend on the degree of saturation. In Maquaire et al. (2003), it is stated that cohesion due to carbonated bridges decreases on soaking, which destroys the majority of the bonds.

3. Hydraulic conductivity (permeability) and seepage

Slope instability can be caused by water flow. As water flows through the soil, there is a transfer of energy to the soil skeleton that causes a seepage force to act on the soil skeleton. In other words, the flow of water through the pore space is accompanied by a friction force between the flowing fluid and the soil skeleton, named the seepage force. Seepage can reduce effective stresses (provided there is vertical flow) and can lead to erosion of the soil. Seepage properties of clay soils are characterised by very low permeability, less than 10^{-5} m/s (mixtures of sand, silt and clay, stratified clay, etc.). Homogeneous clays below the weathering zone can be described as impervious with permeability values less than 10^{-9} m/s. Permeability of fine grained soils can be determined by e.g. falling head permeability tests. Meschyan & Petrosyan (2005) significantly increased the cross-sectional area of the specimen being tested while conducting their experiment and raised the flow rate of seepage water to

improve the accuracy in determining seepage properties of clay soils. Factors influencing the permeability of clays and their relative importance are presented in Murray et al. (1997).

4. Unsaturated soil properties, loss of apparent cohesion and increase in hydraulic conductivity Independent of the type of clay (CA, CB or CO) and independent of the type of clay mineral, the presence of apparent cohesion is characteristic of all unsaturated soils. Clayey soils with a degree of saturation lower than 1 can be accompanied by very high matric suction (negative pore water pressure) values that act as an additional strengthening component, which is often described as apparent cohesion. As soon as the material reaches a degree of saturation that is nearly one due to e.g. a rising groundwater table or rainfall, the apparent cohesion vanishes which means that shear resistance decreases. For example, the water retention properties of intact Boom clay samples have been determined by Le et al. (2008), using different experimental techniques. Alonso & Pinyol (2008) report typical suction values of low plasticity silty clay from Barcelona and a high plasticity soil, Boom clay, which are illustrated for different compaction stresses. Romero et al. (1999) pointed out that high values of suction are mainly controlled by intra-aggregate voids in fine-grained soils.

Not only shear strength, but also hydraulic conductivity, is dependent on the degree of saturation (Fredlund et al., 1994). Unsaturated soil permeability is rarely measured since the methods proposed in the literature are difficult to implement as they involve extremely low flow rates, especially at high suctions. Therefore unsaturated hydraulic conductivity is often predicted indirectly based on water retention data (Peroni et al., 2006).

2.1.3 The specific case of pyroclastic soils and ashes

(AMRA/UNISA)

During recent years, extensive experimental programmes have been conducted to investigate the mechanical and hydraulic properties of pyroclastic soils, which make up a large part of slopes that are highly susceptible to rainfall-induced landslides. Flowslides and debris flows affect pyroclastic granular soils accumulated in the last tens of thousands of years over the limestone massifs of the Western Appennine and the tuffaceous slopes surrounding the city of Naples, as a result of intense volcanic activity of the volcanic centres of Roccamonfina, Campi Flegrei and Somma-Vesuvio (Fig. 2).

Rainfall-induced landslides of the flow-type, affecting a large portion of the Campania Region (southern Italy), can be considered to be one of the most insidious landslide phenomena because of their potential for causing casualties and huge economic damage. They involve unsaturated pyroclastic soil covers, originating from the explosive phases of different volcanic apparatus, which mantle the limestone and tuffaceous slopes of the region.

These landslides can be considered complex slope instability phenomena since they exhibit distinct kinematic characteristics during the failure, post-failure and propagation stages (Fell et al., 2000; Leroueil, 2004; Cascini et al., 2010). The failure stage is characterised by the formation of a continuous shear surface through the entire soil mass (Leroueil, 2001). The post-failure stage is represented by the rapid generation of large plastic strains and the consequent sudden acceleration of the failed soil mass (Hungri, 2004). In the literature, the acceleration of the failed mass during the post-failure stage is mainly attributed to static liquefaction, a process in which a soil mass, sheared under undrained condition, loses a large

part of its shear strength as a result of induced high pore-water pressure, and consequently flows like a fluid.

Previous studies show that, depending on the distance from the eruptive centre and the mechanism of deposition, the properties of these pyroclastic materials are quite variable (Picarelli et al., 2006). A first distinction concerns deposits formed by air-fall, flow and surge sediments. The air-fall deposits are well represented in the distal area of the Somma-Vesuvius region where pyroclastic flows and surges do not reach; they are characterized by well sorted deposits of bomb and black scoria, coarse lapilli and small bombs and blocks, fine lapilli and ash. Flow and surges due to collapses of volcanic columns formed very thick deposits in the proximal area of Campi Flegrei and Vesuvius; they are less sorted than air-fall.

The first part of this section concentrates on the characterisation of pyroclastic soils in distal areas (air-fall ash) carried by AMRA. In the second part the main results of a large research project, aimed to characterise the mechanical behaviour both at failure and post failure stages of typical pyroclastic soils of the Campania Region, are presented by UNISA.

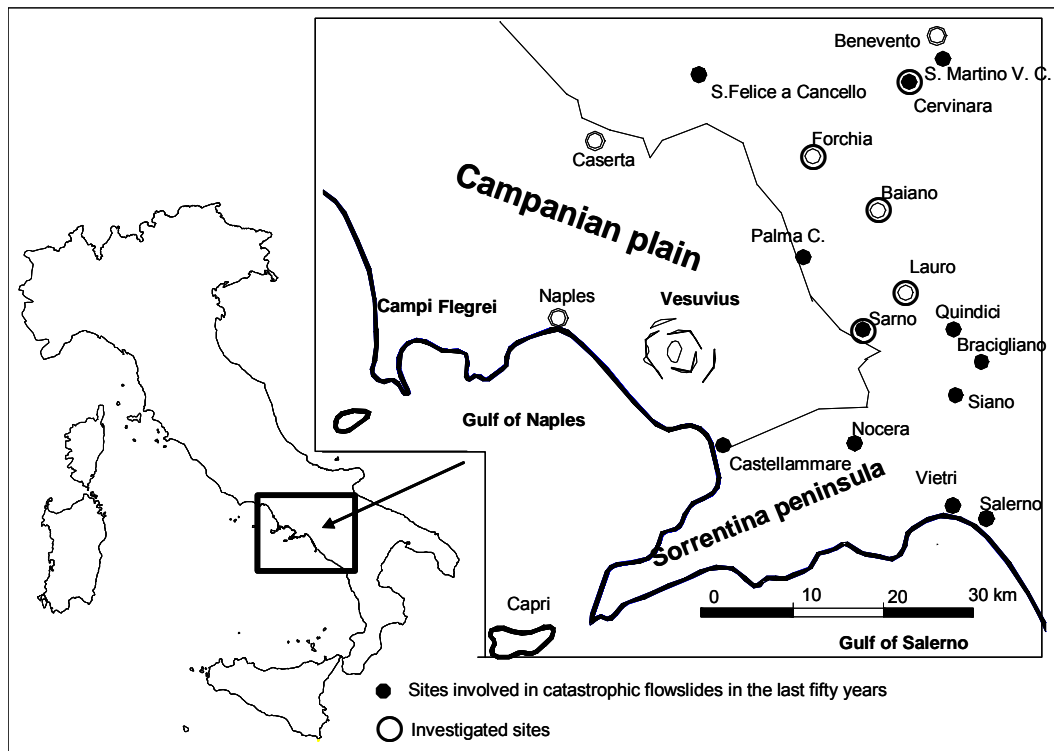


Figure 2 - The area of Campania (South Italy) that is prone to flow-like slope movements.

Characterisation of pyroclastic soils in distal areas (air-fall ash)

(AMRA)

1. Fabric and physical properties

The pyroclastic soils present in the distal area of the Somma-Vesuvius volcanic centre consist of alternating regular layers of ashy soils and pumices, as shown in Figure 3. This cover is 3-4 metres in depth, resting on slopes with an angle of higher than 35°. A deep investigation was carried out at the Monteforte Irpino site in the Avella Mountains (Fig. 4; Papa et al., 2008).



Figure 3 - Cut slope on the Partenio Mt. in the distal area of Somma-Vesuvius. Depth of excavation is 1.20 m.

The pyroclastic cover consists as a regular series of layers essentially parallel to the ground surface, as follows (Fig. 3): 1) topsoil; 2) weathered and humified ash; 3) coarse pumices from the Avellino eruption (3.7 ky b.p.); 4) paleosoil consisting of weathered volcanic ash; 5) fine pumices from the Ottaviano eruption (8.0 ky b.p.); 6) palaeosoil; 7) volcanic sand; 8) altered fine-grained ash.

Similar situations may be found in the Partenio Mountains (Olivares & Picarelli, 2003), while the stratigraphies along the Sarno Mountains are more complex, as this area is nearest to the Vesuvius volcano and, as a result, has been covered by the products of more eruptions. However, the following schematic classification may be adopted since a detailed distinction is not necessary for this study:

- soil A, which includes coarse (A1) and fine pumices (A2);

- soil B, which includes the top soil of pyroclastic nature (B1) and the volcanic ash (B2), which is usually located in the middle of the stratigraphic succession
- soil C, i.e. altered fine-grained ash.

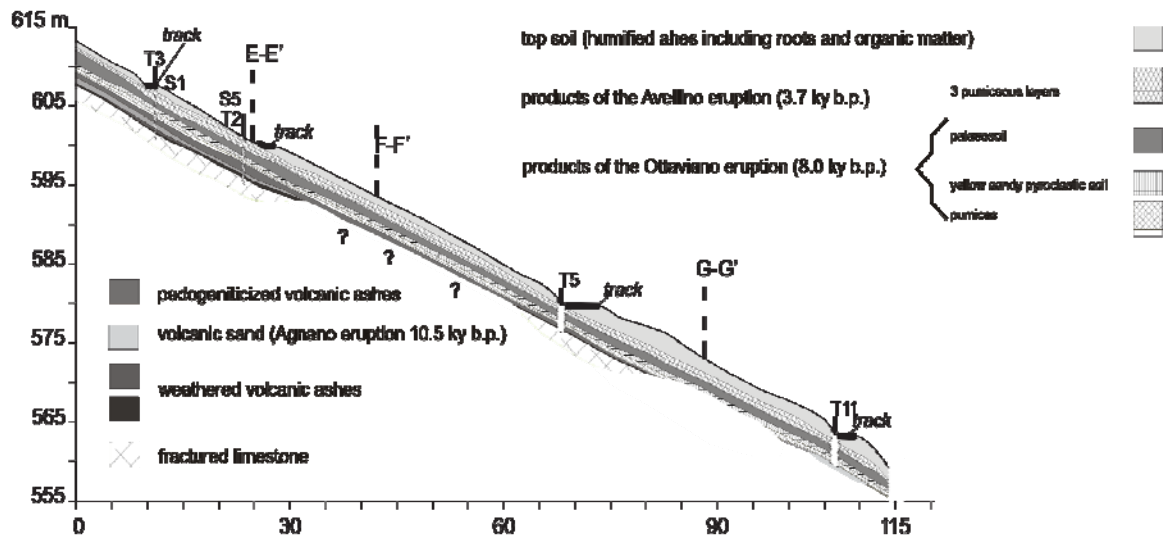


Figure 4 - Stratigraphic succession at Monteforte Irpino site (from Papa et al., 2008).

Figure 5 shows the grain size of samples taken in the three areas of Partenio, Avella and Sarno Mt. In particular, it can be remarked that:

- the grain size of the shallowest ash layers (B1 in Fig. 4) is quite similar to those of intermediate soils (B2), which are well-graded and display a high sandy component and a significant amount of non-plastic silt, which is essentially constituted by very poorly ordered minerals, sanidine and pyroxenes (Picarelli et al., 2006);
- the altered ash (C) is finer than soils of the B type;
- pumices fall in the domain of sandy gravel (A1) and gravelly sand (A2).

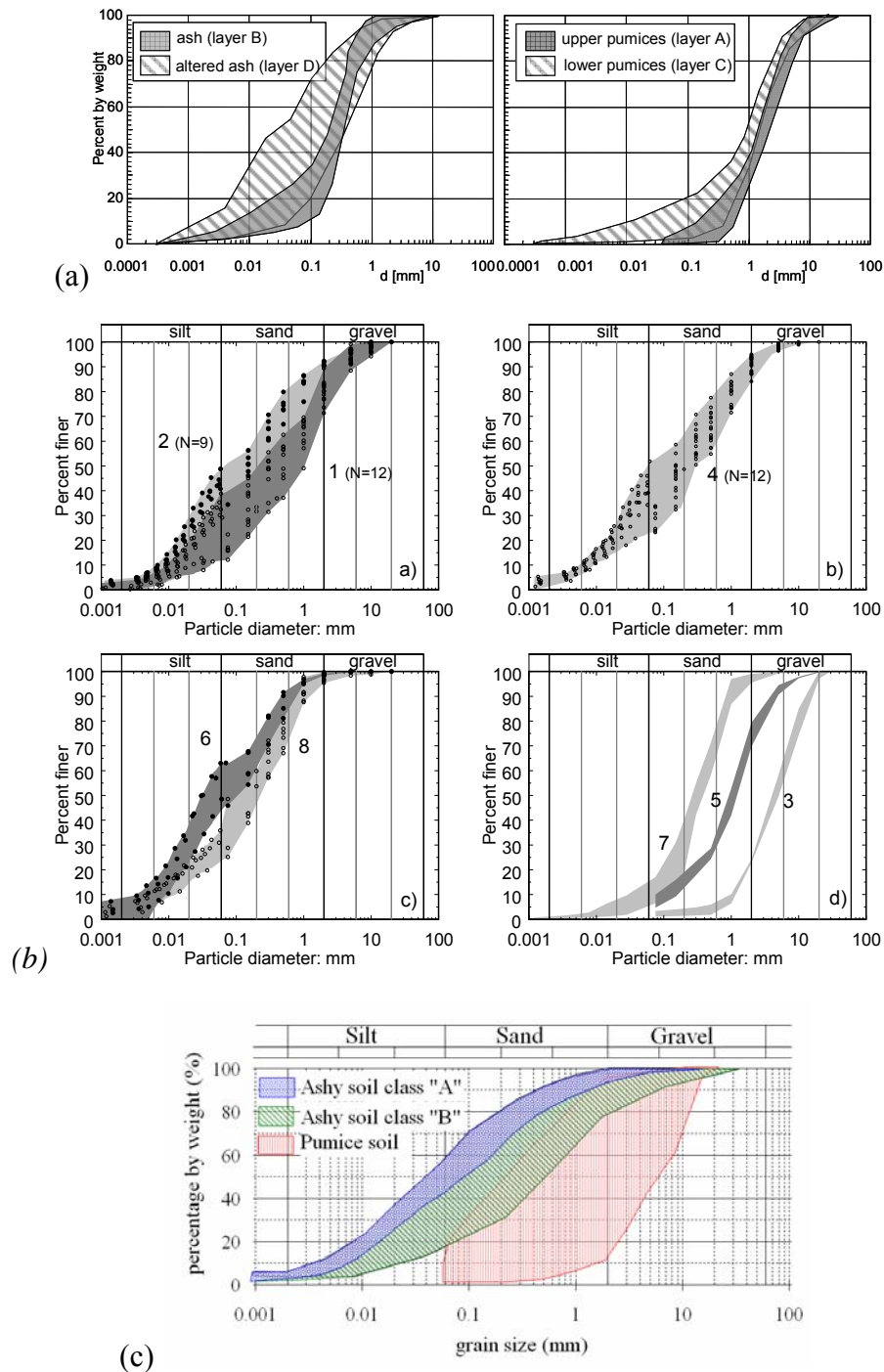


Figure 5- Grain size distribution of pyroclastic soils from: a) Mt. Partenio (from Olivares and Picarelli, 2003); b) Mt. Avella (from Papa et al., 2008) (soils are distinguished with numbers from 1 to 8 following the stratigraphic succession from top to bottom) and c) Mt. Sarno (from Sorbino et al., 2010).

Tables 1, 2 and 3 report the mean values of physical properties of soils sampled respectively in Cervinara, Monteforte Irpino and on the slopes of the Pizzo d'Alvano massifs (Sarno Mt). It is worth mentioning that such properties are not so different from site to site, even if the

slopes investigated are some tens of kilometres from each other.

The soils are unsaturated. Undisturbed sampling is possible because of the suctions that stabilise the specimens. The specific unit weight of ash B varies within quite a wide range ($G_s=2.53\text{-}2.69\text{kN/m}^3$), while the overall porosity is very high, ranging between 69% and 72%. Differently, the fine ash, C, is characterised by a lower porosity (about 58%) and a greater dry unit weight. The value reported for pumices are indicative, since recovering of high quality pumice samples is impossible.

Layer	Material	d_{max} (mm)	U	γ_s (kN/m^3)	γ (kN/m^3)	w*	n (%)	S_r^* (%)
A1	coarse pumices	20	5	25	13	25	52	36
A2	pumices	20	42	26	14	40	50	40
B2	volcanic ashes	10	5	26	14	67	69	84
C	altered fine ashes	10	25	26	16	54	54	75

* w and S_r obtained from samples taken at the end of the wet season

Table 1 - Physical properties of Cervinara pyroclastic soils (modified after Olivares & Picarelli, 2003). d_{max} : maximum diameter of soil particle, U: coefficient of uniformity, γ_s : specific unit weight, γ : unit weight, w: water content, n: porosity, S_r : saturation degree.

Layer	Material	G_s	γ_d (kN/m^3)	γ (kN/m^3)	n (%)	S_r (%)
B1	top soil	2.65÷2.66	7.8÷8.1	11.9÷12.5	69÷70	57÷69
B2	volcanic ashes	2.50÷2.57	7.1÷7.7	11.9÷12.5	69÷72	64÷77
C	altered fine ashes	2.47÷2.49	10.64	15.49	58	87

Table 2 - Physical properties of Monteforte Irpino pyroclastic soils (from Papa et al., 2008). G_s : specific unit weight, γ_d : dry unit weight, γ : unit weight, n: porosity, S_r : saturation degree.

Layer	Material	γ_d (kN/m^3)	γ_{sat} (kN/m^3)	n (%)
A	pumices	6.20	13.1	69
B1/B2	volcanic ashes	7.30	13.1	69
C	altered fine ashes	9.10	15.7	58

Table 3 - Physical properties of Sarno pyroclastic soils (from Cascini et al., 2010): γ_d : dry unit weight, γ_{sat} : saturated unit weight, n: porosity, S_r : saturation degree.

2. Saturated and unsaturated hydraulic properties

A hydraulic characterisation has been carried out on undisturbed and reconstituted specimens recovered from pits cut along some slopes (see Fig. 1). The saturated hydraulic conductivity of Cervinara pumices (A) has been obtained by constant head permeability tests on reconstituted samples (Damiano & Olivares, 2010): the results indicate a value of about $1.0 \cdot 10^{-5}$ m/s for coarse pumices (A1) and of $5.0 \cdot 10^{-6}$ m/s for fine pumices (soil type A2).

The saturated conductivity of natural samples of Cervinara ashes has been measured through constant head tests performed in the triaxial cell under different effective stresses (100-

500kPa). Under the lowest confining pressures of 100 and 200kPa it is about $3.0 \cdot 10^{-6}$ m/s in the top-soil (B1), about one order of magnitude less in the intermediate layer (B2) till values of about $5 \cdot 10^{-8}$ m/s in the lowermost altered layer (C). The hydraulic conductivity decreases by about two-four orders of magnitude in unsaturated conditions, in range of suction between 0 and 100 kPa. Figure 7 illustrates the soil water retention curves (SWRC) and the hydraulic conductivity function of the Monteforte Irpino ashes, determined through forced evaporation tests and drying tests in a pressure plate apparatus, starting from totally saturated conditions (Papa, 2007). The shallowest layers (soil B1 and top-soil) exhibit the greatest range of variation, starting from a value of about 10^{-6} m/s in saturated conditions to values in the order of 10^{-9} m/s under a suction of 50 kPa. The altered ash C presents the smallest range of variation (Evangelista et al., 2008). Similarly, the unsaturated conductivity of Cervinara ash B2 (Fig. 7a) obtained from the interpretation of the transient phase of suction equalisation (Kunze et al., 1965) during suction controlled triaxial tests (Fig. 6a) in the range of suction between 0 and 80 kPa, decreases by about two orders of magnitude as suction increases (Picarelli et al., 2006).

All the soils investigated have water retention properties (Figs. 6 and 7b) that are indicative of coarse-grained materials. They display low air entry values, in the range from 4–8 kPa to 12 kPa, low values of residual water content (for matric suction around 100 kPa) and large changes of the volumetric water content in the transition zone. However, some differences can be recognised by comparing the SWRC of different soils (Fig. 6), between the shallower and intermediate layers (B1 and B2), and the deepest one (C), which displays a higher air entry value and a less steep curve in the transition zone: this is probably due to the different grain-size distributions.

The hysteretic behaviour of these soils has not been yet investigated since the most of the experimental data has been obtained along drying paths. However, an indication for soil C is given by Sorbino & Foresta (2002), who did not find any significant hysteretic effect under net vertical stress in the 0 – 20 kPa range, while the SWRC shows flattening and small hysteretic phenomena for values of the net vertical stress greater than 20 kPa, due to collapse during the wetting path.

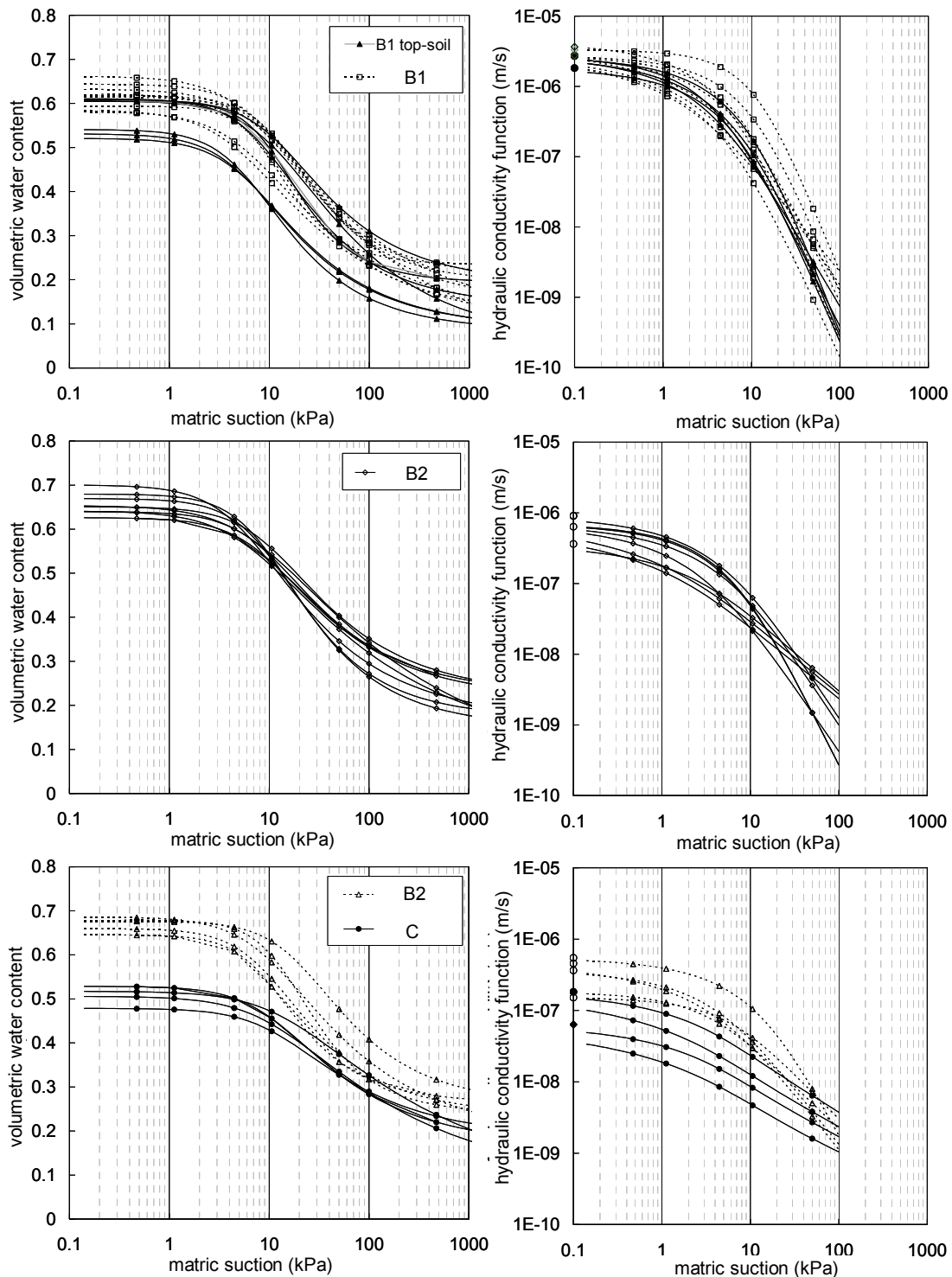


Figure 6 - Monteforte Irpino ashes (layers B1, B2, C): retention curves and hydraulic conductivity functions (from Evangelista et al., 2008).

Figure 8b shows experimental data for Cervinara ash B2, obtained from both wetting (SCTX tests at the end of suction equalisation, conventional long-term infiltration tests on natural and

reconstituted samples) and drying stages (conventional long-term evaporation tests): no appreciable difference can be found suggesting that any hysteretic effects are unimportant.

Further data for Cervinara ash B2 have been obtained from flume tests (see section 1.2.3) on reconstituted small-scale model slopes. Coupling suction measured by tensiometers with volumetric water content obtained by TDR installed near the tensiometers, the water retention curve has been extracted during infiltration. These curves are compared with those obtained through conventional long-term laboratory techniques in Figure 8, where the two experimental results are fitted by the van Genuchten (1980) expression. In spite of some scattering, the characteristic curve extrapolated by flume tests (crosses in Fig. 8) clearly shows that for θ_w higher than 0.38, suction is lower than the value obtained by conventional laboratory tests (curve 1 in Fig. 8). Probably this effect can be explained accounting for the nature of the particle shape and texture. The size of the pores between the particles (intergranular pores) is significantly larger than that of internal pores (intragranular pores). Consequently, the amount of retained water required to cause a given suction is a function of the exposure time. Indeed only long exposure times (as in the conventional tests) enable the intragranular pores to absorb water (Damiano and Olivares, 2010).

Infiltration tests on layered slopes including a pumice layer included between two ash layers (B2), enabled to extrapolate the water retention curve of pumice (Damiano and Olivares, 2010).

The water retention curve in Figure 9 has been obtained by assuming that the same value of suction is found at the ash-pumice interface, by coupling the suction measured in the two ash layers near the interface, with the volumetric water content (θ_w) of pumices obtained by a

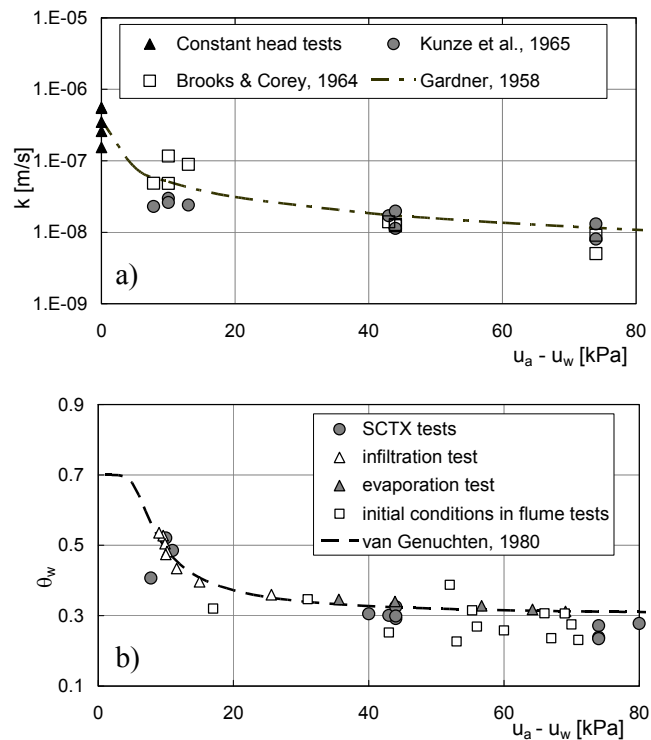


Figure 7- Cervinara ashes (layer B2): a) unsaturated permeability; b) retention curve (from Picarelli et al., 2006).

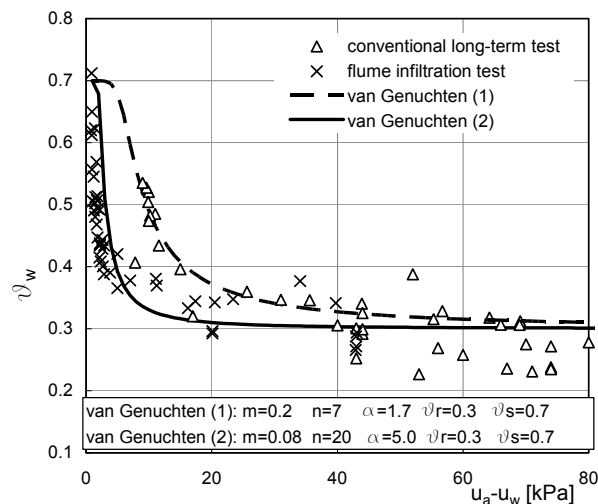


Figure 8- Comparison between SWRC of volcanic ash derived from flume infiltration tests and conventional long-term laboratory tests (from Damiano & Olivares, 2010).

TDR probe. Such a curve, presenting a very steep front in the capillary zone and a very small air-entry value, represents one of the few available data in the literature for pumices. As expected, comparison between the retention curves of pumices and ash shows that pumices are characterised by a lower air-entry value, a steeper slope in the capillary zone and lower residual water content.

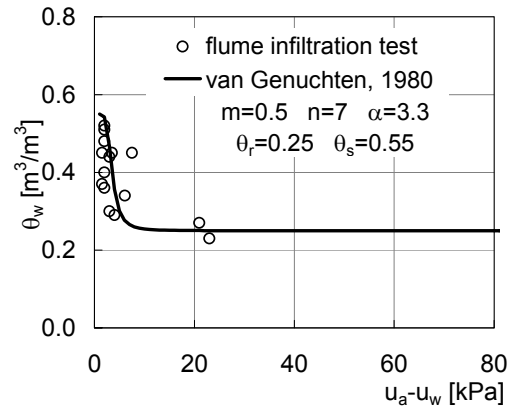


Figure 9 - SWRC of pumices during infiltration tests on small scale layered slopes (from Damiano & Olivares, 2010).

3. Saturated and unsaturated shear strength

Extensive experimental programmes have been conducted in the last decade to investigate the shear strength of volcanic ashes. Since saturation of natural loose samples can induce a strong volumetric collapse (essentially soils of type B), a flushing technique using de-aired water or carbon dioxide (Olivares, 2001) is carried out under very low effective confining stress. Testing is often performed under stresses similar to in situ values.

Results of CIDC and CIUC triaxial tests on saturated natural samples of ashes B1, B2 and C from different sites are shown in Figure 10. Both soils B1 and B2 show a contractive and ductile behaviour, while soil C behaviour is brittle in the entire stress range investigated (Papa et al., 2008; Olivares, 2001). The cohesion, c' , is always very low, while the friction angle ϕ' is quite high. Both ashes have virtually no cohesion, while the soil B1 is characterised by a friction angle ranging between 33° - 36° and the soil B2 by a friction angle of 37° - 40° . The altered ash C has a peak and critical state strength characterized by ϕ' and c' in the range of 30° - 32° and 5 - 11 kPa and 35° - 37° and 0 respectively. The altered ash C has a peak and critical state strength characterized by ϕ' and c' in the range of 30° - 32° and 5 - 11 kPa and 35° - 37° and 0 respectively.

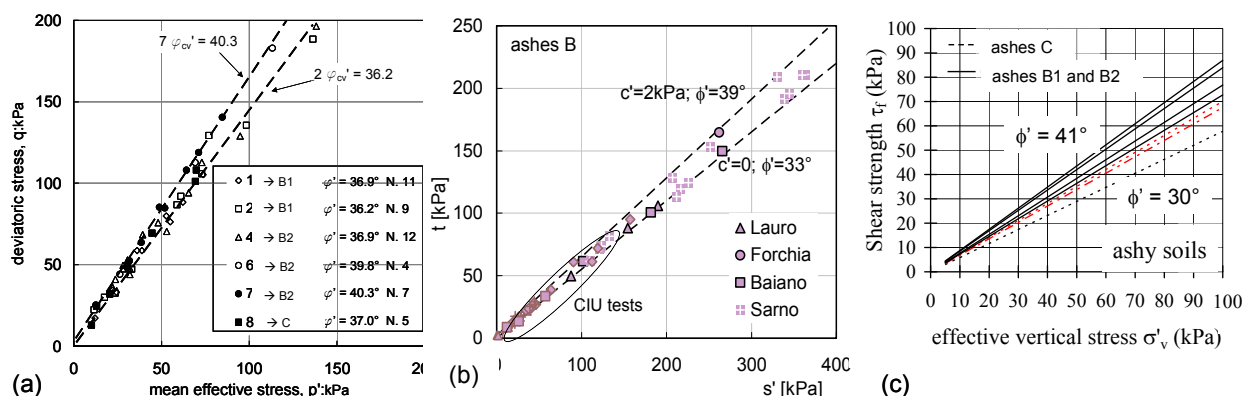


Figure 10 - Results of triaxial compression tests on saturated samples of volcanic ashes collected at: a) Monteforte Irpino (from Papa et al., 2008); b) Partenio, Avella and Sarno Mountains (modified after Olivares, 2001); c) Sarno (modified from Bilotta et al., 2005).

Since suction strongly governs hydraulic properties and strength, a significant part of the test programmes were carried out using apparatus especially suited to unsaturated soils. The analysis concerns mainly the volcanic ashes B2 tested in the range of suction from 0-80 kPa.

Olivares & Picarelli (2003) measured the shear strength of Cervinara ash B2 by means of suction-controlled triaxial tests (SCTX) using a mean net stress ($p-u_a$) between 20 and 200 kPa and a suction (u_a-u_w). The strength measured at different suction values is reported in Figure 11a against the saturated shear strength envelope ($c'=0; \phi'=38^\circ$). All data show the significant role of suction, even at small values of suction (Fig. 11b): in particular, the intercept of apparent cohesion is 2-6 kPa for a suction of 4-8 kPa (Olivares, 2001). These values are sufficient to justify the stability of shallow soil deposits on steep slopes.

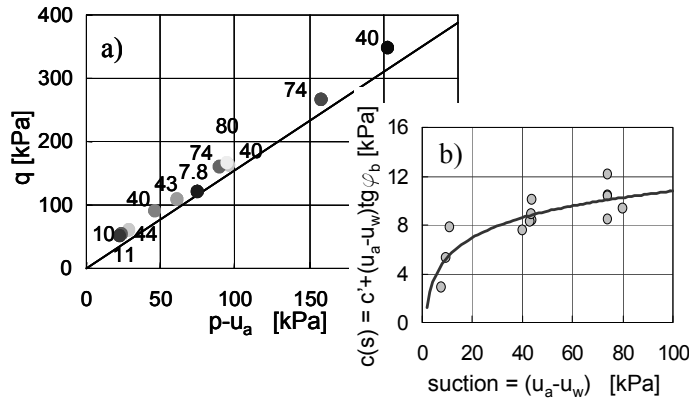


Figure 11- Unsaturated shear strength of Mt. Partenio ashes B2: a) stress plane (numbers indicate the suction imposed); b) cohesive intercept as a function of suction (from Olivares & Picarelli, 2003).

Bilotta et al. (2005) and Papa et al. (2008) investigated the role of suction on the shear strength of

Sarno and Monteforte Irpino B2 ashes, by means of direct shear and triaxial tests performed at different water contents and under different applied suctions, showing that volcanic ashes present a non-linear envelope of the shear strength with respect to the degree of saturation.

4. Response to undrained loading

In spite of the ductile behaviour exhibited in drained triaxial tests, the undrained behaviour of natural ashes B2 is highly unstable and suggests that for very low confining stresses, a mechanism of liquefaction can develop. This is clearly shown in Figure 12a, which reports the results of CIUC triaxial tests carried out on natural saturated specimens taken from air-fall deposits located to the North and East of Naples (Olivares & Picarelli, 2001). In all cases, and in a stress range comparable to the natural one, the stress paths show a peak, which is reached slightly before the Steady State Line, followed by a drop in strength occurring along the same line, as a consequence of increasing positive excess pore pressures.

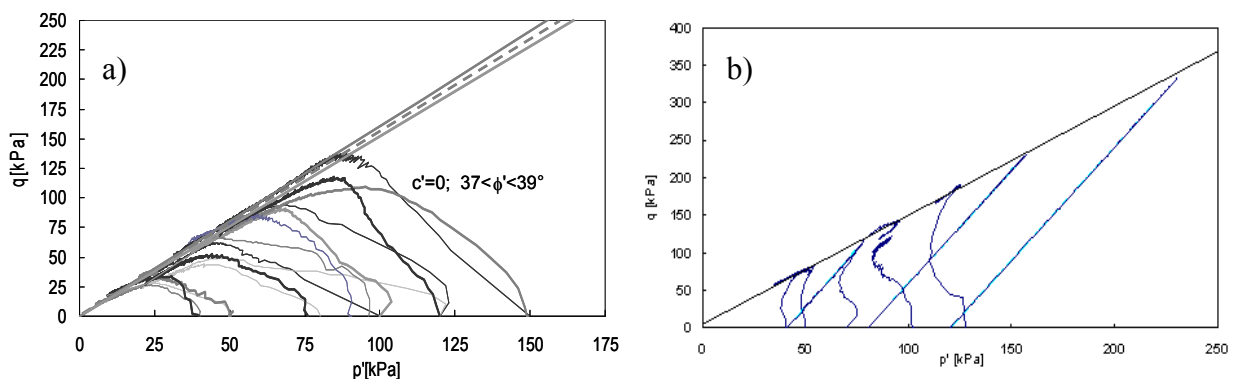


Figure 12- Behaviour during triaxial tests: a) CIUC on Cervinara, Lauro, Sarno volcanic ashes (from Olivares & Picarelli, 2001); b) CIUC and CIDC on Forchia ash.

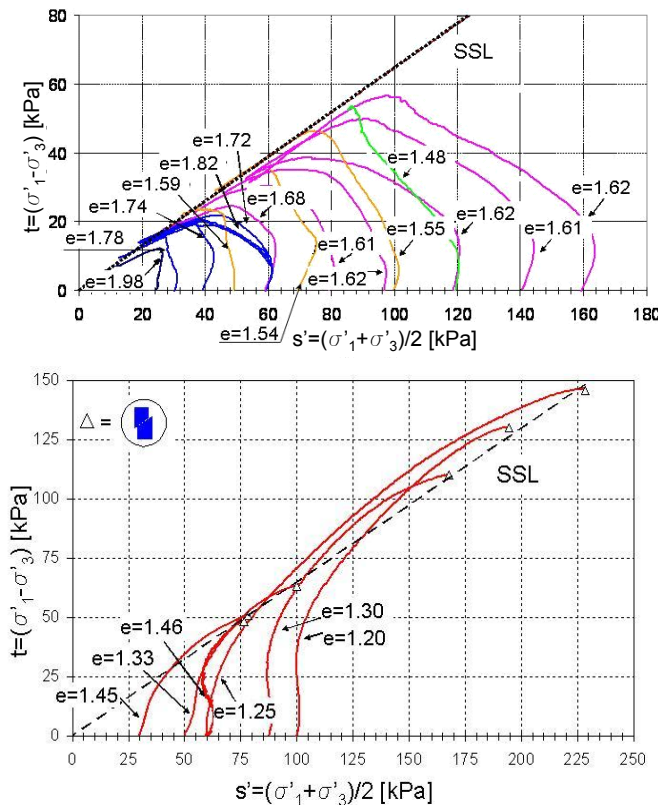


Figure 13- Results of undrained compression triaxial tests on reconstituted specimens of the Cervinara ash (from Lampitiello, 2004): a) loose specimens; b) dense specimens.

regardless of the initial state and type of test, while the mobilised strength strongly depends on the pore pressure that develops in the shear stage. This is clearly shown in the compression plane of Figure 14, which summarises all tests performed on reconstituted specimens. The diagram demonstrates the relationship of the initial void ratio and the Steady State Line, SSL in distinguishing between specimens, which are susceptible to liquefaction (having an initial void ratio above the Steady-State Line, SSL), and specimens which are not susceptible to liquefaction (below the SSL). Such data are extremely useful to identify the deposits, which can give rise to flow-like landslides as a consequence of slope failure (Olivares & Picarelli, 2001).

This behaviour is explained by the high void ratio ($n > 65\%$) and the specific fabric of the materials investigated, which are metastable, displaying a tendency towards volumetric collapse under shear.

In contrast, the response of ashes with a relatively low void ratio is different. This is the case of the Forchia ash ($n=61\%$) whose behaviour in CIUC and CIDC tests is shown in Figure 12b. The soil exhibits quite stable behaviour, even if the shear strength shows a slight decrease after the peak.

The influence of the void ratio on the soil behaviour has been checked through CIUC tests on reconstituted specimens (Lampitiello, 2004). The results show that even a small change in porosity can cause a strong change in soil behaviour, turning from unstable to stable, even though the failure envelope is the same (Fig. 13).

All experimental data presented confirms that the Steady State Line in the stress plane is unique,

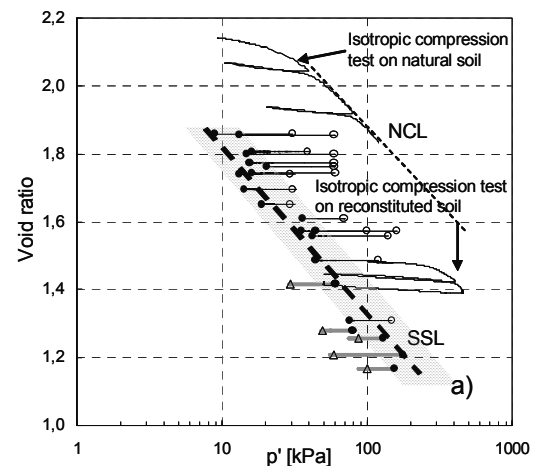
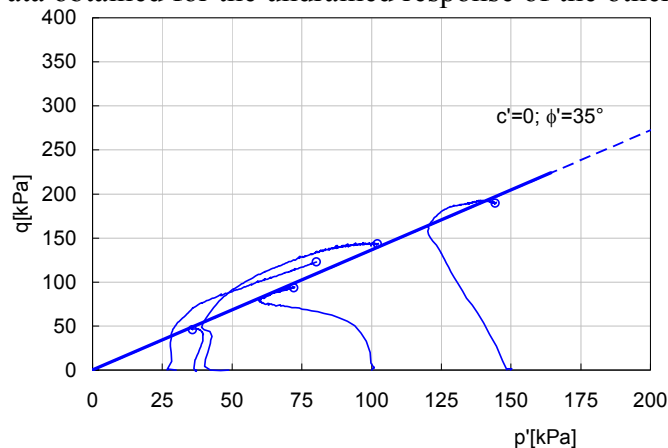


Figure 14- Compression plane: results of undrained triaxial compression tests on reconstituted specimens of Cervinara ash, (from Olivares et al., 2003).

Data obtained for the undrained response of the other types of volcanic ashes tested in triaxial



compression are not so consistent. However, the results of some CIUC tests on altered Cervinara ash, C, show that its behaviour is essentially stable or temporarily unstable for all the investigated confining stresses (Fig. 15). This can be essentially attributed to its lower porosity (about 55%).

Figure 15- Results of CIUC tests on saturated natural specimens of Cervinara altered ash C at $n \sim 55\%$.

Characterisation of the mechanical behaviour at failure and post failure stages of typical pyroclastic soils of the Campania Region (UNISA)

1. Soil properties

An extensive laboratory testing programme on undisturbed and remoulded samples was carried out in recent years at the University of Salerno for an area of about 60 km² of the Campania region recently affected by huge landslides of the flow-type, with the aim of characterising both the physical and mechanical properties of pyroclastic soil deposits. While referring to Cascini et al. (2000), Sorbino & Foresta (2002) and Bilotta et al. (2005) for a detailed description of the methodologies and experimental procedures employed, the main results concerning the hydraulic and shear strength properties of pyroclastic soils are summarised.

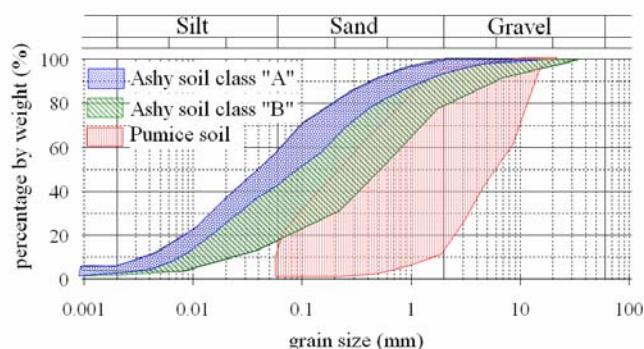


Figure 17- Grain size distribution of pyroclastic soils from Pizzo d'Alvano massif in Campania (southern Italy) (modified from Sorbino & Foresta 2002; Bilotta et al. 2005).

As already discussed in Deliverable D1.2, the pyroclastic soil deposits are characterised by a high variability in their physical and mechanical properties. However, three main soil classes were recognised by Bilotta et al. (2005) consisting of pumice soils and ashy soil layers (class A and B) (Fig. 17). The shallow ashy soil (class B) is generally coarser than the deeper layers (class A), as confirmed by laboratory tests aimed to assess hydraulic and shear strength properties in saturated and unsaturated conditions.

The hydraulic properties of ashy soils in saturated conditions were investigated through conventional permeameter tests that led to the determination of conductivities ranging between 5.0×10^{-6} m/s and 4.8×10^{-5} m/s; while hydraulic conductivity values for the pumice soils ranging between 1.0×10^{-5} and 1.0×10^{-2} m/s were assumed, according to the data available in the literature (Pellegrino, 1967; Whitam & Sparks, 1986).

The Suction Controlled Oedometer, the Volumetric Pressure Plate Extractor and the Richard Pressure Plate furnished the Water Retention Curves describing the unsaturated conditions of the ashy soils, shown in Figure 18; the same Figure also shows the volumetric water content and the hydraulic conductivity curves for pumice soils, obtained by using empirical relationships based on their grain size distribution (Bilotta et al., 2005).

The saturated shear strength envelopes for ashy soils provided effective friction angles ranging from 32° to 35° for class A soil, and

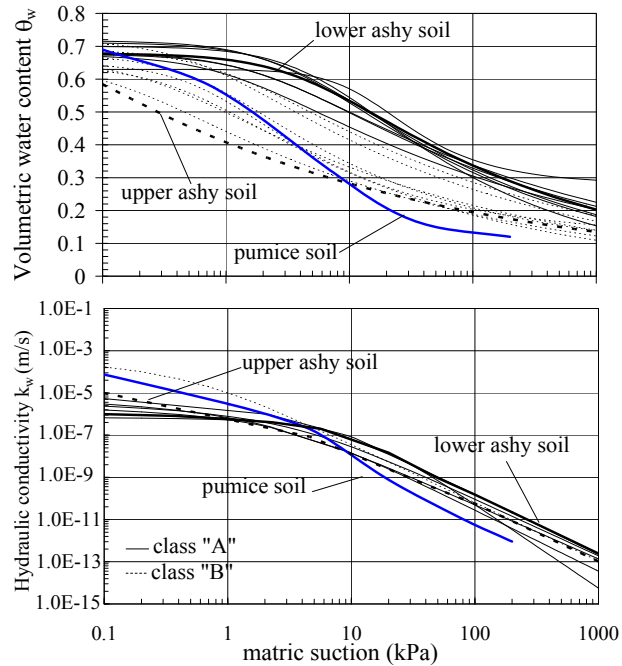


Figure 18- Soil Water Retention Curves (modified from Sorbino & Foresta, 2002; Bilotta et al., 2005).

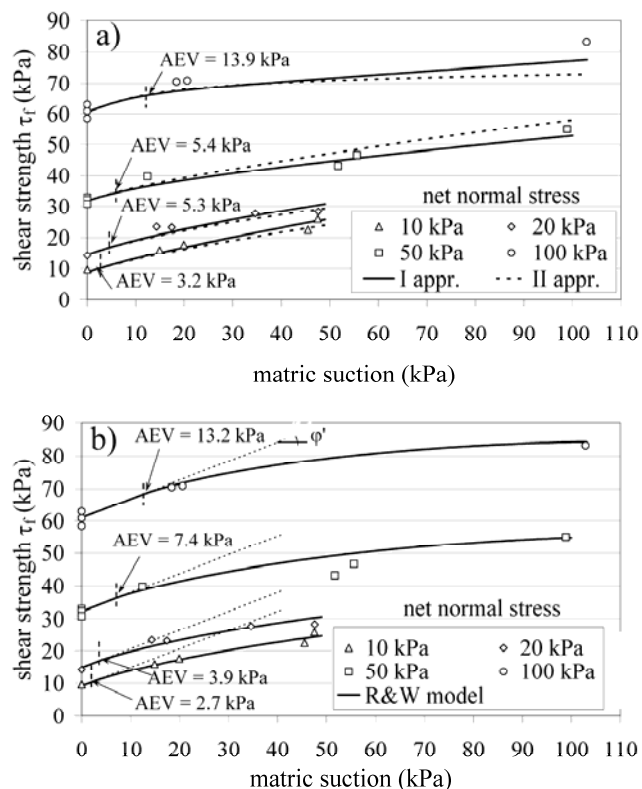


Figure 19- Experimental and predicted shear strength envelopes: (a) Vanapalli et al. (1996) model and (b) Rassam and Williams (1999) model (from Bilotta et al., 2005).

from 36° to 41° for the class B soil. Moreover, when these soils are remoulded, when reworked they show a significant increase in the friction angle and a decrease in the porosity.

The unsaturated shear strength was investigated on undisturbed ash specimens by means of direct shear tests, as well as triaxial tests respectively at different water contents and at variable applied suctions, in order to reproduce the different in-situ conditions during the hydrologic year. The shear strength criterion adopted to model the unsaturated shear strength of the soils was that proposed by Fredlund et al. (1978), who extends the Mohr–Coulomb failure envelope for saturated soils. The experimental laboratory results obtained clearly show a non-linear envelope of the shear strength with respect to matric suction (Fig. 3). The non-linearity of this envelope is reported in the literature by several researchers (Escario & Saez, 1986; Gan et al., 1988; de Campos & Carrillo, 1995; Oloo & Fredlund, 1996; Vanapalli et al., 1996; Oberg & Sallfors, 1997; Rassam & Williams, 1999; Vanapalli et al., 1999). The increase of shear strength with suction was modelled by using the two approaches proposed by Vanapalli et al. (1996) and Rassam & Williams (1999). The class “A” soils are shown in Figure 19 to be strongly independent from the range of suction values detected in-situ, whereas the class “B” ash soils do not show any significant dependence for suction values exceeding 30 kPa (Bilotta et al., 2005). Finally, the angle of shearing resistance with respect to suction, was found to be a decreasing function of matric suction for both soil classes (Fig. 20).

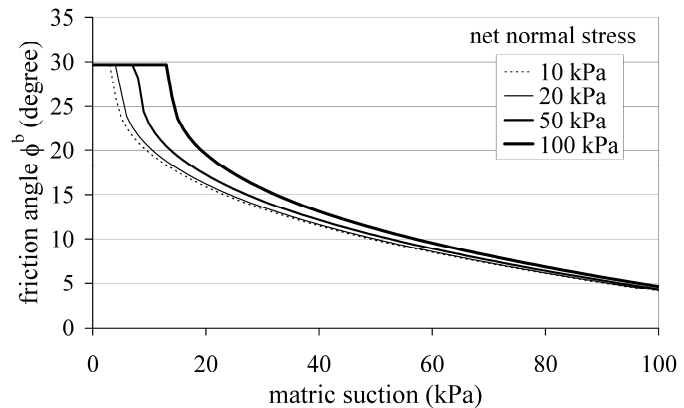


Figure 20- Variation of friction angle ϕ^b of shearing resistance versus matric suction (from Bilotta et al., 2005).

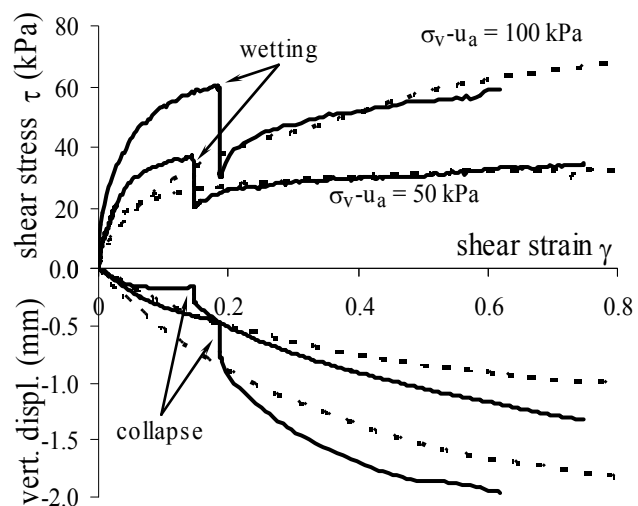


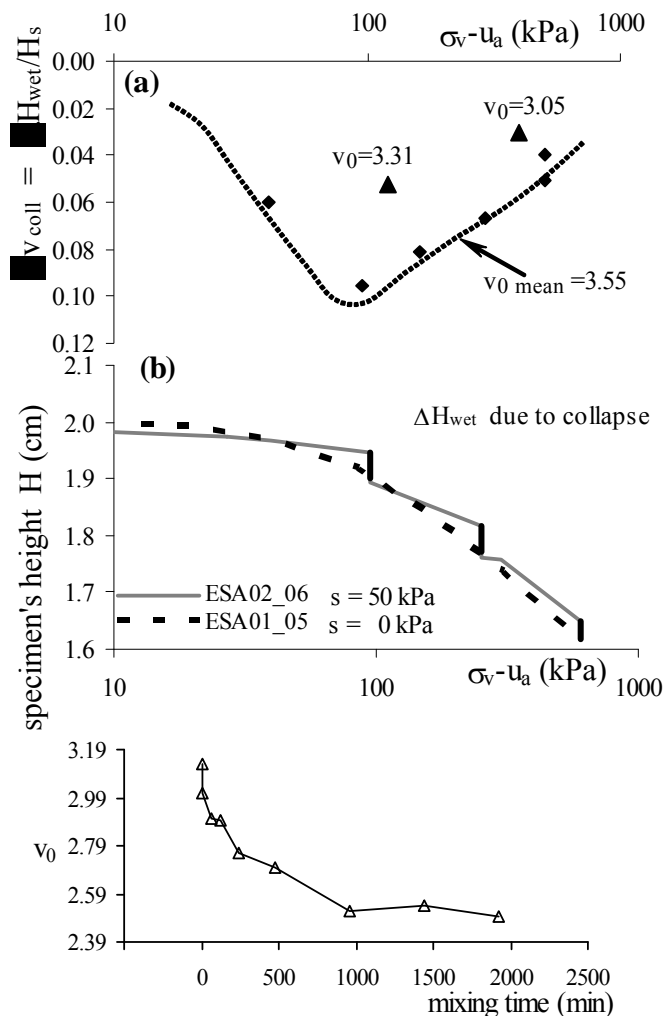
Figure 21- Stress-strain relationship shown in strain controlled shear tests: dashed line (A1 test) and continuous line (A2 test) (from Sorbino et al., 2010).

Another peculiarity of the mechanical behaviour of the pyroclastic soils analysed was examined by performing suction controlled oedometer tests and simple shear suction

controlled tests. In particular, collapsible (Bilotta et al., 2006) and unstable (Sorbino et al., 2010) behaviour were in evidence during the wetting path.

An intensive experimental laboratory investigation was started into the mechanical behaviour, to assess the post-failure mechanisms (i.e. the liquefaction potential) of the pyroclastic soils, by using a new simple shear apparatus designed at the University of Salerno (Sorbino & Foresta in prep.). A summary of the preliminary data obtained is reported.

All the specimens tested were first brought to an imposed value of suction, ranging from 0 kPa for tests “A1, C1” to 50 kPa for tests “A2, B and C2”. A maximum time of 48 hours was sufficient to obtain pore water pressure equalisation within the specimen, whereupon the net vertical stress was applied and about 24 hours were needed to complete the consolidation



phase. Finally, the shear phase was performed at constant suction (type A1, C1) or at variable suction (type A2, B, C2). A detailed description of both methodologies and experimental procedures are reported in Sorbino et al. (2010). The main results obtained are illustrated in Figure 5, showing the results obtained from strain-controlled tests (A1 and A2 tests) carried out at a constant vertical stress of 50 kPa and 100 kPa. From Figure 21 it can be observed that the two specimens tested under saturated conditions (A1 tests) show typical stress-strain behaviour of a contractive material. The results for the A2 tests, obtained through a rapid decrease in suction, are also reported in the same figure, showing a volumetric collapse and a drop in the shear stress mobilised. In both the tested specimens, this drop results in shear stress values that are lower than those attained, at the same shear strain, in the saturated specimens.

Figure 22- (a) Specific volume variation due to wetting collapse vs. vertical net stress for specimens with initial specific volume from 3.64 to 3.45; (b) specimen height variation with net vertical stress in a saturated condition and during repeated wetting-drying paths; (c) Variation of initial specific volume of ashy soils specimens for different mixing times (modified from Migliaro, 2008).

After this drop, both the specimens show an increase in the shear stress with shear strain and approach the stress-strain curves of the saturated specimens. The attainment of shear stress values lower than those shown by the saturated specimens could be explained by an increase of the pore water pressure due to volumetric collapse during wetting. The increase in pore water pressure seems to be confirmed by a stress-controlled shear test at constant vertical stress (B test). A value of the shear stress lower than the saturated shear strength was applied in this test, and maintained constantly during the saturation stage.

As could be expected, volumetric collapse develops during wetting. A sudden increase of the shear strain rate was also observed during this stage of the test. This behaviour highlights that the applied shear stress at collapse is higher than the available shear strength of the soil. This means that an increase in pore water pressure must have been developed in the specimen. These results confirm that the volumetric collapse is responsible for pore water pressure increase during wetting. The observed behaviour is, however, a necessary, but not a sufficient, condition for the development of liquefaction phenomena. This may become sufficient if the amount of volumetric collapse is sufficient to induce a pore water pressure in the specimen equal to the mean total stress. Migliaro (2008) also showed that the potential amount of volumetric collapse can be related to two different conditions: the wetting paths on unsaturated specimens and the modification of the soil structure.

The influence of structural change of the soil on volumetric collapse has been investigated by performing a series of oedometer tests in saturated conditions on undisturbed and remoulded samples.

Remoulded samples were obtained by adopting different techniques of mechanical

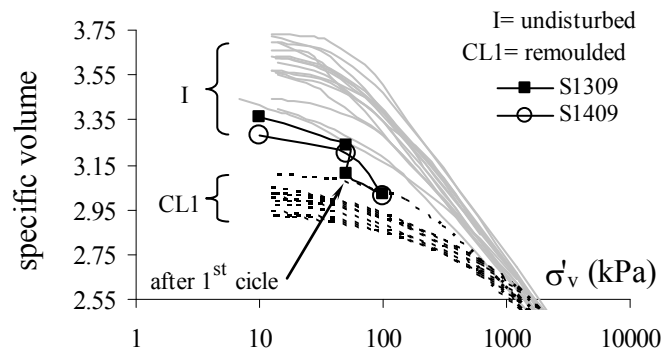


Figure 23 - Comparison between the results for oedometer tests performed on undisturbed and remoulded specimens and the values of specific volume - after reconsolidation - of two specimens exposed to cyclic shearing in simple shear tests (from Sorbino et al., 2010).

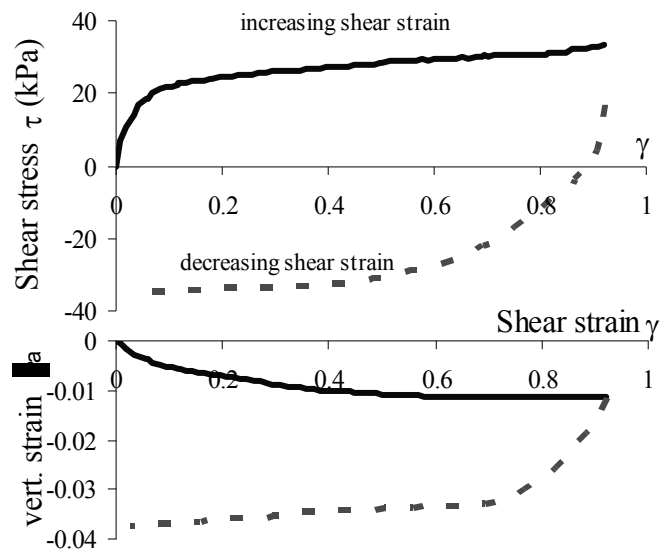


Figure 24 - Stress-strain behaviour for S1309 saturated specimen during cyclic drained simple shear test (from Sorbino et al., 2010).

mixing (Migliaro, 2008). Figure 21c shows the effect of mixing time on the reduction of the initial specific volume (v_0) of the tested specimens. This specific volume reduction is due to macro-aggregate destruction (destruction) without any variation in the soil's grain size distribution (Migliaro, 2008). Figure 22a shows the results obtained from the oedometer tests. By comparing Figure 22a and Figure 23, it can be noted that the amount of the volumetric collapse due to the destruction (i.e. the difference between the specific volumes of the undisturbed and remoulded specimens at a given effective vertical stress) is larger than the value obtained from wetting paths.

The destruction of macro-aggregates can be also reproduced by performing cyclic drained simple shear tests on undisturbed samples. Typical results from this type of test are illustrated in Figure 24, where most of the volume reduction of the specimen is attained when reversing the shear strain. The destruction of the specimen during this cycle is confirmed by the oedometric reconsolidation of specimen S1309 that travels from the undisturbed compressibility domain to the remoulded one (Fig. 23).

Confirmation of the destruction of the specimen is given by the results obtained from constant volume simple shear tests (C1 test) carried out at vertical stress of 100 kPa and 150 kPa. Figure 25 shows the results of these tests in terms of dimensionless stress paths (i.e. the values of shear stress and effective vertical stress referred to effective vertical stress at the end of the consolidation phase " σ'_c "), where the specimen shows a marked dilative behaviour that is typical of remoulded dense material.

In order to evaluate the influence on the potential for liquefaction of the volumetric collapse due to both wetting paths and destructuring, a specific simple shear test was carried out (C2 test). The specimen was initially equalised at an imposed suction of 50 kPa during this test, and then consolidated under 50 kPa net vertical stress. The specimen was sheared to a constant rate of shear strain at the end of the consolidation phase by imposing a constant volume condition. Figure 26 shows the dimensionless stress path (i.e. the shear stress and net

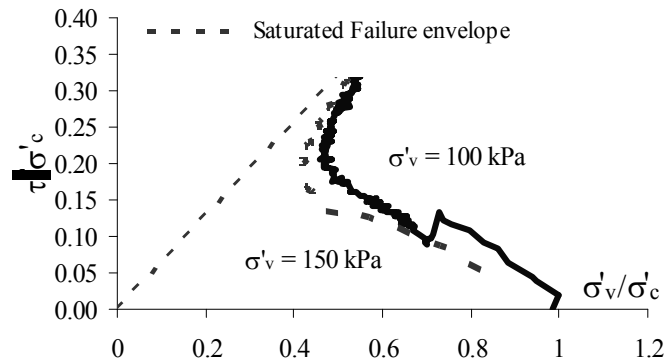


Figure 25 - Normalized stress paths during a constant volume shear for reconsolidated S1309 saturated specimen (from Sorbino et al., 2010).

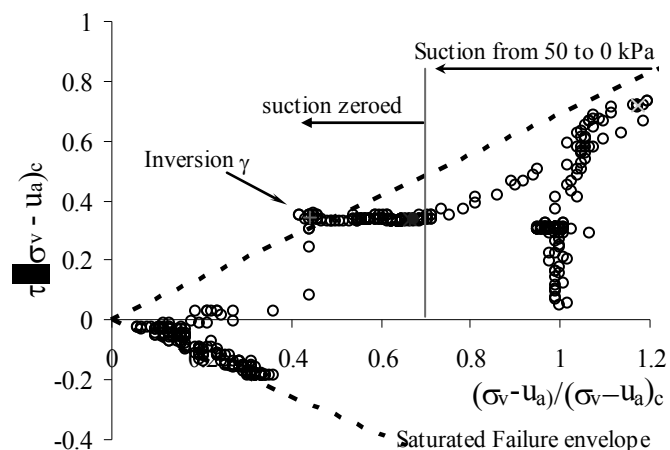


Figure 26 - Normalized stress-path for S1409 specimen during the constant volume shear test (from Sorbino et al 2010)

vertical stresses referred to the value of the net vertical stress at the end of the consolidation phase ($(\sigma_v - u_a)_c$) followed by the specimen during the shear phase. The specimen shows an initial tendency to dilate during this stage of the test, which is shown by the progressive increase of the applied net vertical stress (Fig. 26). In the subsequent stage of the test, suction was rapidly reduced from the initial value of 50 kPa to 0 kPa by flooding the specimen, which was accompanied by an initial decrease of the shear stress. As the shear strain increases, a continuous decrease of the net vertical stress at constant shear stress was experienced by the specimen, probably due to dissipation of excess pore water pressure generated by wetting.

The decrease of effective vertical stress leads the specimen to approach the failure envelope in saturated conditions under an effective vertical stress greater than zero. The relatively dense initial packing meant that the contractive behaviour of the soil was avoided, as was collapse during wetting, so that the specimen was unable to approach liquefaction.

An inversion in the shear strain was applied to the specimen in the final stage of the test in order to simulate soil destructuration. The shear stress mobilised by the specimen immediately reduces and vertical stresses approach the zero stress conditions (soil liquefaction). This behaviour is due to a more consistent volume variation tendency that the specimen develops through destructuration. After the occurrence of the liquefaction phenomena, the specimen exhibits a dilative behaviour once more. This last circumstance can be ascribed to the denser state achieved by the soil following destructuration.

Simple shear tests performed up to now on undisturbed pyroclastic soils highlight an unstable volumetric behaviour when subjected to wetting paths during shearing. This instability, which can be attributed to the collapsible tendency of the soils investigated, is shown both in constant vertical load and constant volume shear tests. However, the amount of the volumetric collapse, due to transition versus saturated conditions, seems to be insufficient to induce liquefaction. More consistent volumetric strains, such as those produced by destructuration of the soil structure, are needed. Additional volumetric strains that can be attained in the soil specimens by reversing shear strain in simple shear tests seem to be responsible for the occurrence of liquefaction.

A strain reversal can take place in situ, when, in addition to rainfall, further hydraulic boundary conditions (coming for example from buried springs) act at the base of the loose pyroclastic covers. It is also evident from Figure 22 that soil skeleton structure can be progressively lost due to either loading or mixing. A soil specimen that is not completely destructured can thus experience consistent volume decrease. From the results obtained up to the time of writing, it seems that the occurrence of liquefaction could be possible also for the same soil in a medium/dense state.

2.1.4 The specific case of fissured stiff clays

(AMRA)

The class of highly overconsolidated clays includes indurated and fissured materials, whose behaviour sometimes escapes from the general framework usually adopted for dense and OC soils. This poses significant problems in the selection of both testing procedures and parameters to use during analysis with particular reference to slope stability problems.

Some bonding, due to either precipitation of salts or carbonates and other compounds, has been frequently proposed to explain the behaviour of stiff OC clays, and has been investigated through laboratory experiments and comparison of the mechanical response of both natural

and reconstituted soils. General, comprehensive considerations on the influence of bonding on material behaviour have been reported by Leroueil and Vaughan (1990) and Burland (1990). The role of bonding on soil behaviour is dealt with in Deliverable D1.1 of this project. In a few words, bonding causes an expansion of the yielding surface beyond the theoretical size associated with the current value of the void ratio, giving rise to a stiffer and more resistant, brittle material. In the case of initially anisotropic soils, it also causes a change in the shape of the yielding surface due to a decrease in the degree of anisotropy of soil. Due to bonding, general and popular theories, such as the Critical State Theory (and the consequent Cam-Clay model) that have been conceived for uncemented materials, whose behaviour is essentially governed by the current void ratio and the induced state of stress, present some weaknesses that are being accounted for by more recent approaches.

A crucial point is that many stiff and indurated clays contain sets of discontinuities and fissures. This is a further problem since the approaches and models, which can account for bonding, are not able to consider the presence of discontinuities and fissures too.

The fundamental question, which arises when dealing with such materials, is whether laboratory samples are representative of the formation as a whole. Typical materials of this class are the so called jointed stiff clays (Esu, 1966; D'Elia et al., 1998), which present sets of joints and bedding surfaces. In principle, these formations can be investigated and modelled following the principles of Rock Mechanics, i.e. looking at the material as a discontinuum. In such a case, any investigation should primarily focus on the role of discontinuities. Other typical materials are stiff fissured clays, which generally are treated following the principles of the Soil Mechanics, i.e. looking at the material as a continuum. Some considerations on jointed stiff clays are reported in Deliverable D.1.2 of this project. This section is essentially devoted to them, with special emphasis to highly fissured tectonized clay shales.

Different studies in the Sixties and Seventies (Bishop and Little, 1967; Marsland and Butler, 1969; Skempton et al., 1969; Lo, 1970; Morgenstern, 1977) pointed out the importance of fissures on the behaviour of clayey formations stressing the role of fissures on the parameters, which are measured through laboratory tests, and the need to select large specimens in order to obtain correct data for any analysis looking at the soils as a continuum (Fig. 27). Another method is to perform in situ tests, which enable investigation of the hydraulic or mechanical response of large soil volumes. For soils containing well oriented fissures, assessing the soil anisotropy is another prominent intent of any investigation.

The role of fissures cannot be easily dealt with since they present highly variable features. Walker et al. (1987) suggest consideration of five basic parameters, namely: continuity, orientation, shape, spacing and surface features (Fig. 28). The combination of such parameters can lead to very different behaviours and properties. An extreme situation is the one of slightly fissured soils (high spacing between fissures) with randomly oriented irregular and rough fissures with a few intersections: these could display similar properties to non-fissured soils having the same index and state properties. An opposite situation is the one of intensely fissured soils (low spacing) with well oriented planar and slickensided fissures: these are much weaker, displaying an anisotropic behaviour with a shear strength, in the direction of fissures, very close to residual.

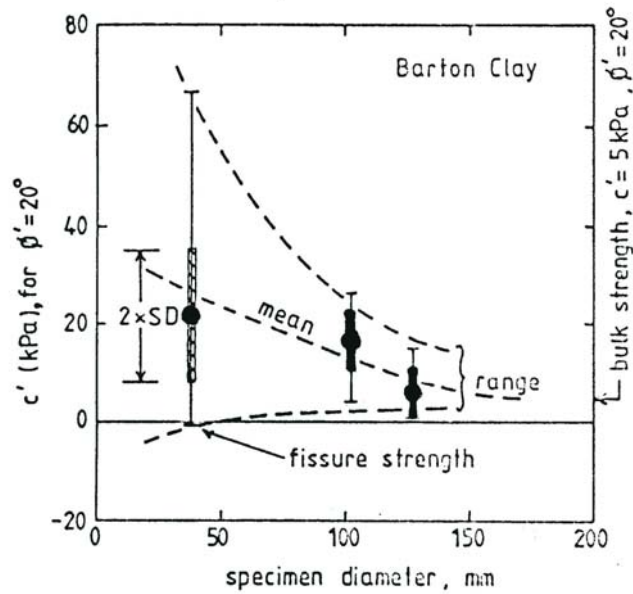


Figure 27 - Dependence of the effective cohesion, c' , of Barton clay on the size of specimens tested (from Chandler, 1984).

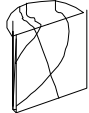
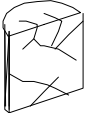
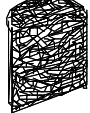

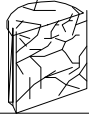



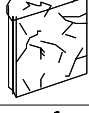
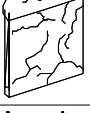



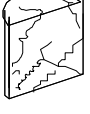
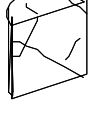

N	Continuity	Orientation	Shape	Spacing	Surface
1	continuous 	actual measured angle(s) to horizontal	planar 	< 5mm 	striated or slickensided 
2	not continuous; many intersections 		undulose 	5 to 10mm 	polished 
3	some intersections 		conchoidal 	10 to 40mm 	smooth 
4	very few intersections 		irregular 	> 40mm 	rough 

Figure 28 - Classification of fissured materials according to Walker et al. (1967).

Tectonized clay shales (AGI, 1977; Picarelli, 1986) represent a special category of stiff fissured clays, which are widespread in the Apennines chain, Italy, but outcrop also in other countries in Europe. Such materials are the result of the geological events, which led to the formation of the Apennines. Tectonized clay shales are sheared, fine-grained, indurated soils consisting of very small shear lenses (called scales or fragments) separated by minor shears (Fig. 29). The size of the shear lenses varies from a few millimetres to a few centimetres. Figure 29 suggests that fissures are not continuous with many intersections, and can be locally oriented; their shape is practically planar (or slightly curved); spacing ranges between some millimetres and a few centimetres; their surface ranges from polished to slickensided. However, the network of minor shears can also be seen as an intricate system of larger continuous and undulose fissures (resulting from the continuity of small single fissures); on the other side, the material as a whole can be seen as a granular soil consisting of single weak elements (indurated clay) having a low intergranular friction.



Figure 29 – *The Bisaccia tectonised clay shale.*

No doubt that in such a case, any analysis should be carried out looking at the soil as a continuum, but special attention must be paid to the size of specimens to test and care has to be used in the sampling procedure. In general, spacing among fissures is so small that testing can be carried out on specimens of usual size, but there are materials whose scales are large enough to impose the selection of specimens of larger size. Especially in the case of low plasticity materials, sampling and carving of specimens should be carried out with great care, since the intergranular mobility (i.e. the movements of the shear lenses) can give rise to significant changes in the mesofabric of soil and to specimens of poor quality.

The influence of fabric on the hydraulic and mechanical response of such materials has been the topic of a number of papers published in the in the last three decades (AGI, 1977; Bilotta et al., 1985); Picarelli et al., 1998, 2002).

Urciuoli (1992) reports the results of constant head permeability tests on the highly plastic Bisaccia clay shale, carried out in the triaxial cell under an anisotropic state of stress corresponding to field conditions. He shows that the relationship between the hydraulic conductivity and the void ratio is more or less the same, regardless of whether the tests have been carried out on undisturbed or reconstituted specimens. This can be justified only if fissures are closed. However, further data regarding other tectonized clay shales taken from the Basento valley suggest that some aperture of fissures can produce significant differences in permeability, which increases as the confining stress decreases (Urciuoli, 1994). In addition, the field value measured by in situ constant head permeability tests is often higher than the one obtained in the laboratory, probably due to the presence of opened fissures or of macro-discontinuities.

Such data suggest that in slope stability problems the short-term condition is as significant as in other fine-grained formations.

The influence of fissuring on the mechanical soil response is negligible every time the stress change is characterised by a substantial increase of its isotropic component, as in the case of surcharges caused by large man made works such as dams. This is shown by experience and documented data (Picarelli et al., 1998). In such a case, in fact, the mobility between scales is practically inhibited and the deformation of soil (essentially compression) is regulated by the stiffness of single elements (in turn depending on bonding) rather than by the mobility of scales along minor shears.

This is clearly shown by both isotropic and oedometer tests that suggest that no significant differences exist between the conceptual behaviour of tectonized clay shales and that of intact clays. Figure 30 shows the values of the void ratio at the end of the isotropic consolidation stage of triaxial tests carried out on undisturbed saturated specimens of the highly plastic Bisaccia Clay Shale and the isotropic virgin line of the same material, obtained through isotropic compression tests performed on reconstituted specimens. As shown, the void ratio of the natural soil enters the zone of “impossible states”; therefore, “yielding” is the result of soil destructuration, i.e. of breaking of interparticle bonds. However, there are cases in which the compression line does not trespass the virgin line because of destructuration occurring before reaching the virgin line: such a situation may occur in the case of soil having a low void ratio and weak bonds (Aversa et al., 1993).

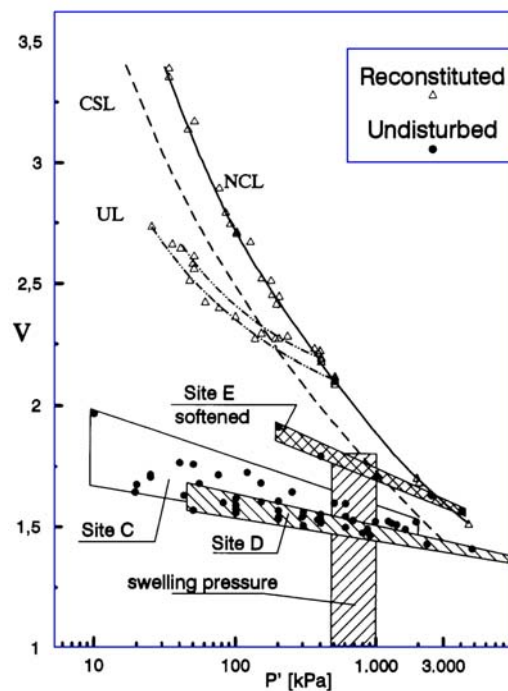


Figure 30 - Relationship between void ratio and effective stress for the highly fissured Bisaccia clay shale subjected to isotropic compression (Picarelli et al., 2002).

The soil response when the deviatoric stress component prevails is very different; this is the case of slopes, cuttings and tunnels. In such situations, the soil may experience high shear strains and display a low shear strength. This is confirmed by experience, which shows that

the main problems posed by tectonized clay shales are landslides triggered from cuttings and natural slopes, and high deformation of tunnels caused by an unusually thick plastic lining (Picarelli et al., 1998).

Useful data have been provided by CIU tests carried out in a Bishop-Wesley stress path controlled triaxial cell instrumented with some microtransducers to measure local axial, radial strains and excess pore pressures (Fig. 31).

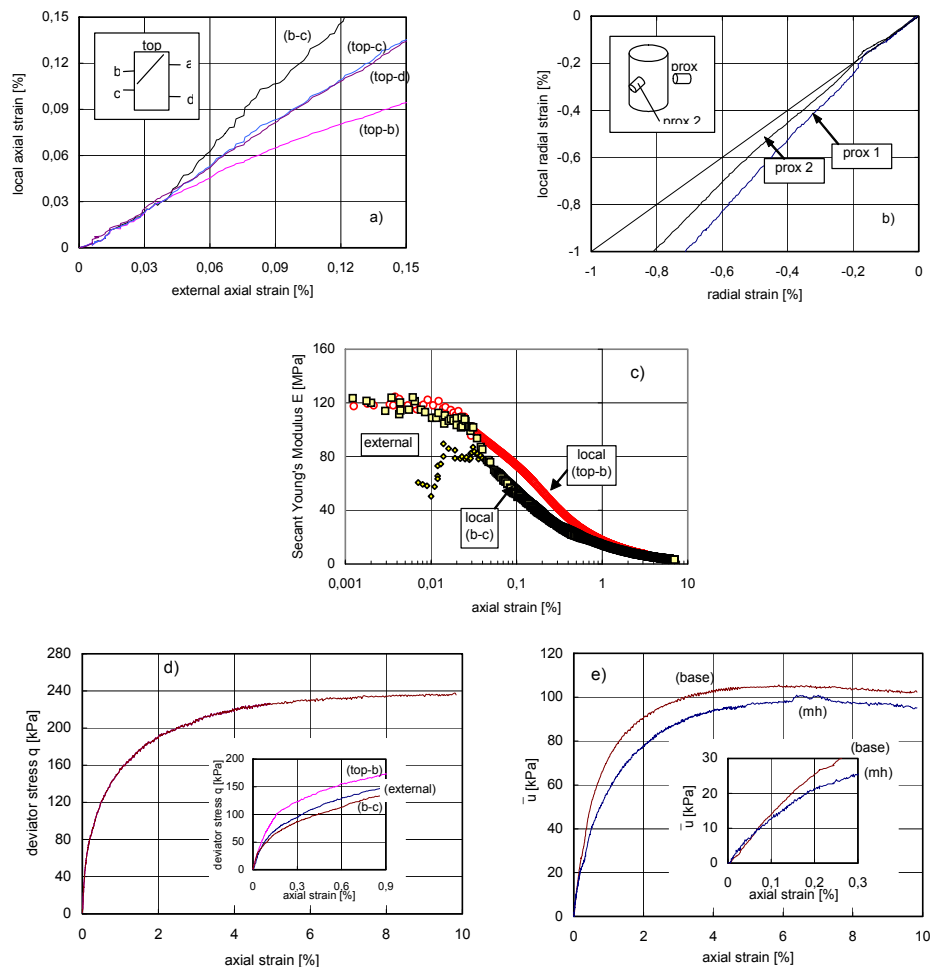


Figure 31 - Results of undrained triaxial CIU test on an undisturbed specimen of the Bisaccia clay shale: a) axial strains; b) radial strains; c) secant Young modulus; d) axial stress-axial strain curve; e) excess pore pressures (Picarelli et al., 2002).

Figure 31 reports the results of a CIU test on an undisturbed specimen subjected to a confining pressure of 400 kPa. As shown in Figure 5a, induced internal strains are quite uniform for axial strains (obtained from external measurements) less than 0.05 %, then local values diverge as a consequence of “strain localisation”, i.e. of formation of a slip surface which develops along contacts between the shear lenses. In fact, the “strain” occurring in the intermediate part of the specimen (b-c) is much higher than the strains measured in the

vicinity of the bases of the specimen (Fig. 31a). The same phenomenon is revealed by radial strains (Fig. 31b). Figure 31c reports the secant modulus, which is quite high until the soil stiffness converges at axial strains greater than 1%. The measured excess pore pressures are reported in Figure 31e, which shows that the values measured at the base (“external” measurement) are higher than those measured at mid-height (“local” measurements), once again presumed to be due to strain localisation. Finally, Figure 31d shows that the stress-strain curve (from “external” measurements) is ductile in spite of the high OCR of the soil.

Accounting for the fabric described, these observations suggest that what is defined as “strain” is the result of the movements of shear lenses along shear fissures, leading to separation of the specimen into two or more parts. For small “global” strains, the soil stiffness is relatively high because the meso-fabric is not yet mobilised, while the soil stiffness drops for higher strains, as a consequence of the mobility of shear lenses along their bounding fissures. This also governs the volumetric soil response and the brittleness, which is generally moderate or nil.

Figure 31 reports the failure envelope obtained by CID and CIU tests on undisturbed specimens: it is clearly non-linear. In contrast, the Critical State Line of the reconstituted material is linear. For small confining stresses, the shear strength of undisturbed specimens is higher than the critical strength; for high stresses it is smaller. Once again, this can be explained by the role played by fissures. We can imagine that the shear strength along fissures is very low, possibly close to the residual strength. As shown in Figure 32, the shear strength should depend on both a basic friction angle, corresponding to the one, which can be mobilised along fissures, and a dilation angle which depends on the shear surface profile. This, in turn, should depend on the features of the network of fissures, i.e. on their continuity, shape and superficial features, which govern the “roughness” of the “global” shear surface. For high stresses, when dilation drops to zero, the shear strength tends towards the basic friction angle, which is close to the residual one, thus smaller than the critical value; for small stresses, the contribution of the “dilation angle” and of the basic friction angle can lead to a shear strength greater than critical. This suggests that the overconsolidation ratio does not play a significant role, the one of the fissure network being much higher.

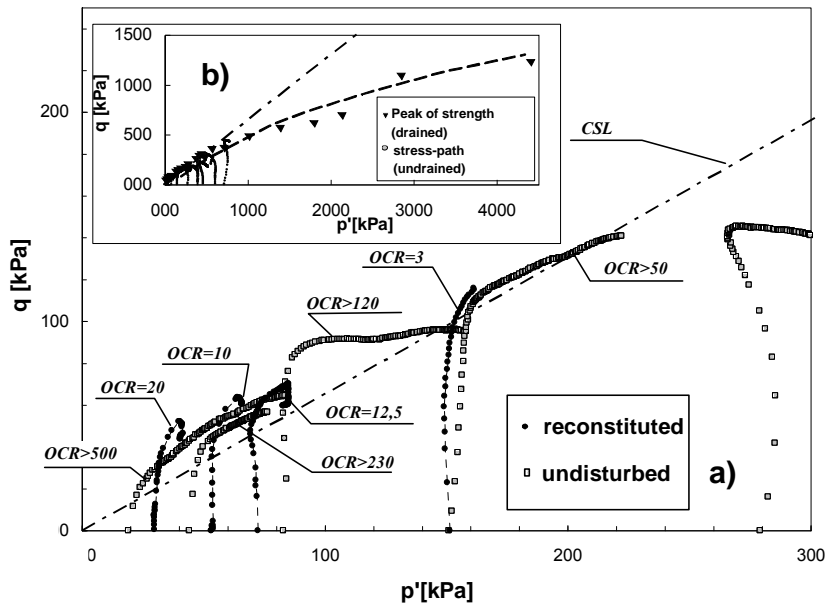


Figure 31 - Failure envelopes: a) undisturbed and reconstituted specimens in CID and CIU triaxial tests for $p' < 300$ kPa; b) peak drained strength and CIU stress path for p' to 4000 kPa (Picarelli et al., 2002).

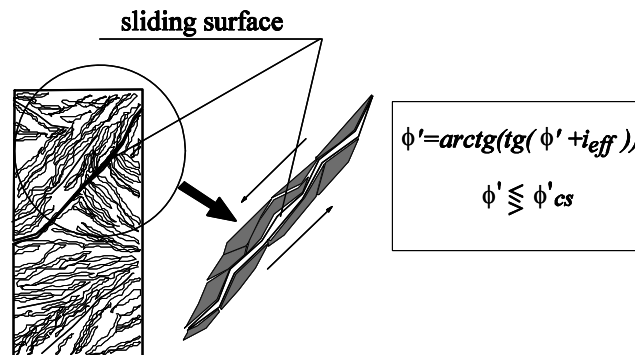


Figure 32 - Mechanism of rupture of tectonized clay shales (Picarelli et al., 2002).

Such data do agree with the lesson coming from experience, which suggests that first-time slides mobilise a low shear strength, characterized by a value of the cohesion, which is practically nil, and a friction angle generally comprised between the critical and residual friction angle.

Unlike what is generally indicated by experience on other materials, both the critical and the residual strength are higher than the values measured on reconstituted specimens (Leroueil et al., 1997; Picarelli, 2009). This is due to the shear lenses, which play the same role as particles in granular soils giving rise to a relatively “coarse effective grain size” (critical strength) and inhibit the formation of a really planar slip surface (residual strength).

A last consideration concerns the high deteriorability of these materials, associated with positive volumetric strains (Bilotta et al., 1985; Picarelli et al., 2002; Picarelli and Di Maio, 2010). Swelling under low stresses is often as high as in expansive soils, causing destructuration and a decrease of the influence of fissures on the mechanical soil behaviour, accompanied by a surprising increase of the shear strength. Such behaviour can explain the serious problems posed by deep excavations (Picarelli et al., 1998) and, possibly, the typical occurrence of mudslides in these materials (Picarelli, 2009). The reason of their high expansivity seems associated with physical-chemical phenomena occurring at the microscale (ionic exchanges occurring when the soil absorbs water having a low salt content), favoured by the opening of fissures (Picarelli and Di Maio, 2010).

2.2 FAILURE MECHANISMS OBSERVED IN SMALL-SCALE FLUME EXPERIMENTS

2.2.1 Results of flume experiments on saturated and unsaturated sands (ETHZ)

Generally the landslides induced by rainfall occur as a result of increase in pore pressures and/or seepage forces during and after heavy rainfall events (Terzaghi, 1950; Sidle & Swanston, 1982; Sitar et al., 1992; Anderson & Sitar, 1995). It is the increased pore pressure that decreases the effective stress in the soil and thus reduces the soil shear strength, eventually resulting in slope failure (Brand, 1981; Brenner et al., 1985). Further studies have illustrated that in some cases of rainfall-induced landslides, movement along the sliding surface leads to crushing of the soil grains, which results in the liquefaction along this surface, finally resulting in rapid movement and long runout distance (Sassa, 1996, 1998a, b; Gerolymos et al., 2007; Gerolymos, 2010). The occurrence of flowslides due to static effects has also been studied. It was found that the static liquefaction resistance of sand is influenced by a number of factors, including relative density, confining pressure and initial shear stress conditions, as well as grain angularity, over-consolidation ratio, stress history, length of time under sustained pressure, grain structure or fabric, and loading rate (Castro, 1969; Casagrande, 1971; Castro & Poulos, 1997; Chu et al., 2003; Casini et al., 2010).

In recent decades, many small-scale landslides have been triggered under laboratory conditions. For example, Sassa (1972, 1974) performed a series of flume tests on Toyoura sand (Japanese standard sand) and concluded that the changes in rigidity of sand and upper yield strain within a slope are essential to the analysis of slope stability. Further studies on liquefied landslides revealed that the increasing pore pressure, due to restriction of dissipation by an undrained soil layer, caused slope failure during rainfall and that the generation of pore pressure was a result of sudden initiation of subsidence (Sassa & Takei, 1977; Sassa, 1984). Eckersley (1990) triggered flowslides in coking-coal stockpiles by raising the water table, and inferred that excess pore pressures were generated during, rather than before, the movement. Another laboratory flowslide study was conducted on loose saturated fine quartz sands, in which the motion of liquefied sands and pore pressures during motion were analyzed (Spence & Guymer, 1997). Kubota (1997) performed a series of tests on silica sand and loess to study the mechanisms of flowslides under rainfall conditions. He concluded that the generation of

pore pressure was a result of a sudden initiation of subsidence. Iverson and his colleagues triggered landslides and debris flows in a large flume, with emphasis on examination of landslide movement and intergranular pore pressures (Iverson & LaHusen, 1989; Iverson, 1997; Iverson et al., 1997, 2000; Major & Iverson, 1999). These studies showed that landslide rates depend significantly on the initial soil porosity, and that rapid fluidised landsliding involves partial or complete liquefaction of the lower density mass by high pore fluid pressure. It was also concluded that the magnitude of pore pressure change induced by porosity change during landsliding depends not only on initial porosity, but also on the relative time scales for soil deformation and pore pressure diffusion; pore pressures fluctuated dynamically during rapid steady-shear deformation of water-saturated granular materials, and dissipated significantly only during post-depositional sediment consolidation (e.g. Moriwaki et al., 2004).

The factors affecting the mechanisms of initiation and spreading of landslides in sandy soils due to precipitation, based on flume tests, will be discussed in this report.

1. Initial void ratio (based on Iverson and LaHusen, 1989; Iverson, 1997; Iverson et al., 1997, 2000; Wang & Sassa 2001, 2003)

As soils approach specific critical-state porosities during shear deformation, it has been suggested that landslide behaviour may depend on initial soil porosity (Casagrande & Boston, 1936; Schofield & Wroth, 1968). Tests on small soil specimens indicate that dense soils (initially less porous than critical) dilate as they begin to shear, whereas loose soils (initially more porous than critical) contract (e.g. Castro, 1969, among others). Dilation can reduce pore water pressures and thereby retard continued deformation by increasing normal stresses and frictional strength at grain contacts, whereas contraction can increase pore water pressures and thereby reduce frictional strength (Reynolds, 1886). To isolate the effect of initial soil porosity on landslide style and rate, Iverson et al. (2000 & 1997) conducted large-scale experiments under closely controlled conditions using a 95 m long, 2 m wide concrete chute with a 31° slope, roughened bed, and smooth side walls (Iverson et al., 1992). In each experiment, a tabular prism of 6.1 to 6.4 m³ of moist, granular soil was formed by dumping and shovelling it behind a rigid, 0.65 m high retaining wall installed near the head of the flume (Iverson et al., 1997). The landslide experiments included individual tests with initial porosities ranging from 0.39 ± 0.03 to 0.55 ± 0.01 (± 1 SD sampling error for an individual experiment). Ancillary tests of the same soil in a ring-shear device and a triaxial cell under various initial densities produced dilative shear failure when initial porosity was ≤ 0.41 and contractive shear failure when initial porosity was ≥ 0.46 .

Landslides developing in soils with differing porosities displayed sharply contrasting dynamics (compare Figs. 1 and 2). Landslides with initial porosities > 0.5 failed abruptly and accelerated within 1 s to speeds > 1 m/s. The surfaces of these landslides appeared to be fluid and smooth, and data from dynamic piezometers confirmed that pore water pressures rose rapidly during failure and reached levels nearly sufficient to balance total normal stresses and liquefy the soil (Fig. 1).

Three landslides with initial porosities indistinguishable from the critical porosity (0.44 ± 0.03 , 0.44 ± 0.03 , and 0.42 ± 0.03) displayed inconsistent behaviour, including slow slumping of a single soil block, episodic slumping of multiple blocks, and moderately rapid (~ 0.1 m/s)

slumping that ceased after <0.5 m displacement. Dynamic piezometer data from these experiments revealed a complex mix of dilative and contractive soil behaviour during failure. In experiments with landslides in initially dense soil, failure geometry similar to that of the loose soil was observed but the data revealed markedly different landslide dynamics (Fig. 2). Precursory pore water pressures necessary to trigger failure of the dense soil developed relatively slowly (owing to relatively low hydraulic conductivity due to smaller pore spaces), and were roughly twice as large as the pore pressures necessary to trigger failure of the loose soil (owing to high peak strength of the dense soil). On average, motion of the landslide with dense soil proceeded about 300 times more slowly than motion of the landslide with loose soil (compare Figs. 1 and 2). The landslide with the lowest and least variable initial porosity (0.41 ± 0.01) displayed the clearest dilative soil behaviour as it underwent slow episodic motion (Fig. 2). The attempt to induce a landslide with still lower porosity (0.39 ± 0.03) ended uneventfully because it was not possible to infiltrate water fast enough to impart pore water pressures sufficient to trigger slope failure.

However, if fluid pressure can diffuse into or away from contracting or dilating soil as quickly as the soil deforms, pressure equilibration keeps pace with deformation and the effects of porosity change diminish. However, the time scale for pore pressure diffusion is h^2/D , where h is the typical thickness of the deforming soil mass and D is the typical hydraulic diffusivity. Even sandy soils with high diffusivity commonly have $D < 100 \text{ cm}^2/\text{s}$. Thus, the time scale for diffusive pore pressure equilibration in deforming soil masses with $h \sim 1$ m typically surpasses 10 s. In comparison, the time scale for landslide acceleration in response to basal pore-pressure change is $\sqrt{h/g}$ (Iverson, 2000), which yields values < 1 s for $h \sim 1$ m. Accordingly, it is concluded that pore pressure diffusion can seldom keep pace with soil deformation and that relatively small variations in porosity can influence landslide behaviour profoundly.

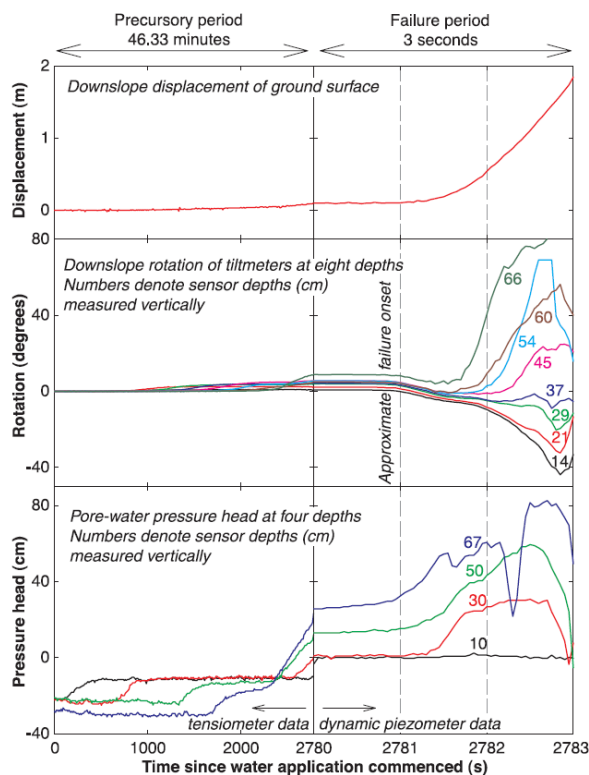


Figure 1 - Data recorded in a landslide experiment with loose soil (initial porosity 0.52 ± 0.02). The time axis is expanded 927 times to reveal details of behaviour during the 3 s failure period (after Iverson et al., 2000).

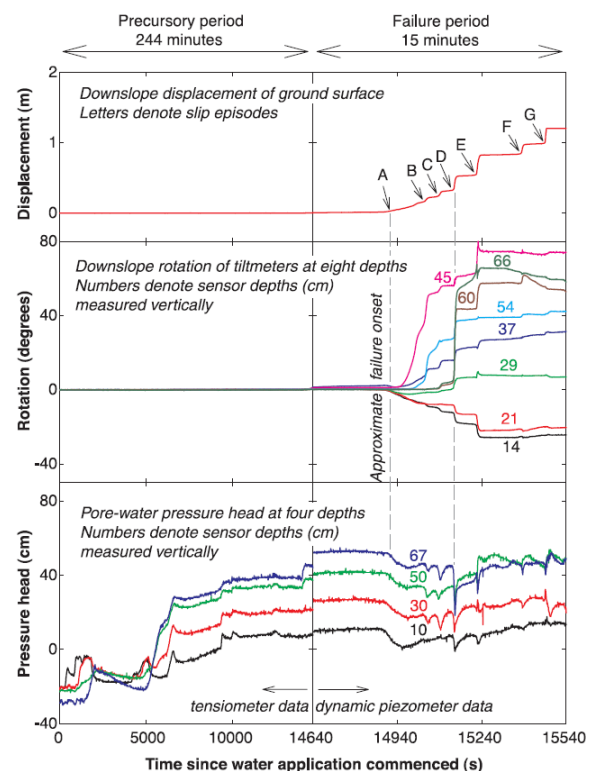


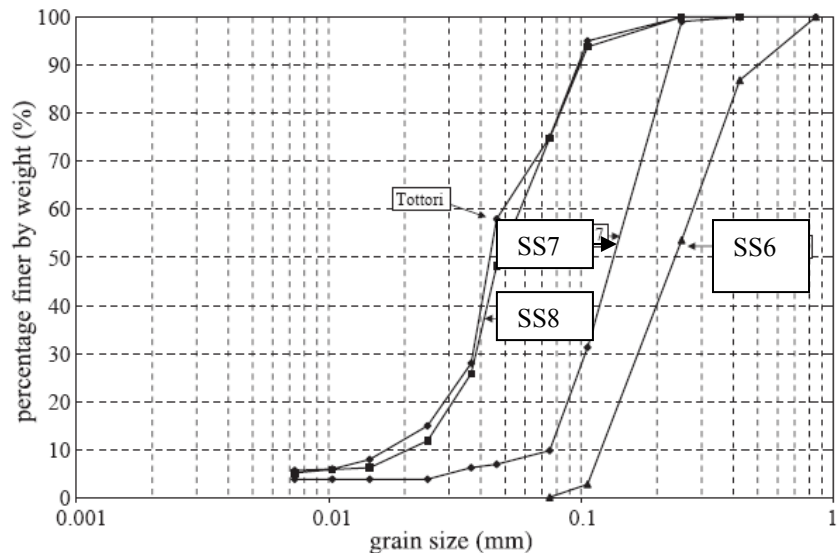
Figure 2 - Data recorded in a landslide experiment with dense soil (initial porosity 0.41 ± 0.01). The time axis is expanded 16 times to reveal details of behaviour during the 15 min failure period (after Iverson et al., 2000).

Wang & Sassa (2001, 2003) conducted a series of tests on silica sand no. 7 ($D_{50} = 0.13$ mm) and no. 8 ($D_{50} = 0.05$ mm) (Fig. 3) to investigate the effect of initial dry densities on pore-pressure generation and failure behaviour of a landslide mass.

Different types of failure modes were observed. Each failure type was divided into 4 periods:

- (1) **Wetting**: after sprinkling, the water gradually flowed toward the base, and the wetting front was approximately parallel to the base. During this period, obvious normal displacement appeared in the tests on extremely loose samples;
- (2) **Precursory slides**: after the wetting front reached the base, retrogressive compound shallow sliding appeared at the toe part of the slope as the saturation degree increased;
- (3) **Major failure**: major failure occurred following the retrogressive compound shallow sliding. The displaced soil slid a certain of distance (ΔS , as shown in Fig. 4), and then stopped;
- (4) **Successive movement**: the failed landslide soil began to move again after the major failure, as sprinkling was continued, and flowed downward slowly.

Figure 3 - Grain-size distribution curves for silica sand no. 6 to 8 (after Lourenco et al., 2006).



Failure mode	Wetting	Precursory slides	Major failure	Successive motion
Type A $I_d \leq 0.01$ Retrogressive sliding	 Visible normal displacement	 Slow retrogressive toe sliding	 Sudden multiple sliding	 Very shallow flowslide
Type B $0.01 < I_d \leq 0.49$ Retrogressive sliding	 No visible normal displacement	 Slow retrogressive toe sliding	 Slow retrogressive sliding	 Very shallow flowslide
Type C $-0.14 \leq I_d \leq 0.30$ Flowsliding	 With ($I_d < 0$)/without ($I_d \geq 0$) visible normal displacement	 Slow retrogressive toe sliding with visible deformation as a whole	 Flowsliding with relative motion between soil layers	 Slow sliding
Type D $0.30 < I_d \leq 0.46$ Flowsliding	 Without visible normal displacement	 Slow retrogressive toe sliding without visible deformation as a whole	 Retrogressive sliding followed by movements with relative motion between soil layers	 Slow sliding

Figure 4 - Summary of the failure modes, types A and B observed in samples with S7, and types C and D observed in samples with S8 (after Wang & Sassa, 2003).

Each failure mode was greatly affected by the initial density in these series of tests. Usually, in the series of tests on S7, the sand with density index ($I_d \leq 0.01$ ($I_d = (e_{max} - e) / (e_{max} - e_{min})$)) was likely to suffer from a Type A failure (Fig. 4), but when the initial density indexes ranged

from 0.17 to 0.49, the samples were more likely to suffer from a Type B failure. A Type C failure occurred in the series tests on S8, when $0.14 \leq I_d \leq 0.30$, and failure of type D when $0.30 \leq I_d \leq 0.46$.

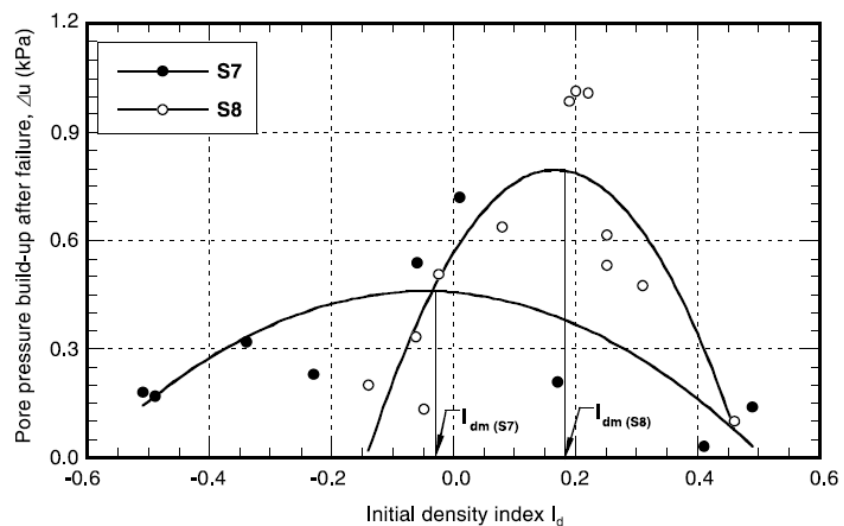
2. Effect of initial density on pore-pressure build-up

Recent studies have revealed that pore-water generation in fluidised motion is greatly dependent on initial density as well as thickness of soil layers (Eckersley, 1990; Iverson et al., 2000; Wang & Sassa, 2001). Presenting a time series for pore pressure and sliding distance, Wang & Sassa (2001) found that high pore pressure was built-up after, not prior to, the initiation of failure. In the analysis of the relationship between pore-water pressure build-up after initiation, the major failure, and the motion of failed landslide mass, they plotted the pore-pressure build-up after onset of failure (Δu), against the initial density index (I_d) for each test, and found that there was an optimal density index (I_{dm}) at which Δu reaches a maximum value (Fig. 5). They interpreted the existence of I_{dm} as a combined effect of factors as follows:

1. For tests in which $I_d < I_{dm}$, the permeability is greater, thus the dissipation must be quicker. Accordingly, the effect of greater pore pressure dissipation rate is likely to exceed the effect of greater pore pressure generation.
2. For tests in which $I_d > I_{dm}$, the volume reduction during shear is small, thus less pore water pressure generation is likely to accompany the failure.

As shown in Fig. 5, the optimal density index (I_{dm}) for S7 differs from that of S8. This shift can be interpreted by the volume-reduction potential, which is directly related to the generation of pore-water pressure for a saturated sample under undrained conditions during shearing. In fact, if S7 has the same volume-reduction potential as S8, it should have a smaller density index than S8 soil.

Figure 5 - Pore-pressure build-up after failure versus initial density index (after Wang & Sassa, 2003).



3. Soil thickness overlaying the sliding surface (based on Wang & Sassa, 2001, 2003; Eckersley, 1990)

As shown by triaxial laboratory tests, the initial shear stress under drained conditions strongly affects static liquefaction resistance (Kramer & Seed, 1988; Hird & Hassona, 1990; Ishihara, 1993). Eckersley (1990) also found that the build up of pore pressures might be affected by

shear deformation, dissipation, thickness of mass overlying the sliding surface, and other factors that are not yet completely understood.

Wang & Sassa (2001) performed two series of flume tests with different values of soil thickness. They plotted the pore pressure build up after the initiation of major failure against initial density index. In both series of tests, they observed an optimum value for density index (I_d) that leads to the highest value of excess pore pressure. However, the maximum value of pore pressure for the tests with the most thickness is greater than that for the thinner sample, while the optimum density index is lower. They interpreted this data by attributing lower values of dissipation rates of pore pressure and the existence of higher initial stress state to the thicker slopes (Fig. 6). Also they measured higher peak velocities of the sliding mass for the thicker sample, which can be due to the greater build up of pore pressure because of the lower dissipation rate in the initially thicker sample.

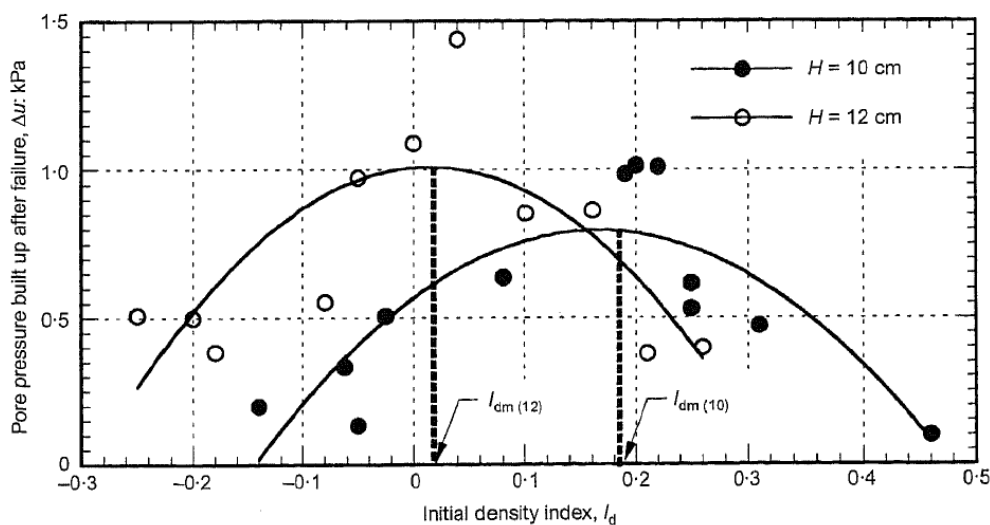


Figure 6 - Relationship between pore pressure build up after failure and initial density index for samples with different thicknesses (after Wang & Sassa, 2003).

4. Fine-particle content (based on Wang & Sassa, 2001, 2003; Iverson & LaHusen, 1989; and Iverson et al., 1997)

The pore-pressure build-up after the initiation of failure for S8 is generally greater than that for S7 (Fig. 5), indicating that higher pore pressure developed more easily in the finer sand S8. This could be because S7 has a greater permeability (Fig. 3). In the analysis of pore pressure generation during slope failure and sliding, Iverson & LaHusen (1989) and Iverson et al. (1997) pointed out that the pore-pressure build-up mainly depends on the rate of landslide motion and soil deformation, as well as the soil permeability. If the moving velocity of a failed landslide mass is the same, quicker dissipation will occur in the soil with greater permeability, and thus pore-pressure build-up will be smaller. The optimal density index (I_{dm}) for S7 was found to differ from that of S8. This shift of I_{dm} can be interpreted by the volume-reduction potential, which is directly related to the generation of pore-water pressure for a saturated sample under undrained conditions during shearing. In fact, if S7 has the same volume-reduction potential as S8, it should have a smaller density index than the S8 soil.

Wang & Sassa (2001, 2003) pointed out that the influence of grain size on the type of movement of the landslide mass is significant. As introduced in Figure 4 for the tests on S7, retrogressive slides were initiated, whereas rapid flowslides occurred in the tests on S8, showing a completely different failure mode. The main reasons for the different failure modes for S7 and S8, can be considered to be due to: (1) the pore-pressure build-up after failure, which is normally smaller for tests on S7, as shown in Figure 5; (2) the generated pore-water pressure that is dissipated very quickly for S7 during movement because of its greater permeability, as shown in Fig. 3; (3) the smaller grains in S8 that are more likely to float during movement.

5. Effect of layering (based on Lourenco et al., 2006)

Permeability variations in natural slopes can be due to lateral and vertical variations of porosity and grain size distribution, existence of a shallow hard impermeable bedrock, and impermeable geological structures (e.g. faults filled by clayey material) where water could accumulate and perched water tables can be formed. These permeability variations, which could reach two orders difference of magnitude at shallow depths, act as physical barriers to groundwater flow, creating pore water pressure gradients and endangering the slope stability. Lourenco et al. (2006) studied pore water pressure generation and the corresponding failure mode in flume models, typically 1 m in length and 40 cm in height, in soils with different permeabilities. Experiments were conducted for different arrangements of soil layers (by changing the soil layer position), and infiltration direction (downward infiltration by sprinkling water on the soil, and upward infiltration from the bottom of the lower soil layer). All experiments used two industrial sands: a coarse grained sand, silica sand no. 6; and a very fine sand, silica sand no. 8 (Fig. 3). Sand was deposited in the loosest possible conditions for both layers in every test. The permeability for sand no. 8 in a loose condition was approximately $5.0 \cdot 10^{-5}$ m/s, as obtained by laboratory experiments (Wang & Sassa, 2001); whereas Terzaghi's (1955) formula for uniform sands was adopted for no. 6 sand, giving $3.9 \cdot 10^{-4}$ m/s. They found out that variations in permeability can greatly influence the failure onset. Seepage erosion was found to dominate failure if the lower layer was coarser, while retrogressive failure of the upper layer was the most relevant failure mechanism if the lower layer was finer. However, a gradation between these two styles was observed for certain model arrangements. Regarding the effect of infiltration direction, upward infiltration resulted in a rise in the pore water pressure from the bottom to the top whereas perched conditions were formed within the upper finer layer during downward infiltration.

6. Failure processes (based on Moriwaki et al., 2004)

To clarify the failure process of a landslide triggered by rainfall, Moriwaki et al. (2004) conducted a full-scale model landslide experiment. A 23 m long and about 8 m high flume was used and the slope was instrumented by surface displacement meters, pore-water pressure gauges, and piezometers (Fig. 7). The flume was filled with loose coarse sand ($D_{50} = 0.4$ mm) and sprinkled at a constant intensity of 100 mm/h. The landslide occurred first in the upper slope about 154 min after the sprinkling started, following a creep movement within 41 min. The sliding mass reached a maximum speed of 1.2 m/s and stopped in about 5 s, compressing soils in the lower gentle slope and horizontal sections.

The authors observed that the velocity curve of surface displacements developing, up until the rapid landslide occurred, can be approximately classified into three stages: (A) an asymptotic increase, (B) an exponential increase, and (C) a linear increase (Fig. 8).

Figure 9 shows changes in piezometric levels (P.L.) during the rapid slide. Surface displacement at the middle part of the 30° slope (D-3) is also shown for reference. Values throughout the slope and horizontal section increased rapidly. The peak value at each sensor in the 30° slope was low because the original piezometric levels were low just prior to the rapid slide. On the other hand, piezometric levels in the lower part of the 10° slope, and in the horizontal layer, were higher than in the upper part of the slope and the peak occurred at the connecting point at the downslope end of the 10° slope. Small oscillations (1–2.5 Hz) in waveform were observed at sensors G-1, G-3, and G-5 in the 30° slope, where the soil layer slid down parallel to the slope. The other sensors showed no remarkable cyclic fluctuations. Iverson & LaHusen (1989) reported a generation of a 1 Hz fluctuation in a 10 m long slope failure experiment. The small pressure increase in the upper slope was likely to have been caused by the soil shearing, whereas the higher pressures in the horizontal layer and the lower part of the slope were likely caused by a mix of soil compression and shearing by the sliding mass. High pore-water pressures also developed outside of the landslide mass due to the compression induced by the landslide mass, as shown by G-11.

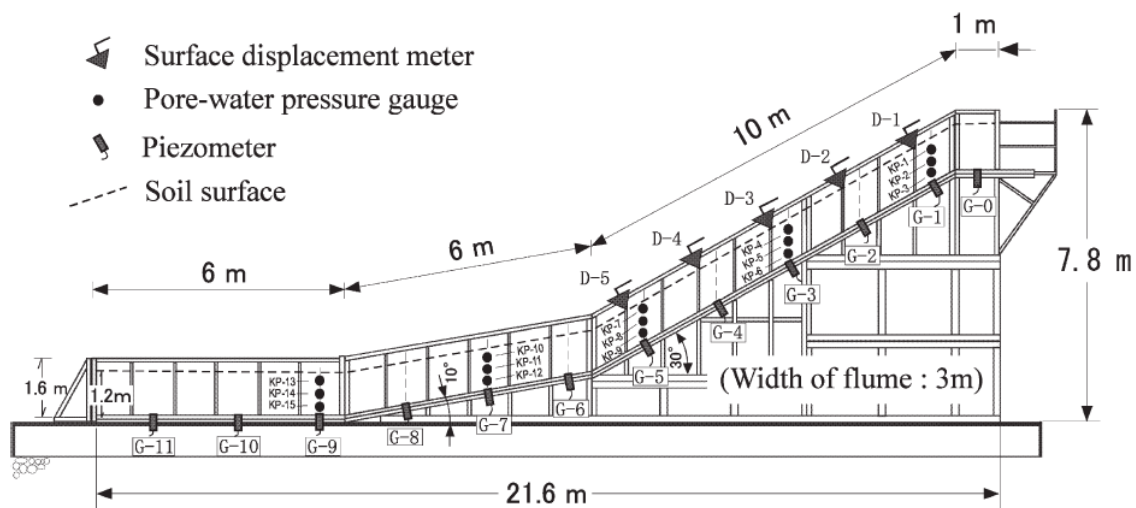


Figure 7 - Model slope and location of sensors (after Moriwaki et al., 2004).

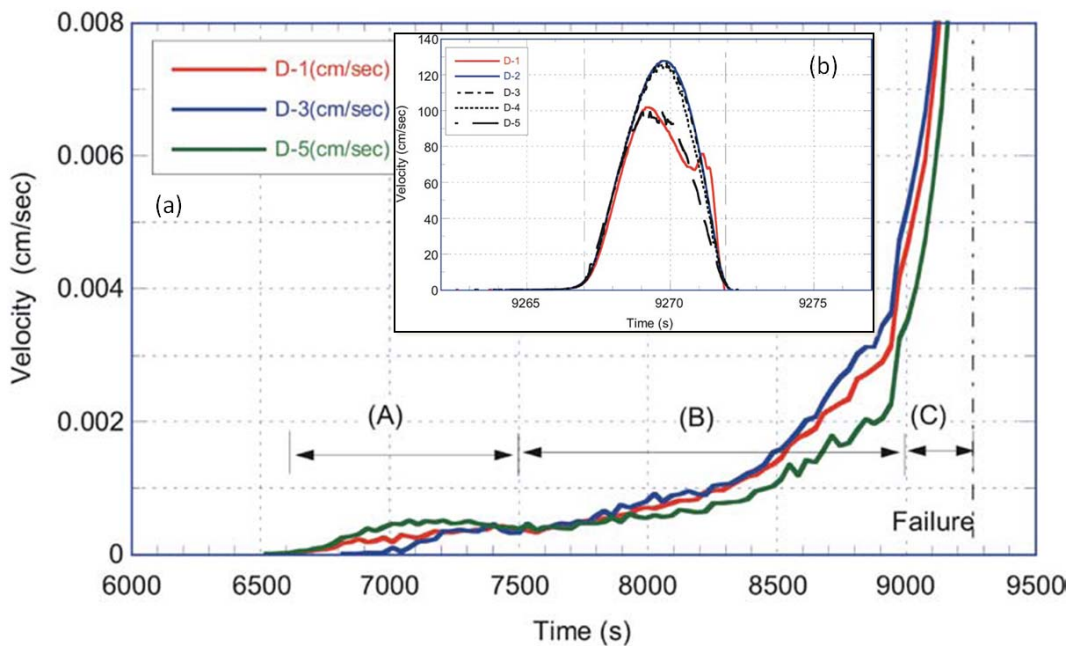


Figure 8 - a) Change in velocity of surface displacement before the slide (computed using each 30 s of data, after Moriwaki et al., 2004). b) Velocity of surface displacement during the rapid slide.

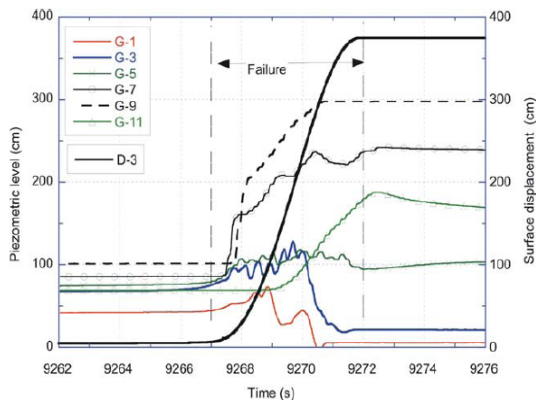


Figure 9 - Fluctuation of piezometric levels during the slide (D-3; surface displacement, after Moriwaki et al., 2004).

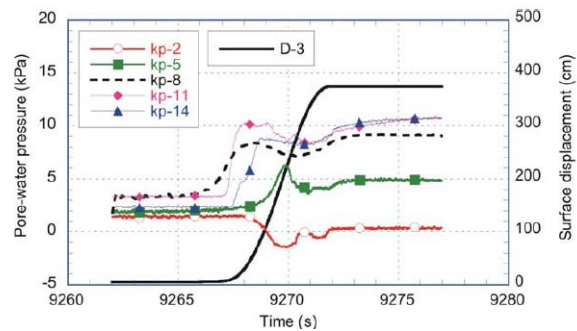


Figure 10 - Fluctuation of pore-water pressures at 60 cm depth throughout the soil during rapid failure (after Moriwaki et al., 2004).

The pore-water pressures inside the soil mass rapidly increased throughout the slope as soon as rapid failure occurred. Figure 10 shows all pore-water pressure changes at a depth of 60 cm. Pore-water pressures in the 10° slope (kp-8, kp-11) and the horizontal section (kp-14) responded sequentially starting from upslope. On the other hand, those in the 30° slope (kp-2, kp-5) reacted late and pressure at the top of the slope decreased after the soil moved downslope. From the time sequence of pore-water pressure increase and the deformations observed, it is inferred that shear deformation appeared at first near kp-8, and then extended gradually downwards and upwards. The smaller tendency of pore-water pressure in kp-2

might be the result of the extensive deformations and the unsaturated state. Most pressures peaked at 1–2 s after the slide started and then receded slowly.

7. Conclusions

Iverson et al. (2000) conducted large-scale experiments under closely controlled conditions to isolate the effect of initial soil porosity on landslide style and rate. They found landslides with differing porosities displayed sharply contrasting dynamics. Landslides with *initial porosities* > *critical porosity*, failed abruptly and accelerated within 1 s to speeds > 1 m/s. The landslides with initial porosities indistinguishable from the critical porosity displayed inconsistent behaviour, including slow slumping of a single soil block, episodic slumping of multiple blocks, and moderately rapid (~0.1 m/s) slumping. Data from the experiment with dense soil implied failure geometry similar to that of the loose soil but revealed markedly different landslide dynamics. On average, motion of the landslide with dense soil proceeded about 300 times more slowly than motion of the landslide with loose soil.

Wang & Sassa (2001, 2003) conducted a series of tests on silica sand to investigate the effect of initial dry densities on pore-pressure generation and failure behaviour of a landslide mass. They observed different types of failure modes and divided each failure type into four periods: Wetting, Precursory slides, Major failure, and Successive movement. Each failure mode was greatly affected by the initial density in these series of tests. In presenting a time series for pore pressure and sliding distance, they found that high pore pressure was built-up after, not prior to, the initiation of failure. In the analysis of the relationship between pore-water pressure build-up after initiation, the major failure and the motion of failed landslide mass, they plotted the excess pore pressure build-up after onset of failure (Δu), against the initial density index (I_d) for each test, and found that there was an optimal density index (I_{dm}) at which Δu reaches maximum.

Eckersley (1990) concluded that the build up of pore pressures might be affected by shear deformation, dissipation, thickness of mass overlying the sliding surface, and other factors that were, as yet, unclear.

Lourenco et al. (2006) found that variations in permeability can greatly influence the failure onset. Seepage erosion was found to dominate failure if the lower layer was coarser, while retrogressive failure of the upper layer was the most relevant failure mechanism if the lower layer was finer.

During failure in a full-scale landslide experiment, Moriwaki et al. (2004) observed rapid increase of subsurface water pressure in the slope and horizontal soil layers. It was inferred that the increased water pressures in the upper slope resulted from collapse of the loose soil structure during shearing in the translational slide, whereas those in the lower portion of the slope and horizontal sections resulted from a mix of soil compression and shearing by the sliding mass.

2.2.2 Results of flume experiments on saturated clays

(CNRS)

Small-scale landslides are triggered in the laboratory by means of flume experiments to gain a better understanding of the failure behaviour of clayey slopes (Spickermann et al., 2009). Tests are carried out on two different kinds of clayey material, clay from Zoelen, the Netherlands and in the reworked (i.e. displaced and weathered) black marls of the Super-Sauze landslide, France. The grain size distributions are given in Figure 11.

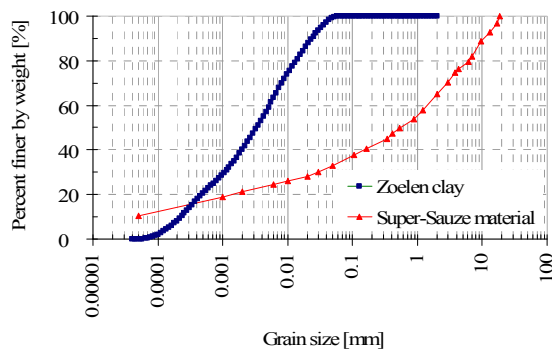


Figure 11 - Grain size distributions of the two materials tested.

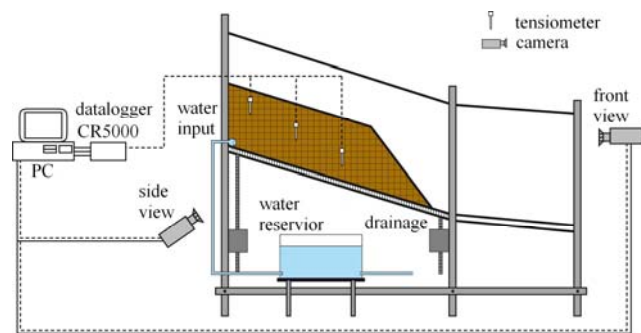


Figure 12 - Cross section of the flume device.

1. Flume test apparatus and test procedure

The test apparatus is depicted in Figure 12. The inner dimensions of the flume are 250 cm in length, 60 cm in height and 60 cm in width. The flume angle α can be changed for different test requirements. The test apparatus boasts one transparent side. Images are taken at defined intervals from this side, from the front or from the top. Displacements fields are computed from correlation of multi-temporal optical images (CIV). Pore water pressure is monitored by tensiometers. The tensiometers, developed and constructed in the Laboratory for Physical Geography, Utrecht University, consist of a ceramic cup, 6 mm in diameter, which is attached to a direct reading miniature pressure gauge. Water is permitted to infiltrate from the back at the bottom of the slope using a pump to investigate the hydrological triggering, and a defined top water level that is kept constant (upward constant head infiltration).

2. Analysis of flume test on Zoelen clay

The first experiment was carried out on Zoelen clay. Before the slope was built, the material was mixed with water in buckets to obtain a homogeneous slope model with an initial water content lower than the liquid limit. The densely packed slope model has a height of 40 cm, a width of 60 cm, a length of 57 cm and a slope angle of 35° with respect to a horizontal flume surface ($\alpha = 0^\circ$). The flume was tilted back with a flume angle of -21° (26-09-08), that gives a total slope angle of $\gamma = 16^\circ$. After three days of drying, water infiltration was started (29-09-08). After another two days, the flume was tilted to $\alpha = 11^\circ$ (01-10-08), which gives a total slope angle of $\gamma = 46^\circ$. Final failure occurred after an additional three weeks of water supply (24/25-10-08).

Displacements in time are measured using two points on the slope surface (Fig. 13). Figure 17 presents the time displacement curves of the whole failure process (25 days). Only very slow movements took place from 01-10-2008 until 24-10-2008, with displacements of about 5 mm during that period. Then the movement velocity increases and final failure occurs. The time

displacement graphs (Fig. 16) of the final failure event (Fig. 14) indicate that this takes place in two stages, both on the 25-10-08, the first between 0:28 and 03:24 and the second between 5:20 and 7:20. Even if the movement along the slip surface in this phase is faster than the movement before 25-10-08, it can be described as rather moderate. Figure 14 shows the slope after failure on the 26-10-2008 including the final positions of the observed points A and B. The whole failure process lasts about three weeks.

Pore water pressure measurements were taken at nine locations from the cross section in the centre of the slope (Fig. 15). The pore water pressure measurements of all tensiometers are presented for the whole test period in Figure 17. Only tensiometers T1 and T2, which are located at the base, show positive values. Figure 16 gives the pore water pressures p measured during the time of final failure of tensiometers T2, T3 and T6. An increase of pore water pressures is not observed before final failure. The pore water pressures determined from tensiometers T7 and T9 seem to decrease, which may be due to evaporation at the slope surface. After final failure, pore water pressure measured by tensiometer T7 drops abruptly, since it was located in the shear zone. The development of measurements by tensiometers T1 to T6 and T8 can be characterised by pore water pressure fluctuation.



Figure 13 - Initial test conditions and observation points for the flume test on Zoelen clay.

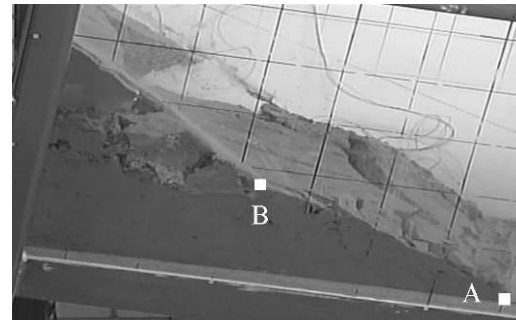


Figure 14 - Slope after failure, 26-10-2008, inclusive of final positions of observation points A, B for the flume test on Zoelen clay.

In general, it is assumed that progressive failure is caused by the decrease of shear resistance, i.e. the reduction of shear parameters, such as apparent cohesion due to suction. According to Petley et al. (2005), small displacements in the first part of the failure process are caused by microcrack formation. Even if the microcracks weaken the slope slightly, it is still in a stable state. Shear surface formation starts when the microcrack density reaches the point at which interaction between them begins. Petley et al. (2005) propose that during this early phase of shear surface development, a reduction of pore pressure can stop the deformation. It is assumed that pore water pressure fluctuation supports the development of microcracks and further the formation of a slip surface. The acceleration to failure in the time displacement curve starts when shear stress exceeds shear strength. From this point, pore pressures become increasingly unimportant in causing further deformation. To summarise, pore water pressure fluctuation together with initial and ongoing microcracking and gradual reduction of suctions in the clay could be responsible for a progressive initiation of failure.

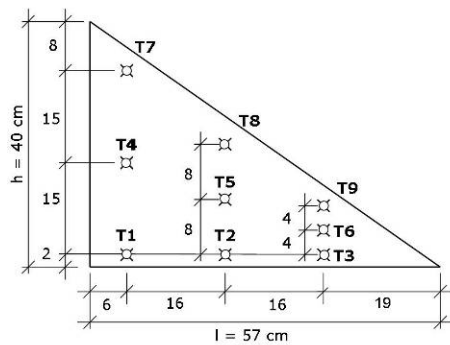


Figure 15 - Position of tensiometers in the middle cross section of the slope consisting of Zoelen clay.

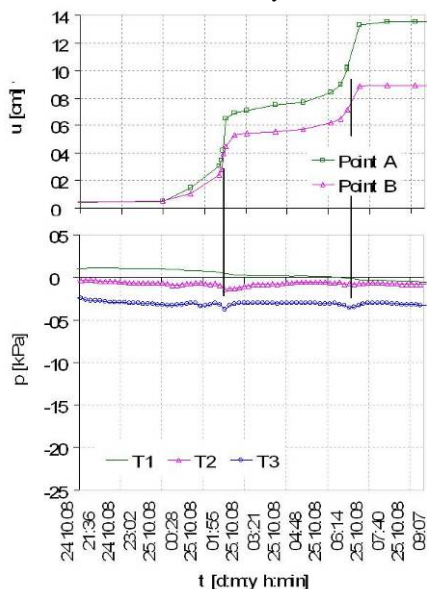


Figure 16 - Time displacement curves for the last failure phase in the Zoelen clay test; tensiometer pore pressure measurements of T1, T2 and T3.

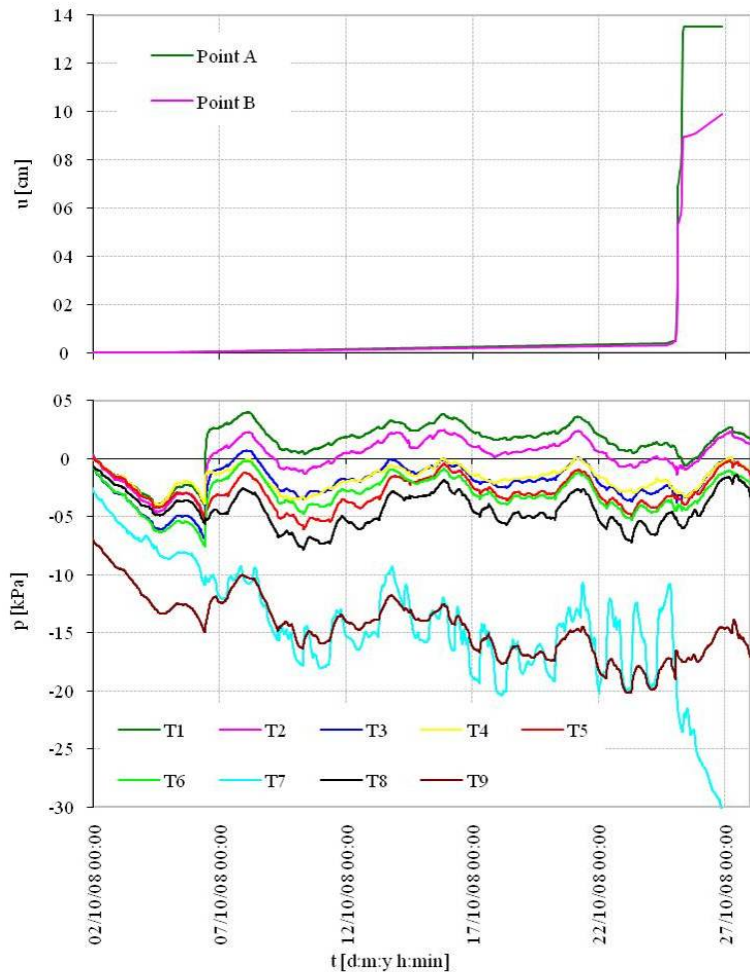


Figure 17 - Time displacement curves of points A and B at the slope surface of the flume test on Zoelen clay and pore water pressure measurements during the whole experiment.

3. Analysis of flume test on black marls

A series of tests is carried out on reworked Callovo-Oxfordian black marls of the South French Alps, a material that is highly prone to hydrologically triggered landslides (Malet, 2003; Malet et al., 2007). One of the first preliminary experiments was performed on dry, loosely packed material. Slope dimensions were 23 cm in height and 90 cm in length.

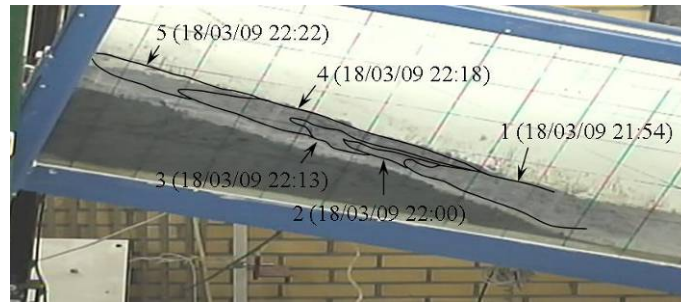


Figure 18 - Final state of flume experiment on dry, loose black marls showing retrogressive slumping.



Figure 19 - Initial test conditions (height = 26 cm, width = 60 cm, length = 91 cm) and observation point A.

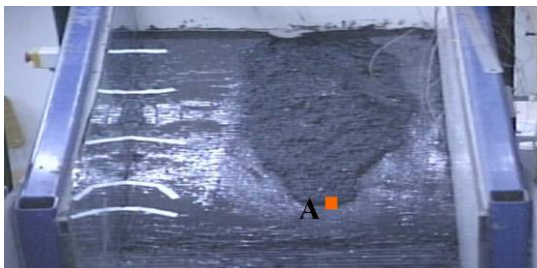


Figure 20 - Final state and observation point A.

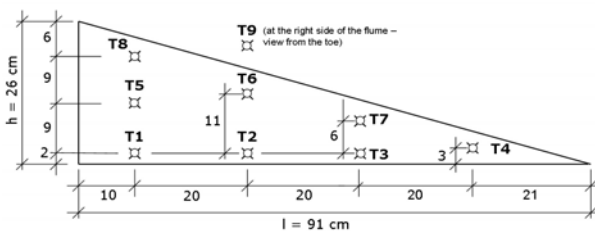


Figure 21 - Position of tensiometers in the middle cross section of the slope.

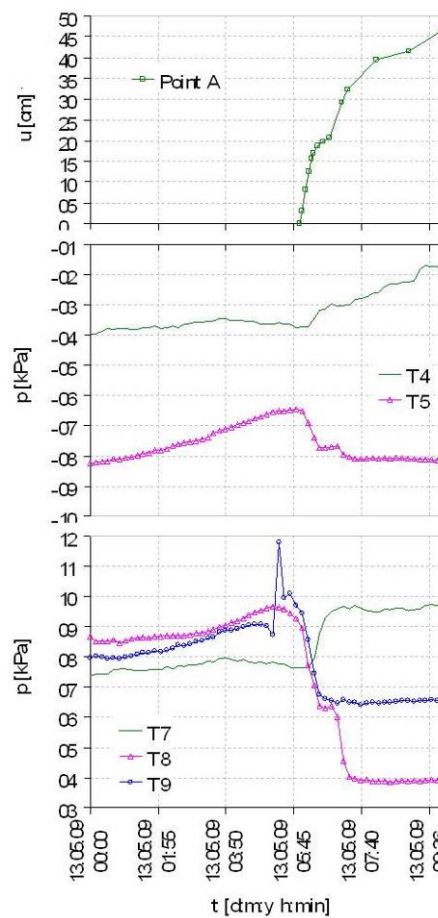


Figure 22 - Pore water pressure measurements of tensiometers T4, T5, T7, T8 and T9 during final failure (time period: 10 h).

Water infiltration started when the flume surface was horizontal on 13-03-2009. The flume inclination was increased gradually to an angle of 18° until 18-03-2009 (16:00), which, when combined with the slope angle of about 14°, generates a total slope angle of about 32°. Failure

starts at the toe at the right side of the flume, as seen from the front, on 18-03-2009 at 21:45, and it continues in the direction of the crest. The slump development is displayed in Figure 18. Failure occurs as sudden multiple superficial slides, with subsequent slow movement of the whole failure mass. The total time span of the failure event is about 8 hours, and the failure process can be characterised as retrogressive slumping. However the behaviour at the beginning of failure is not clearly identified. It is supposed that a first slip surface (slump 1) is formed due to seepage at the toe.

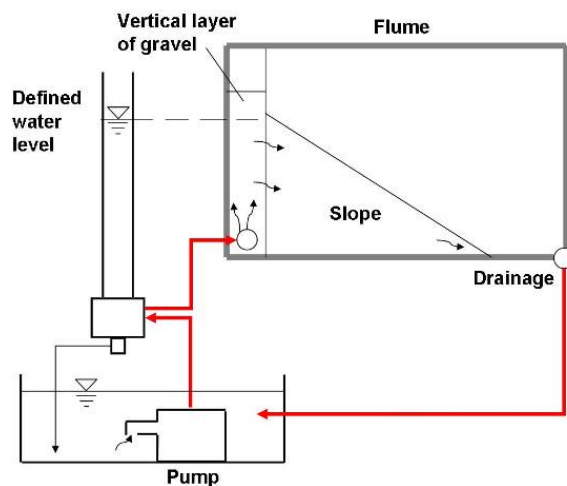


Figure 23 - Scheme of water circulation used in flume and centrifuge tests (Spickermann et al., in prep.).

Material parameters	
initial dry density ρ_{dini} [g/cm ³]	1,72
density of saturated soil ρ_{sat} [g/cm ³]	2,04
initial water content w_{ini} [%]	18,6
void ratio [-]	0,58
porosity [-]	0,37
Dimensions	
height = 23 cm	
width = 60 cm	
length = 65.5 cm	

Figure 24 - Initial material parameters used in flume tests on black marls.

Another preliminary experiment was performed with a relatively high initial water content and low density (Fig. 19, Fig. 20). The development of pore pressure of selected tensiometers is depicted in Figure 22 in a time period of 10 h, and compared with the displacements. T5, T8, T9 show an increase in pore pressure before movement begins. It is believed that such a failure is induced by boundary effects, e.g. preferential flow between the slope material and the back panel of the flume.

After a couple of tests, the model setup was improved to have a more uniform water infiltration from the back by using a gravel pillar (Fig. 23). Furthermore, initial test conditions have been fixed, such as the geometry of the slope, density and water content (Fig. 24). The initial water content is equal to 18.6%, which is higher than the optimum water content and lower than the liquid limit.

Figure 25 shows the final state of one of the tests using the fixed parameters (Spickermann et al., in prep.). After several hours of water supply, the movement starts with the development of a first failure surface that is indicated by fissure number 1. The tensiometers show an increase in pore water pressure until about 20/03/2010, 3:30 (Fig. 26). These measurements suggest that slope saturation, or the loss of apparent cohesion, contributes to the initiation of failure, i.e. to the development of tension crack 1.

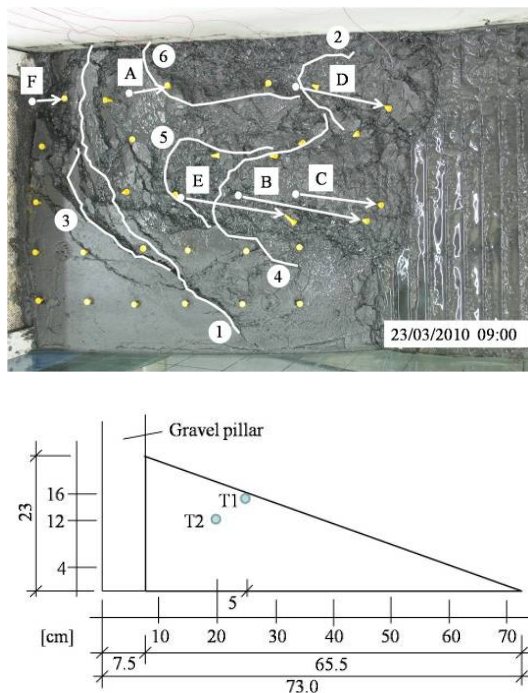


Figure 25 - Flume test model from above after failure and location of tensiometers; A-F: observation points; 1-6: failure development; T1-T2: location of tensiometers (Spickermann et al., in prep.)

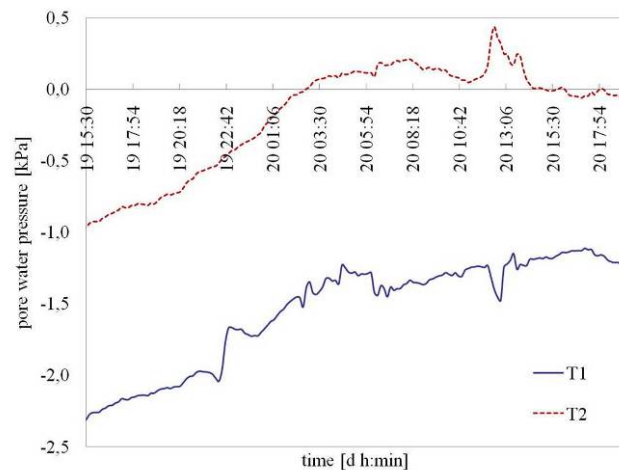


Figure 26 - Time pore water pressure curves of tensiometers T1 and T2 starting from 19/03/2010 at 15:30 (Spickermann et al., in prep.).

2.2.3 Results of flume experiments on pyroclastic soils

(AMRA)

Extensive areas of the Campania region in South Italy are subjected to rainfall-induced landslides, some of which evolve into flows. These phenomena occur in unsaturated air-fall pyroclastic deposits, which mantle the steep slopes of Apennines surrounding Vesuvius. A series of tests on small-scale slopes have been carried out at the Geotechnical Laboratory of the Department of Civil Engineering, Second University of Naples, where an instrumented small-scale physical model 2.2 m long and 0.5 m wide has been built in order to investigate the mechanics of such landslides (Damiano, 2004; Olivares et al., 2009).

The research has been addressed to investigate the response of the slope to rainfall, which can be reproduced by a system, which allows imposition of different rainfall intensities. The apparatus is heavily instrumented in order to capture all of the fundamental mechanical aspects of the slope behaviour, and to assess the role played by single factors, such as geometry, initial and boundary conditions and soil properties, on the mechanics of rupture. The instrumentation allows measurement of any changes of soil state (such as water content, porosity), state of stress (matric suction, pore pressure) and displacement pattern. Volumetric water content is measured through a TDR probe, while porosity is determined indirectly,

during the first infiltration stage, from measurements of settlements at ground surface. The pore pressure is measured by micro-transducers, i.e. tensiometers, and pore pressure probes installed at the base of the slope. The displacement field is obtained through laser transducers and video-cameras. During the early post-failure phase, monitoring enables measurement of excess pore pressures induced by rupture and early post-rupture soil deformation (liquefaction and, eventually, fluidisation). Miniature pore pressure transducers and high-definition mobile video-cameras have a prominent role in achieving this. Details of the instrumented flume can be found in Olivares et al. (2009) (Fig. 27).

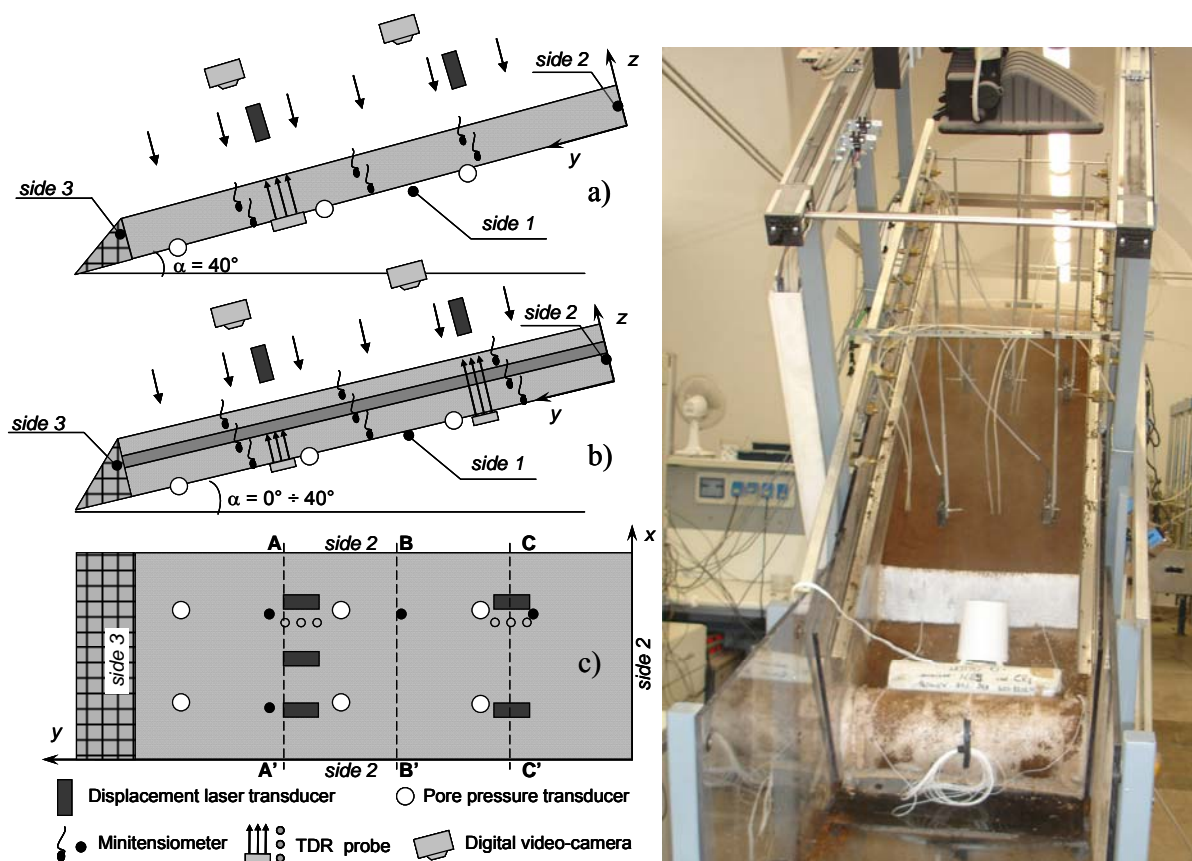


Figure 27 - Sketch of the instrumented flume.

In order to investigate the role of the void ratio on the mechanics of failure, a number of tests have been performed on homogeneous ashy layers reconstituted at different initial porosities: the results are illustrated in the two following sections, distinguishing tests on loose layers from tests on dense layers. In the context of small-scale experiments on 10-20 cm thick slopes, the definition “dense (or loose) soil” has to be interpreted with reference to the low net stress states applied.

The small-scale slopes have been reconstituted by a moist-tamping technique (Olivares & Damiano, 2007). The adopted thickness/length ratio smaller than 1/10, allows consideration of the experiment as though it were being conducted on an infinite slope, since this represents the most frequent case in the concerned area. Slope inclination was, in all cases, set to 38°-40°, slightly larger than the friction angle of the saturated soil (38°). A boundary condition with an impervious bottom was reproduced (allowing investigation of a typical scenario

characterised by the presence of a less pervious layer at the top of fractured limestone), while a geotextile drain was placed at the toe of the slope, in order to let free water outflow when soil approached saturation. With the exception of two experiments (FL21_1 and FL22_2), all the tests were carried out under uniform and constant rainfall until the occurrence of slope failure. A summary of the experimental programme, including tests on layered deposits, is reported in Table 1, including the geometry, initial conditions and the intensity of artificial rainfall.

The experiments have been conducted on pyroclastic soils that have repeatedly been responsible for the development of catastrophic landslides, taken from Cervinara (Olivares & Picarelli, 2003), Monteforte Irpino (Papa et al., 2008) and Bracigliano, north-east of Naples. The properties of these soils are reported in section 1.1.1.

Table 1 - Test conditions.

Test	Soil	Geometry			Initial conditions				i [mm/h]
		α [°]	L [m]	h [m]	w	n [%]	S_r [%]	$(u_a - u_w)$ [kPa]	
FL1	Cervinara	40	1.00	0.08	0.18	62.6	27.9	70.0	20
FL2		40	1.00	0.08	0.30	70.8	32.0	53.0	20
FL3		40	1.20	0.12	0.25	67.7	31.1	57.0	40
FL4		40	1.20	0.10	0.30	70.0	33.4	32.0	40
FL5		40	1.20	0.10	0.32	63.2	48.4	29.0	40
FL6		40	1.00	0.09	0.35	69.0	40.9	20.0	40
FL7		40	1.00	0.16	0.31	71.1	33.2	67.0	80
FL8		40	1.10	0.10	0.30	70.4	32.8	70.0	60
FL9		40	1.10	0.10	0.37	73.1	35.3	59.2	60
FL10		40	1.10	0.10	0.43	65.0	59.6	51.7	60
FL11		40	1.30	0.12	0.41	72.7	30.3	-	60
FL12		40	1.00	0.10	0.40	69.8	45.0	55.3	60
FL13	Bracigliano	35	1.25	0.14	0.64	79.0	43.6	34.3	60
FL14	Cervinara	40	1.30	0.16	0.43	74.0	39.3	75.0	60
FL15		40	1.00	0.10	0.50	75.4	42.4	17.5	55
FL16	Bracigliano	40	1.00	0.10	0.40	75.7	33.3	41.0	56
FL17		38	1.20	0.10	0.52	77.4	39.6	62.8	40
FL18	Monteforte Irpino	40	1.40	0.14	0.42	75.8	35.4	54.0	50
FL19		40	1.10	0.10	0.39	68.8	46.7	68.5	54
FL20		40	1.10	0.11	0.50	71.6	52.4	31.0	55
FL21_1		40	1.10	0.10	0.47	76.1	39.0	38.0	50
FL21_2		40	1.10	-	-	-	-	15.5	55
FL22_1		40	1.10	0.10	0.43	75.9	36.0	28.0	50
FL22_2	40	1.10	-	-	-	-	15.0	45	

1. Flume tests of inclined slopes of loose ashes subjected to rainfall infiltration to failure

The results of tests are summarised in Figures 28, 29 and 30, which respectively report: suction at two different depths (in the middle and at the bottom of the layer) and settlement of the ground surface (Fig. 28), pore pressure at the base of the slope and settlement of the ground surface (Fig. 29) and rate of displacement at the ground surface (Fig. 30). The process will be described by distinguishing three different phases: the first, from wetting toward failure ($t < t_f$); the second, failure ($t = t_f$) and, finally, the post-failure evolution ($t > t_f$).

During infiltration ($t < t_f$), the layer experiences a marked decrease in suction and exhibits a large volumetric collapse due to the initial high porosity of the soil (Fig. 28). Indeed, all the tensiometers recorded a strong decrease in suction (greater than 50 kPa in about 20 minutes) while the infiltration front gradually moved from the ground surface to the base: this is clearly shown by the delay of suction revealed by the devices located near the bottom (deep tensiometers). In the very first phase, the volumetric strain is about 1% and remains almost uniform, until the deep tensiometers measure a negligible suction decrease (Δt_1 in Fig. 28); the collapse becomes increasingly severe when the deepest devices record an abrupt reduction in suction (Δt_2 in Fig. 28). Stability is still ensured during this stage, by the effect of suction on the shear strength of soil.

Subsequently, a few minutes before failure (Δt_3), the superficial tensiometers reach small and practically constant values of suction (about 2-3 kPa), while this practically vanishes at the level of the deepest devices and the pore pressure transducers start to record a positive pore pressure, testifying the presence of water ponding whose height increases continuously in the time, giving rise to seepage parallel to the slope, up to failure ($t = t_f$). At the same stage, settlement readings indicate a significant volumetric collapse (about 8%) (Fig. 28). The settlement is about 15 mm just before the onset of instability and the volumetric strain can be estimated to be about 10%. Figure 29 shows the pore pressure measured at the base of the slope. The onset of instability is marked by a clear discontinuity in the pore pressures. In fact, after rupture ($t > t_f$) a sudden increase in pore pressure appears for a few seconds in most of the soil mass. In accordance with other authors (Eckersley, 1990; Wang & Sassa, 2001), this occurs only after failure leading to a rapid acceleration of the soil mass.

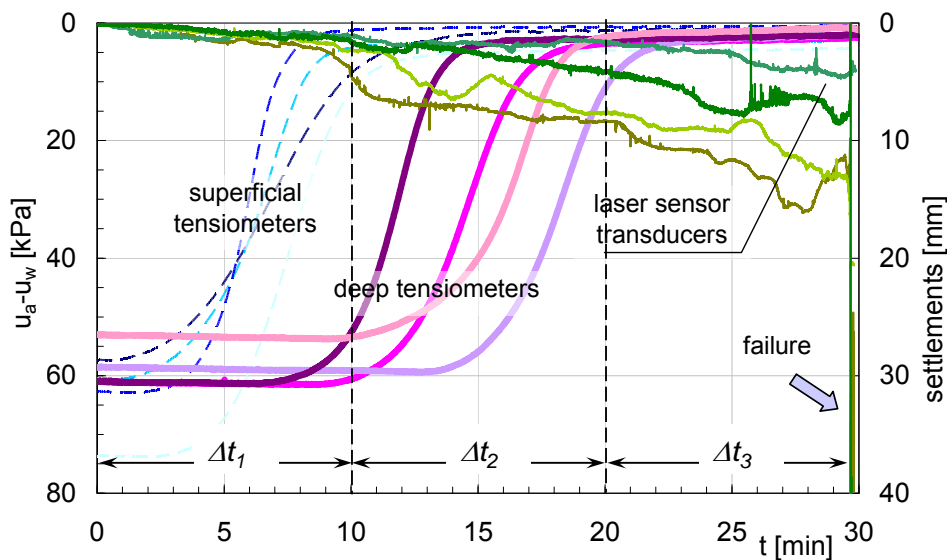


Figure 28 - From wetting to failure: typical response of loose ash deposits in the inclined flume.

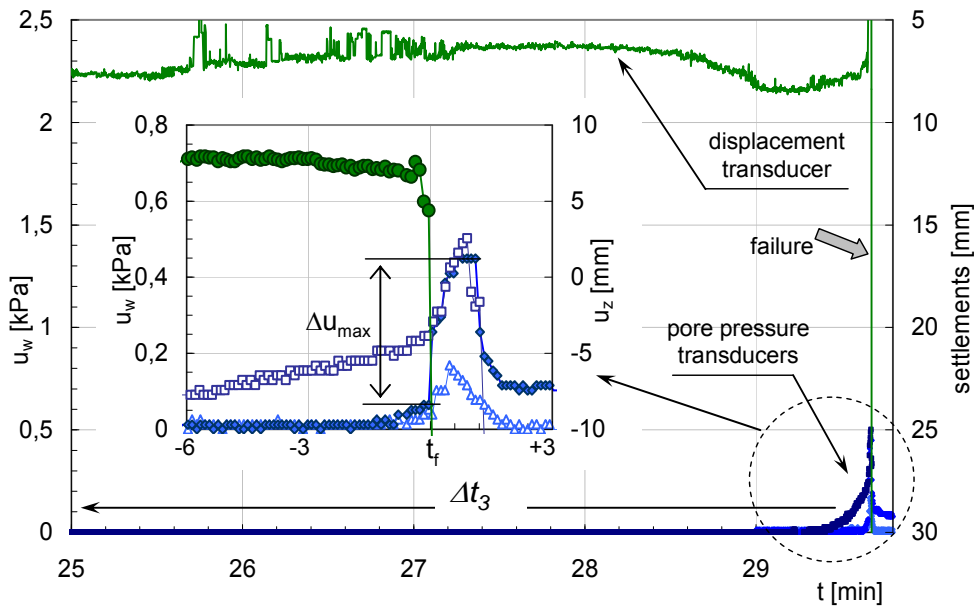


Figure 29 - Typical response at failure of loose ash deposits in the inclined flume.

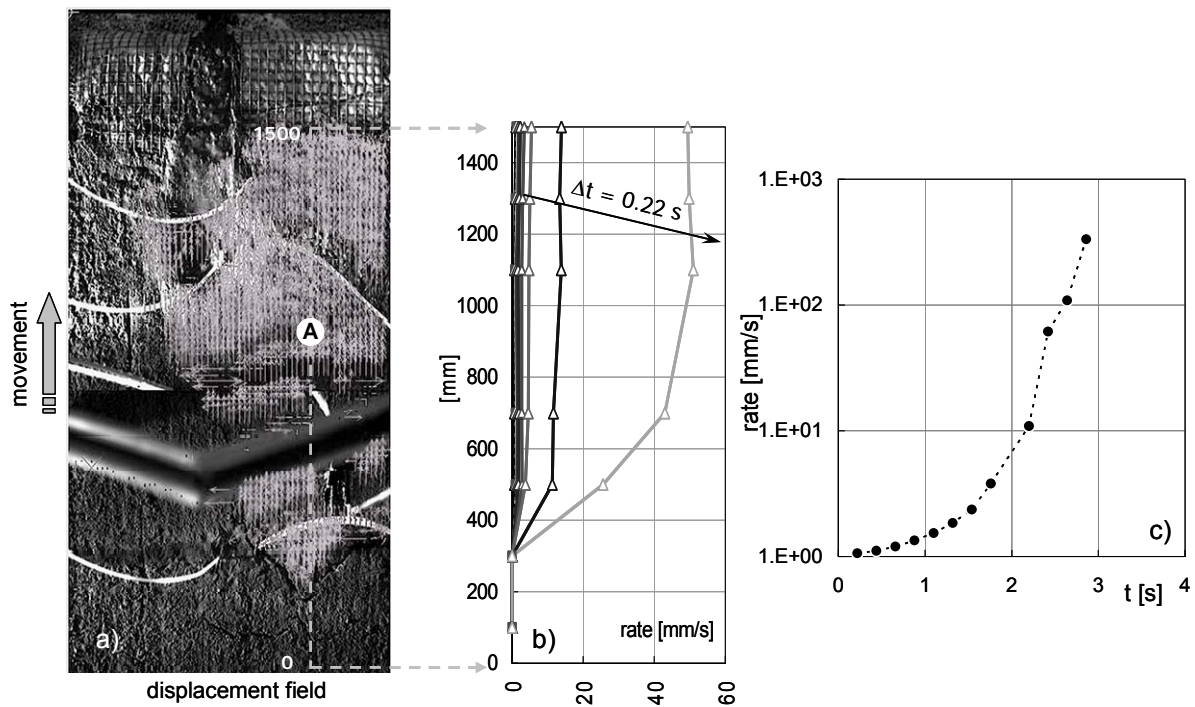


Figure 30 - Post-failure evolution: typical response of loose ash deposits in the inclined flume.

In the case of tests FL8 and FL9, the excess pore pressure assumes a high value, close to the total stress, which should cause a complete loss of shear resistance. Subsequently, a reduction in pore pressure is observed when the transducer is left partially uncovered by the soil. Therefore, in order to correctly capture pore pressures up to complete fluidisation, the transducers should be able to follow the soil mass during any movement.

A representative scenario of the slope behaviour can be traced from the displacement field obtained from the digital video-system. This is illustrated in Figure 30a, which shows the displacement field immediately after rupture and in Figure 30b, which reports the evolution of the displacement rate each 0.2 seconds. After failure, a sudden acceleration involves much of the slope and, just few seconds after ($t_f < t < 3s$), the rate of displacement (Fig. 30c) increases from 0.001 m/s (after $t = 0.22s$) to over 0.3 m/s (after $t = 2.8s$). This result, together with the sudden increase in pore pressure, is the experimental evidence of the establishment of partial or fully undrained conditions, which leads to a flow-like movement (Olivares & Damiano, 2007).

2. Flume tests of inclined slopes of dense homogeneous ashes subjected to rainfall infiltration to failure

Tests performed on ashy deposits reconstituted at an initial porosity lower than 70% reveal some different features. Even if the first stage of infiltration is qualitatively similar to what occurs in loose deposits, some different aspects can be observed. Firstly, by tamping the soil with higher energy in order to reach the desired selected porosity, both permeability and time to failure are affected. Comparing the results in terms of trend of suction during the test previously shown (Fig. 28), which was performed on a deposit reconstituted at an initial porosity of 73%, and the test illustrated in Figure 31 performed on a deposit reconstituted at a porosity of 65%, subjected to the same rainfall intensity (60 mm/h), it can be noted that the advance of the wetting front is slower in the denser deposit, which requires a longer period of rainfall to fail, despite an initially higher water content.

Moreover, the reduction in suction is not accompanied by a marked volumetric collapse: even when a strong suction decrease interests the whole layer, settlements at the ground surface indicate that the densest soil experiences only small strains. In contrast to the loosest soils, only a small void ratio increase becomes apparent along the whole slope during the approach of instability, as shown by negative displacement measurements reported in Figure 31, probably associated with some dilation occurring at the base of the layer.

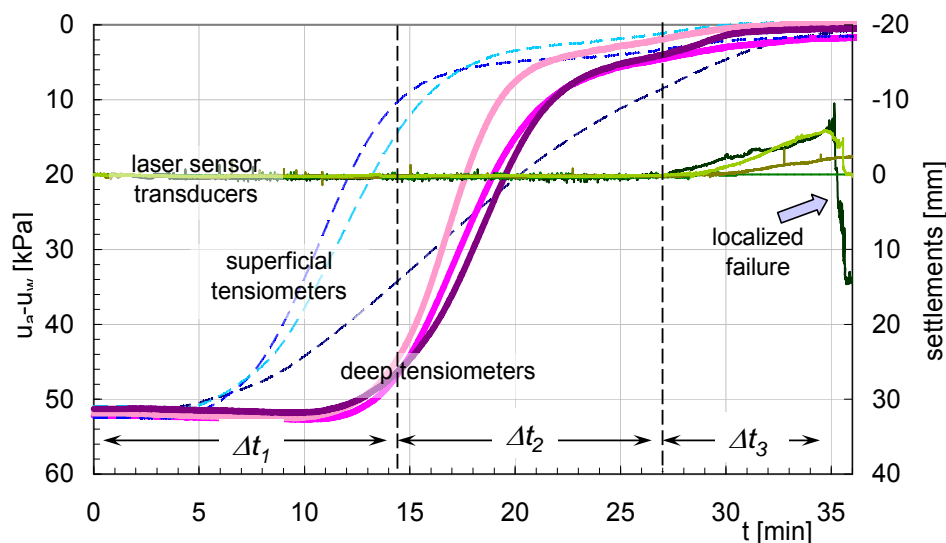


Figure 31 - From wetting to failure: typical response of dense ash deposits in the inclined flume.

As in the case of loosest deposits before failure, a fully saturated condition is established at the base of the slope but, pore pressures remain more or less constant at failure (Fig. 32). Hence, the instability process is not accompanied by a reduction of shear strength along the slip surface and the failure is followed by the evolution of a slide. In most cases, rupture is characterised by successive superficial slips and subsequent movements do not display a clear flow-like evolution. This is confirmed by the velocity of soil particles at the ground surface.

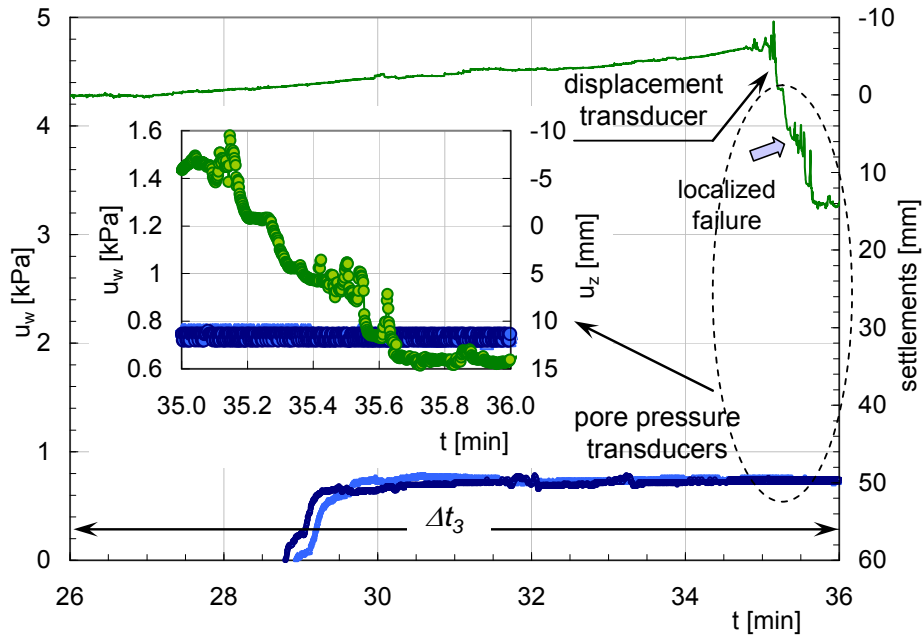


Figure 32 - Typical response at failure of dense ash deposits in the inclined flume.

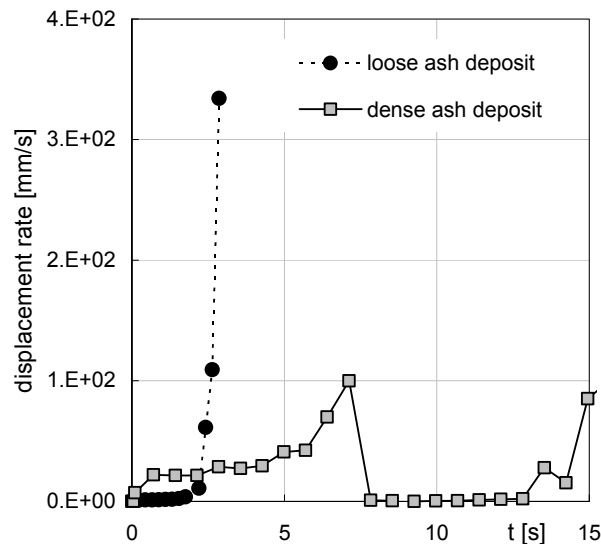


Figure 33 - Post-failure evolution: comparison between velocity of loose and dense layer in ash deposits in the inclined flume.

The velocities of a point inside the sliding soil mass are compared in Figure 33 for both loose and dense deposits. The different mode and type of movements is demonstrated clearly and it can be noted, in particular, that loose deposits are characterised by a more rapid evolution of downslope movement while movements in the dense deposits develop more slowly and demonstrate, in some cases, intermittent movements typical of retrogressive slides. In fact, in the case of a denser deposit, the detached soil mass moves with slower velocity, reaching a value of 0.1 m/s and stopping after about 7 seconds; the soil moves again after the soil mass behind it, which in the meantime reaches a failure condition, applies further compression.

3. Conclusions

Tests on homogeneous model slopes in volcanic ashes show that porosity influences both the time of infiltration and the mode of failure. In fact, in all tests performed on loose soil (porosity higher than 73%), failure developed in the whole layer, which displayed a clear flow-like evolution; in contrast, in tests performed on relatively dense soil (porosity lower than 69%), failure occurred only in the uppermost part of the slope, and any evolution into a flowslide was not so evident.

In experiments performed on loose model slopes with an angle equal to the saturated friction angle of the soil, failure occurred after an essentially drained wetting stage, the stability conditions being ensured by the enhancing effect of suction on shear strength. When it is dissipated, the slope fails and a rapid acceleration occurs as a consequence of a sudden increase in positive pore pressure (static liquefaction). Both the high shear strain rate and the maximum pore pressure recorded at the base indicate that the process evolves towards complete fluidisation (Olivares & Damiano, 2007).

Conversely, tests performed on relatively dense soil show that the suction reduction is not accompanied by volumetric collapse and the failure exhibits the features of a slide rather than a flowslide.

Such data, in conjunction with the results of conventional and unconventional laboratory triaxial tests on natural specimens (Olivares & Damiano, 2007), demonstrate that in situ void ratios might enable discrimination between deposits, which are prone to liquefaction and can give rise to catastrophic debris flows, and deposits whose post-failure behaviour would tend to form a slide, giving rise to a potentially less catastrophic event. For typical thickness of pyroclastic covers, thus accounting for the average state of stress, the critical void ratio could be established as around 1.8, which is generally less than the natural void ratio of the most air-fall deposits. However, further aspects, such as the probability of progressive failure, should be accounted for in boundary value problems (Picarelli et al., 2008).

2.3 FAILURE MECHANISMS OBSERVED IN CENTRIFUGE TESTS

2.3.1 Results of centrifuge experiments on unsaturated sands

(ETHZ)

1. Introduction

The physical modelling of landslide processes in the laboratory can potentially create well documented, highly-instrumented case-studies of slope behaviour in which the material

properties, initial state, and boundary conditions are all well defined. However, practical constraints such as laboratory space, personnel, and large material quantities make full-scale (or even slightly reduced scale) modelling prohibitively costly. However, the reproduction of the process at a greatly reduced scale is widely acknowledged not to be fully representative of full-scale behaviour due to the difference in stress levels between model and prototype (Schofield, 1980; Take et al., 2004). If an model is downscaled by a factor N and subjected to an acceleration field N times greater than Earth's gravity, the gradient of body stresses within the model will be similar to the prototype, ensuring similarity of effective stresses and groundwater pressures at equivalent depths.

During raining over model slopes in centrifuge tests, seepage dominates in the movement of water through the fills, implying that Darcy's law holds for this case (Kimura et al., 1991). It is generally accepted that the seepage velocity in the centrifugal field of Ng is N times that in the gravitational field, as long as the identical material is used for the model and prototype soil at the same void ratio (Goodings, 1984; Garnier et al., 2007). Since the intensity of rain has the same dimension as the seepage velocity, the intensity of rain in the Ng field is N times that in the gravitational field.

Several mechanisms have been investigated by researchers in centrifuges modelling of sandy slope failures due to rainfall. Kimura et al. (1991) performed 21 tests on sandy slopes varying the initial conditions of the soil in terms of water content and void ratio, the inclination of the slopes and the rain intensities. Their tests indicate the occurrence of mainly two types of failures; complete failure along a well-defined deep slip surface, where the wetting front has already passed, and local instabilities at the toe after appearance of groundwater flow. Take et al. (2004) and Lee & Bolton (2006) performed a series of tests to evaluate different triggering mechanisms of slips and flowslides due to heavy rainfalls. The hypotheses that were explored during these tests were static liquefaction and localised build up of transient pore water pressures due to layering and significant changes in the inclination of the underlying lower permeability layers.

In the following sections, the mechanisms of failure in sandy slopes observed in centrifuge tests are reviewed and the parameters affecting these mechanisms will be explained.

2. Effect of initial conditions of slopes on the failure mechanism (based on Kimura et al., 1991)

Kimura et al. (1991) carried out a series of centrifuge tests to investigate the stability of fills subjected to heavy rains. They used an artificial mixture of 50% of Kanto loam with 33% Toyoura sand and 17% crushed Toyoura sand, which was classified as SM. Their focus was mainly on the effect of initial conditions of the fill such as the initial void ratio and water content on some cases (case I, Figure 1) and the influence of rain intensity and slope inclination in other cases (case II, Figure 2). All of the tests were done under a nominal centrifugal acceleration of $50g$. In case I, 11 tests (Tab. 1) were done on slopes of 45° inclination and the rain was applied by 10 nozzles arranged in 2 lines with an intensity of 600 mm/hr, which is identical to 12.0 mm/hr in the prototype. While 10 tests (Tab. 2) were performed for case II, with rain intensities of 2250, 1400 and 700 mm/hr (45, 28 and 14

mm/hr at prototype scale, respectively) and the slope angle was 60°, 45° and 30° for the tests conducted.

Sheets of filter paper were laid on the slope prepared under case II conditions to prevent erosion due to rain. Pore pressure transducers and conductivity sensors were installed at locations shown in Figure 2. Deformation features for the fills and movement of the wetting front were recorded by photographing the models for both test cases I and II. The fills described as complete failure in Tables 1 and 2, failed along a well-defined deep slip surface and the description as local failure indicates local instabilities at the toe of the slopes.

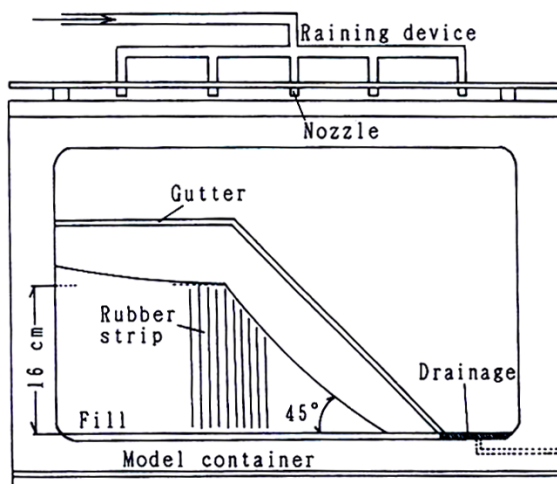


Figure 1 - Setup test for test case I (after Kimura et al., 1991).

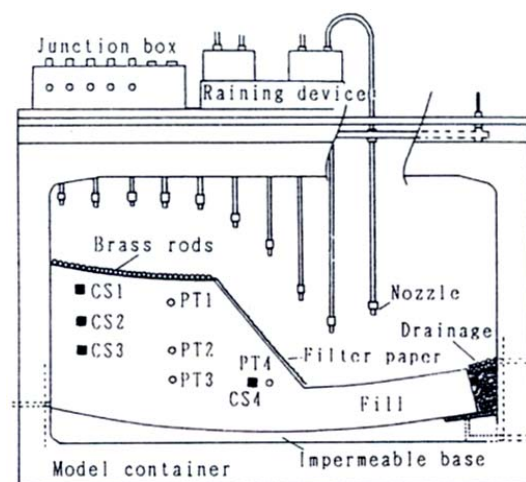


Figure 2 - Setup test for test case II (after Kimura et al., 1991).

Table 1 - Test conditions and results for test case I (after Kimura et al., 1991).

Test No.	Initial condition		Time to failure (s)	Pattern of failure
	e_{ini}	w_{ini}		
A-1	1.75	27.9	--	No failure
A-2	1.81	27.3	--	No failure
A-3	1.86	25.5	--	Local
A-4	1.86	24	--	Local
B-1	1.66	36.2	--	No failure
B-2	1.72	36.6	44	Complete
B-3	1.81	38.3	48	Complete
C-1	2	25.5	50	Complete
C-2	2.02	27.6	42	Complete
D-1	1.94	37.1	30	Complete
D-2	2	33.2	13	Complete

Table 2 - Test conditions and results for test case II (after Kimura et al., 1991).

Test No.	Angle of slope (°)	Rain intensity (mm/hr)	Time to failure (s)	Pattern of failure
E-60 (1)	60	2250 (45)*	35	Complete failure
.(2)	60		36.8	
E-45 (1)	45		66	
.(2)	45		50.5	
E-30 (1)	30	1400 (28)*	97	Local failure
.(2)	30		90	
F-45	45	700 (14)*	58	Complete failure
G-60	60	700 (14)*	61.5	Complete failure
G-45	45		250	Local failure
G-30	30		400	

* Bracketed figures are at prototype scale

(The average initial void ratio $e = 1.87$ and water content $w = 28.5\%$)

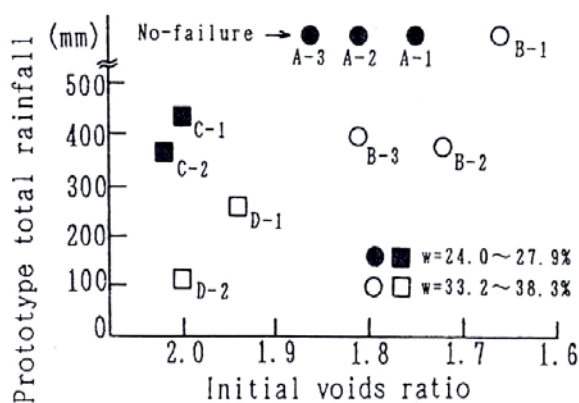


Figure 3 - Relationship between prototype total rain and initial void ratio (after Kimura et al., 1991).

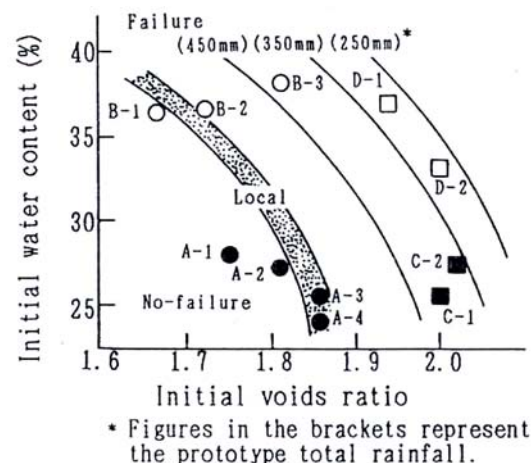


Figure 4 - Effect of the initial conditions of fills on the stability (after Kimura et al., 1991).

The fills with higher initial void ratios failed at lower rain intensities (Fig. 3). When the initial void ratios were similar, more rainfall was necessary to cause failure in the fills with lower initial water content. Figure 4 shows that the zones of no-failure, local failure and complete failure can roughly be established together with the contours of equal rainfall.

The movement of the wetting front was recorded by pore pressure transducers and conductivity sensors. The responses of conductivity sensors and pore pressure transducers are shown in Figures 5 and 6, respectively for test G-30. The increase of the conductivity for sensor CS4, observed between 200 and 300 seconds, may reflect that the groundwater flow developed after the wetting front reached the impermeable base.

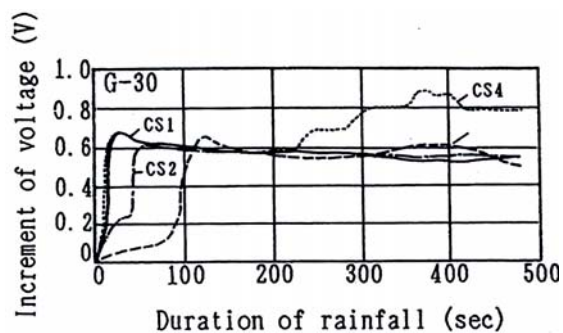


Figure 5 - Observed variation of conductivity (after Kimura et al., 1991).

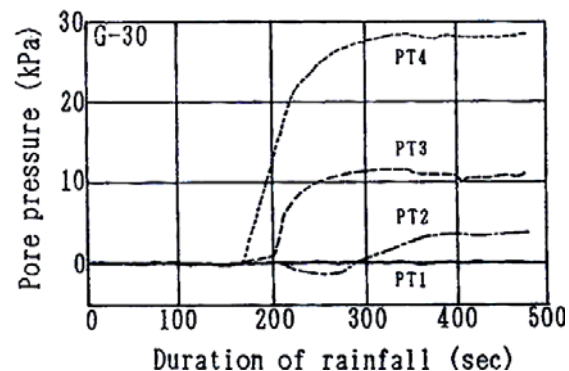


Figure 6 - Observed variation of pore pressures (after Kimura et al., 1991).

Evaluation of the *static liquefaction* and the effect of *localised transient pore pressure* as mechanisms of landslides (based on Take et al., 2004 and Lee & Bolton, 2006)

Take et al. (2004) performed a series of tests on highly instrumented centrifuge models to evaluate two candidates for the triggering mechanisms of slips and flowslides due to heavy rainfalls. The two hypotheses that were explored during these tests were static liquefaction and transition from slide to flow due to localised transient pore water pressures.

The soil used in the model fill experiments was decomposed granite. Index tests performed in Hong Kong by the Public Works Central Laboratory on this material indicated that the soil is a slightly clayey, silty, very gravelly sand (GEO, 1999) with a mean grain size of 1.1 to 1.4 mm and approximately 16% of relatively low-plasticity fines (plasticity index of 11–14%). To reduce the unrealistic influence of large particles on the behaviour of the small scale fill slopes, the fill material was first sieved to remove all particles in excess of 5 mm in diameter. Proctor compaction tests indicated that the maximum dry density of the soil is 1.920 kg/m³ and is achieved at an optimum water content of approximately 11–12%.

3. Evaluation of the static liquefaction mechanism

Terzaghi (1956) referred to the phenomenon of sudden change of loose deposits of sand into flows, due to a slight disturbance, as spontaneous liquefaction accompanied by substantial shear strength reduction of the soil when subjected to undrained shearing. Static liquefaction is widely described as the loss of strength of the loose contractive material and the consequent conversion of the fill into a fast moving slide (or flow) (Knill et al., 1976, Olson et al., 2000, Chu et al., 2003, Casini et al., 2010).

The speed of movement and permeability of any failing material could ensure that undrained conditions pertain as soon as yielding begins. Laboratory tests indicate that dense soils dilate as they begin to shear, whereas loose soils contract (Figure 7.a) (Schofield & Wroth, 1968). For saturated specimens that compress, undrained conditions lead to effective stress paths with decreasing shear stresses, and run-away instability is observed provided the yield surface opens up in the outward direction of the hydrostatic axis. Thus, instability occurs inside the failure surface. Instability is not synonymous with failure, although both may lead to catastrophic events (Lade, 1989). For undrained conditions and compressive material, the instability is self-sustaining and unconditional, i.e., it is not dependent on conditions outside the soil element. Loose, fine sands and silts have relatively low permeabilities and small

disturbances in load or even small amounts of volumetric creep may produce undrained conditions in such soils, and instability of the soil mass follows. As long as the soil remains drained, it will remain stable in the region of potential instability. When potential instability is reached, the soil may not be able to sustain the current stress state. This stress state corresponds to the top of the current yield surface as shown schematically in the diagram of effective mean normal stress (p') versus deviatoric stress (q) (Fig. 7). Following this point of maximum q , the soil can deform plastically under decreasing stresses. Figure 7 shows a schematic p' versus q diagram in which the line connecting the tops of a series of effective stress paths from undrained tests on loose soil provides the lower limit of the region of potential instability. In the region above this instability line, the soil can deform plastically under decreasing stresses. Experiments show that this line is straight. Since it goes through the top points of the yield surfaces, which evolve from the origin, the instability line also intersects the stress origin (Lade, 1993).

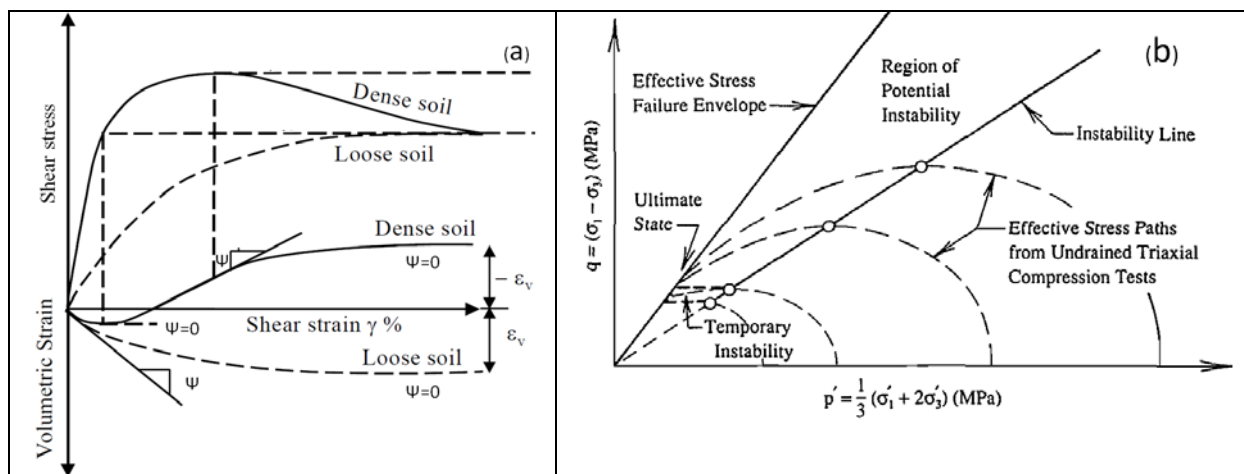


Figure 7 - a) typical behavior of soils in shear tests b) Schematic diagram showing the location of instability line (after Lade, 1993).

Figure 7.b also shows a region of temporary instability, which is located in the upper part of a dilating zone. It is a region where instability may initially occur, but conditions allow the soil to dilate after the initial instability, thus causing the soil to become stable again (Lade, 1993). In drained triaxial compression tests, the fill material used by Take et al. (2004) was observed to have a critical state angle of friction of 34° . When placed very loose, similar decomposed granite fill materials have a well documented susceptibility to static liquefaction in saturated triaxial tests (e.g. Ng et al., 2004). Undrained triaxial tests performed on very loose samples of the Beacon Hill decomposed granite (relative compaction about 70% of Proctor optimum compacted density, circa 0% relative density) indicate that the model fill material is similarly collapsible with an instability line representing a mobilised angle of friction of 22° . Thus, if it is maintained at this large void ratio of about unity while it becomes saturated, and if collapse is so fast that excess pore pressures can not dissipate, static liquefaction could occur at a stress ratio much lower than the critical state (Take et al., 2004).

Rainfall infiltration was reproduced in the model test to investigate the mechanism of static liquefaction by uniformly applying atomised mist in two rows of five nozzles placed just above the soil surface (Fig. 8). The size of the nozzles was chosen to provide small droplet sizes and to reproduce a continuous rainfall intensity of 250 mm/hr at 60g centrifugal

acceleration, representing a severe weekly rainfall in Hong Kong (4.2 mm/hr). To avoid unintentional drying of the model during centrifuge testing, the experiments were conducted in a sealed atmospheric chamber (Take & Bolton, 2002). As shown in Figure 8, a no-flow boundary condition is provided on all boundaries of the model fill slope, with the exception of the bottom right-hand corner, in which seepage water is allowed to spill to overflow once the water level has reached the elevation of the toe of the slope. Pore water pressures are measured using a network of miniature (7 mm in diameter) pore pressure and tension transducers (PPTT) buried within the model fill at each of locations indicated by open circles in Figure 8. The deformations of the model fill slopes have been measured by a new image-based system of deformation measurement, which combines the technologies of digital imaging, the image processing technique of particle image velocimetry (PIV), and close range photogrammetry (White et al., 2003).

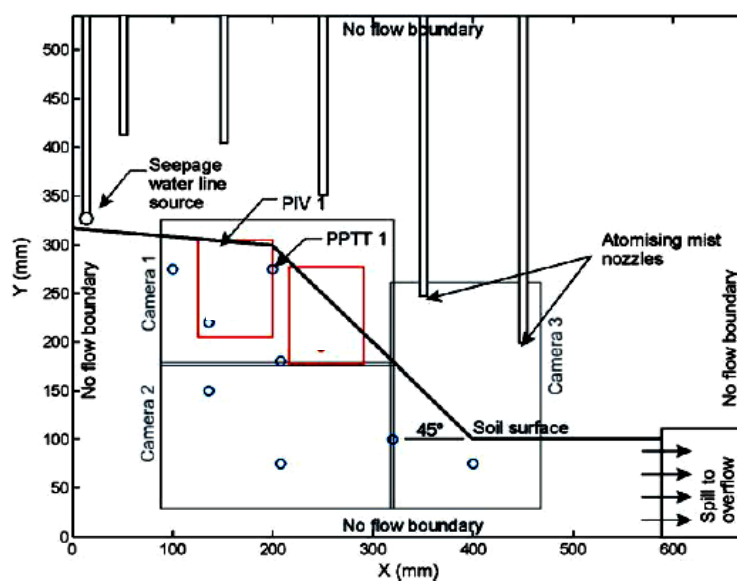


Figure 8 - Static liquefaction model test geometry (after Take et al., 2004).

The model fill was slowly brought to the testing acceleration of 60 g in 10 g increments. As the loose fill material becomes incrementally heavier, a cumulatively larger percentage of the loose fill can no longer support this increase in total stress and rapidly decreases its void ratio. As increments of “gravity” are progressively turned on, the height of the fill above the phreatic surface effectively becomes higher, requiring progressively higher capillary forces to be developed if the volumetric water content is to be retained. As a result, the biggest pores shed their pore water vertically downwards into the fill, creating an initial suction distribution, which increases with elevation from a value of approximately zero at the toe to -25 kPa at the crest (PPTT1 in Fig. 9b). Large settlements at the crest of the fill (Fig. 9c) correspond to a settlement of over 2 m at prototype scale and represent a vertical strain of 10%, when averaged over the entire fill height. The high compressibility observed in these loading increments indicates that the material in the entire fill slope is in a state on the normal compression line. Therefore, it is impossible to have a looser slope at the current effective stress levels (Take et al., 2004).

The fill slope was subjected to the equivalent of six weekly periods of rainfall infiltration (Fig. 9a). As shown in Fig. 9b, the arrival of rainfall on the slope surface at time A destroys a

significant portion of the soil suction very rapidly at the shallow location of PPTT1. The loose model fill responds immediately to this loss of surface tension, as the macro-voids, which had survived self-weight consolidation, collapse. The resulting settlement of the bench above the fill slope is purely vertical. Similarly, the loss of suction in the region of static shear stress (i.e. beneath the sloping portion of the embankment) also causes macro-voids to collapse, with a significant down-slope displacement. Despite being subjected to an additional five infiltration events of identical severity, the model slope was observed neither to achieve positive pore water pressures nor to experience any significant additional deformation (Take et al., 2004).

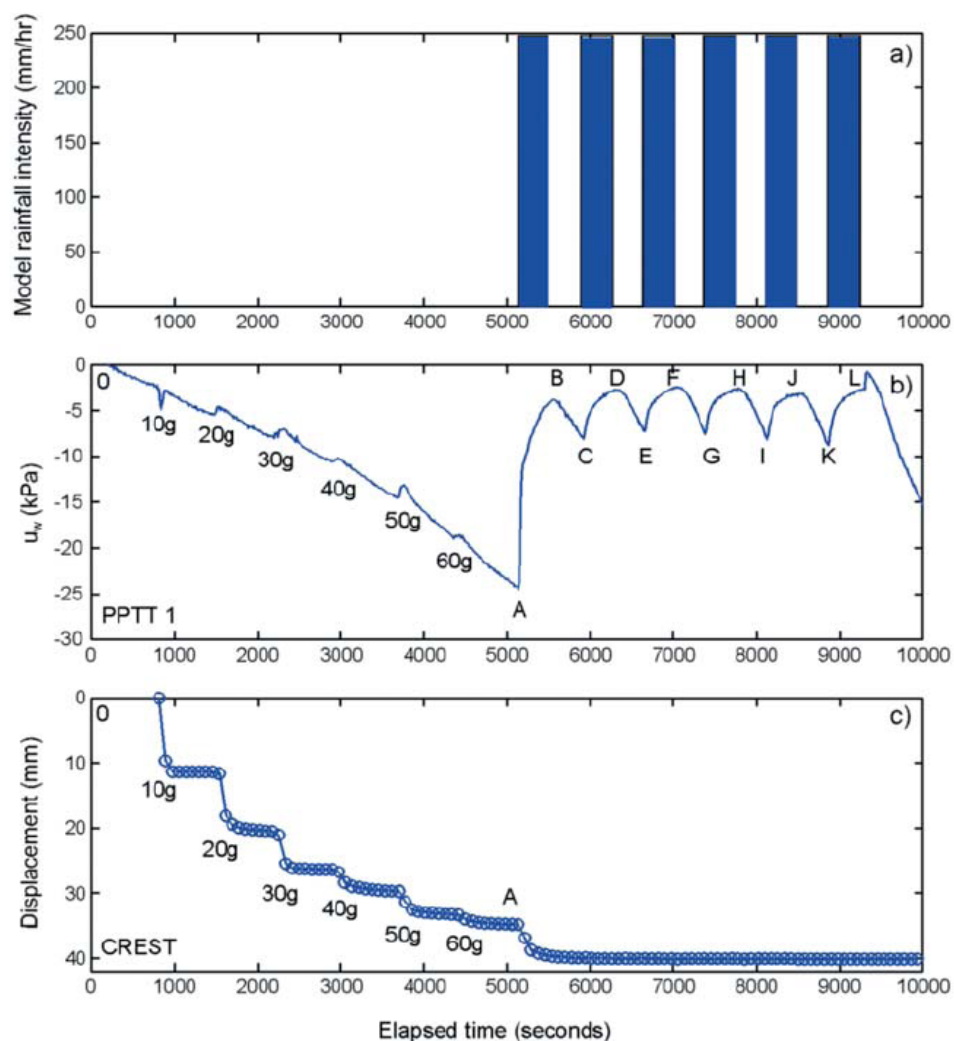


Figure 9 - Observed behaviour of static liquefaction model (after Take et al., 2004).

Although the fill has experienced instability, a flow failure has not been triggered by the mechanism of static liquefaction. In triaxial tests on loose, saturated, samples of the same fill material, static liquefaction was observed to occur when the model fill was unable to drain during attempted volume reduction. The fill material in the model test remained very loose near the surface, despite being subjected to an increased self-weight. It is likely, therefore, that the difference in observed behaviour relates to the model fill slope's ability to

accommodate the wetting collapse through the compressibility and ease of migration of the pore air. Thus, the unsaturated nature of the fill material, and the lack of groundwater ponding, has eliminated the possibility of creating static liquefaction in this model (Take et al., 2004).

The infinite slope analysis predicts that a 45° slope (such as the above mentioned model fill slope) is potentially in danger of failure. However, due to the high compressibility of the fill material, the model fill slope achieved an average angle of inclination of 33.5° prior to rainfall infiltration. Here, as was observed in the model fill experiment, the unsaturated infinite slope may experience instability but, if the voids can collapse, undrained failure will be averted and the stress path remains inside the failure line (Take et al., 2004).

Accordingly, the mechanism of static liquefaction, although easy to reproduce in saturated triaxial specimens, is much more elusive in physical models. Particularly, the unsaturated nature of the fill material, and the lack of groundwater ponding, has eliminated the possibility of creating static liquefaction in this model. The results indicate that CDG is too permeable to develop a sufficient depth of the wetting front (Yeung, 2002) and then to turn into a flow, as water can quickly drain out from the soil pores. In addition, static liquefaction is unlikely to occur if the model fill is unsaturated and the bedrock is deep enough. Since the air in the unsaturated voids is highly compressible, the model fill slope may exhibit wetting collapse instead of undrained failure (Take et al., 2004).

However, Take et al. (2004) concluded that the non-appearance of an event in certain circumstances can not be taken to mean that the event will never occur under any circumstance. Therefore, the conventional understanding of static liquefaction in loose CDG fill slopes can not be dismissed on the evidence of one centrifuge test. Furthermore, there is a factor arising out of centrifuge testing that may indeed have militated against liquefaction. Inertial events such as the duration of a pressure pulse due to soil collapse will take the form $t_{\text{pulse}} \propto \sqrt{h/g}$. In centrifuge tests, fall distances h are reduced by factor N whereas accelerations are increased by factor N . Accordingly, $t_{\text{pulse, model}} = t_{\text{pulse, field}} / N$. Diffusion processes, such as the release of air or water from a collapsing void, have durations of the form $t_{\text{dissipation}} \propto h/v$ where the flowrate v may be deduced from Darcy's Law. As explained before, v is increased by factor N and h reduced by factor N in a centrifuge test, so $t_{\text{dissipation, model}} = t_{\text{dissipation, field}} / N^2$. This means that the release of trapped pressure in a centrifuge model, during a collapse event, will be greater in proportion than that found at full scale. This problem is well-known in centrifuge earthquake liquefaction studies (Taylor, 1995). Two corrective strategies are to slow down the rate of dissipation by a factor N by increasing fluid viscosities by factor N , or to reduce pore sizes (i.e. grain sizes) by a factor \sqrt{N} . Further studies on this point will be valuable in the clarification and classification of fast landslides (Take et al., 2004).

4. Evaluation of the slide to flow mechanism due to localised build up of transient pore pressures

An alternative hypothesis of the triggering mechanism of fill slope failures has been proposed by Take et al. (2004) and Lee & Bolton (2006). Take et al. (2004) performed two centrifuge model tests at 30g to investigate this transformation of initially slow moving slopes to flowslides in both loose and dense fill slopes. The geometry adopted for both fill slopes is presented in Figure 10.

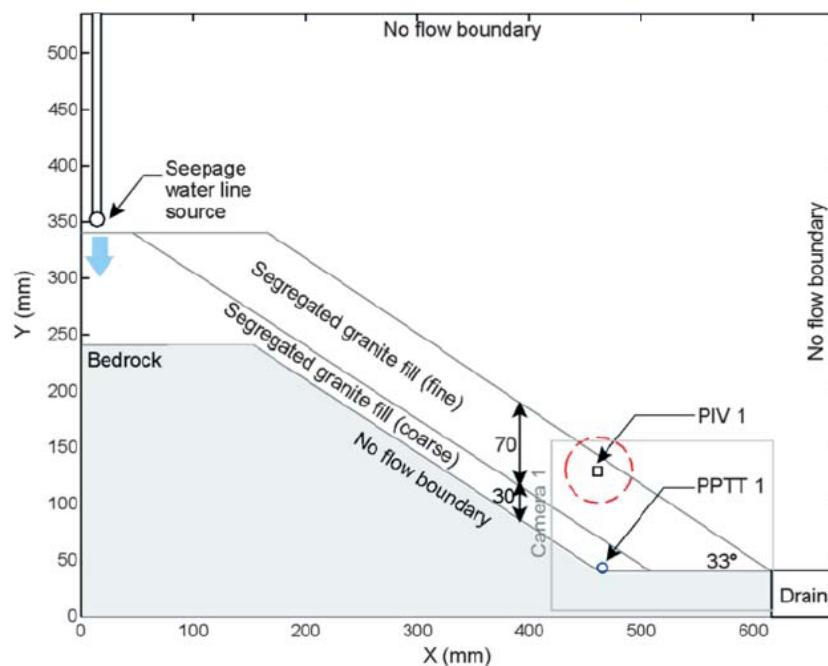


Figure 10 - Slide-to-flow landslide triggering mechanism model (after Take et al., 2004).

The intended triggering mechanism combines the two closely related pore pressure generation scenarios of flow constriction and heterogeneity, thereby compounding the landslide risk. Firstly, elevated transient pore water pressures will be generated at the toe as the inclination change of the impermeable bedrock will constrict seepage flow. Water must be stored at this location, and will be forced to seep through the fill material at the toe of the slope, thus reducing the effective stresses at this critical location. The chosen soil profile for the model fill also represents an idealised case of layering, in which the decomposed granite fill material has been sieved and separated into its coarse and fine fractions and placed one on top of the other to form a layered backfill. In this scenario, the layer is enclosed within the toe of the slope, which is also notably the location of the flow constriction. The presence of the layering in this model will reduce the intensity and duration of rainfall infiltration required for failure (Take et al., 2004).

5. Fill slope with loose layers

The density of the fill material in the first layered slope model was intended to be representative of tipped fill and was placed with only a minimal compaction effort. The resulting layered slope is very loose, with an approximate relative compaction of 77%. As expected, the loose model fill material experienced significant settlement due to increased acceleration (Take et al., 2004).

The measured pore pressure versus time after the first arrival of the seepage water is plotted in Figure 11. The local pore water pressure was observed to increase at nearly a constant rate, reaching a maximum value of 16 kPa at point B in Fig. 11a. As intended, the rate of water transfer into the toe region has exceeded the seepage velocity through the model fill, causing a transient increase in pore water pressure at the toe. As this seepage front has been progressing towards the toe, the slope has been slowly creeping. Image analysis performed on the images prior to final acceleration of the failure (times B and C in Figure 11a), indicates that the toe is

accelerating horizontally with an average velocity of approximately 6 mm/s (Fig. 12). The observed displacement field over this time interval indicates that the surface of the model fill is moving down-slope at a slower velocity. As the toe continues to accelerate horizontally, the surface of the model fill accelerates towards the toe, with the velocity increasing (Fig. 11b). When the fill material has finally come to rest, it has formed a low-angle run-out (Take et al., 2004).

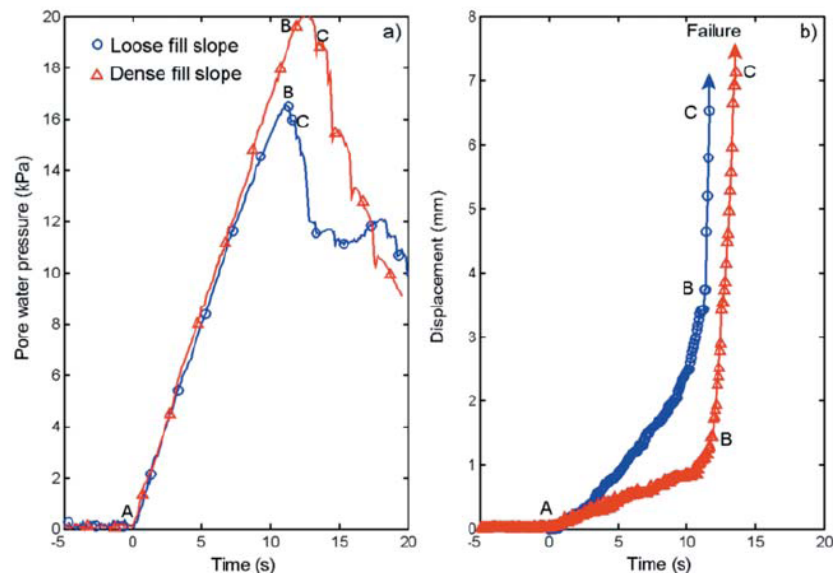


Figure 11 - Observed behaviour of slide-to-flow models (after Take et al., 2004).

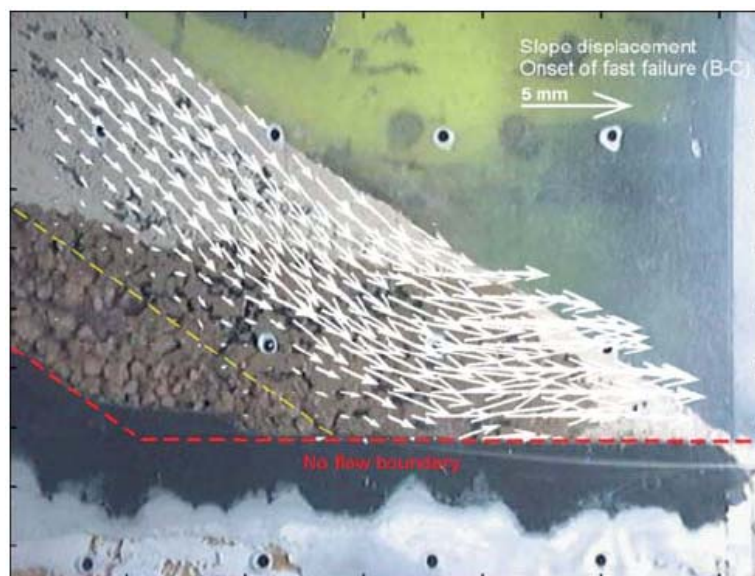


Figure 12 - Displacement field prior to final acceleration of loose fill model (after Take et al., 2004).

6.Fill slope with dense layers

The experiment was repeated with a fill compacted to 95% maximum Proctor density, whilst keeping all other factors constant. After introducing the seepage water to the crest of the fill it was quickly transmitted to the toe of the slope, building up localised transient pore water pressures at an identical rate to the loose fill model (Fig. 11a). The dense slope exhibits a much stiffer response to the build up of pore water pressures, with less than one half of the pre-failure displacements indicating the onset of failure. Just before reaching the failure pore water pressure, the brittle fill material cracked and water rapidly entered the fill. As high pressure water entered this crack, the acceleration of the slide increased. After time B, the slope mass is observed to accelerate, albeit at a slower slide velocity than observed in the loose fill slope (points B-C on Fig. 11b). More dense fill slopes will fail in a more unpredictable, brittle fashion compared to the loose, ductile, fill slopes. The pore water pressure required to trigger the failure has slightly increased (Take et al., 2004).

Lee & Bolton (2006) also conducted two centrifuge tests at 40g on Completely Decomposed Granite (CDG) to investigate the potential importance of layering effects in a fill slope. The geometry of both fill slopes is presented in Figure 13. The slope angle for the model slope is 35°, which is slightly higher than the critical state angle of friction. Infiltration was introduced to the crest of the model slope from a water source located at the end of the model. Presumably, water seeps through and builds up in the gravel layer. Pore water pressure is expected to develop at the interface between layers and this will force the water to seep through the fill material at the mid-slope and trigger a failure. The build up of transient pore water pressure measured by PPT1 at the interface is shown in Figure 14.

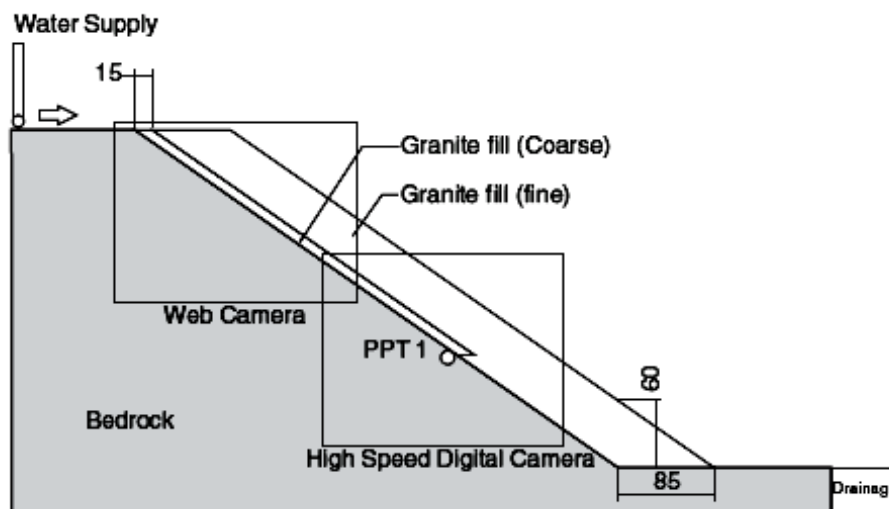


Figure 13- Model geometry of the slope model (after Lee & Bolton, 2006).

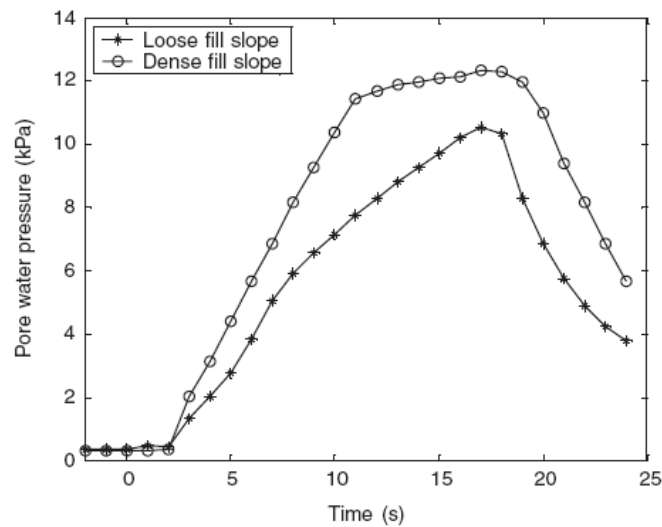


Figure 14 - Development of pore water pressure at the location of porepressure transducer PPT1 in model slopes (after Lee & Bolton, 2006).

Failure was induced when layered fill slopes were subjected to seepage flow from a more permeable layer (Fig. 15). The results indicate that shear failure can be developed when transient pore water pressure is allowed to build up in a more permeable layer underneath a fill slope, even though the top fill layer is compacted to a high degree (Lee & Bolton, 2006).

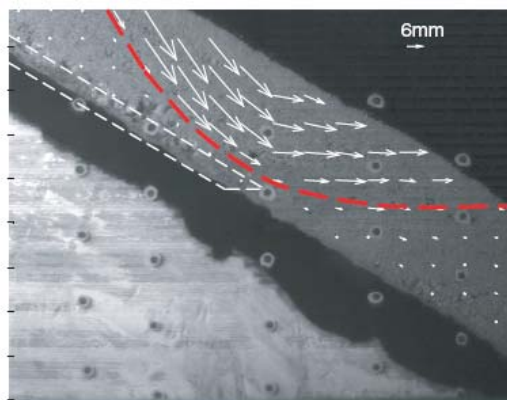


Figure 15 - Displacement vector field of the mid-slope of a layered model in Completely Decomposed Granite (after Lee & Bolton 2006).

7. Summary and conclusions

Kimura et al. (1991) found that two types of failure appear when a fill is subjected to heavy rain. One is the failure along a well-defined deep slip surface taking place in the areas where the wetting front has passed. The other is the failure initiated in the toe areas, that develops after the appearance of the groundwater flow on top of an impermeable base layer. They observed that the downward movement of the wetting front takes place with a constant rate, which is related to the rain intensity and has a shape similar to the geometry of the slope. The fills with higher initial void ratios failed at lower rain intensities. In the case of similar void ratios, more rainfall was necessary to cause failure in the fills with lower initial water contents.

Take et al., (2004) concluded that, in contrast to the static liquefaction mechanism obtained from laboratory element tests, it has been easy to create the slide-to-flow mechanism of landslide triggering by creating local groundwater mounds and hence increases in pore water pressure and local reduction in effective stress where seepage was restricted. The initial slide has been observed to create rapid flow events with low run-out angles, apparently very similar to those occasionally observed in Hong Kong fill slopes. These model flowslides were just as striking in dry, dense fill as in wet, loose fill. If these model events are realistic, the priority in hazard reduction should be in preventing triggering of a slip. Interception of groundwater percolation would be more useful as a remedial measure than densification, although the removal, mixing, and compaction of loose fill would have the coincidental benefit of eliminating permeable layers. Attention should particularly be focussed on regions of slopes where springs of seepage are observed after rainstorms. Shallow horizontal drains would be particularly effective in suppressing slip triggering in such locations.

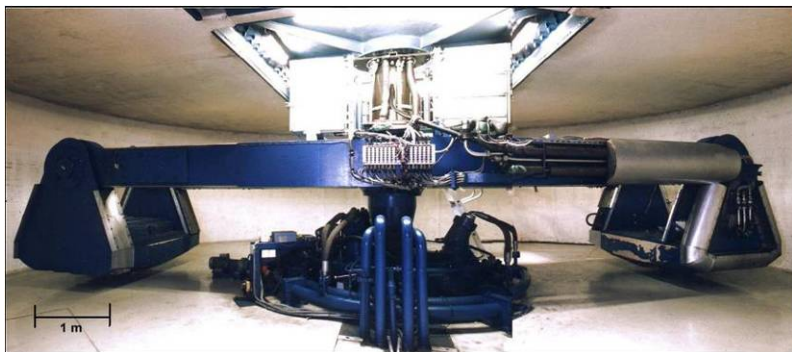
Lee & Bolton (2006) concluded that shear failure can be developed when transient pore water pressure is allowed to build up in a blind layer underneath a fill slope, even though the top fill layer is compacted to a high degree.

2.3.2 Results of centrifuge experiments on unsaturated clays

(CNRS)

Real slope behaviour cannot be reproduced properly with small-scale model tests acting under a gravity field at 1g. This is mainly because self-weight forces are the dominant load and the material behaviour is stress dependent. In order to replicate the gravity-induced stresses of a prototype in a scaled model reduced by $1/n$, it is necessary to test the model in a gravitational field n times larger than that of the prototype. This can be achieved through centrifuge model testing. Experiments on black marls were performed at Ruhr-University Bochum using the geotechnical beam centrifuge Z1 (Jessberger et al., 1988) (Fig. 16). After the slope model and the measurement devices were installed (Fig. 17), the acceleration was increased to 50 g during the consolidation phase that permits effective stresses to equalise in the model, to represent the prototype case. The initial water content of the consolidation phase is equal to 12.3 %, which is almost equal to the optimum water content. This water content is chosen to avoid large displacements or even failure during consolidation. However such an initial water content leads to a very dense model with a very low hydraulic conductivity. As a consequence, the saturation of the slope cannot be executed in a time period that is reasonable for centrifuge testing. The water supply (hydrological trigger) is started after the consolidation phase.

Slope failures occur if the initial water content is too high during consolidation (Figs. 18 & 19). The slope model fails before an acceleration of 50 g can be applied.



Radius: 4.125 m
 Max. acceleration: 250 g
 Max. acceleration in test: 50 g
 Max. weight of model: 2 t

Figure 16 - Geotechnical beam centrifuge Z1 (Jessberger et al., 1988) at Ruhr-University Bochum.

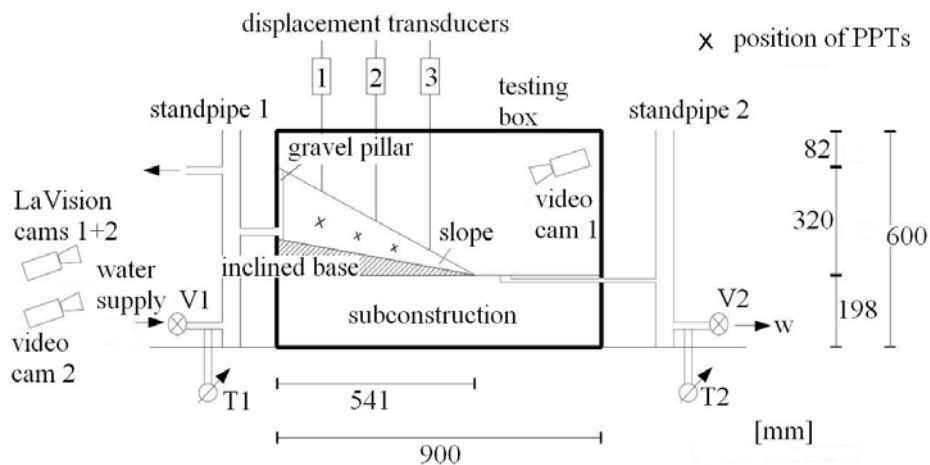


Figure 17 - Scheme of the model setup and measurement devices for the centrifuge tests on unsaturated clay slopes at the Ruhr-University, Bochum.



Figure 18 - Start of the consolidation phase for unsaturated clay with an initial water content higher than the optimum water content (about 18%).



Figure 19 - Failure that occurred during the consolidation phase for unsaturated clay with an initial water content higher than the optimum water content (about 18%).

2.4 SYNTHESIS

It has been shown in the preceding chapters that laboratory tests have provided a firm basis for understanding landslide triggering and have given a compact and useful overview of the state of the art of laboratory testing, with respect to landslide hazards. The main methods described within these chapters are flume and centrifuge experiments, covering a wide range of soils, including clays, sands and pyroclastic deposits. While no laboratory test is fully capable of replicating the natural environment in which landslides occur in every respect, they prove a useful tool in so far as they are cheaper and easier to carry out than either full scale experiments or long-term monitoring sites, and all variables may be controlled. To this end, it is important to compare laboratory and field data, and both have been shown within this deliverable to have been used well in conjunction.

The flume experiments have shown the state of the art with respect to triggering failure due to rainfall infiltration into sands, clays and pyroclastic materials. Landslides in soils with initial porosities greater than the critical porosity have been observed to fail abruptly with high accelerations and a long run out, whereas those where the initial porosity is equal to the critical porosity have inconsistent behaviour varying from slow slumping of a single block, episodic slumping of multiple blocks to moderately rapid slumping. Dense sand exhibited a similar slide geometry to loose sand, but slid at approximately 300 times slower velocities. Tests in unsaturated clays show that high pore water pressure fluctuation, along with initial and ongoing microcracking and gradual reduction of suctions are responsible for progressive initiation of failure and eventual runout with low mobility.

Flume experiments in pyroclastic soils have shown that porosity influences rates of infiltration and therefore the mode of failure. In loose pyroclastic soils, failure was seen in a whole layer which translated into a flow slide. Failure was seen in dense pyroclastic soils in the upper layers only, with no flow slide, and a reduction of suctions did not induce collapse and failure, but promoted a slide rather than a flowslide.

Centrifuge experiments in sands have shown that 2 failure modes are observed in sand fill experiencing heavy rainfall. Failure may occur along a well defined slip surface or at the toe of the slope. The wetting front moved downwards, and the fills with higher initial void ratios failed at lower rain intensities. Where the void ratios are lower, more rainfall was necessary to cause failure in the fills with lower initial water contents. Centrifuge tests in clays have proved difficult to prepare and run effectively, with the slope often failing before reaching the target acceleration.

3 KNOWLEDGE OF SLOPE FAILURE MECHANISMS FROM FULL-SCALE IN – SITU EXPERIMENTS

3.1 FULL – SCALE SLOPE FAILURE EXPERIMENTS IN COARSE – GRAINED SOILS AND MORAINES.

1. Gruben

Two areas at about 2800 m above sea level (masl) at Gruben (Canton Wallis) were selected as field test sites and instrumented for artificial rainfall tests in the summers of 1999 and 2000, to investigate the hydro-mechanical mechanisms. One slope had an average gradient of 31° and $\sim 100 \text{ m}^2$ plan area (Field 1), and was used in both years. A steeper slope of 42° and approximately 55 m^2 plan area was also instrumented in 2000 (Field 2).

The Gruben glacier overlies the gneiss or muscovite (mica) slates of the Fletschhorn crystalline group, which form the oldest part of the (Pretriassic) Bernhard Plate. The moraine from the glacier forefield is composed from these parent rocks, based on faulted muscovite-rich gneiss or slate with some albite, chlorite and biotite present. When there is sufficient melt-water or runoff from rain, a series of depressions have formed natural peri- and proglacial lakes, and these constitute a major natural hazard. Excessive discharge has caused regular overtopping of the natural barriers around the lakes. Hence catastrophic outbursts and extensive erosion events have occurred. Five major glacier floods or debris flows were documented for the village of Saas-Balen (Saas Valley, Wallis, Switzerland) during the 19th and 20th centuries. The latest was in 1970 (Haeberli, 1992). Prevention measures against this hazard have already been designed to control and disperse the flow through the lakes and to provide sufficient additional storage to absorb peak flows (Haeberli et al., 1996). Construction was completed in 1997 at a cost of 1.5 Mio SFr and has been very effective to date.

The field test sites were instrumented with devices to measure suctions and volumetric water content, pore water pressures, rainfall intensity, and were provided with apparatus to create artificial rain as uniformly as possible (Springman & Teyssere, 2001). The soil characterisation tests included in situ and laboratory experiments on both saturated and partially saturated samples to determine densities (maximum, minimum, in situ and optimum - from standard Proctor compaction tests) together with permeability (saturated) as a function of normal stress, void ratio and particle size. A series of bender element tests were also set up to obtain shear wave velocity v_s (and hence small strain shear modulus) as a function of maximum particle size, effective stress and void ratio, and to link results to the field determination of compression wave velocity v_p (Cortona, 2000) whereby $v_p = \text{approximately } \{2(1 + \nu')\}^{0.5} v_s \sim 1.6 v_s$ (ν' = Poisson's ratio).

The test field is located at $\sim 2750 \text{ m}$ above sea level (masl), below Lake 1. The moraine is extremely heterogeneous with a significant range of particle sizes represented in the overlying 1-2 m on the slope. Seismic refraction, D.C. resistivity and gravimetry soundings were performed during a former geophysical campaign (Vonder Mühll et al., 1996). The results indicated a maximum thickness of nearly 100 m of moraine, with looser packing in a top layer (low compression velocities $v_p = 400\text{--}600 \text{ m/s}$ in the top 5 m at the site and $v_p = 700\text{--}1400 \text{ m/s}$ for the next 15 m and $v_p = 1100\text{--}1400 \text{ m/s}$ over the next 80 m), whereas the underlying moraine appears to have been well compacted with v_p increasing with depth (Springman et al., 2001, 2003). Resistivities from 2 to 10 $\text{k}\Omega\text{m}$ were obtained. Rock lies beneath the moraine with $v_p = 4400\text{--}4800 \text{ m/s}$. Instabilities were expected to develop primarily in the surface layers, where data relating to the in situ density and water content were obtained from an

average of five sand replacement tests and nine neutron-gamma probe tests (Springman et al., 2001).

Grain size distributions were determined from representative surface samples (originally 1-2 tonnes, from up to 1 m depth), taken adjacent to Field 1. Typical grain size distributions are given in Figure 1a for unlimited maximum fraction and for three fractions extracted from the “whole” sample and restricted to < 45 mm, < 16 mm, and < 2 mm. The fines content is significant. These have controlled the permeability and some aspects of the shear strength.

A sprinkler system was constructed to supply controlled artificial rainfall, the intensity of which was also measured. A base rate of circa 10 mm/h was supplied almost continuously for one week in 1999, including peaks of between 30 and 40 mm/h. There were two unplanned pauses, each for a few hours, early in the week when the water supply stopped. Rainfall was supplied more evenly in 2000, but only for two days and two hours, with an average of 16 mm/h for the first day and 12 mm/h for the second day. It was noted (Teysseire et al., 2000) that wetting during initial infiltration followed a steep hyperbolic path, as if along the main wetting curve of the WRC from a nominally dry state, whereas pauses in rainfall caused an exponential reduction of S_r with time (along a hysteretic scanning WRC). On rewetting (also along a hysteretic scanning WRC), resaturation up to the immediate past maximum S_r occurred significantly quicker than for the drying phase, whereupon further saturation continued at the previous rate (main wetting curve).

Details of extreme rainfall events for the nearest climatic station in Simplon Dorf (1495 masl), \square 5 km east, which also has high rainfall amounts and intensities (Molnar, 2002, private communication) are: (a) observed maxima for 2- and 7-day storms of 5.9 and 2.3 mm/h rainfall intensity respectively (both in 1977: period 1900–1980); (b) 500-year return period: predictions for 2- and 7-day storms give 9 and 3.5 mm/h.

The artificial rainfall events exceeded any observed storms of that duration at Simplon and have a return period greater than 500 years. This therefore provided a worst-case scenario.

A typical instrumentation plan is shown in Fig. 1(c). Time domain reflectometry (TDR) and moisture point (MP) devices were installed for accurate measurement of changes in volumetric water content (θ_v) and determination of S_r in the top 20 cm and top 1 m respectively. Suctions were also measured by tensiometers (T), although some difficulties were experienced in the harsh alpine conditions, which led to the malfunction of a number of instruments.

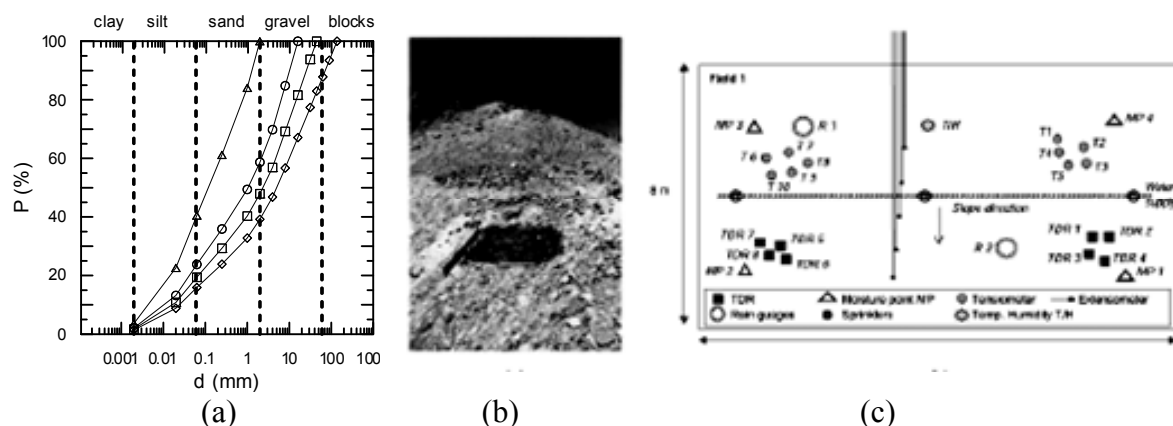


Figure 1 - (a) Grain size distributions; (b) view of the moraine slope field 1; (c) plan of instrumentation field 1/1999 (after Springman et al., 2001).

A continuous water supply was created by pumping from Lake 1, so that artificial rainfall could be simulated on a slope over a test field area of approximately 100 m². Intensities varied between approximately 10-30 mm/h, depending on the local wind conditions, corresponding to an extreme rainstorm. It is known that there are differences between artificial and natural rainfall, so response was also to be monitored following the artificial storm. Several smaller, but nonetheless significant, natural events were recorded. The duration of the test was 7 days with a total amount of rainfall of approximately 1.9 m, followed by a further 42 day period (Field 1/1999).

In year 2000, both test fields were to be subjected to a lower rainfall intensity (actually between 8-22 mm/h) over a longer period, with calibration of response from 1999 to 2000 from using the same Field 1 (but with slightly less instrumentation). However after ~2 days (Fig. 2), the 42° slope failed, and the tests were stopped. The common water supply system led to slight variations in rainfall, but these were in phase with each other, so that the rainfall distribution was similar for both fields.

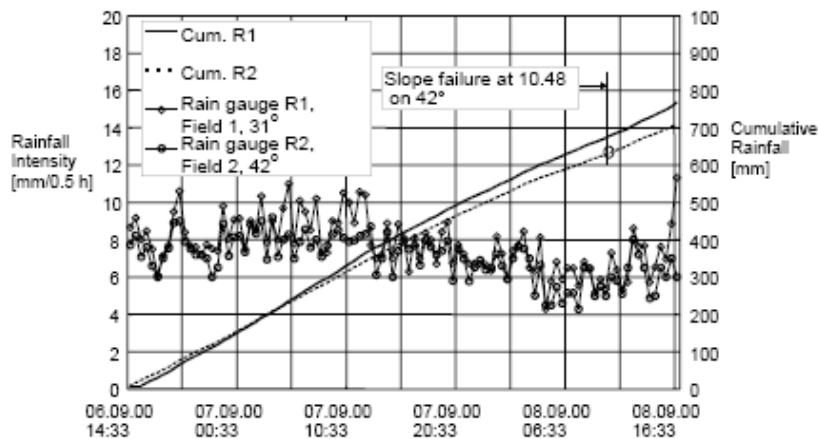


Figure 2 - Rainfall intensity for 2000 (after Springman et al., 2001).

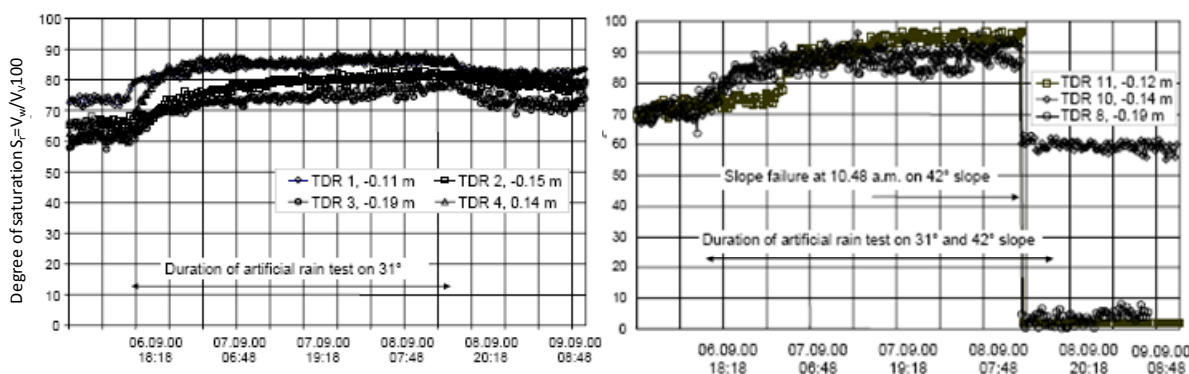


Figure 3 - TDR measurements (artificial rain): (a) Field 1/2000; (b) Field 2/2000 (after Springman et al., 2001).

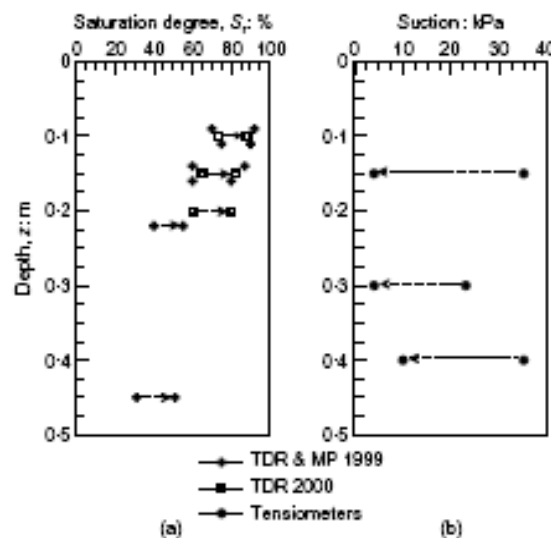


Figure 4 - Immediate pre and post-rainfall event data: (a) saturation degree determined from TDR and MP probes, fields 1/1999 and 1/2000; (b) suctions determined from tensiometers, field 1/2000 Gruben ((after Springman et al., 2003).

Figure 3a shows four sets of TDR measurements (TDR 1, 2, 3, 4) over 2 days of intense rainfall (field 1/2000), during which the degree of saturation in the surface layers increased from ~60% to around 75-88%. The degree of saturation did not reach an asymptotic value over 2 days. Suctions were also measured at three depths between 0.16 m-0.4 m. Data of pre- and post-rainfall event values of suctions are also plotted with depth for Field 1/2000, and are assumed to represent typical suction response (Fig. 4b). Since the beginning of the rainfall, suctions reduced most quickly in the shallower layers, from roughly -30 kPa to a minimum value of -4 kPa (Fig. 4b). The reduction in suction is particularly important given the accompanying decrease in effective stress, and hence mobilised shear strength. Data from 1999 and 2000 show in Figure 4a that initial values and increments of S_r are similar for both years.

Figure 3b shows three sets of TDR measurements (TDR 8, 10, 11) over 2 days of intense rainfall (field 2/2000), the qualitative response is similar to field 1 (Fig. 3a). Higher values of S_r (~95%) have been reached when the failure occurred. The data suggest that when $S_r > 90\%$, occluded air bubbles may have inhibited further saturation for field 1. These data highlight the role of suction in the stability of the moraine slopes. The suctions experienced by these soils are relatively small; nevertheless, suctions greater than 4 kPa appear to be sufficient to maintain slope stability. Instability occurred in the steepest slope only when S_r approached 0.95, corresponding to small, although still positive, values of suction.

Soils existing on steep slopes have experienced a highly anisotropic stress path (Zhu & Anderson, 1998). Therefore preparatory stress paths plotted in deviator stress q ($= \sigma_1 - \sigma_3$) and mean effective stress p' ($= (\sigma_1 + 2\sigma_3)/3$) space (Fig. 5a), where σ_1 and σ_3 are the axial and radial effective stresses as well as the principal stresses, have followed an initial isotropic consolidation (IC) up to a value of p'_I , and a further anisotropic consolidation (AC) phase to a principal stress ratio (σ_1/σ_3) of 2.5 (described by σ'_{1A} , σ'_{3A} , q_A and p'_A). Shearing to failure (F) was achieved by decreasing p' as q was maintained constant: σ_1 and σ_3 are reduced at the same rate (0.5 kPa/h) until failure is reached (σ'_{1F} , σ'_{3F} , q_F and p'_F : Fig. 5a). This models the expected loss of p' due to a net increase in pore pressure without change in the total stresses.

The gradient M of the critical-state line drawn in q - p' space, through the failure state of the three tests, is 1.59. This may be used to deduce a value of $\phi' = 39^\circ$ at failure. As p' reduces, ε_a increases (Fig. 5b). The stiffest response occurs due to unloading from higher initial stress states, whereas the initial volumetric response indicates a small degree of dilation.

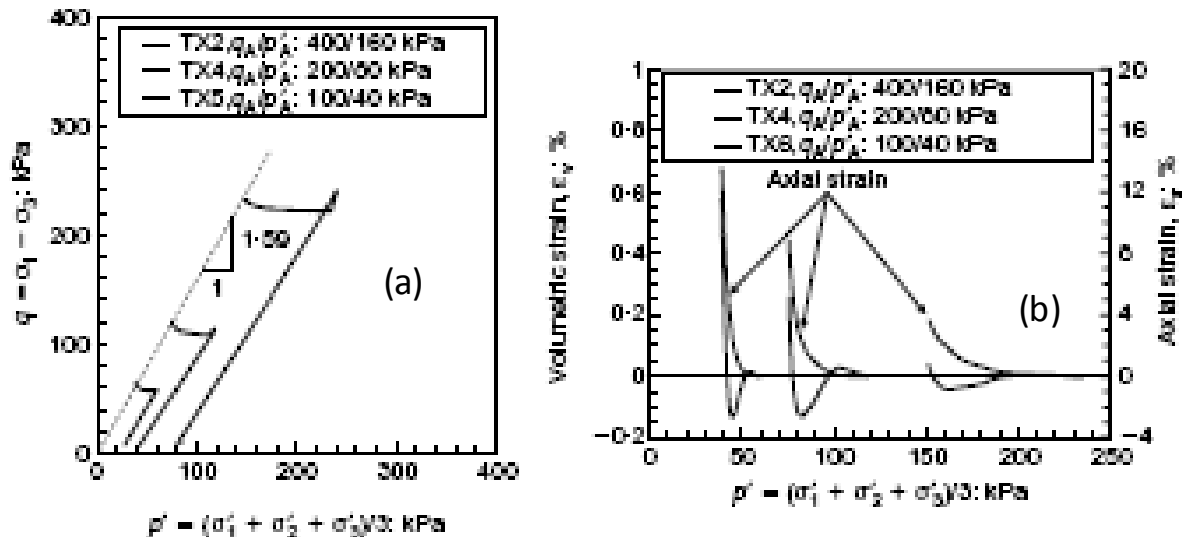


Figure 5 - CSD triaxial tests, Gruben moraine: (a) stress path data; (b) axial and volumetric strain against mean effective stress (after Springman et al., 2003).

Prediction of an ‘apparent cohesion’ term has been made by Springman et al. (2003), adopting a factor of safety equal to unity and describing this by two different assumptions for the mobilised shear strength at failure. Field shear box data have been used to determine parameters for a Mohr–Coulomb analysis assuming the effect of suction is modelled by this apparent cohesion, which depends on the saturation degree. Alternatively, suction may be estimated from the saturation degree at various depths and included in a shear strength envelope, which is dependent on suction and saturation degree. Despite the simplicity of the analyses and extreme heterogeneity of the moraine, it was found in both cases that the factor of safety reduced almost to unity at depths of between 0.2 to 0.5 m for the 42° slope, as had been observed from the field test.

2. Rüdlingen

A landslide triggering experiment was carried out near Ruedlingen in North East Switzerland in autumn 2008 and spring 2009 to replicate the effects of a heavy rainfall event from May 2002, in which 100 mm rain fell in 40 minutes (Fischer et al., 2003), causing 42 superficial landslides. The slope was subjected to extreme rainfall by artificial means in October 2008 over a period of 4 days, with a rainfall intensity of 15 mm/h for the first two days and an intensity of 30 mm/h for the last two days. The sprinklers were distributed at constant spacing along the central line of the slope. Some surface movements were detected during this extreme event, although failure did not occur. Subsequently, a range of measures was implemented, such as relocating the distribution of the sprinklers to provide more rainfall to the upper part of the slope, so that a failure mechanism was triggered in March 2009,

incorporating about 130 m³ of debris (Springman et al., 2009; Casini et al., 2010; Askarinejad et al., 2010).

The experimental area selected is located on an east facing slope on the banks of the river Rhine. The altitude is about 350 masl. The average gradient was determined using a total station theodolite to be 38° with maximum of 43° in the middle of the slope. The surface is slightly concave; the middle longitudinal line is 0.3 to 0.5 m lower than the sides, except that the slope drains marginally to the north at the bottom.

The experimental slope was originally covered by forest, with coverages of circa 80%, at heights of 5-20 m. Shrubs up to 1-5 m high and a free herb layer each cover circa 50% of the surface. The preliminary root reinforcement was quantified by Schwarz & Rickli (2008), using measured distribution of the roots, standard models and samples for small field tension tests.

The site is located in the Swiss lowlands. The bedrock consists mainly of Molasse, which is the sediment that was deposited in the foreland basin of the Alps. The Molasse consists of alternate layers of sea deposits under the Tethys Sea (Seawater Molasse) and land deposits (Freshwater Molasse). Several augured samples as well as an outcrop of the bedrock about 20 m above the selected field revealed horizontal layering of the (fine grained sand- and marl/mudstone) sedimentary rocks at the experimental slope (Tacher & Locher, 2008). The saturation and drainage characteristics of a slope may exert a major control on the prevention, or triggering, as well as the shape of any failure. Depending on the efficiency of preferential flow, and on how this flow is initiated, soils saturate differently (Kienzler & Naef, 2008). Therefore, infiltration characteristics at the Ruedlingen experimental slope were evaluated with combined sprinkling and dye tracer tests (Springman et al., 2009). The experiments revealed a high infiltration capacity of the soil. No overland flow was observed during the sprinkling at any of the three locations. After excavation, flow paths of the infiltrated water were clearly visible by the dye patterns (Fig. 6a). In all of the soil profiles, staining of the soil was mainly homogeneous and little preferential flow was visible. The dye patterns showed complete and homogeneous saturation of the whole soil profile with only little preferential drainage and with perched saturation above the sandstone bedrock. These results confirmed the high vulnerability of the slope to failure and led to expectations of a deeper-seated failure above the transition to bedrock rather than a more surficial failure that is typical for many rainfall-induced landslides (Springman et al., 2003). However, stained fractures below the subsoil revealed that substantial drainage might occur into the bedrock, which could prevent complete saturation and failure of the instrumented slope.

The behaviour of soil was investigated under saturated and unsaturated conditions. Soil was collected from Test Pits excavated to different depths. The grain size distributions with depth for TP 1 are shown in Figure 6b. The clay fraction increases with depth from 4% at shallow depths to 10% at around 2 m. The silt fraction also increases with depth from 25% to 32%, while the sand decreases from 67% to 56% (Fig. 6b). The clay is active in the upper part ($I_A > 1.25$) and is normal below 1 m depth ($0.75 < I_A < 1.25$). The soil can be classified as medium-low plasticity silty sand (ML) according to USCS. The fines content played a significant role in the behaviour of slopes, and on the mode of failure, because the strength, amount and rate of infiltration, and therefore the change in degree of saturation were strongly influenced by this.

The results for isotropic consolidation – standard drained compression (CIDC) and undrained (CIUC) triaxial tests, plotted all together in the $\sigma_q - \sigma$ (where $\sigma_q = 2/3(\sigma_a - \sigma_r)$, $\sigma = q/p'$; $\sigma_a = \sigma_h/h$; $\sigma_v = -\sigma V/V_0$; $\sigma_r = (\sigma_v - \sigma_a)/2$; $q = \sigma_1 - \sigma_3$; $p' = (\sigma_1 + 2\sigma_3)/3 - u$) plane (Fig. 7a), were

exploited to detect a possible critical state stress ratio. In spite of the data variability, typical of natural samples, a value of $\eta_{CS} = 1.30$, corresponding to a critical state friction angle of about $\theta'_{CS} = 32.5^\circ$, seems to represent the critical state conditions for this soil fairly well. The only exception is noted in test TX4 (Fig. 7a), which was carried out at the lowest confining pressure (Fig. 7b), in which disturbance and low stress conditions may cause some variability. The entire set of stress paths followed by the soil elements in the standard tests is summarised in Figure 7b, where the assumed critical state line (CSL) is drawn (Casini et al., 2010).

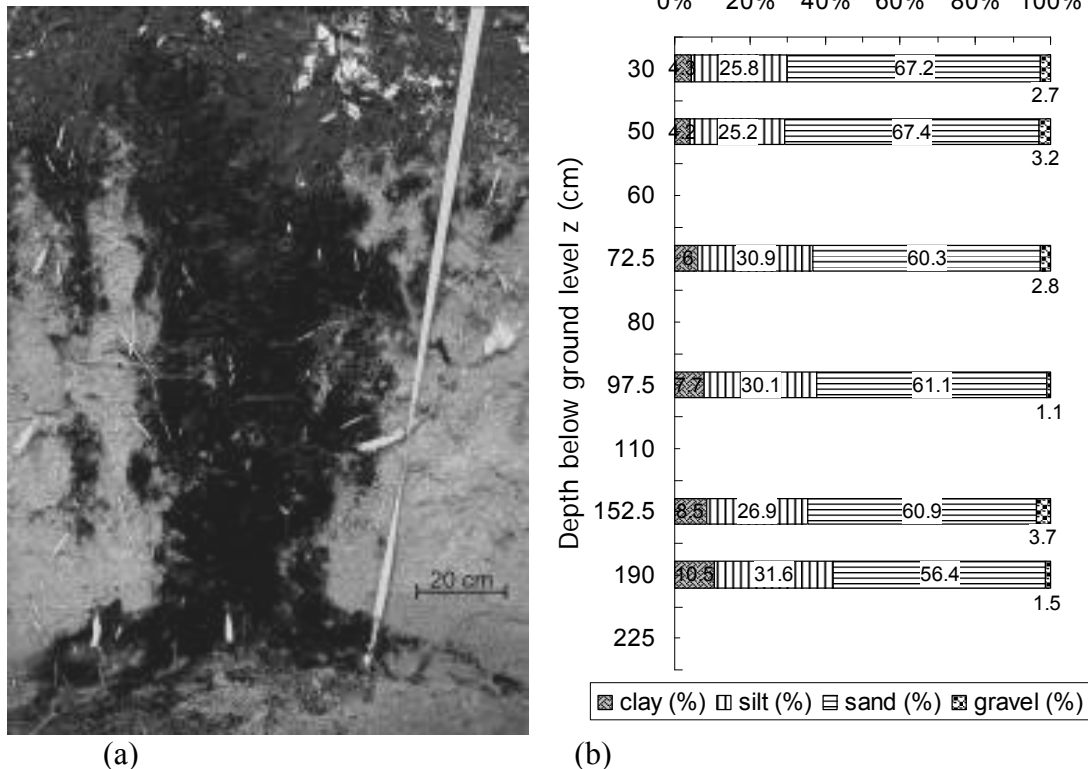


Figure 6 - (a) Dye pattern in the middle section of a test pit; (b) grain size distribution with depth.

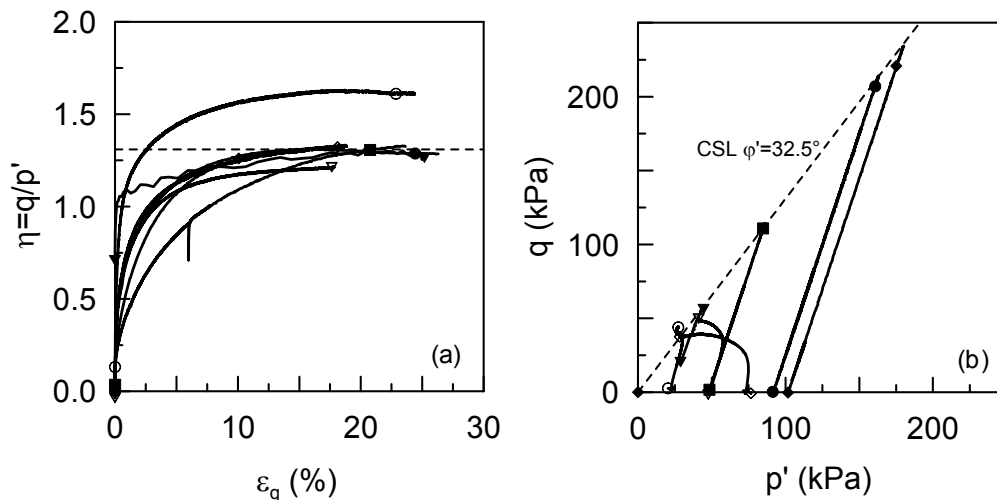


Figure 7 - Triaxial tests results for natural sample in saturated conditions: (a) ϵ_q - η plane ; (b)

p'-q plane (after Casini et al., 2010).

Figure 8 shows 3 sets of TDR measurements over 16 hours of intense rainfall in March 2009, when the distribution of the sprinklers was relocated to provide more rainfall to the upper part of the slope, during which time the volumetric water content of the surface layers increased from ~25% to around 55%. Pore water pressures were also measured at six depths between 0.15 m - 1.5 m. Since the beginning of the rainfall, negative pore water pressures reduced most quickly in the deeper layers, from roughly -7 kPa to becoming positive with a maximum value of 9 kPa. The increase in pore water pressure to positive values (saturated conditions) is particularly important given the accompanying decrease in effective stress and hence reduction in mobilised shear strength that may lead to failure. A slope stability analysis was performed using the same approach as Springman et al. (2003) but extended to a laterally limited rectangular slide. A critical depth of $z = 1.12$ m is obtained for a pore water pressure of -2.9 kPa. All the other depths investigated needed less suction for a safety of factor $FoS = 1$. The approach used is quite simple with all the limitations of limit equilibrium analyses. But it can be applied to predict the zone of potential failure, which in the field experiment was located at a depth $z \sim 1.25$ m. The pore water pressure mobilised at failure was higher than the critical value determined here. This is due to a more complex response of the soil in comparison to the simplified hypothesis of limit equilibrium analyses (Casini et al., 2010). The slope before and after failure is shown in Figure 9 (Springman et al., 2009).

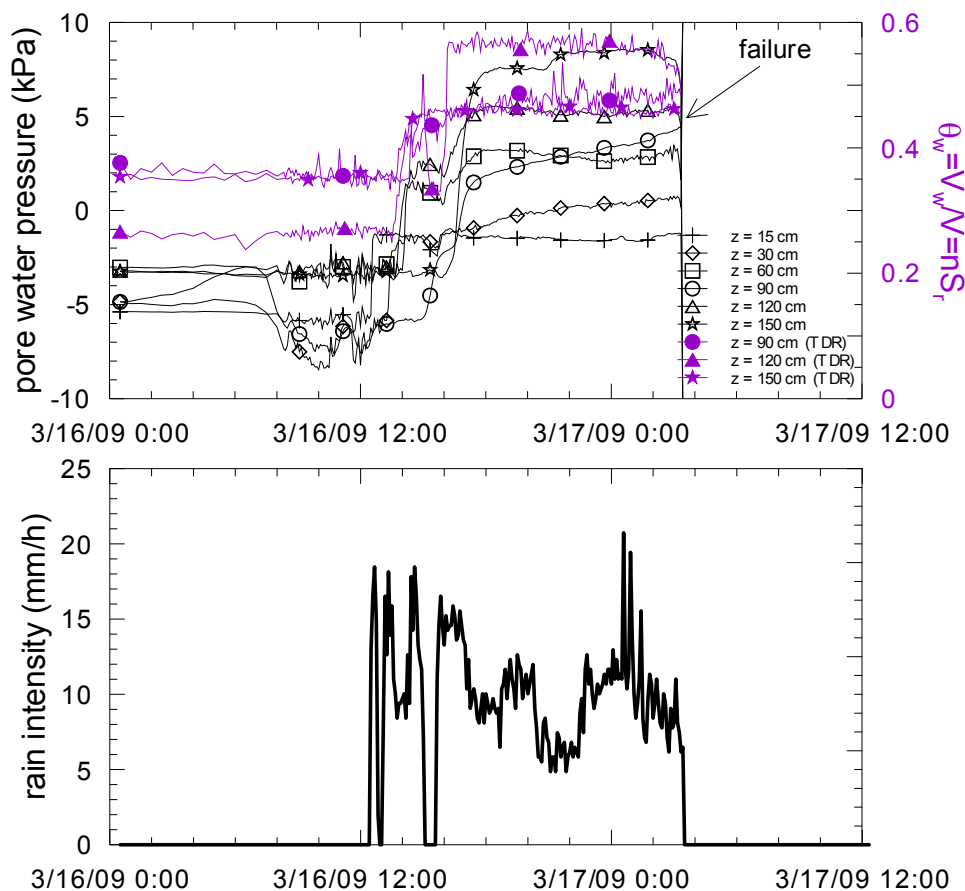


Figure 8 - Tensiometer, TDR measurements, rain intensity with time, March 2009 in

Rüdlingen.

Figure 9- Rüdlingen slope: before and after failure on 17th March.

3.2 FULL-SCALE SLOPE EXPERIMENTS IN FINE GRAINED SOILS (CNRS)

This section summarises the knowledge gained from hillslope hydrology experiments whose objectives were to understand the mechanism of water infiltration (Darcy matrix flow, preferential flow in fissures and macropores) in the topsoil of two landslides developed in black marls (Super-Sauze mudslide, Laval landslide). The two landslides are characterised by different initial hydrological conditions: nearly saturated conditions for the Super-Sauze landslide and unsaturated conditions for the Laval landslide (Figs. 1 & 2). A multi-technique approach was set up to monitor soil deformation (DGPS, terrestrial laser scanning) and soil hydrology (e.g. groundwater level measurements, soil water content monitoring, chemical tracer analysis (chlorure and bromure), seismic tomography and Electrical Resistivity Tomography -ERT-, Travelletti et al., in press).

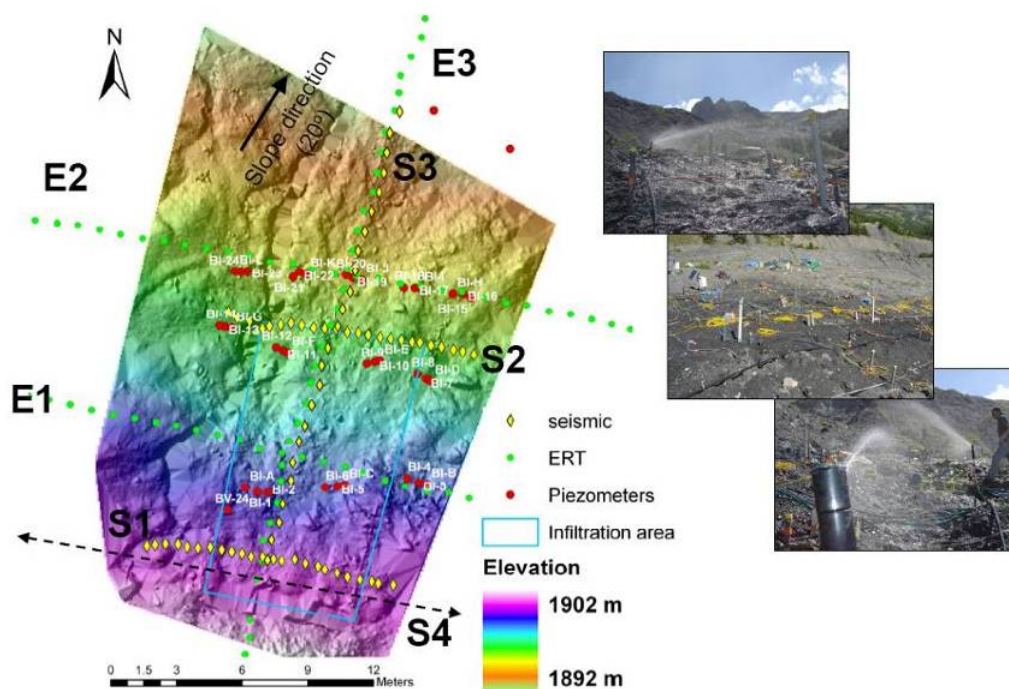


Figure 1 - Hillslope hydrology experiments on the Super-Sauze mudslide: topography of the rain experiment area with the ERT--seismic surveys and the position of the piezometers.

The objective of the hillslope hydrology experiments is to understand the hydrological system of the landslide better and to quantify the impacts of preferential flows on the hydrological behaviour. This section presents a summary of the water movement analysis based on the interpretation of Electrical Resistivity Tomography monitoring (ERT), using a time-lapse inversion approach. The specific objectives are: (i) to characterise the spatial and temporal development of the water infiltration front and the subsurface flow in the soil and, (ii) to identify the time when the conditions of steady-state flow (e.g. constant water flow rate) is reached.

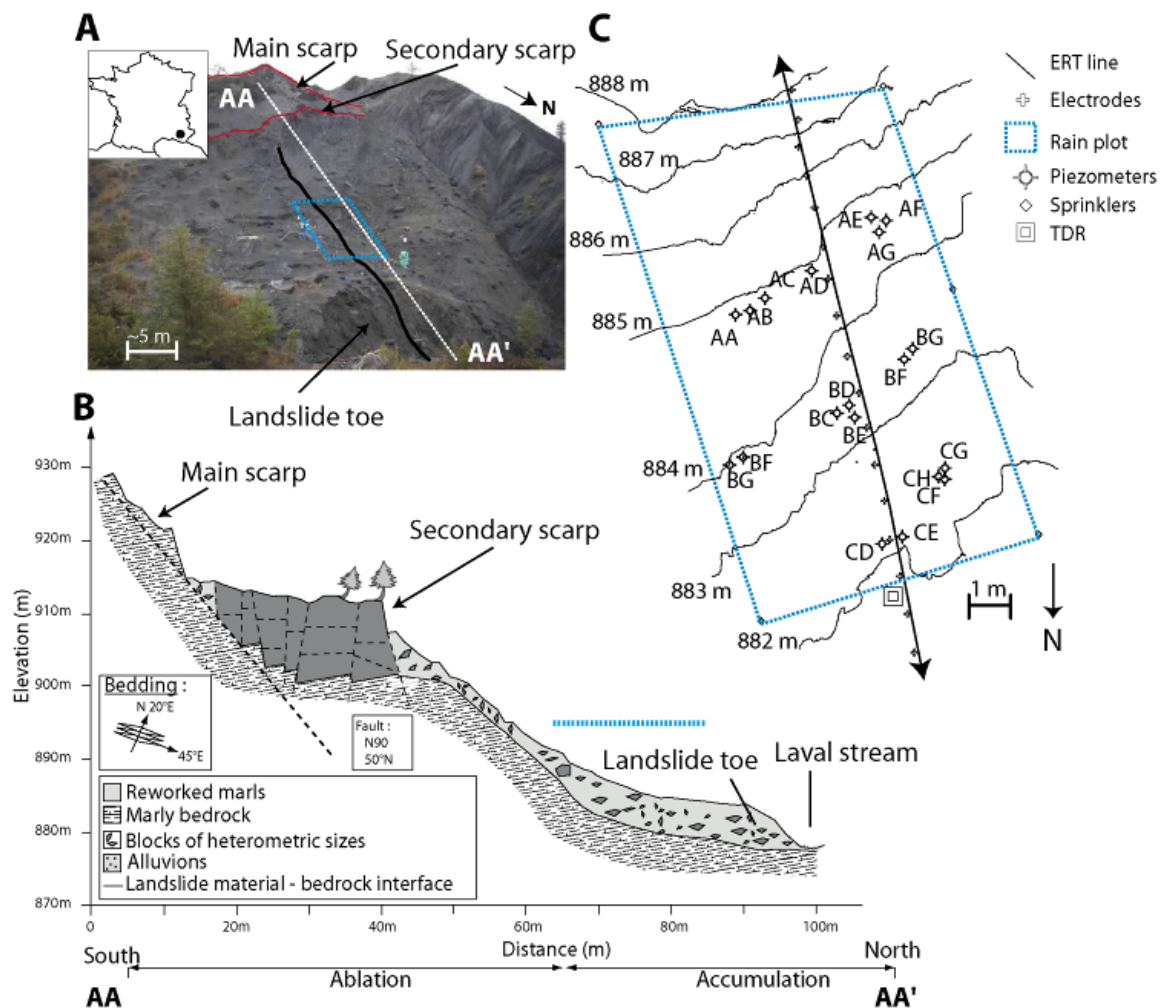


Figure 2 - Hillslope hydrology experiments on the Laval landslide: (a) Photograph of the Laval landslide. The rain experiment plot and the location of the ERT line are detailed. (b) Cross section of the landslide. (c) Monitoring equipment installed on the rain experiment plot.

1. Methods

The rainfall experiment was conducted on a representative plot of about 100 m² during several days with a mean rain intensity of 11 mm/h. The artificial rain was produced using a water pump and six sprinklers located along the borders of the experimental plots.

The ERT tomography lines crossed the central part of the experimental plots (Figure 1a, c; Figure 2) and the ERT lines coincide with the centre of the experimental plot. The upstream part of the ERT line (Laval landslide) and the extremities of the transversal ERT lines (Super-Sauze landslide) are located outside of the artificial rain in an area called the ‘dry plot’. The system features an internal switch-system board for 48 electrodes with 1 m inter-electrode spacing. Thus the image resolution is expected to be high enough to image the global development of water infiltration and subsurface flow in the slope. Hydrological processes occurring at the centimetre scale are not detected with this electrode spacing. Three to six stacks were systematically replaced for each quadripole in order to obtain a maximum standard deviation of 3% for the repeated measurements. Data acquisition lasted approximately 15 minutes; an acquisition was conducted every 1 to 3 hours. For the first

experiment in Super-Sauze, a Wenner-Schlumberger configuration was applied because it offers a good compromise in the signal/noise ratio. Then a Dipole-Dipole configuration was used in the Laval landslide because the resistivity value measurements were more accurate and there was low electrical noise of the surroundings (Rings & Hauk, 2009).

2.Data analysis: influence of temperature on the resistivity values

Soil temperature was monitored near the experimental plot along a vertical profile at different depths to determine the effects of soil temperature on the resistivity values. The temperature influences on the resistivity values were found to be negligible below 0.5 m in reworked black marls (Figure 3), using the relationship proposed by Keller & Frischknecht (1966),

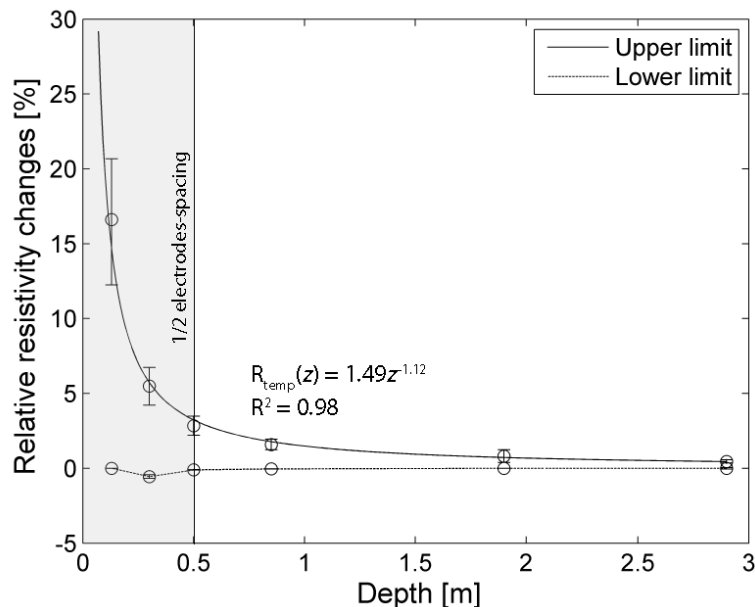


Figure 3 - Maximum of relative resistivity variation caused by soil temperature changes. The maximum in the relative resistivity changes are located above 0.5 m depth. Above that depth, the inverted resistivity models are poorly resolved (less than $1/2$ electrode-spacing).

3.Data analysis: approach used for time-lapse inversion

The apparent resistivity values were inverted using the time-lapse approach based on cross-models implemented in the *RES2DINV inversion software* (Loke, 2006). Several types of cross-models were used to estimate any errors in the inverted resistivity values. The Root Mean Square error (RMS) and the stability through time of the inverted resistivity values observed in the dry plot of the inverted models are used to select the best inverted cross model (Fig. 4).

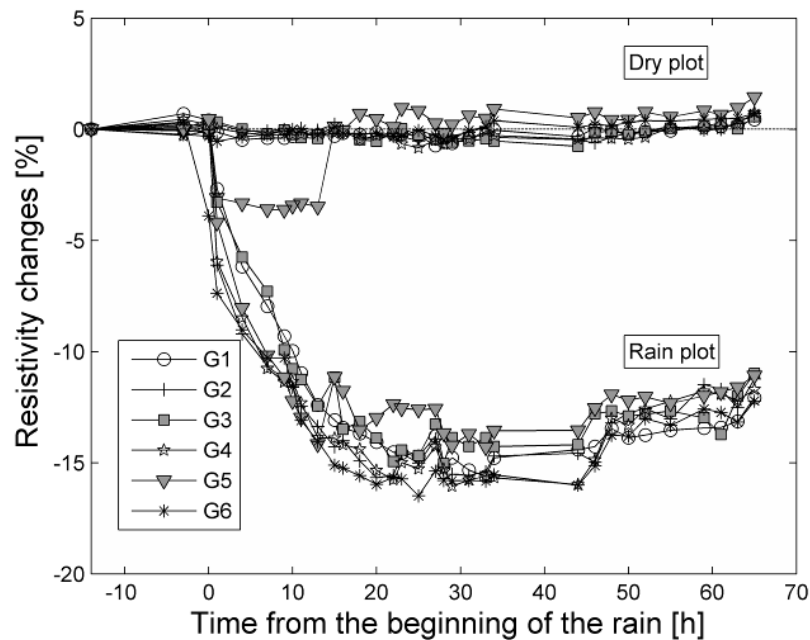


Figure 4 - Inverted resistivity changes within the dry plot (149 nodes) and within the rain plot (207 nodes) for six cross models groups “G” for the data acquired in the Laval landslide experiment.

4.Results: Super Sauze mudslide experiments (initially saturated conditions)

The signal/noise ratio is too low to detect an evolution of the infiltration front: the resistivity changes in the rain plot are similar to those measured in the dry plot (Fig. 5). The variations observed in the electrical resistivity are mainly due to the changes in water salinity. Water runoff measured at the surface shows that a relatively small quantity of water infiltrated the rain plot. This illustrates that the initial hydrological condition plays an important role in the detection of resistivity changes in these environments.

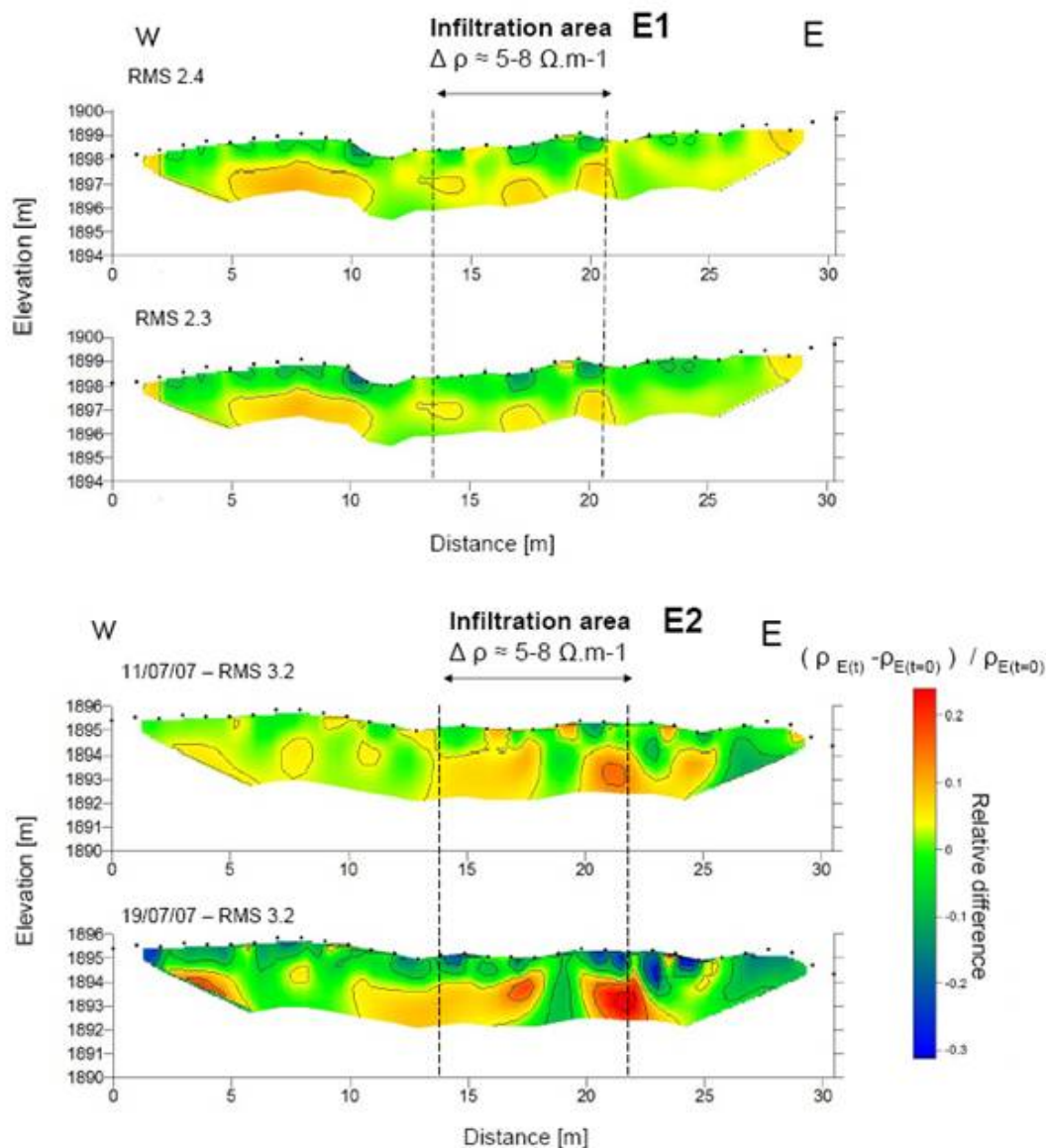


Figure 5 - Relative comparison of E2 & E1 (Fig. 1 for the location) to the reference before the start of the rain experiment.

5. Results: Laval landslide experiments (initial unsaturated conditions)

The signal/noise ratio is better than in the Super-Sauze experiment. The clear response in the resistivity values allows the timing of steady-state flows to be determined and leads to the establishment of a conceptual hydrological model.

6. Determination of steady-state flow time:

The steady state flow time is strongly correlated with time of constant resistivity values (validated by constant water levels observed in the piezometers) (Fig. 6). Steady state flow conditions are reached 21 h after starting the rain. The topsoil is characterised by relatively short times varying between 5 h and 15 h \pm 1 h while deeper locations mostly reached steady-

state flow conditions after 20 h to 28 h \pm 1 h (Fig. 6). More time is needed for locations downstream outside the rain plot (30 h to 35 h \pm 5 h) to reach steady-state conditions. This time difference between areas outside and inside the rain plot strongly suggests the development of subsurface lateral flow during the rain experiment. The steady-state flow times are in agreement with the time when constant water levels are measured in the piezometers. Two preferential flow paths could be detected near the abrupt change of slope delimiting the landslide toe from the other part of the landslide body (Fig. 6). These flow paths induce fast water infiltration until the weathered clay-shales / bedrock interface thus leading to steady-state conditions after a short time of rain experiment (ca. 15 h \pm 2 h). These preferential flows are probably connected through the interface between the weathered clay-shales and the bedrock. An apparent hydraulic conductivity value K_s of $1.7 \cdot 10^{-4}$ m/s can be derived, based on the determination of the steady state flow times and the average hydraulic charge of the piezometers. This relatively high apparent saturated hydraulic conductivity shows how fast the soil is draining the infiltrated water as soon as steady state conditions are reached.

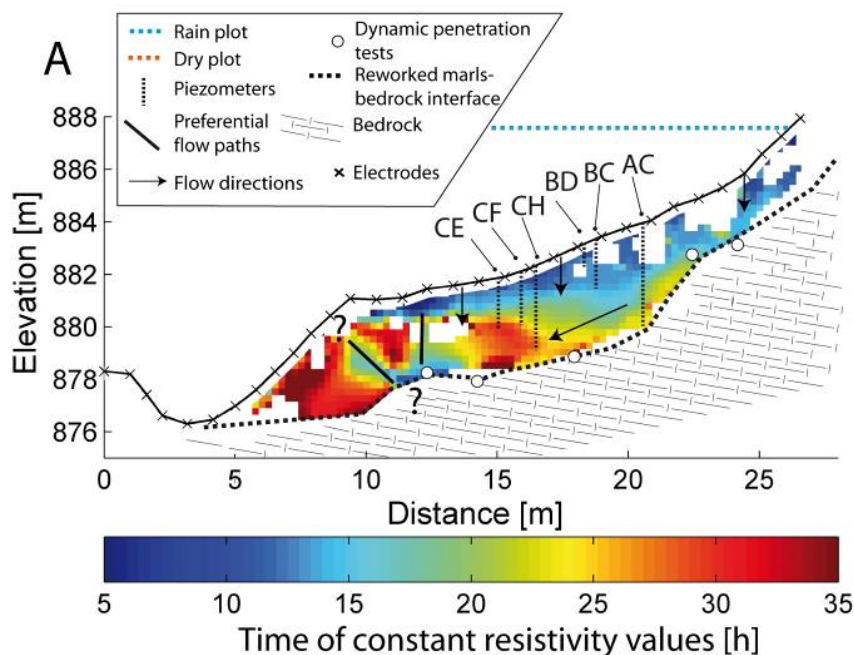


Figure 6 - Times to reach constant resistivity values. Two preferential flow paths are suspected near the Laval landslide toe. The development of a subsurface lateral flow inside the rain plot at depth is also suspected.

7. Conceptual hydrological model:

A decrease of resistivity (e.g. negative anomaly) is observed with time directly following the onset of the rain (Fig. 7). This observation reflects the development of a wetting front, progressing mainly vertically during the first 10 h of the experiment. The area located downstream and outside the rain plot is then affected by a negative anomaly showing that a lateral subsurface flow is developing. After 30 h of rain, this lateral subsurface flow may have reached the Laval stream (Fig. 7). A conceptual hydrological model can be proposed based on the time evolution of resistivity changes and the location of steady-state flow conditions

inside the rain plot. The wetting front is estimated by the isovalue of -5% of the resistivity change (Fig. 8).

- t_0-t_{0+5h} : in the first hours of the rain experiment, the wetting front has already penetrated the first metre of the top soil. The preferential flow paths located near the landslide toe allow water to reach the bedrock interface rapidly;
- $t_{0+5h}-t_{0+12h}$: vertical water infiltration is still dominant. Steady-state flow conditions are reached in the topsoil. Consequently, the groundwater level observed in piezometer BD stays at its maximal level. In the deepest piezometers CH and AC, the groundwater levels start to rise progressively. At the same time, water infiltration occurs on the top of the landslide toe, probably supplied by surface water runoff coming from the rain plot. In that area, the preferential flow paths are still draining water to the bedrock depth, where steady-flow conditions are reached progressively. The wetting front starts infiltrating downslope, showing the formation of subsurface lateral flow that is draining water to outside the rain plot;
- $t_{0+12h}-t_{0+15h}$: inside the rain plot, steady-state flow conditions are progressing faster in depth than outside the rain plot. The wetting front reaches the bedrock interface;
- $t_{0+15h}-t_{0+20h}$: the surrounding soil of the preferential flow paths progressively entered in steady-state flow conditions and the ground could be considered to be very close to saturation. Consequently, subsurface lateral flow starts to develop inside the landslide toe. Surface water runoff contributes also to infiltrating water at the toe;
- $t_{0+20h}-t_{0+25h}$: the entire rain plot is under steady-state flow conditions. Groundwater levels remain at a constant level in nearly all piezometers;
- $t_{0+25h}-t_{0+30h}$: the subsurface lateral flow may have connected the Laval stream. Steady-state flow conditions are reached both in the landslide toe and in the rain plot.

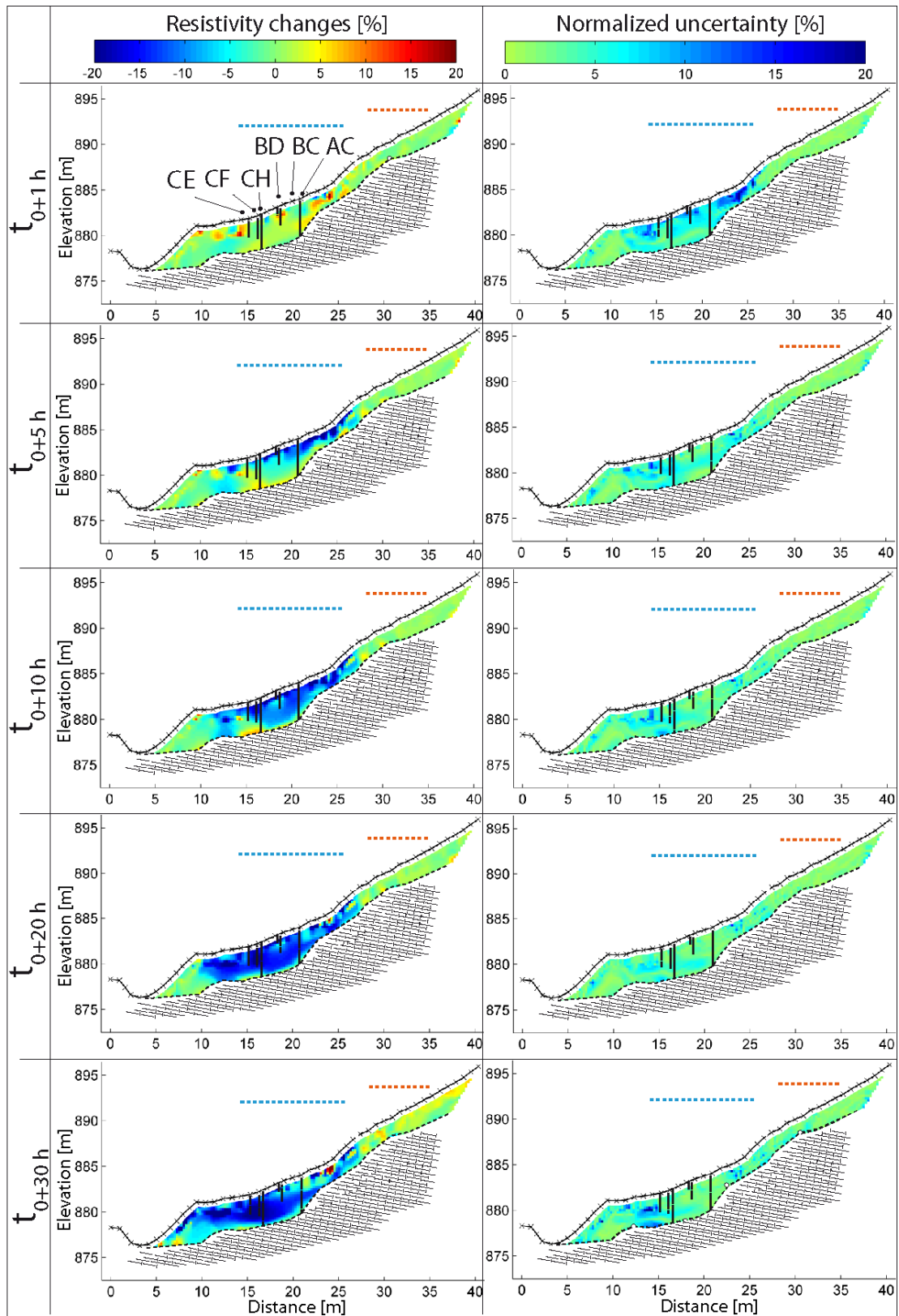


Figure 7 - Resistivity changes during the rain experiment on the Laval landslide with the associated uncertainty. The development of subsurface lateral flows can be highlighted.

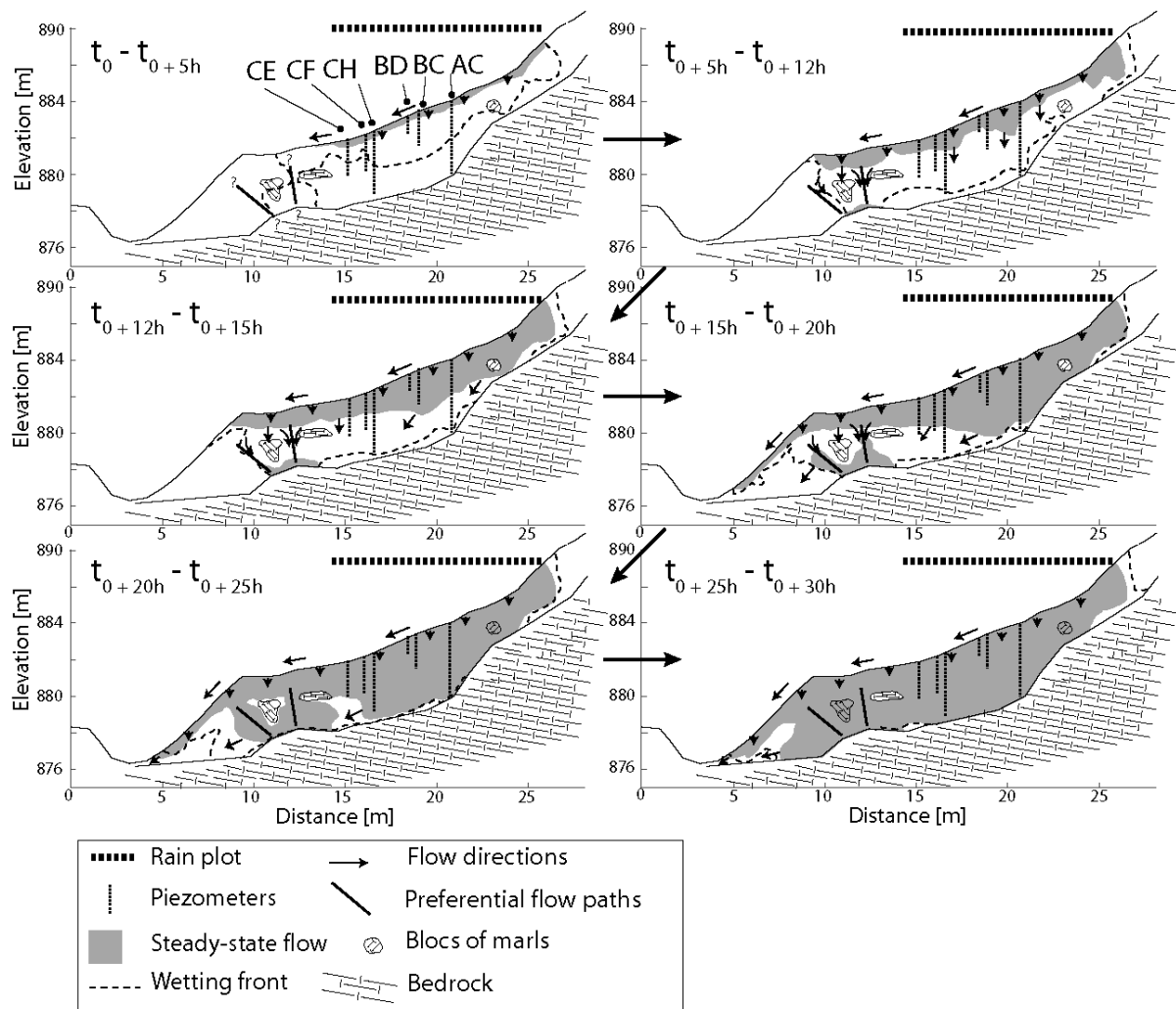


Figure 8 - Hydrological concept of water infiltration during the rain experiment. In the first hours, vertical infiltration is dominant, then lateral subsurface flows develop along the landslide material-bedrock interface. Two preferential flow paths near the landslide toe allow water to reach the bedrock in a short time after the beginning of rainfall. Areas characterised with longer times to reach steady-state flow conditions are identified as marly blocks.

3.3 SYNTHESIS

The reproduction of landslide processes at a greatly reduced scale is widely acknowledged not to be fully representative of full-scale behaviour due to the difference in stress levels between model and landslide. This problem is overcome by conducting full-scale experiments in the field.

Two field test sites in moraine at Gruben (Canton Wallis), Field 1 with an area of about 100 m² and an average slope gradient of 31° and Field 2 with an area of about 55 m² and an average slope gradient of 42°, were instrumented for artificial rainfall tests. Devices were installed to measure suctions and volumetric water content, pore water pressures and rainfall intensity, to investigate the hydro-mechanical slope response. In a test period in summer 2000 the 42° slope (Field 2) failed after two days of artificial rainfall, during which the degree of saturation, S_r , increased to 95%. It was noted that the degree of saturation did not reach an asymptotic value over 2 days. Suctions reduced in the shallower layers, from roughly -30 kPa to a minimum value of -4 kPa, steeper than the internal angle of friction. It is concluded that the reduction in suction is particularly important in the stability of the moraine slopes. Suctions greater than 4 kPa appeared to be sufficient to maintain slope stability. Instability occurred in the steepest slope only when S_r approached 0.95.

Another experiment was carried out in autumn 2008 and spring 2009 at a slope with an average gradient of 38°, with a maximum of 43° in the middle of the slope, in coarse-grained soils near Rüdlingen in North East Switzerland to replicate the effects of a heavy rainfall event from May 2002. Failure was triggered in March 2009 incorporating about 130 m³ of debris. Measurements have shown that the volumetric water content of the surface layers increased from 25% to 55%. Negative pore water pressures reduced most quickly in the deeper layers, from roughly -7 kPa to becoming positive with a maximum value of 9 kPa. As in the first example the increase in pore water pressure to positive values (saturated conditions) is particularly important given the accompanying decrease in effective stress and hence reduction in mobilised shear strength that may lead to failure. A limit equilibrium analysis was performed to validate the results.

Two full-scale hydrology experiments that were performed in the topsoil of two landslides developed in black marls (Super-Sauze mudslide, Laval landslide) are presented in order to understand the mechanism of water infiltration (Darcy matrix flow, preferential flow in fissures and macropores). The rainfall experiments were conducted on a representative plot of about 100 m² during several days with a mean rain intensity of 11 mm/h. Information, such as infiltration times, flow velocities, apparent hydraulic conductivities obtained from those experiments at a large scale are necessary to establish hydrological concepts for the hydro-mechanical modelling and interpretation of hydrologically triggered failure processes.

4 KNOWLEDGE OF SLOPE FAILURE MECHANISMS FROM LONG-TERM MONITORING OF NATURAL SLOPES

4.1 SYNTHESIS OF MONITORED SITES ON COARSE-GRAINED SOILS AND MORAINES (BOTH SHALLOW AND DEEP-SEATED, SATURATED AND UNSATURATED) (ETHZ)

4.1.1 Tössegg, Canton Zürich

A grass covered test slope, with an average inclination of 27° in the North of Switzerland was identified as being suitable for this experiment. In the area surrounding the slope, a series of 42 surficial landslides had occurred in May 2002 after a rainfall event, in which 100 mm rain fell in 40 minutes (Fischer et al., 2003). Most of these slopes, consisting of weathered sandstone, have been stable due to suctions, which have been reduced to a critical value due to this extreme event. Many such failure events had been observed in the slopes along the Rhine between the villages of Rüdlingen and Eglisau, over the prior five years, characterised by saturation of a relatively porous soil (weathered sandstone) layer (of around 1 m in depth) and slip along a planar soil-rock interface (Thielen et al., 2010).

Prior to the design of the experimental setup, a combination of geophysical, geological and geotechnical methods was applied during a multiphase site investigation (Thielen et al., 2005; Friedel et al., 2006), which yielded a model of the subsurface (Fig. 1). Interestingly, the investigations revealed a layered soil structure, with a less permeable layer overlying a more permeable one, and this was found to influence the soil response quite markedly. A layer of clayey sand, up to 1.5 m thick, overlies weathered sandstone (silty sand) just above the rock surface. The sampling procedures are described in Thielen et al. (2005) and provide information about the soil properties (grain size distribution, plasticity index, permeability and density) for both soil types, which are summarised in Table 1 (Thielen, 2010).

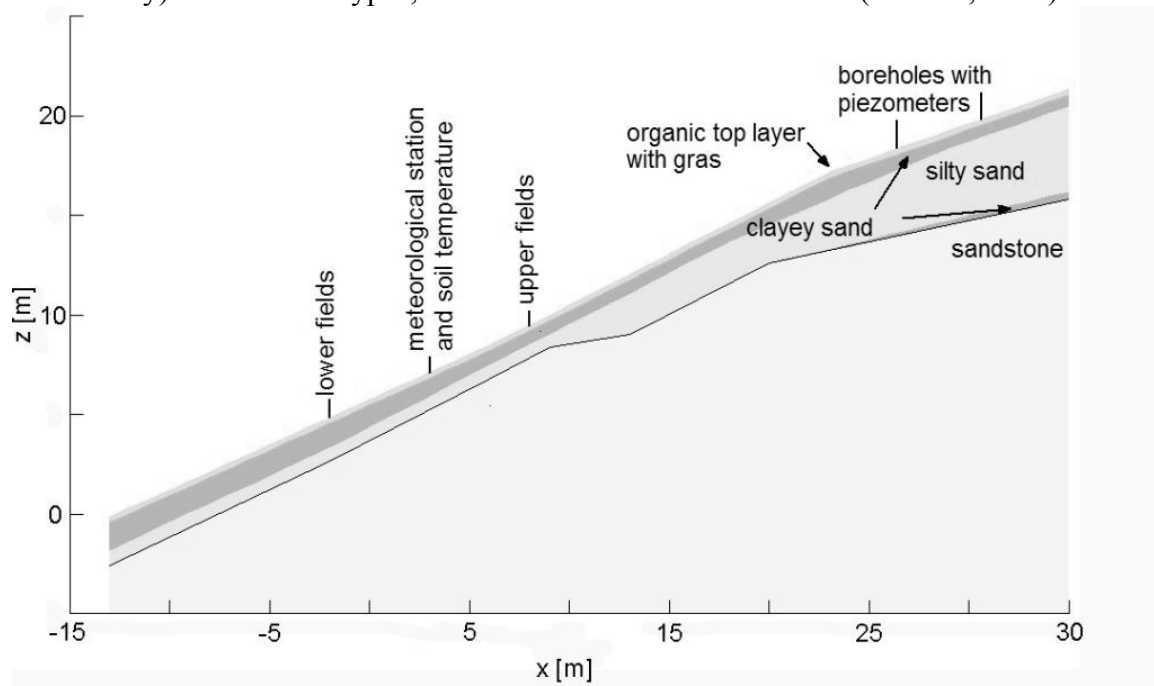


Figure 5 - Model of the longitudinal section through the slope (after Thielen et al., 2005).

Table 1 - Soil properties (after Thielen et al., 2005).

	Clayey sand	Silty sand
Grain size distribution		
Grain size [mm]	% passing	% passing
< 31.5	100.0	100.0
< 0.5	97.0	98.3
< 0.06	41.2	26.8
< 0.02	23.3	15.8
< 0.002	7.1	5.6
Plasticity analysis		
I _p [%]	7.3-17.8	3.3-5.9
w _L [%]	22.6-35.5	22.6-25.1
Saturated permeability [m/s]	~3*10 ⁻⁸	~5*10 ⁻⁶
Dry bulk density [g/cm³]	1.29-1.49	1.29-1.40

The years 2003 and 2004 differed significantly in the amount of rainfall (www.meteoschweiz.ch) and resulting differences in water content were measured in the layer on top of the sandstone. The placement of sensor probes could then be optimised for the monitoring experiment with the help of this information. The instrumented 200 m² test site was located in a part of the field that resembled the critical cross sections from the 2002 storm event, with the added advantage that the above mentioned layers of interest could be reached at relatively low depths.

Figure 2 shows a photograph of the test slope together with the plan and the vertical distribution of the instrumentation. Four clusters of instruments were installed, with matching sets at key depths, as well as a central location for soil temperature and meteorological measurements.

The volumetric water content of the soil was measured using two types of Time Domain Reflectometry (TDR and Moisture point (www.esica.com)). Useful experience has been obtained with this combination of instruments in moraine by Teyssere et al. (2000), Springman & Teyssere (2001) and Springman et al. (2003). Two types of tensiometers were used for the measurement of suction: tensiometers with electronic pressure transducers for continuous data logging (grey points in Fig. 2a) and tensiometers for manual readout installed to verify the continuous data (grey quads in Fig. 2a).

The locations of three piezometers that have been installed in boreholes in the upper part of the slope, in order to observe the level of local water tables, are shown in Figure 1. These were important in trying to understand the local hydrology of the slope, in terms of subterranean flow into the underlying silty sand layer. A more detailed description of the instrumental setup and the measuring devices and calibrations can be found in Thielen & Springman (2005) and Thielen (2007).

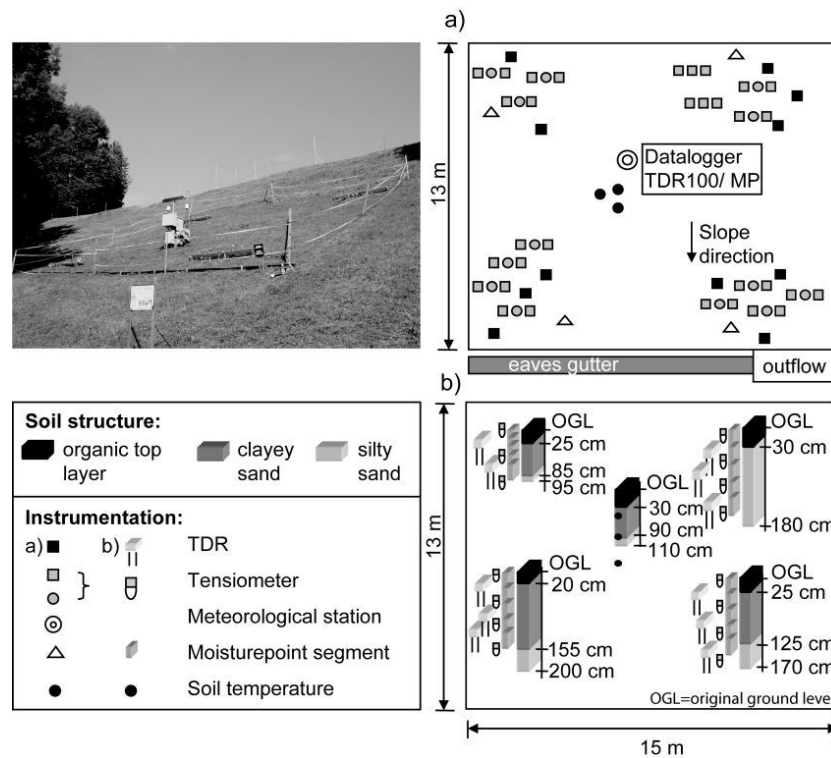


Figure 6 - Picture of the test slope and instrumentation design of the test site (a) plan view, (b) vertical distribution of sensor probes and layers of the soil model. OGL is Original Ground Level.

The measurements of every device were recorded by the data logger every 10 to 15 minutes from August 2004 until July 2006. The manual readout tensiometers yielded weekly data. Although there were some gaps in data, a number of significant rain events (52 events; Thielen, 2007) were recorded, although none of these approached the severity of the May 2002 storm.

Seasonal response of the soil-water balance in the test slope could be observed for the four instrumented fields (Fig. 3). In particular, two extremes of behaviour were identified, in which the upper clayey sand layer was saturated with suctions approaching zero (winter regime), and a summer regime with suctions exceeding about 80 kPa, measurable by tensiometers due to cavitation and lower values for the volumetric water content. The variations of volumetric water content in the soil (θ_v) with depth are subject to seasonal fluctuations, which tend to reduce with increasing depth. In summer, the water content in the top soil layers is dependent upon climatic influences. In autumn, the top clayey sand layer becomes saturated and water starts to infiltrate into, and recharge, the underlying more permeable layer, which is also more liable to flow parallel, downslope or into the bedrock. Additional recharge from any preferential flow paths in upper layers or upslope contributes to the more dynamic fluctuations in water balance in this lower layer. The upper clayey sand layer more or less remains saturated during the winter period. Onset of saturation and desaturation tends to occur later with depth, the phase shift ranging by up to two months.

Figure 3 shows suction and volumetric water content data for the entire measuring period, for different depths for the right side of the field. Highlighted in grey are the zones with measurements in silty sand, the other zones consist of clayey sand. Interestingly, the layering

is rather different with 15 cm of soil on the upper right location and 120 cm of the clayey sand on the lower right of the field, but this is below all sets of instruments at 15, 60, 120 and 150 cm in depth. The silty layers play a greater role on the right side of the field (see Figs. 2 & 3).

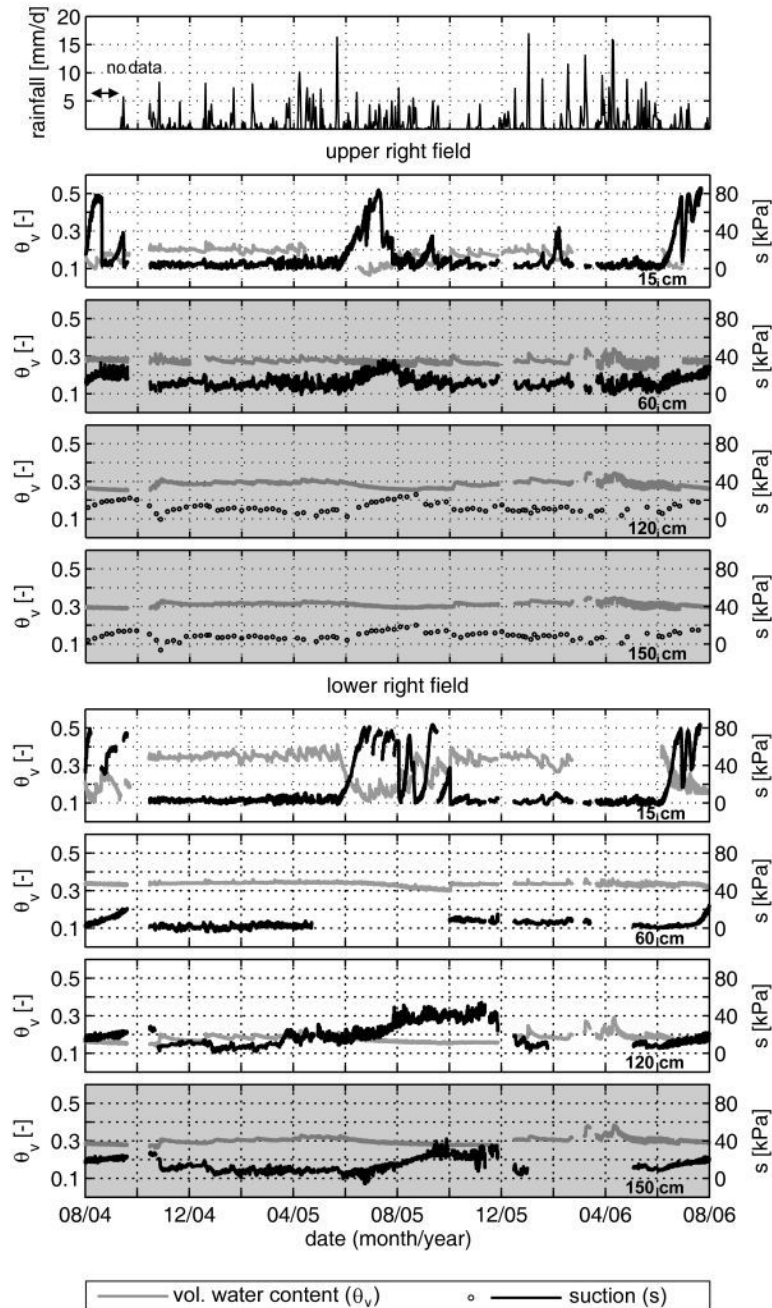


Figure 7 - Rainfall, volumetric water content (Moisturepoint/TDR data) and suction (Tensiometer data) for the right field side during the monitoring experiment.

The tensiometer data generally agrees with the corresponding TDR or Moisturepoint data. Increases in volumetric water content are accompanied by a decrease in suction, and a decrease in volumetric water content is accompanied by an increase in suction. In the summer periods (August 04 until September 04, June 05 until October 05 and after June 06), the water

content in the top soil layer fluctuates markedly due to climatic influences (e.g. rainfall, temperature, air humidity, evapotranspiration). These short term variations can be observed up to a depth of 45 cm. At a depth of 60 cm, the data appears to be smoother; the water content decreases continuously with increasing suctions, and climatic conditions do not influence the water content very much. The most important hydrological finding of the experiment was the seasonal two-phase soil moisture behaviour of the slope with a typical summer and a typical winter character. This typical winter and summer characteristic could be observed in terms of the influence of the respective rainfall events.

4.1.2 Gruben, Canton Wallis

Two surface areas at approximately 2800 masl near to the Gruben glacier were selected as field test sites (slopes of 31° field 1 & 42° field 2), to investigate the influence of relative density and degree of saturation of the soil on the slope stability in a moraine. A sprinkler system was constructed in the middle of these test areas to supply sustained rainfall over several days. The steeper slope failed. The soil response in terms of water content and suctions was measured (more details are reported in deliverable 2.1). A layout of the instrumentation installed in Field 1 and Field 2 is given in Figures 4a, b & c. The instrumentation was removed prior to the winter of 1999/2000 and then a marginally different setup was reinstalled for 2000. Extensometers were set up in 1999 to obtain a line series of surface deformations. Up to 2 mm downslope extension was measured. Following difficulty in 1999, tensiometers were used successfully in 2000 to measure suctions during the intermittent artificial and natural rainfall and the subsequent recovery periods on the 31° slope. Runoff was ~ 80% for this slope and type of storm.

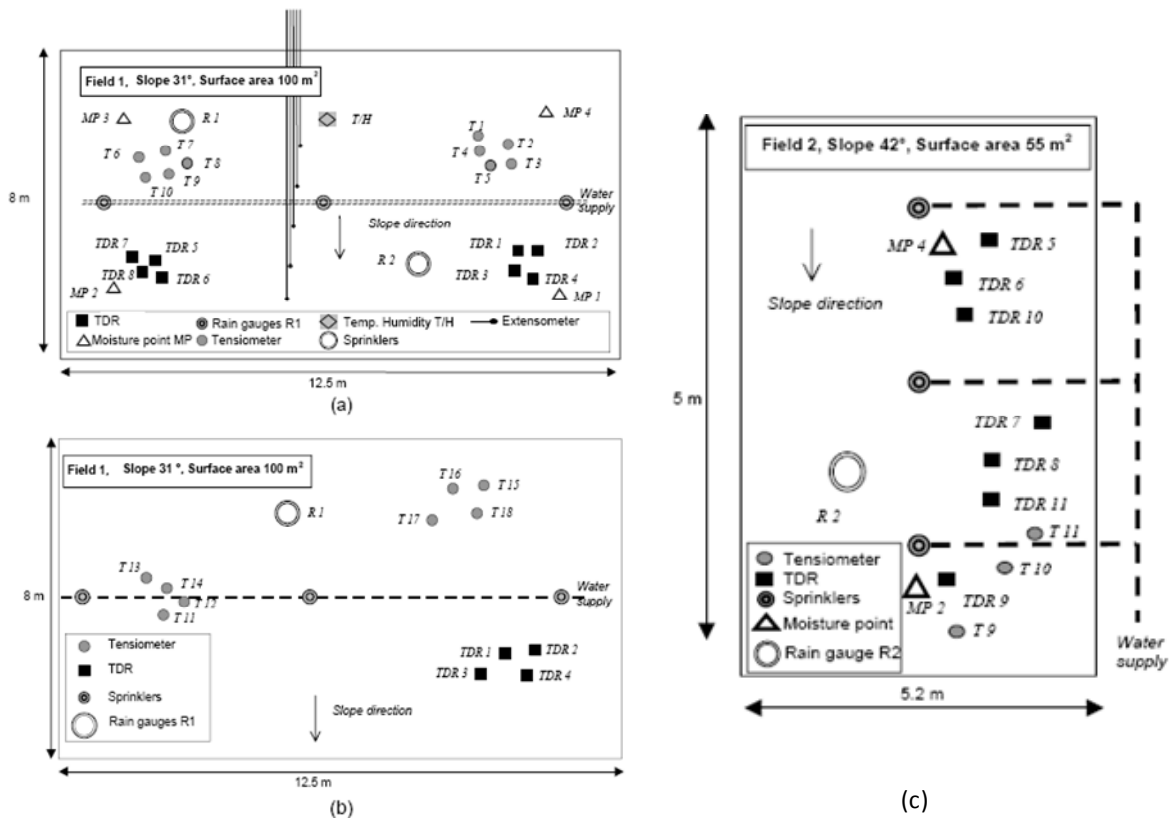


Figure 8 - Test field and instrumentation layout: (a) Field 1/1999; (b) Field 1/2000; (c) Field 2/2000 (after Springman et al., 2001).

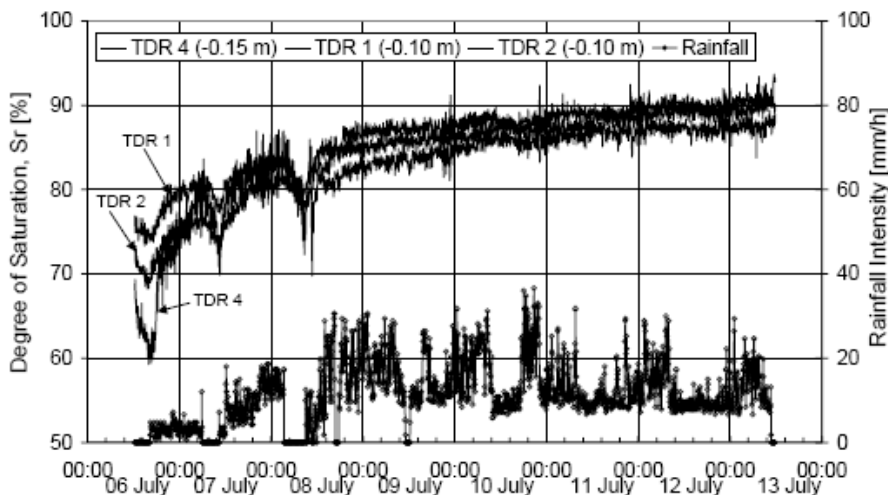


Figure 9 - TDR and rainfall measurements (artificial rain). Field 1/1999 (after Teyssere et al., 2000; Springman et al., 2001).

1. Testing Procedure: Field 1/1999

A continuous water supply was created by pumping from Lake 1 (Fig. 2) so that artificial rainfall could be simulated on a slope over a test field area of approximately 100 m². Intensities varied between approximately 10-30 mm/h, depending on the local wind

conditions, corresponding to an extreme rainstorm (Fig. 5). It is known that there are differences between artificial and natural rainfall, so response was also monitored following the artificial storm. Several smaller, but nonetheless significant, natural events were recorded. The duration of the artificial rainfall test was 7 days with a total amount of rainfall of approximately 1.9 m, followed by a further 42 day period of natural rainfall.

2. Testing Procedure: Field 1/2000 and Field 2/2000

In year 2000, both test fields were to be subjected to a lower rainfall intensity (actually between 8-22 mm/h) over a longer period, with calibration of response from 1999 to 2000 from using the same Field 1 (but with slightly less instrumentation). However after ~2 days, the 42° slope failed and the tests were stopped (see deliverable 2.1). The common water supply system led to slight variations in rainfall, but these were in phase with each other, so that the rainfall distribution was similar for both fields.

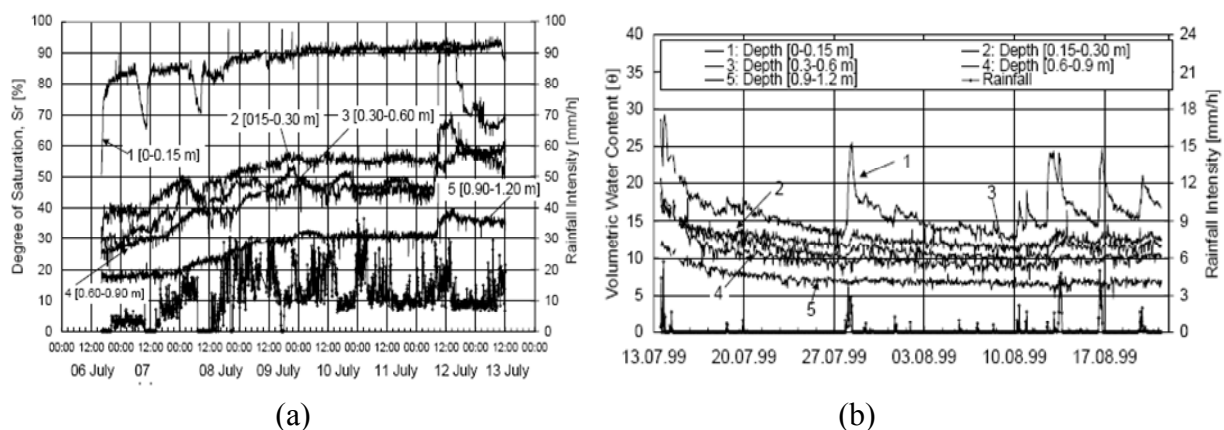


Figure 10 - Moisture Point measurements Field 1/1999: (a) artificial rain; (b) period following test (after Teyssere et al., 2000; Springman et al., 2001).

Figure 5 shows three sets of TDR measurements (TDR 1, 2, 4) compared to rainfall intensity over 7 days of intense rainfall, during which time, the degree of saturation in the surface layers increased from 60–75 % up to around 90 %. Pauses in the rainfall (during the 1st and 2nd days) are clearly seen on the response curves, with very little delay between the change and the measurement of a reduction in saturation. Figure 6a shows the extent of the water penetration for depths up to 1.2 m from the MPs in terms of the degree of saturation S_r . The top segment (No. 1) between 0 and 0.15 m confirms the response measured by the TDRs, and is very sensitive to any changes in the rainfall intensity. The decrease in S_r (i.e. from MP No. 2 to No. 3 to No. 4 and No. 5) develops slower with increasing depth. Figure 6b shows the reduction in volumetric water content θ or θ_v for the period following the test, and hence implies that there will be recovery of suctions after the artificial rain was stopped. The field was only subjected to natural rainfall for 42 days after the test.

To reach unstable conditions in such soils on a slope slightly less steep than the critical state friction angle requires large changes in the water content and a flow regime. The steep trend observed in Figure 6a suggests that by increasing θ and hence S_r by 10-30 % immediately in response to rainfall, small, but nevertheless significant, decreases in suction will also be caused inducing decrease in the mobilised shear strength. As soon as critical conditions develop within the soil mass, sudden movements can occur and the unstable soil mass will fail (Springman et al., 2001).

4.1.3 Rüdlingen, Canton Schaffhausen

The selected experimental area is a steep, forested slope in Ruedlingen, North Switzerland, where 42 surficial landslides occurred (Fischer et al., 2003) in spring 2002, after extreme rainfall (100 mm fell in 40 minutes). Asprinkling experiment was carried out in autumn 2008 to investigate the hydrological and mechanical behaviour of the slope. This test was followed by a triggering experiment in spring 2009 (more detail in deliverable 2.1).

The area is located on an east facing slope on the banks of the river Rhine (Springman et al., 2009). The altitude is about 350 masl. The average gradient of the slope was determined using a total station theodolite to be 38°. During the preliminary investigations, sandstone and marlstone were located at a depth of between 0.5 m to more than 5 m along the 30 m x 7.5 m plan section (Askarnejad et al., 2010). The behaviour of soil was investigated under saturated and unsaturated conditions (Springman et al., 2009; Casini et al., 2010a & b). The average saturated permeability of soil was determined to be $k_{\text{sat}} = 1 \cdot 10^{-7}$ m/s. The soil can be classified as medium-low plasticity silty sand (ML) according to USCS.

An extensive instrumentation plan was designed to measure hydrological and geo-mechanical responses of the slope. Detailed measurements of soil suction, water level and soil volumetric water content were combined with an investigation of subsurface flow at the lowest part of the slope by means of tracer experiments. Deformations were monitored during the experiment, both on the surface via photogrammetrical methods and within the soil mass, using a flexible probe equipped with strain gauges at different points and two axis inclinometers on the top (Askarnejad, 2009). The instruments were installed, mainly in three clusters, in the slope. The instruments included jet-fill tensiometers, TDRs, Decagon TDRs, piezometers, a soil temperature sensor, deformation probes, earth pressure cells, acoustic sensors and rain gauges (Fig. 7). The tensiometers were installed at depths of 15, 30, 60, 90, 120, and 150 cm below the ground surface in each cluster. Decagons were installed at shallow depths of 15 to 60 cm every 15 cm, and TDRs from 60 cm to 150 cm, with a spacing of 30 cm. All the instruments were calibrated and checked in the laboratory to ensure that they functioned properly before installation in the field. The hydrological responses of the soil were measured during the experiment with a logging interval of 5 minutes.

The artificial rainfall was applied by means of 10 sprinklers, with equidistant spacing, located on the middle longitudinal line of the field. The lower sprinklers experienced higher hydraulic heads as the water was supplied from the upper part of the slope. Therefore, the rainfall was not uniformly distributed. The average applied rain intensity is shown in Figure 8a, with an average intensity of 35 mm/hr for 3 hours as the first wetting phase (W1), followed by a 20 hour stop allowing the soil to drain (first drying phase D1). Afterwards, the slope was sprinkled for 1.5 days with an average intensity of 17 mm/hr, which increased with a first shock of 45 mm/hr to an average value of 30 mm/hr for another 1.5 days (second wetting phase W2) and then the second drying phase started (D2).

Figures 8b, c, and d show the variations of volumetric water content (VWC) and matric suction at three different depths of 30, 60, and 120 cm, in clusters 1 and 2. After changes in the intensity of applied rainfall, the suction and volumetric water content measurements respond without significant time discrepancy in all 3 depths. This verifies the high infiltration capacity of the soil obtained from the earlier hydrological investigations. At some points during the second wetting phase of the rainfall, the changes in VWC and suction were not contemporaneous. This can be due to either the hysteretic effect of the soil–water retention curve or the difference in the location of the sensors at each depth. The VWC in Figures 8b

and c drops as the suction increases, at the beginning of the second drying phase (D2), but the suction increases up to 2.5 kPa in cluster 2 at a depth of 120 cm (Fig. 8d), and the VWC starts to decrease only after this point. This point can be described as the air entry value of the WRC, which is consistent with the value derived from the laboratory test ($s_{aeV} = 2.7$ kPa).

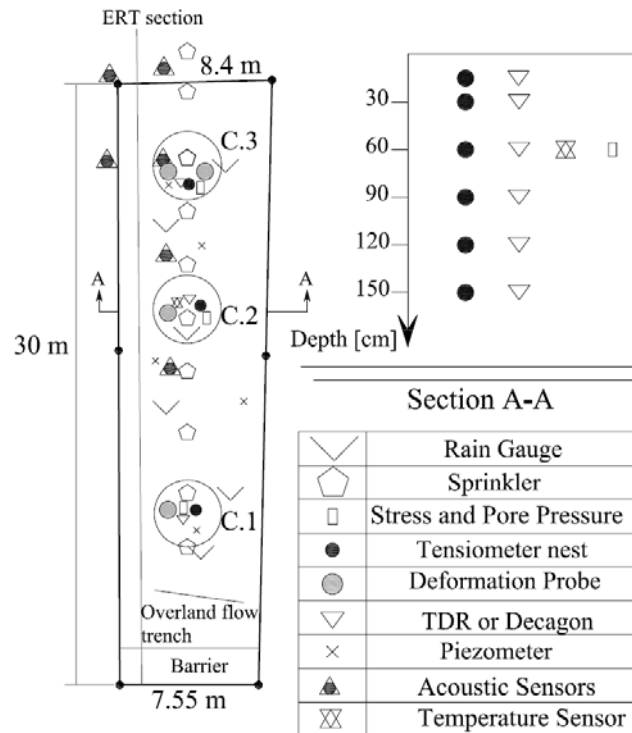


Figure 11 - Instrumentation plan and section (after Askarinejad et al., 2009).

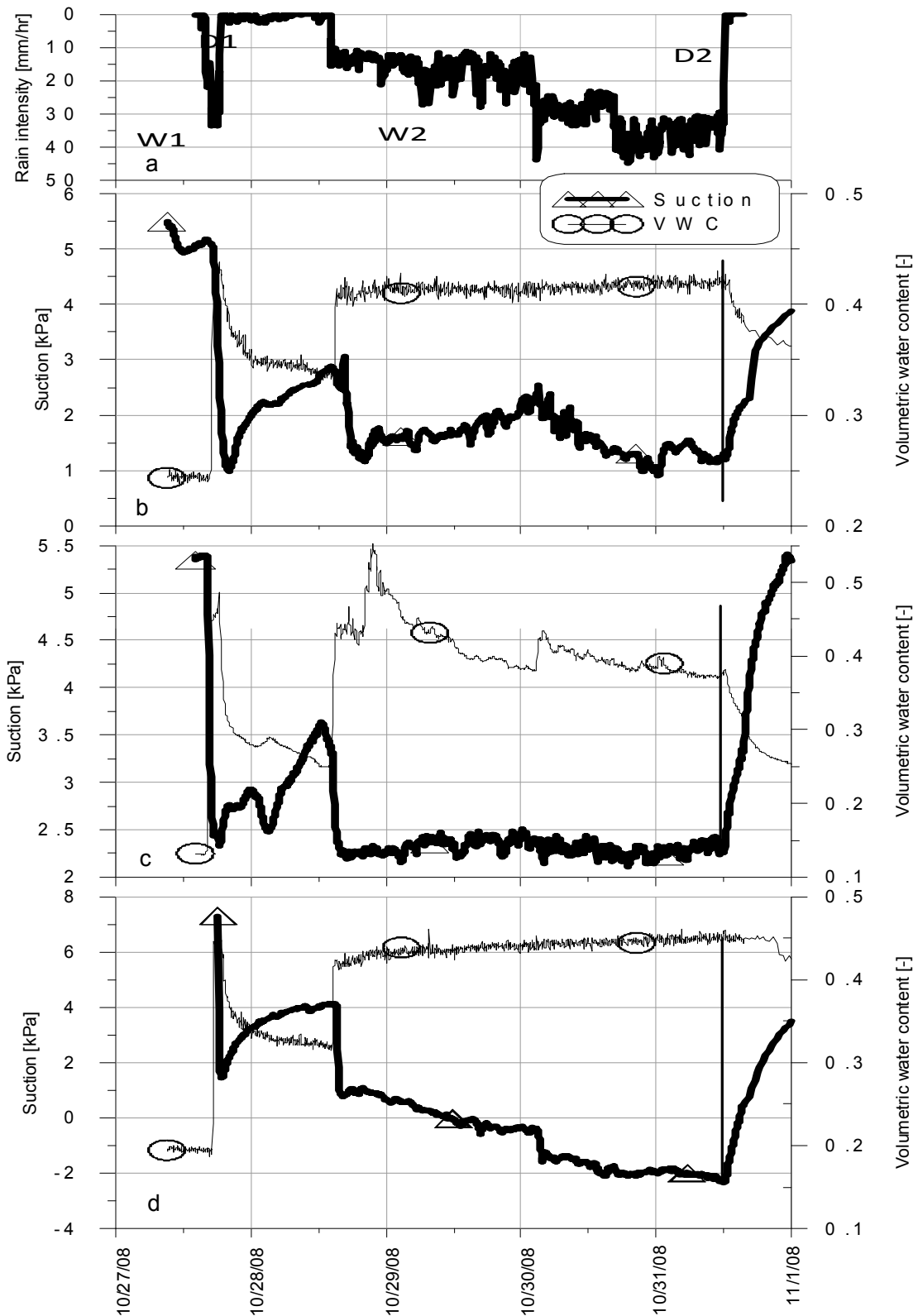


Figure 12 - (a) Average applied rain intensity, (b) Variations of volumetric water content and matric suction in cluster 1 at a depth of 60 cm, (c) cluster 2 at a depth of 30 cm, and (d) cluster 2 at a depth of 120 cm.

4.1.4 La Frasse – Large landslide in tertiary flysch (Swiss Alps)

(EPFL)

1. General context and landslide characterisation

The La Frasse landslide is located in the Pre-Alps of the Vaud Canton in Switzerland (Fig. 9). It's a large landslide, mainly containing decomposed flysch (sandstone and clay schists) with an active, mobilised soil mass of around 42 million m³. Average velocities of the sliding mass are around 10-15 cm/year. The slope has a mean inclination of 11° in the upper, and 20° in the lower part and moves over a length of 2 km, starting at the bottom of the Tours d'Aï, 1500 masl, and going down to the Grande Eau River at a height of 800 masl. It covers an area larger than 2 km². Considering an estimated thickness of 80 m in its upper section and 40 m near the toe, a width between 500 m in the upper and middle part and 800 m in the lower part, the total volume of the sliding mass reaches 73 million m³ (Planchat et al., 2009). The main features of the slide are summarised in Table 1.

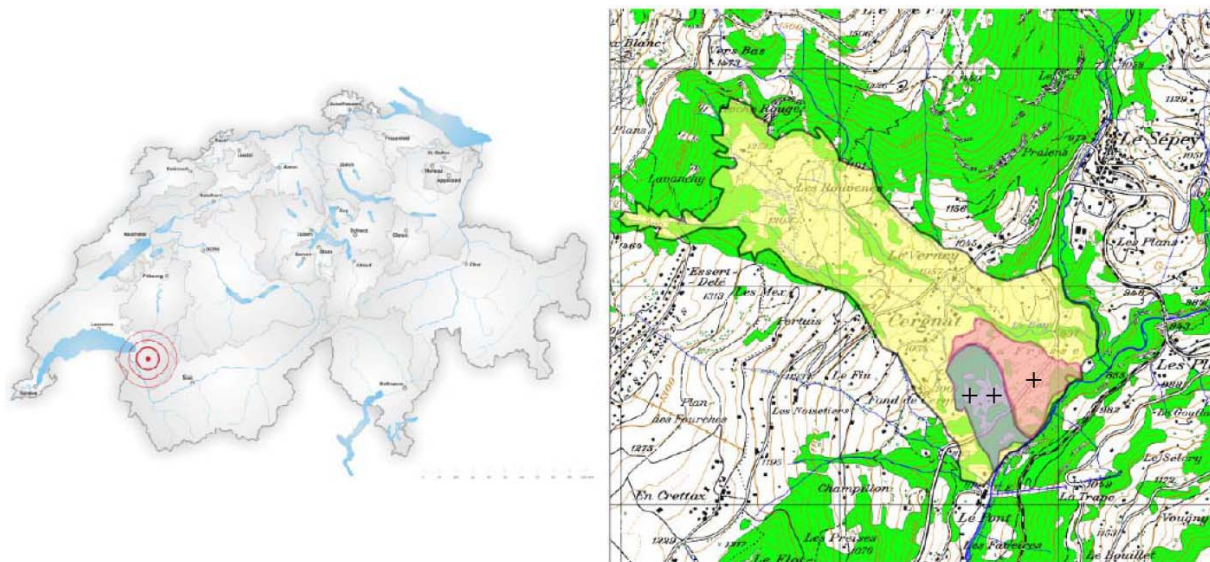


Figure 9 - Location of the La Frasse landslide : within Switzerland (left) ; within its topographic context (right). The most active zones (until installation of a pumping platform in 1994) of the sliding mass include Zone ++ (purple) and Zone + (pink) (Planchat, 2009).

From a geomorphological point of view, an upper and a lower landslide can be distinguished, both of which move in a NW to SE direction along the line of steepest slope (Lugeon, 1922). A secondary scarp zone delineates these two geomorphological features. While sliding velocities reach values of around 5 to 10 cm per year in the upper part of the landslide, the smaller and steeper part below 1000 masl displays variable, higher velocities of up to 20 to 60 cm per year. Inclinator readings in the lower part of the slope have highlighted a well defined and unique failure plane. Deformations are localised along that failure plane, whereas they are relatively small in the sliding body. Some secondary failure planes have been observed in Zone+ (Fig. 9, right).

The main geological feature of the area is a pinched syncline running along a SW-NE axis. The hinge of the syncline is composed of tertiary rocks, namely Eocene siltstone and flysch,

while the outer layers are composed of Triassic dolomite and Malm limestone (Fig. 10). The limestone abutment separating the upper from the lower part of the slope has been heavily eroded during the last Ice Age, but still has a stabilising effect on a volume of 31 million m³ in the upper part of the slope. The sliding mass is mainly composed of flysch, a heterogeneous material containing plastic clay schists and sandstone pebbles crushed by the slope motion and mixed with other rocks (limestone debris or superficial moraine) (Planchat, 2009).

Name	La Frasse landslide
Location	Canton Vaud, Switzerland
Average coordinates	46°21'8''N/7°2'37''E
Active slide area	~ 1 km ²
Max / Min altitude	1500 / 800 m asl
Total length	>2000 m
Average Width	800 m
Average depth	80 m (upper part) / 40 m (lower part)
Volume	~ 42 million m ³ (active slide) / ~73 million m ³ (total slide)
Mean inclination	11° (upper part) / 20° (lower part)
Average velocity	10 – 15 cm/year (upper part) / 20-60 cm/year (lower part)
Geological context	Triassic dolomite, Malm limestones, Eocene siltstones, flysch
Vegetation	Pasture land, wooded zones and swamps
Possible damage	Roads (RC 705 and RC 709), around 40 chalets, hydro-electric plant downstream of the slide and town of Aigle (VD)

Table 1 - General features of the La Frasse landslide (Planchat et al., 2009).

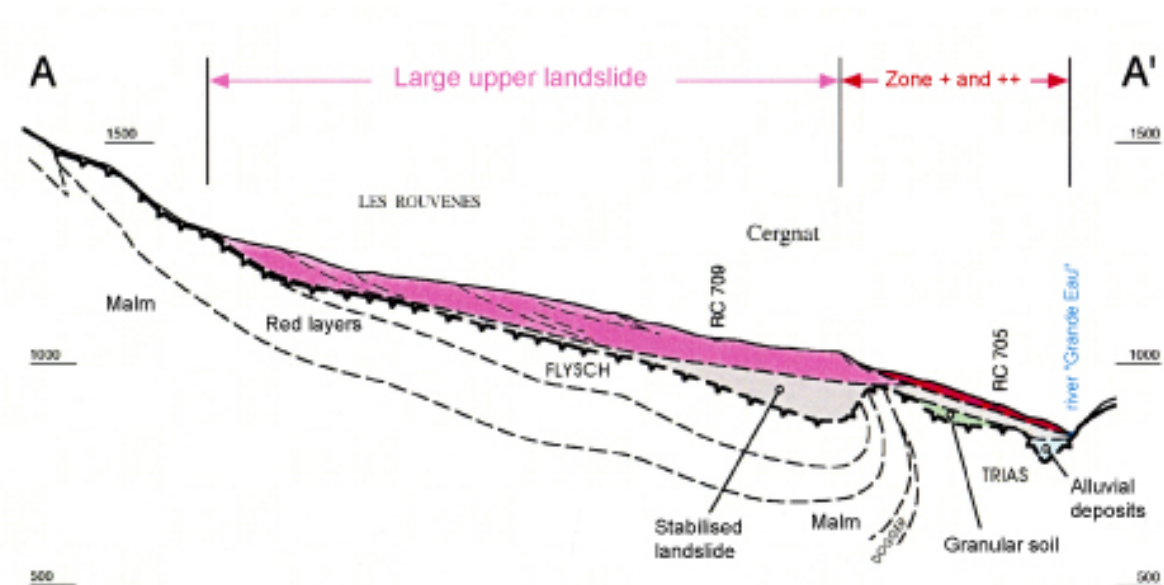


Figure 10 - Geological profile of the La Frasse landslide (NCG-EPFL, 2004).

Due to the heterogeneity of the sliding material, the whole sliding mass can be considered in hydrogeological terms at the landslide scale to be an aquifer (Tacher et al., 2005). Excess

groundwater pressures (artesian levels) have been recorded along the main slip surface, but also within the sliding mass (Tacher et al., 2005). Maximal variations of excess groundwater pressures are measured in the vicinity of the limestone abutment due to the reduced flow section. They are less significant uphill due to gravitational drainage, and at the toe due to the relatively consistent level of the Grande Eau River (Noverraz & Bonnard, 1990). The strong variations of pore water pressures in the aquifer can be related to the low values of the flysch permeability ($\sim 1 \times 10^{-6}$ m/s) and of the coefficient of specific storage ($\sim 1 \times 10^{-4}$ m/s) (Planchat et al., 2009). As reported in the DUTI project (1986), the permeability could locally be much more important due to the presence of gravel channels near the slip surface, but the lack of interconnectivity between the channels was proven by means of pumping tests carried out in 2002, which implies that they are not relevant at the slope scale. There exists no clear relationship between the acceleration phases and either gross rainfall or net infiltration (daily precipitation minus evapotranspiration) (Fig. 11). A better correlation is found if past events up to two years before the day of calculation are considered and if the daily rainfall values below a certain threshold value are neglected (NCG-EPFL, 2004; Tacher et al., 2005). Even then, the contribution of direct surface infiltration remains less important than the subsurface flow. In fact, the La Frasse landslide acts as draining basin for an area of nearly 3 km². The bedrock seems not to be draining the instability. More details on the hydro-geological settings can be found in Tacher et al. (2005).

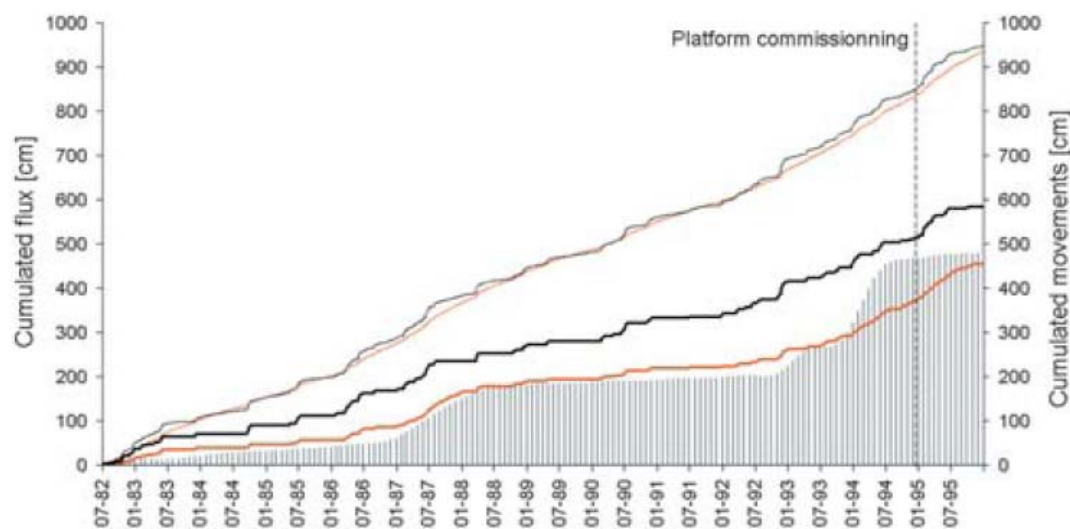


Figure 11 - Relationship between observed horizontal displacements at the RC 705 level and computed flux entering the landslide in a cumulative representation (NCG-EPFL, 2004);

Thin black line: infiltration issued from COUP model (considering temperature, snowmelt, vegetation, soil, sun exposure...); Thin orange line: weighted infiltration; Thick black line: truncated infiltration – daily rainfall < 2 mm/day; Thick orange line: weighted and truncated infiltration; Vertical bars: displacements.

In the past century, several major crises have been recorded (1913-1919, 1966, 1981 and 1994) in which displacement rates were considered to have reached critical values and the landslide has been extensively instrumented. The measurements revealed the presence of two types of triggering mechanisms. The first one is related to external hydrological conditions. Due to prolonged rainfall and low soil water permeability, pore water pressures increase along

the slip surface and in the landslide mass. As a consequence, the shear strength along the slip surface decreases, which leads eventually to the triggering of the instability. The second so called “internal” mechanism is attributed to the sudden occurrence of acceleration phases in periods of rather low precipitation and to the movements recorded between crises. Successive rise and drawdown of the groundwater level, creep deformation or the seepage forces could lead to significant morphological changes. Other factors, such as toe erosion by the Grande Eau River, are supposed to play an important role under certain circumstances (e.g. crisis of 1966).

2. Monitoring history

The current understanding of the La Frasse landslide results from a century long process of investigations and theories of trials and errors. These theories were either accepted or rejected, based on field observations and measurements between and especially during the occurrence of crisis. To this day, there are nearly 60 boreholes and galleries at La Frasse. The first investigation galleries of 95 and 182 m length were commissioned by Lugeon et al. (1922) for their study of the 1913-1919 crisis. In the meantime, these two galleries have disappeared. Displacements of 7.5 m were measured along the cantonal road RC705 between 1913 and 1916, with a further 4 m between 1916 and 1919. This corresponds to sliding velocities of 2.5 m/year and 1.3 m/year, respectively. The significant rainfall between 1910 and 1917 has been highlighted as a likely cause of these accelerations (Lugeon et al., 1922).

Three additional boreholes were commissioned 50 years later by Bersier et al. (1970) for the investigation of the 1966 crisis. After six years of low precipitation, the site experienced heavy rainfall in the second half of 1965. The accumulated snowfall in November and December 1965 reached 518 mm, which represents an augmentation of 135% of the average value (DUTI, 1986). Due to unusually mild conditions, the snowmelt started early, in February, while 163 mm of rainfall was recorded simultaneously that month. Shortly thereafter, the first inhabitants of Cergnat registered claims for damage. At the end of the crisis, in April 1966, the RC705 had moved by 7m in Zone++ (see Fig. 1). The landslide mass in the upper part was affected as well, with displacements amounting to 2 m. Aside from the above hydrological considerations, the impact of the Grande Eau River toe erosion is frequently considered as a triggering, or at least an aggravating, factor for the 1966 crisis.

In 1986, the first inclinometers were installed in a field campaign comprising the creation of 6 boreholes. These works were part of the DUTI study of the 1981 crisis (1986). At the same time, 15 boreholes have been carried out in various stages by the private consultants Norbert & De Cérenville between 1984 and 1989. Between November 1981 and April 1982, the RC705 was displaced by more than 4 m. The acceleration of the landslide was particularly brutal from November 1981 through to the end of the following January. In that period, the average sliding velocity amounted to 10 cm/day. In the upper part of the landslide, the acceleration remained largely unnoticed with velocities of 15 to 18 cm/year recorded near Cergnat until July 1983, compared to the long term average of 10 cm/year. According to the DUTI study (1986), this slight acceleration could have preceded the crisis in the lower part of the landslide.

After a major crisis in 1994, leading to displacements of up to 3 m at the cantonal road RC 705, it was decided to install a pumping platform for drainage purposes and to institute a detailed monitoring campaign. Therefore, 22 boreholes were drilled between 1994 and 1998. As a consequence of the heavy precipitation occurring at the end of 1993, such as the 290 mm

of rainfall recorded in December, the groundwater regime showed significant perturbations. Figure 12 shows the profiles of inclinometer readings in the lower part of the slope (zone++) from 21 November 1994 to 5 January 1995. A rigid body motion can be identified for the sliding mass and a concentration of the displacements along a primary slip surface at 25 m depth.

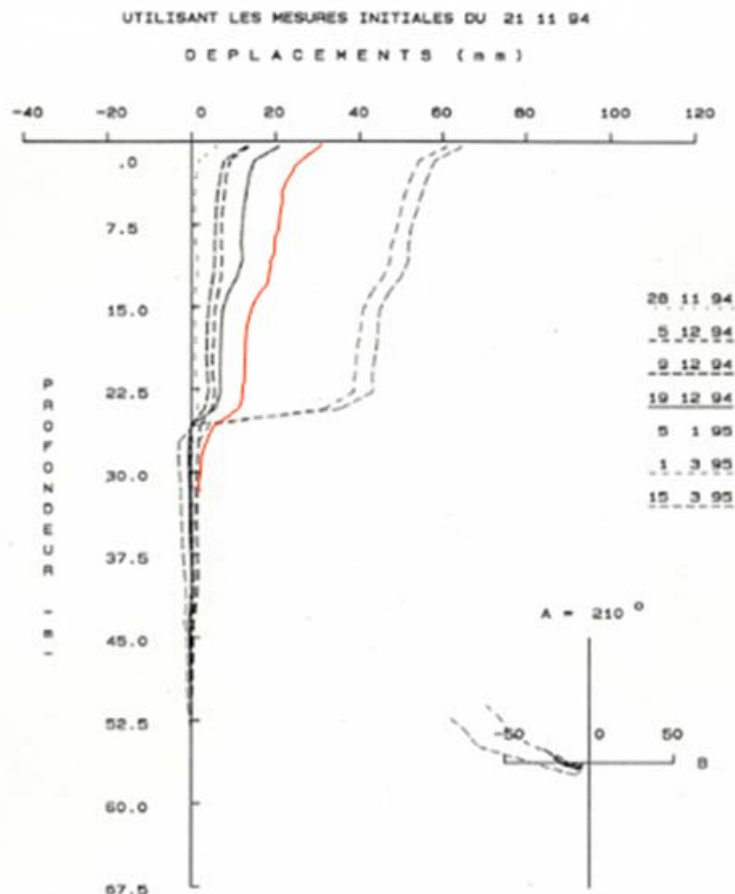


Figure 12 - Inclinometer profile from 21 November 1994 to 5 January 1995 for the La Frasse landslide (Planchat, 2009).

After completion, extracting groundwater from the slope through the pumping platform reduced the displacements significantly, but was only a part of a global stabilisation concept and did not consist in itself in a sustainable solution because of the low tolerance with respect to residual movements and the high costs for maintenance and electricity. In 2004, an expertise group named NCG-EPFL was founded consisting of the two private consultants Norbert Géologues-Conseils SA and De Cérenville Géotechnique SA, as well as the Swiss Federal Institute of Technology in Lausanne. This group was ordered to analyse the past and current situation and evaluate a sustainable solution for a future landslide stabilisation by means of time-dependent, geological, hydrogeological and geomechanical modelling (NCG-EPFL 2004). As a result of the study, it was decided to construct a 900 m long drainage gallery, crossing the whole landslide body. The gallery was completed in March 2009. It is 725 m long with the option to extend it in case the target efficiency is not achieved. 8

additional boreholes were drilled for the study in 2004, and the design of the gallery. The main drainage gallery is equipped with 54 boreholes drilled upwards.

The extensive monitoring campaign since the early 90s was fundamental in assessing the landslide behaviour in more detail. Inclinator and piezometer readings provided essential data that allowed the problem to be approached from a modelling point of view to understand the underlying mechanisms that lead to sudden accelerations of the sliding mass. Several numerical studies have been conducted since, and have greatly assisted in the project for the construction of a drainage gallery (NCG-EPFL, 2004; Commend et al., 2004; Tacher et al., 2005; Laloui et al., 2004; Planchat et al., 2009).

The current monitoring programme comprises subsurface measurements of displacements and pore water pressures, measurements of surface displacements and source outflows. 18 inclinometers are installed for the measurement of subsurface displacements. 32 piezometers measure the pore water pressures at different points in the sliding mass, of which six are equipped with data loggers, which enables real time monitoring of the hydraulic head fluctuations (1 measure/hour). The State of Vaud Department of the Water, Soil and Sanitation Services also closely monitors some of the many springs of the La Frasse landslide. Surface displacements are measured by means of GPS, traditional triangulation with theodolites and, more recently, by a novel laser distance meter. Since 2006, surface displacements are measured by means of a semi-fixed, permanent laser-target installation called ROBOVEC which was developed at the Swiss Federal Institute of Technology in Lausanne in collaboration with the private company GEODEV (Fig. 13).



Figure 13 - Prototype of the ROBOVEC. The laser distance meter is enhanced with a bi-axial modular robotization (Manetti & Steinmann, 2007).

The ROBOVEC has been designed for continuous monitoring of the 3D position of significant points. It allows the distance, horizontal and vertical angles of different points situated on the sliding mass to be measured by means of a laser distance meter and a bi-axial modular robotisation, with a precision of less than 1 cm for a distance of 600 m. The computer piloted ROBOVEC has a wireless connection to the internet. Data can be acquired and the ROBOVEC can be controlled remotely. At La Frasse, the instrument is installed on a concrete pillar on the opposite side of the valley and scans, regularly, the position of 9 geodetic prisms on the sliding mass and 2 reference points outside the sliding area (Fig. 14).



Figure 14 - View of the La Frasse landslide from the opposite side of the valley where the ROBOVEC has been installed in June 2006 (top); one of 9 geodetic prisms that have been installed on the site and a map showing the location of the targets and the ROBOVEC (bottom) (Manetti & Steinmann, 2007).

Figure 15 shows the continuous measurements of surface displacements measured with the ROBOVEC since 2006. The local crisis in August 2007, triggered by heavy rainfalls, is clearly denoted by the surface displacements of points 2, 3, 6, 8 and 11. Total displacements of 50 cm were measured between May and October at point 8. The landslide reached marginal equilibrium in November, but further movements were reactivated at the beginning of December. The sliding mass, moving along a secondary slip surface at approximately 8 m depth, finally reached a stable position in May 2008. 1023 mm of (gross) precipitation was recorded during the first 6 months of 2007, including 600 mm between May and July 2007, compared to a value of 358 mm (an average between 1995 and 2006). Furthermore, two peak events with daily precipitations higher than 40 mm were also observed in July. A correlation between the displacements of points 8 (*Zone+*) and 9 (*Zone++*), and the precipitation, is shown in Figure 16. Unlike major crises in the past, the 2007 crisis seems to show a

reasonable correlation between the two quantities. This observation also tends to reinforce the idea that the 2007 acceleration of the landslide was a rather superficial phenomenon.

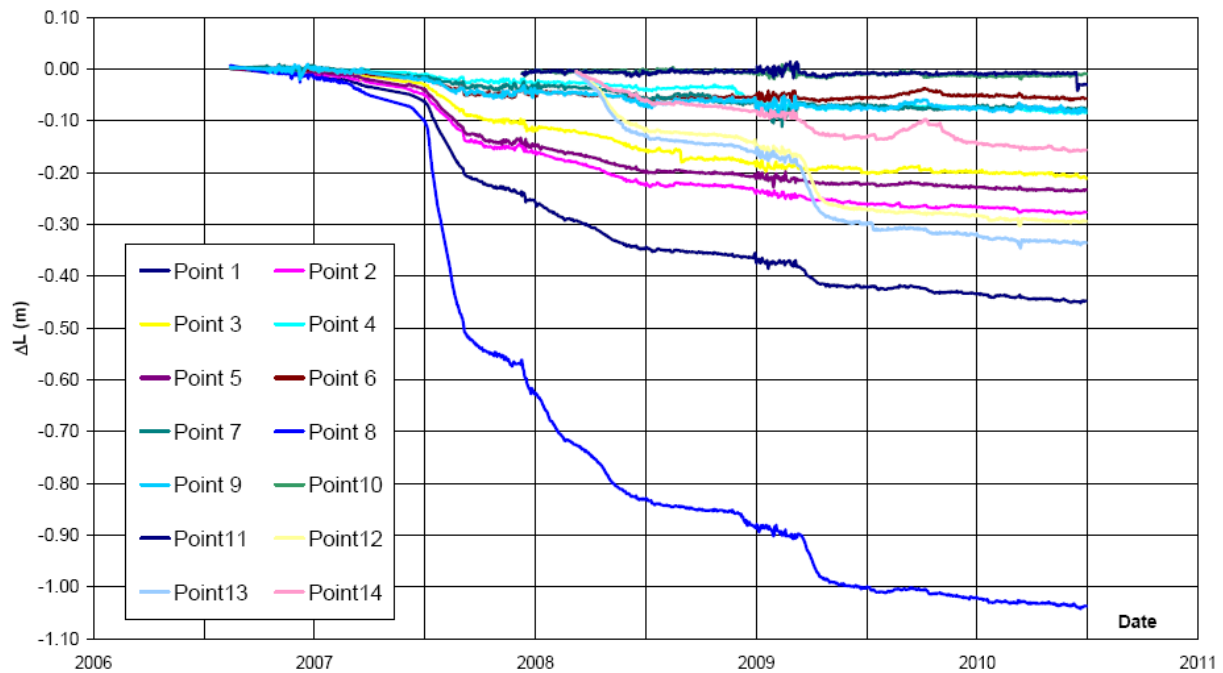


Figure 15 - Time series of absolute surface displacements measured at different points on the landslide (Swiss Geo Testing Ltd., 2009).

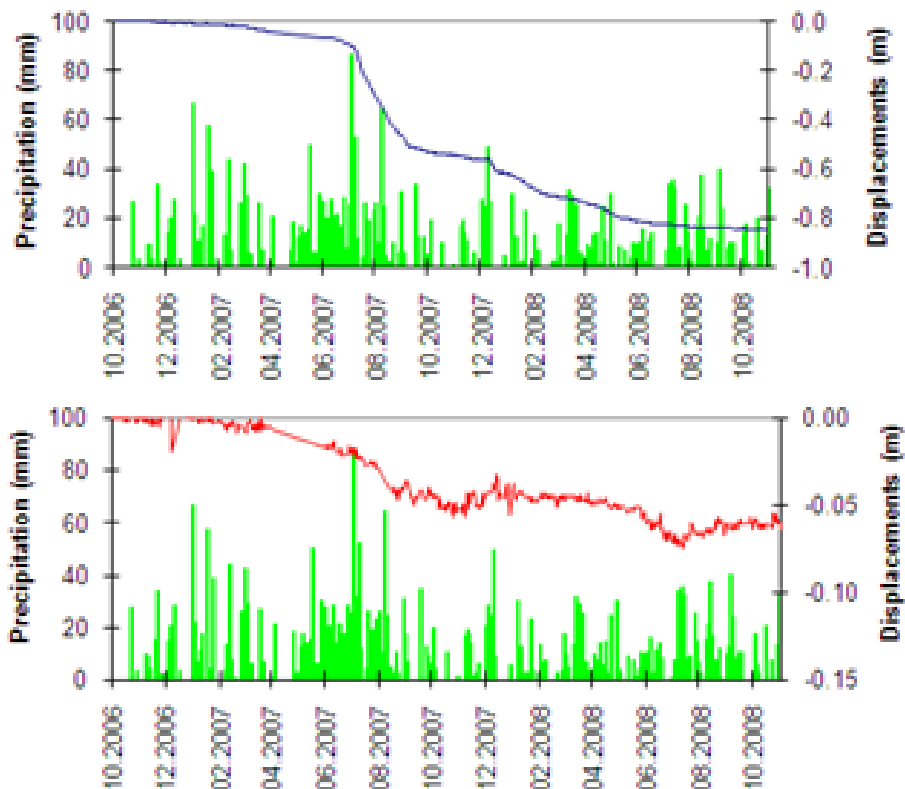


Figure 16 - Surface displacements in relation to gross precipitation over time at point 8 (top) and point 9 (bottom) (Planchat, 2009).

3. Conclusions

The La Frasse landslide has attracted a lot of attention in the past due to its capacity for sudden acceleration phases and the hazard it represents for the roads crossing the slide, the houses, which are built on the unstable mass, and the city of Aigle downstream of the Grand Eau river, which passes at the toe of the large landslide. Since the completion of the cantonal road RC705 in 1867, which constitutes the main connection between the ski resorts Villars, Leysin and Les Diablerets and the Rhone valley, and which traverses the landslide, movements of not less than 80 m have accumulated up to today. Around 35% of the total displacements can be attributed to a handful of crises that lasted a couple of months to several years. The crises mobilised geologists and geotechnical engineers, who have performed many surface and subsurface investigations with the goal of understanding the governing mechanisms driving the slope movement. A continuous monitoring campaign has been led by the Canton of Vaud for the past 20 years, comprising subsurface measurements of displacements and pore water pressures and surface measurements of displacements, rainfall and the activity of springs. The field data was essential for the establishment of mitigation measures, especially for the evaluation of the efficiency of possible drainage galleries to erase peak responses in pore water pressures in the unstable soil mass. The detailed monitoring in the lower part of the landslide allows the behaviour in the local, critical zones to be assessed in real time. The minor crisis of 2007 was characterised by a local acceleration of a part of the landslide along a secondary slip surface. Its movements could be recorded continuously due to the use of a novel laser-target instrument. The availability of continuous data on displacements and pore pressures enables more adequate numerical hydrogeological and

geomechanical modelling to be conducted, in conjunction with advanced laboratory testing of soils. This may lead, in the future, to the achievement of greater insight into the mechanisms governing the behaviour of the large landslide and prediction of ongoing behaviour.

4.2 SYNTHESIS OF MONITORED SITES ON FINE-GRAINED SOILS (OVERCONSOLIDATED AND WEATHERED CLAYS, BOTH SHALLOW AND DEEP-SEATED)

4.2.1 Synthesis of monitored sites on reworked black marls

(CNRS)

This section summarises the knowledge gained from the long-term monitoring of the Super-Sauze mudslide. Mudslides are the most typical landslide type observed in reworked Callovo-Oxfordian black marls of the South French Alps. They are generally the result of complex failures, in which structurally-controlled rock block slides transform progressively into a slow-moving mudslide. Their dynamics may result from sliding and flowing, either singly or in combination. Continuous movement of these mudslides may be maintained over long distances (hectometric to kilometric), depending on the availability of an unobstructed sloping path, and over long periods of time (> 200 years). Typical observed instantaneous velocity ranges from 0.001 to 5.0 m/day in relation to seasonal changes in pore water pressures over the period 1991-2009. Surges of the mudslides have been observed in relation to compression of the material during motion, undrained loading and the development of excess pore water pressure. From a mechanical viewpoint, the mudslides display a complex style of movement with a vertical profile of velocity coupling displacements along a shear band at depth, and diffuse deformations above it.

This section focuses on the analysis of the Super-Sauze mudslide (Fig. 1), because of its representativeness of landslides in Callovo-Oxfordian black marls, and the availability of data from the long monitoring period. The section discusses, in turn, (1) the historical development of the landslides; (2) the structure and geometry of the moving masses; and (3) their kinematics, hydrology and possible mechanisms.

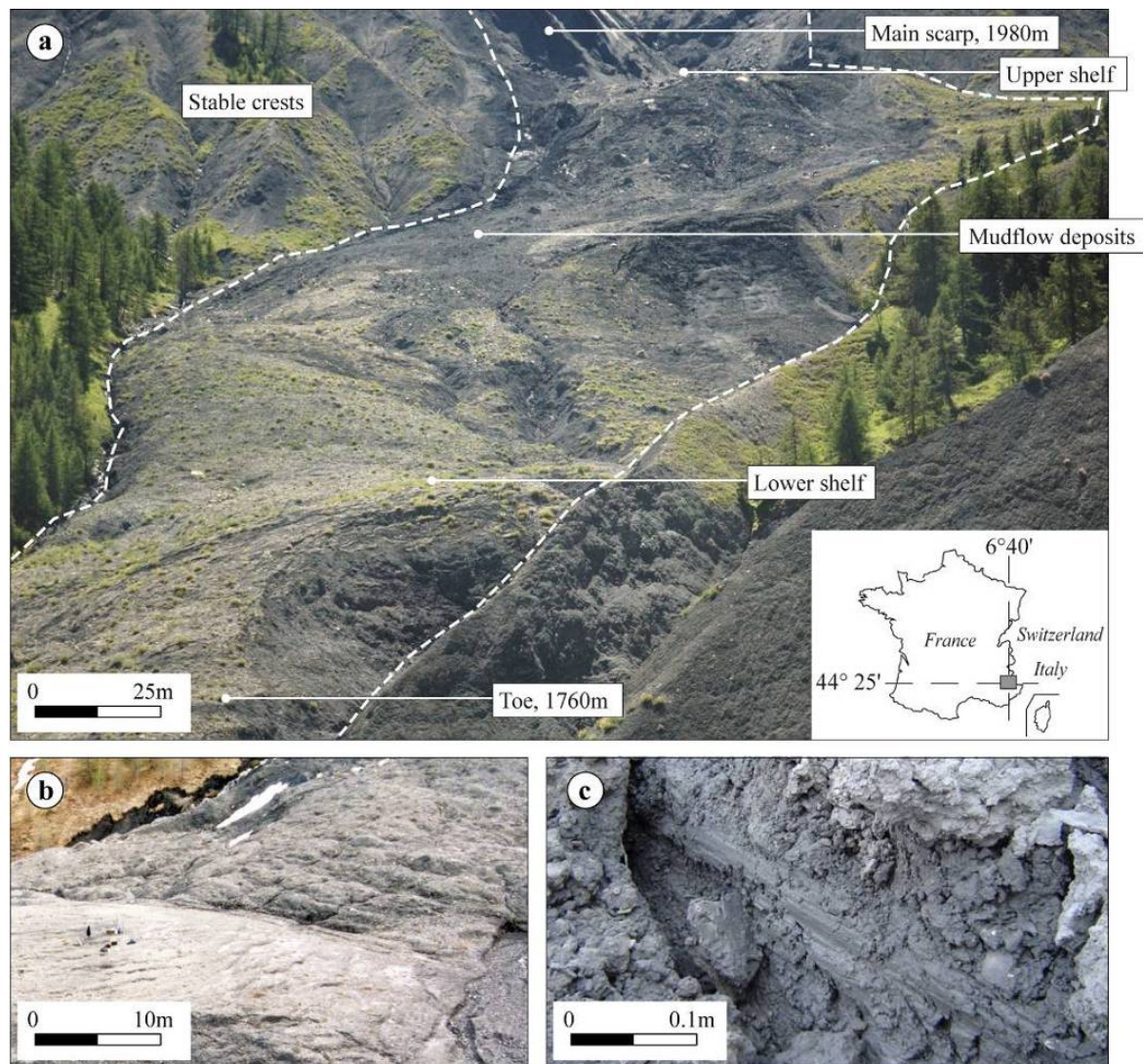


Figure 1 - Geomorphologic features. a) Photograph of the mudslide on 28th July 2008; b) Compression levees in the lower part; c) Striations indicating movement along shear surfaces along a stable in-situ crest in the central part.

1. Historical development of the mudslide

In the beginning of the 1970s, plane and wedge failures occurred respectively on the Eastern and Western sides of the upstream part of the main channel (MC) resulting in an accumulation of large marly rock panels, and in the formation of a main scarp (Fig. 2). The panels have been progressively weathered. A matrix supported soil fabric has developed, integrating marly fragments of different size, and filling up the gullies progressively.

Weathering tests have been carried out on intact black marl rock samples of 0.5 m³ using alternate wetting-drying cycles and freezing-thawing cycles (the procedure is indicated in Fig. 3) and changes in grain size distributions have been evaluated by laser diffraction particle analyses.

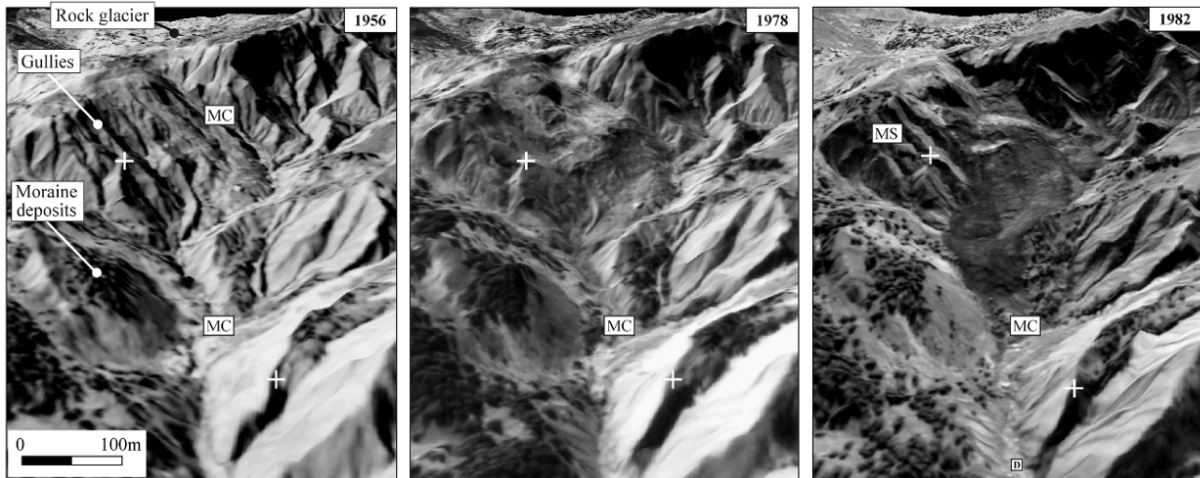


Figure 2- Morphological setting and evolution of the Super-Sauze mudslide, from 1956 (before failure) to 1982. The temporary storage of material at the toe of the main scarp and its weathering is clearly recognisable, before the downstream progression of the material in the main channel. (MC: main channel; MS: main scarp).

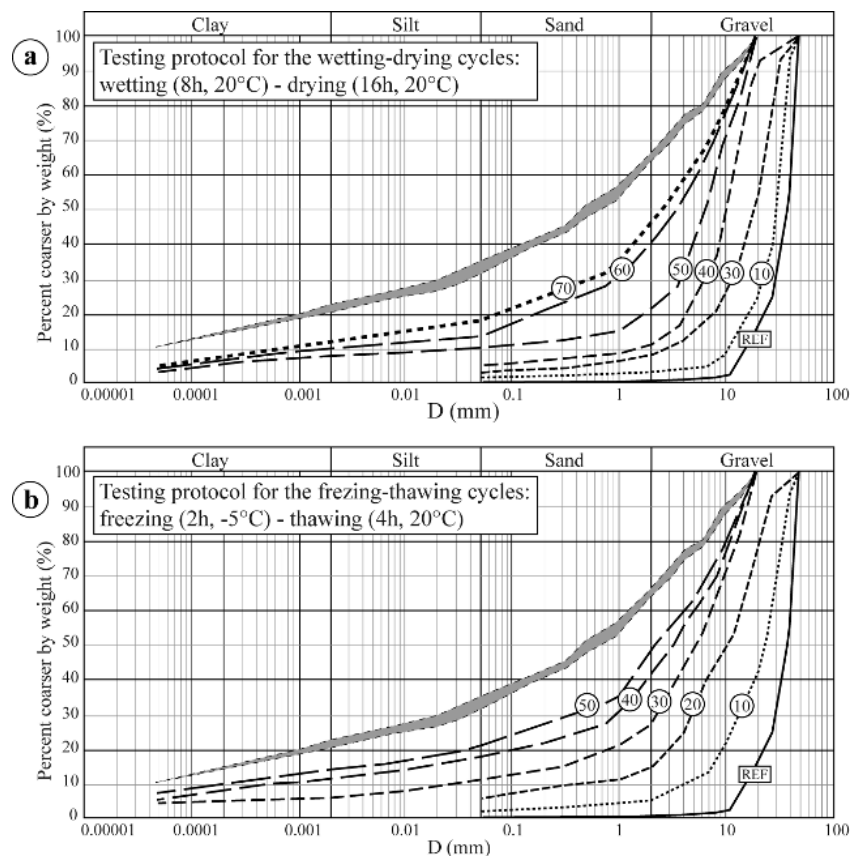


Figure 3 - Changes in grain size distributions of the Super-Sauze black marls for a) wetting-drying cycles, and b) freeze-thaw cycles. The grey colour represents the observed grain size distribution of the surface material of the mudslide; the number in the dots indicates the

number of weathering cycles.

The results indicated that ca. 80 freeze-thaw cycles or ca. 140 wetting-drying cycles are necessary to obtain the observed grain size distribution of the surface material of the mudslide (Fig. 3; Malet, 2003). As the yearly average number of freeze-thaw cycles at Super-Sauze is estimated at 40 from meteorological observations, 3 to 4 years would be necessary in the field for disintegrating a rock sample into a soil sample, with possible water retention capacities. This high weathering rate is a qualitative indicator of the development of a soil matrix for the environmental conditions observed at Super-Sauze, taking into account that the weathering rates strongly reduces with the weathering cycles (Rippa & Picarelli, 1977).

These experimental data are consistent with the information retrieved from the analysis of old photographs (Fig. 2) indicating that the reworked material has started to move downstream 4 to 5 years after the initial rock failures (Fig. 4a).

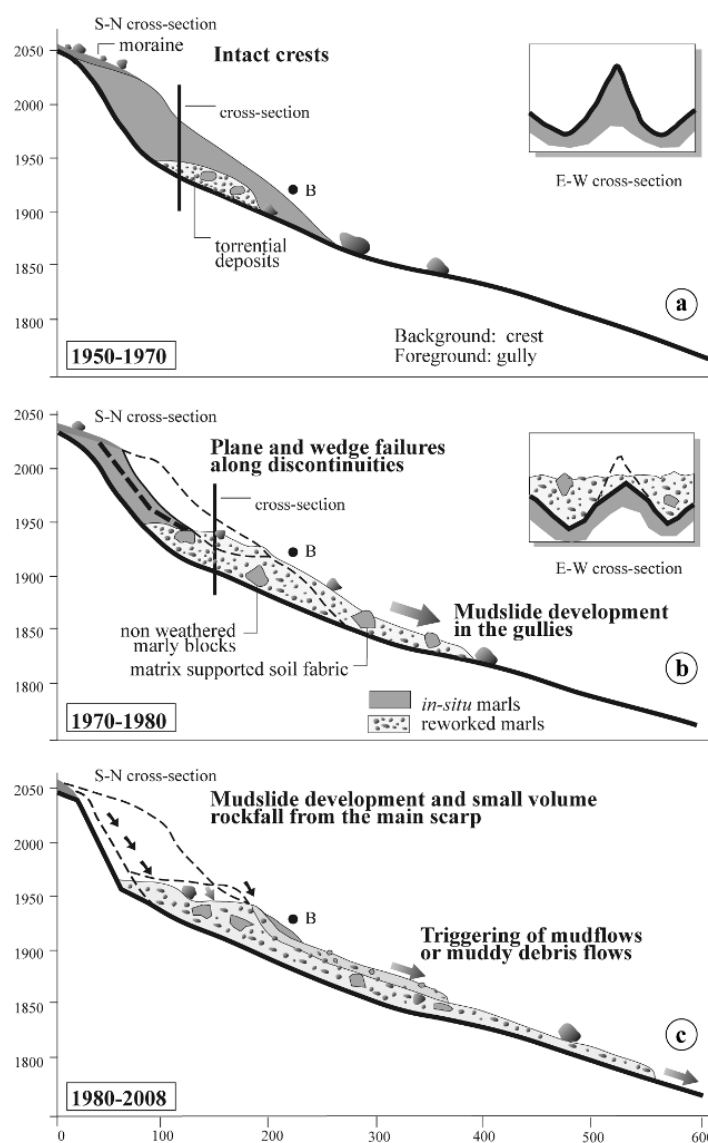


Figure 4 - Conceptual model of development over time of the mudslide. a) Initial conditions before failure; b) Rock failures, weathering of the failed rock panels and progressive filling of

the gullies; c) Actual mudslide development.

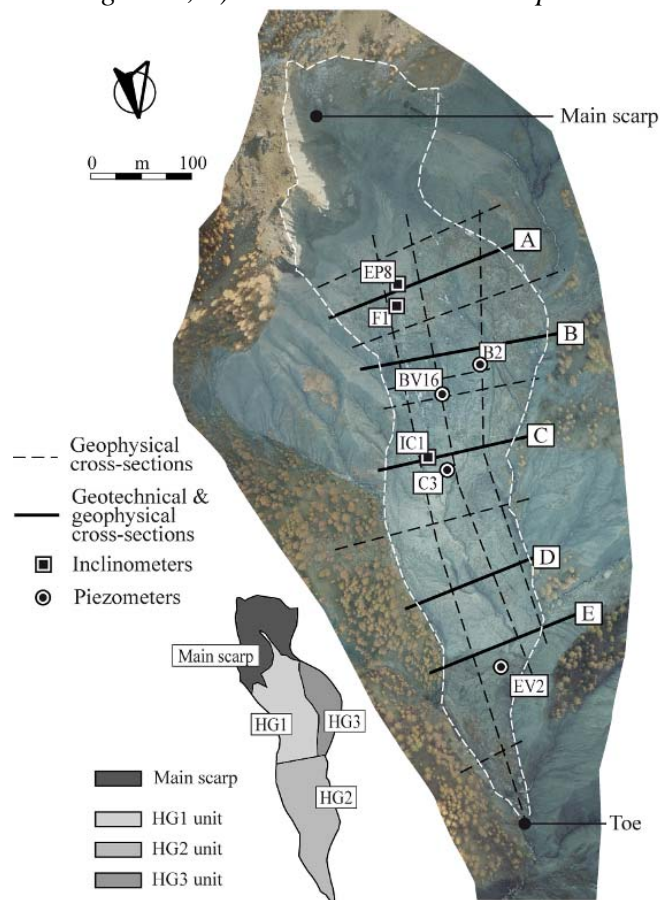


Figure 5 - Location of the geotechnical, geophysical and hydrological investigations on the mudslide, and hydro-geomorphological units (HG) identified from the observations.

Starting in the late 1970s, a rising level of soil accumulation in the gullies is observed (Fig. 4b). Since 1982, the material has progressed downstream by more than 200 m, with some changes in the rate of displacement according to the presence of obstacles. The bedrock geometry corresponds in the upper part to a succession of more or less parallel crests and gullies (as can be observed on cross-section B; Figs. 4b & 6) and, in the medium and lower parts, to a narrow incised channel (as can be observed on cross-sections C, D and E; Fig. 6). Consequently, the thickness of the mudslide is highly variable and varies between 0 and approximately 20 m.

In 2009, the mudslide extended over a horizontal distance of 870 m and occurred between elevations of 2105 masl at the crown and 1760 masl at the toe, with an average 25° slope gradient. The total volume is estimated at 750,000 m³ (Malet & Maquaire, 2003), and the mudslide is bordered by two streams.

The dynamics are controlled by bedrock geometry, rock mass fabric, and hydrology. Morphological features induced by the sliding and flowing mode of the mudslide are easily recognisable. The contact between the mudslide and the stable hillslopes comprises a shearing zone of a few metres width, characterised by tension cracks and shear surfaces marked by scratches in the direction of the movement (Fig. 1c). Compression levees are also clearly

distinguishable locally (Fig. 1b). A detailed morphological description of the mudslide can be found in Weber & Herrmann (2000).

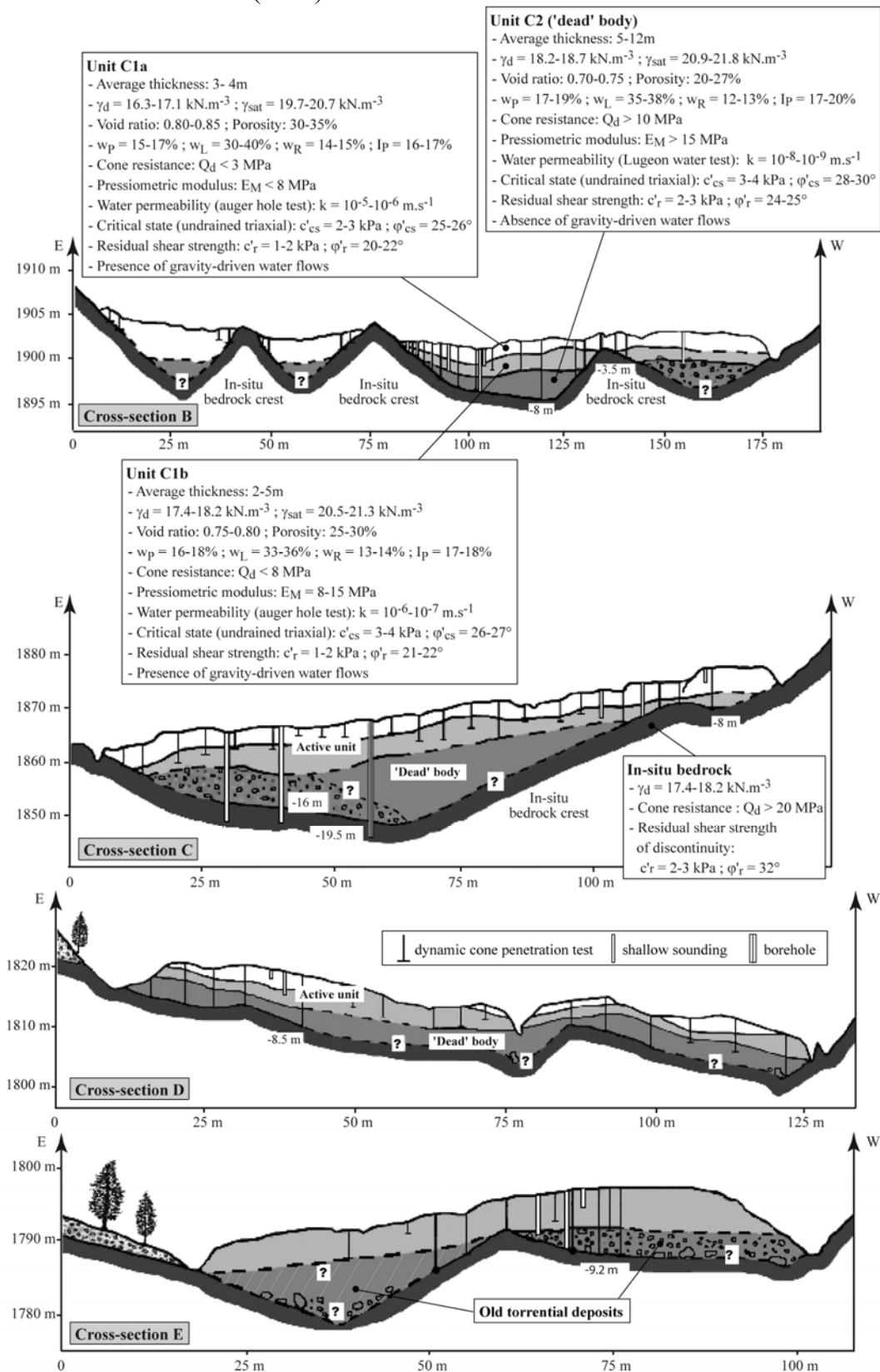


Figure 6 - Internal structure of the mudslide from the upper to the lower part (cross section B to E).

2. Internal structure

Geotechnical and geophysical prospecting have allowed definition of the 3D structure to be made. The geotechnical investigation consisted of six boreholes (up to a depth of 30 m), more than 200 dynamic penetration tests along 5 cross-sections (Fig. 5), inclinometer measurements, several in-situ testing programmes, encompassing pressuremeter and vane shear tests, and soil sampling (Flageollet et al., 2000, 2004; Maquaire et al., 2001; Malet, 2003). The geophysical prospecting consisted of 14 electrical resistivity profiles combined with P-wave and S-wave seismic tomographies (Schmutz et al., 2001; Grandjean et al., 2007; Méric et al., 2007).

According to variation of geotechnical, geophysical and hydrological parameters, the mudslide is comprised of two vertical units: the first unit (C1) is a semi-permeable material of 5 to 10 m thick, while the second unit (C2, with a maximum thickness of 10 m) is a stiff and impervious material (Malet & Maquaire, 2003). Figure 6 details the geometry and structure on cross-sections B to E, and indicates the range of geotechnical parameter values for the different units.

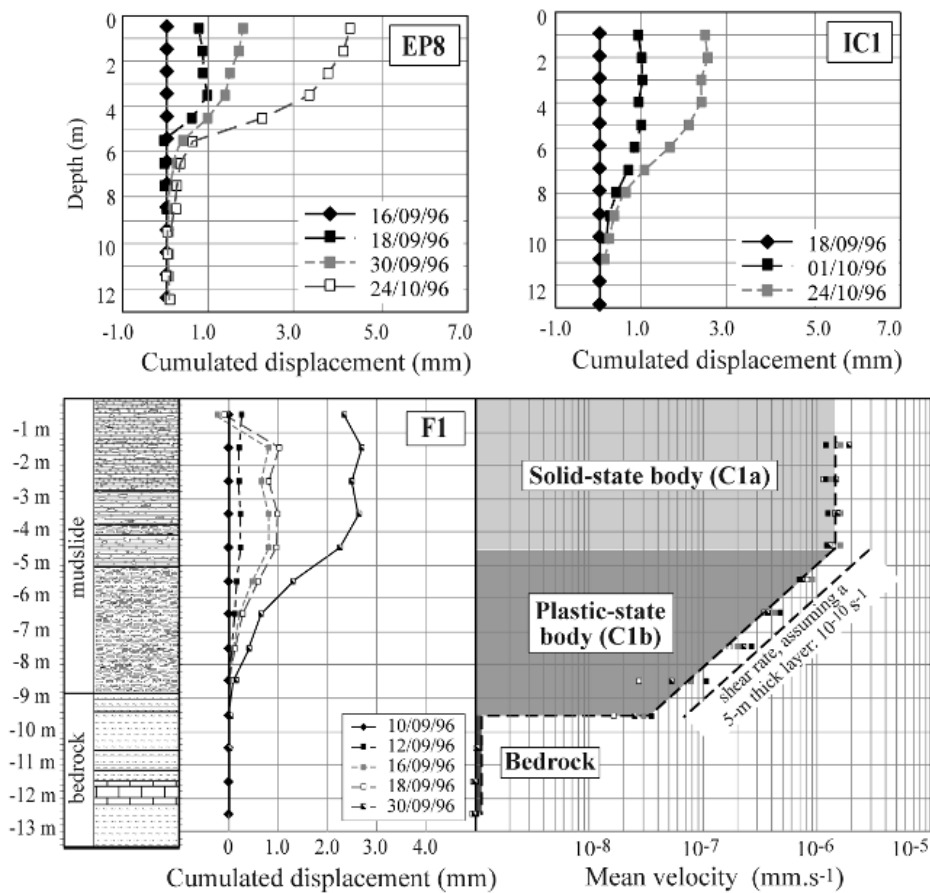


Figure 7- Geomechanical behaviour of the mudslide, interpreted from inclinometer measurements at boreholes EP8, F1 and IC1. The vertical distribution of velocity provides

evidence for the essentially solid-state (rigid body) and plastic-state behaviour of the mudslide.

3. Vertical velocity distribution

Within the active unit (C1) of the mudslide, inclinometer measurements in boreholes F1, EP8 and IC1 (Fig. 7) lead to the identification of a relatively thick shear zone of 3-4 m (C1b), in which strains are relatively homogeneous, and a rigid body of 4 m on top (C1a). This active unit overrides either the in-situ bedrock (at location F1), or the C2 unit, which is called 'dead body' (at locations EP8 and IC1). The examination of soil samples from the boreholes did not produce a clear identification of a shear band.

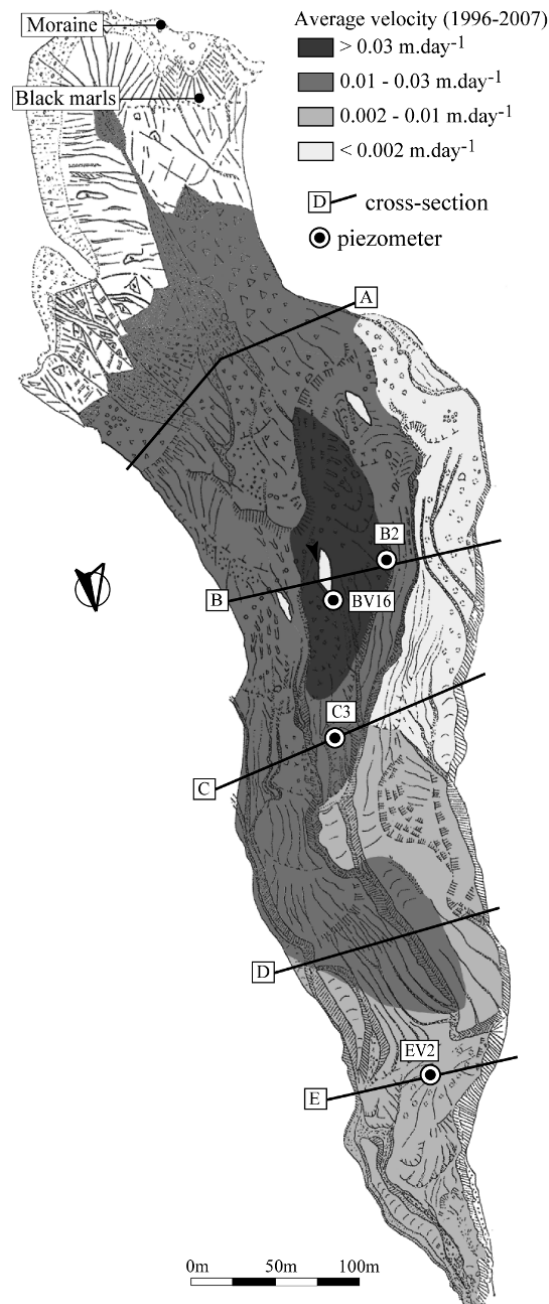


Figure 8- Average velocity field observed during the period 1996-2007, from a network of ca. 40 benchmarks.

4. Kinematics, hydrology and possible mechanisms of the mudslide

The kinematics have been monitored since 1996 by combining total station and dGPS measurements of the displacements of benchmarks and extensometric measurements (Malet et al., 2002); since 2007, the displacements have also been observed from camera recordings and terrestrial laser scanning (Travelletti et al., 2008).

The velocities lie in the range from 0.002 to 0.03 m.day⁻¹ (Fig. 8), but accelerations with velocities up to 0.4 m/day may be observed each spring season (Fig. 9a). Displacements along the mudslide correspond mainly to the line of greatest slope. Figure 9 shows examples of the ‘pore water pressure – displacement’ pattern at the annual (Fig. 9) and event scales (Fig. 10) at several locations for the period 1997-2001. Pore water pressures are monitored automatically in four standpipe piezometers (B2, BV16, C3 and EV2; Fig. 5), which are installed at -4 m in depth with the top of the filter zone at -3 m, sealed with bentonite plugs. The high displacement rates necessitate the installation of new piezometers every two years at the same location to monitor the hydrological pattern over long periods.

The displacement pattern exhibits a seasonal trend with two acceleration periods (Spring and Autumn) and two deceleration periods (Summer and Winter). The maximum daily displacements are observed systematically in the snow melting periods, with peaks from Mid-April to Mid-June, and in the heavy rainfall periods, with peaks from Mid-October to Mid-November (Fig. 9).

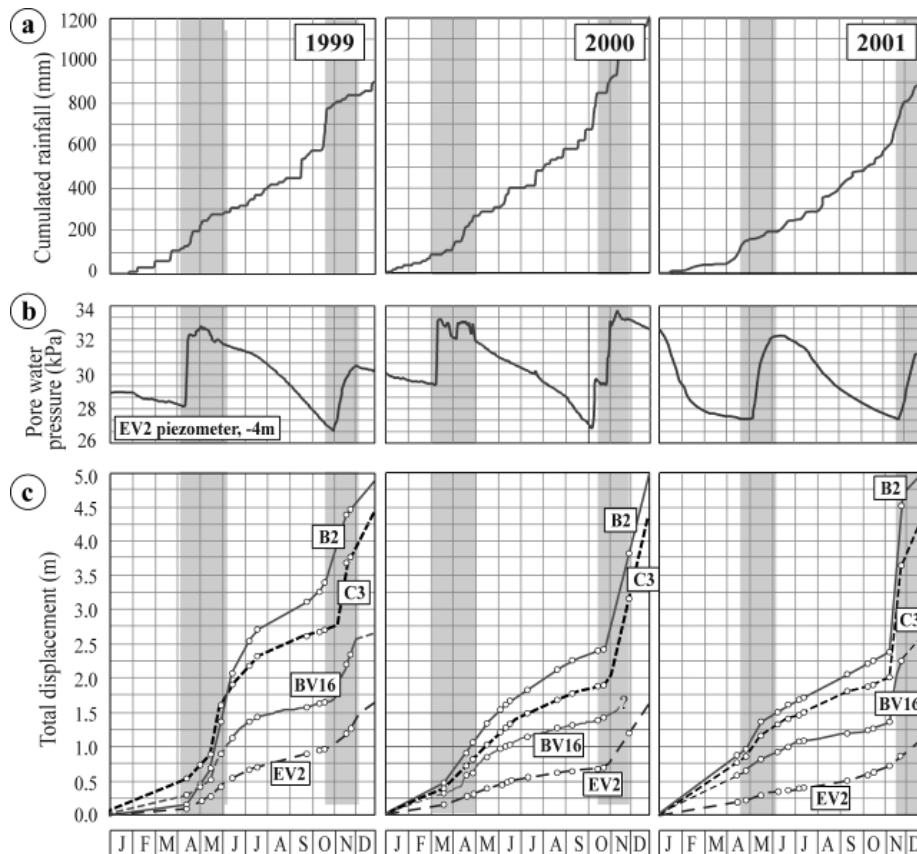


Figure 9- Observed ‘pore water pressure – displacement’ pattern at the annual scale.

a) Cumulative yearly rainfall monitored at BV16 location; b) Pore water pressure monitored at EV2 piezometer at -4 m; c) Total displacements observed on cross-sections by total station measurements (benchmarks B2, C3, BV16 and EV2).

The relative position of the water level is dependent on local conditions, the highest groundwater level being observed in the upper part (cross-section B) and decreasing downslope. Consequently, the displacement rates are variable and decrease from the upper to the lower part of the mudslide (Figs. 8 & 9). One of the most interesting points is the velocity

response of the landslide to increases in pore water pressures both in periods of high (Spring) or low (Autumn) groundwater levels, as observed for instance in May and October 1999 (Fig. 10).

5. Hydrological behavior of the mudslide

Groundwater flow analysis: inferences from field data

Hydrology is the main controlling factor of the landslide mobility. A detailed analysis of multi-parameter time series from 1997 onwards, combined with an extended hydrological investigation, have been used to define a hydrological concept (Malet et al., 2005b).

Inputs (rainfall, snowfall) to, and outputs (surface water, evaporation) from the saturated zone represent the mass balance of the hydrological system. Over the period 1970-2000, the yearly cumulative precipitation is 730 mm (with about 200 to 250 mm as snowfall), but the maximum daily or monthly value varies greatly. A monthly value of 150 to 200 mm can occur, especially in April, May, October or November. The water reservoir of the mudslide consists of C1a, C1b and C2 units (Fig. 6), and the lateral streams are the spatial boundaries of the hydrological system. The total volume of the water reservoir is estimated at 450,000 m³.

Groundwater levels between -0.5 to -2.0 m are observed in the upper parts of the mudslide (cross-sections A-C), while deeper water levels (-2.5 m to -3.5 m) are observed in the western parts of cross-sections B-C. Moreover, the depth of the average position of the groundwater table slowly decreases from the B cross-section (-0.7 m) to the E cross-section (-1 m). In the unsaturated zone, the volumetric water content varies considerably, ranging from 0.10 to 0.35. The range of saturated hydraulic conductivity values (measured in the field with the auger hole method) varies with depth from 10⁻⁵ m/s between -1 m and -2 m to 10⁻⁸ m/s in the lower unit (Fig. 11). Lugeon tests in the bedrock indicate a hydraulic conductivity of 10⁻⁹ m/s. The range of unsaturated hydraulic conductivity values in the topsoil (measured with triple ring disc infiltrometers at multiple suctions) vary greatly from 10⁻⁴ m/s to 10⁻⁸ m/s, according to the soil surface characteristics (Malet et al., 2003). The average transmissivity value (10⁻⁵ m²/s) and the storage coefficient value (e.g. effective porosity; 0.21 ± 0.04) of the soil material have been estimated from twenty one groundwater rises in piezometers BV16 and EV2.

In the first approximation, the C1 unit can be considered to be a fully saturated medium. The piezometric behaviour shows high pore water pressure variations (up to 20-25 kPa at -4 m) with sudden recharge following snowmelt. Pore water pressures may remain high for a long time, due to the medium permeability of the material and the presence of the relatively impermeable layer underneath. Statistical analyses (autocorrelation functions, wavelets) of 6h precipitation and groundwater time series, combined with a hydrochemical survey (de Montety et al., 2007) allow identification of some pattern of piezometric behaviours and definition of three hydro-geomorphological units (Fig. 5).

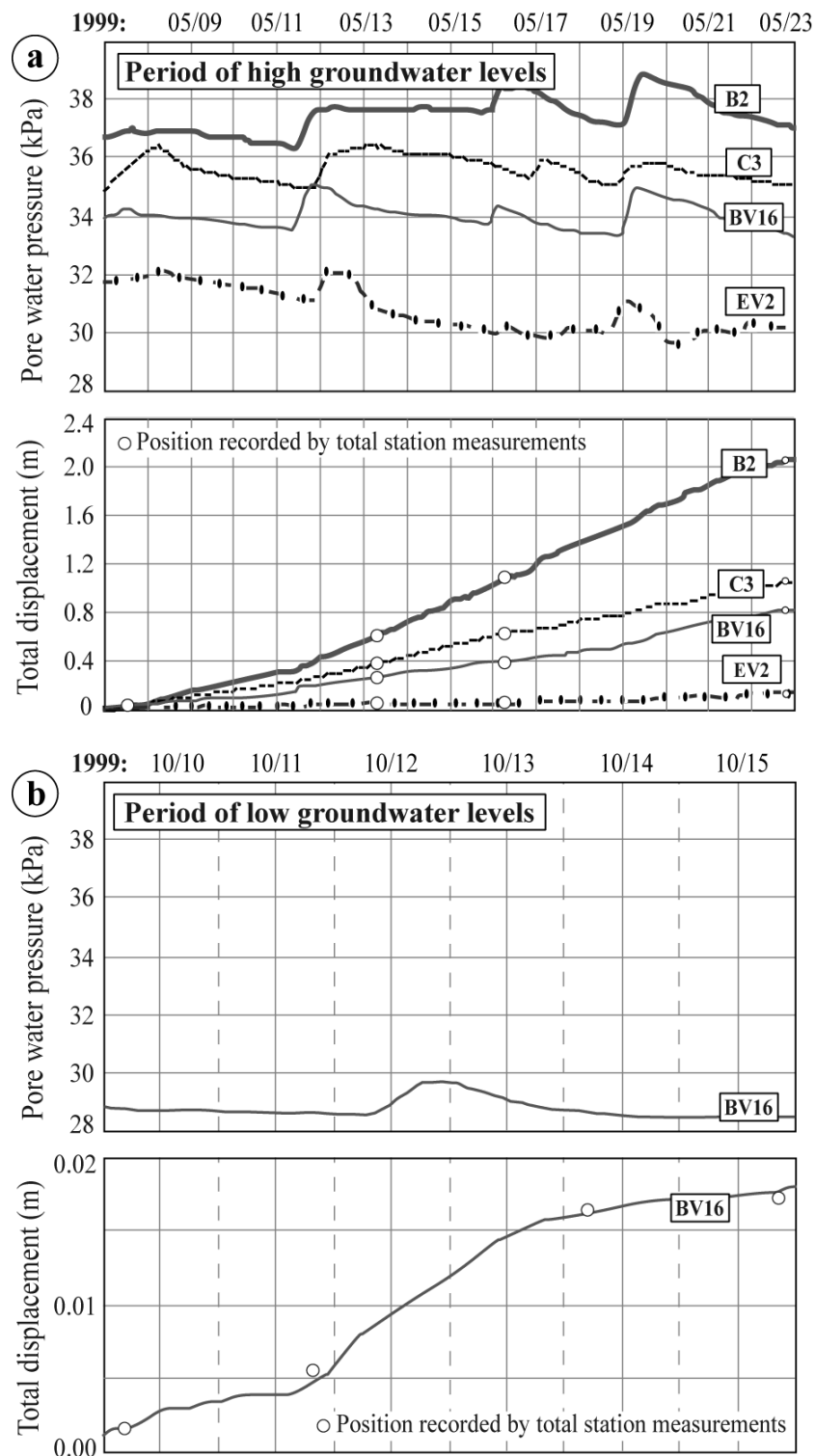


Figure 10 - Observed 'pore water pressure – displacement' pattern at the event scale.
 a) Pore water pressure monitored at several piezometers at -4m and total displacements observed on cross-sections by total station measurements in a period of high groundwater levels (May 1999);
 b) Pore water pressure monitored at piezometer BV16 at -4m and total displacements observed by total station measurements in a period of low groundwater levels

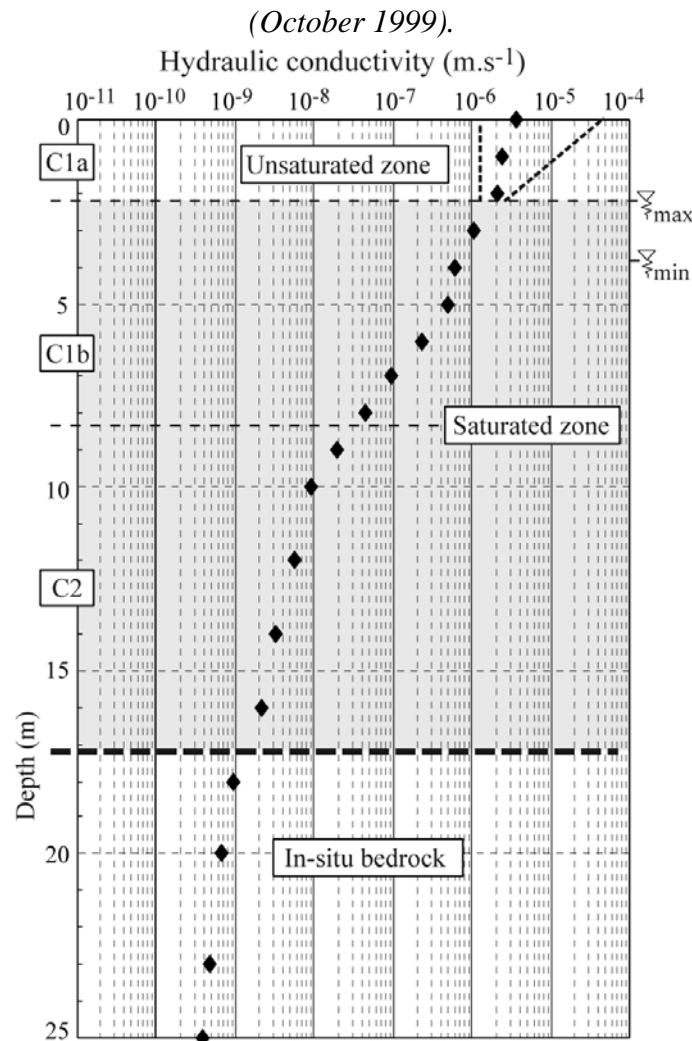


Figure 11 - Variation of hydraulic conductivity with depth at borehole IC1 (cross-section C), and maximal and minimal groundwater levels observed for the period 1997-2001. The grey colour indicates the saturated zone.

For piezometers installed at -4 m in depth, and considering the time delay between the onset of precipitation and the observed rise in groundwater level for characterising the response time, and the time delay between the end of precipitation and the recovery of the pre-event groundwater level for characterising the drainage time:

- the *HG1 unit*, exhibits very rapid piezometric responses (< 1 hour), a significant fluctuation (up to + 0.4 to + 0.8 m) and rapid drainage (3-5 hours);
- the *HG2 unit*, exhibits rapid piezometric responses (2-3 hours), a modest fluctuation (up to + 0.05 to + 0.3m) and relatively quick drainage (12-24 hours);
- the *HG3 unit*, exhibits slow piezometric responses (> 5 hours), low fluctuation (centimetric) and slow drainage (> 24 hours).

Hydrological concept

The multiple sources of information have led to the proposal of the following hydrological concept:

- if the groundwater level is near the surface (between -1.0 m and -1.5 m, according to the location), their fluctuations are invariably rapid (less than a few hours), of moderate magnitude (0.1 to 0.4 m) and of relatively short duration (within days) following rainfalls. Peaks following snowmelts have a longer duration;
- the decline of the groundwater levels below a depth of -1.5 m strongly depends on the season, with faster drainage in summer;
- the hydrological regime is influenced by two important recharge events, one at the end of spring and one at the beginning of autumn.

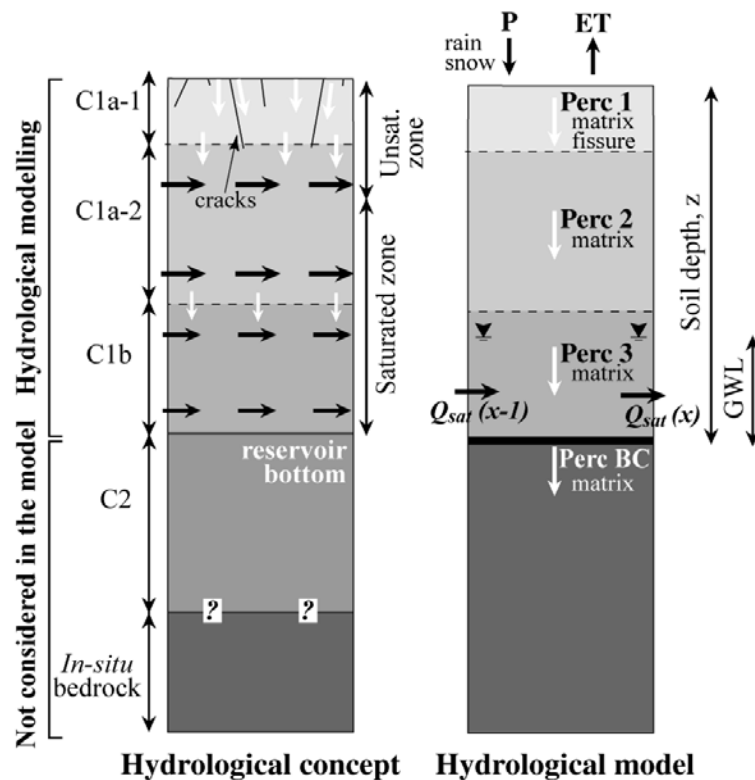


Figure 12- Schematisation of the hydrological concept implemented in the hydrological model.

The rapid (within hours) piezometric responses are attributed to matrix Darcian flows in the nearly fully saturated media combined with fissure flows through a superficial (0.5 – 2 m) system of interconnected cracks. The depth of the crack system coincides very often with the contact between the unsaturated and saturated zones (Fig. 12). Contribution of fissure flows to the recharge of the groundwater table is not the same for all the measurement stations, due to differences in crack density, soil surface characteristics and material compaction, so it can be considered as one of the main reasons for the spatially varying rates of groundwater rise (de Montety et al., 2007).

These considerations are schematised into a hydrological concept with three layers (Fig. 12): a layer with a continuous permeable crack system (C1a₁) overlies two layers marked by different hydraulic conductivity values (C1a₂, C1b). The lower unit (C2) and the *in-situ*

bedrock are considered impervious and thus are not integrated into the hydrological model.

Hydrological modelling

Hydrology of the mudslide has been modelled with the spatially distributed physically-based model STARWARS (Malet et al., 2005b). The model resolves the equation for saturated and unsaturated flows, in the vertical and horizontal directions, assuming freely drainable water, and uses measured distributed values for the parameter values. Antecedent soil moisture in the different reservoirs, infiltration I , evaporation Ep , surficial runoff R , percolation in the unsaturated zone Pe and saturated lateral flow Q_{sat} define the hydrological balance of the system. A complete mathematical description of the model can be found in Malet (2003).

The generation of groundwater is simulated by imposing state-controlled boundary conditions at the bottom and flux-controlled boundary conditions at the surface. A SNOWPACK/MELT sub-model is incorporated as a pre-processor in the hydrological model using a simple conceptual approach describing the energy balance of the topsoil from the time series of net radiation and temperature. A simple conceptual FISSURE FLOW sub-model has been developed to represent shallow bypass flows in fissures as well (Malet et al., 2005b). At each time step, the water flow in excess of the infiltration capacity of the topsoil is directed towards the fissures and that volume of water is transferred directly towards layer C1a₂ within one timestep. The flow in the reverse direction, from the saturated fissures to the soil matrix, is not considered.

The application of the model and its calibration/validation procedure are described by Malet et al. (2005b). The spatial and the timestep resolution of the model are respectively fixed at 2 x 2 m and 6 hours.

Figure 13 shows the simulation results for piezometers EV2 and BV16. The response pattern is reproduced rather well, although some recorded peaks, especially for BV16, are underestimated or missed because of the very simple representation of fissure flows in the model (de Montety et al., 2007).

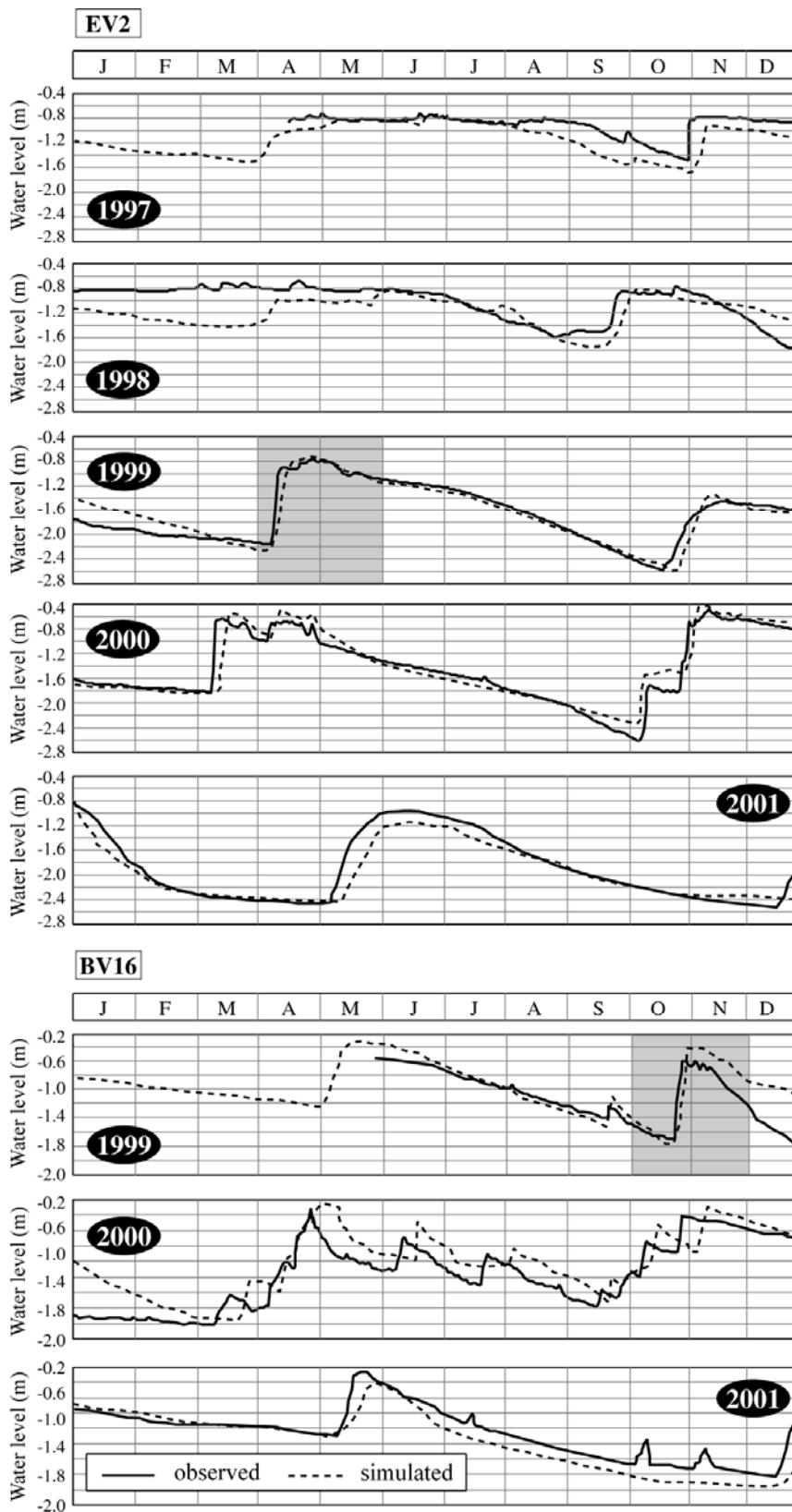


Figure 13 - Examples of observed and simulated groundwater levels over years 1997-2001 at piezometer locations EV2 and BV16 (see Fig. 5 for the location).

6. Mechanical behaviour

From the borehole inclinometer profile (Fig. 7), it appears that shearing of the plastic-state body C1b accounts for at least 80% of the displacement. Interpreting the slope behaviour in terms of effective stresses and critical state parameters, the variable rates of movement are controlled by thresholds in pore water pressures, values of which appear to be constant in time (Fig. 14). For instance, observations over the period 1999-2005 at piezometer BV16 indicated that the ‘Spring acceleration’ is initiated at a pore water pressure threshold value of ca. 30 kPa while the ‘Autumn acceleration’ is triggered by a slightly higher threshold value of ca. 32 kPa. Above these thresholds, the velocity increases non-linearly.

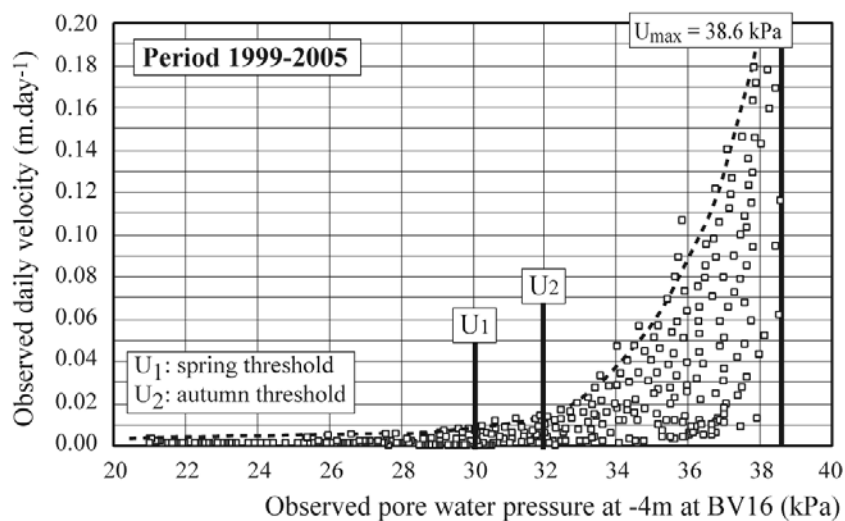


Figure 14- Thresholds in pore water pressures to trigger a surface velocity > 0.01 m/day for different observed rising and falling limbs at the BV16 location.

Detailed analysis of velocity vs. pore water pressure data supports this mechanical hypothesis by indicating that the velocity is higher during the rising limb of the groundwater than during the falling limb (Fig. 15). This hysteresis in the velocity pattern has been observed in other clay-shale landslides (Bertini et al., 1986; Giusti et al., 1996). Possible mechanisms explaining the development of excess pore water pressures are differential movements (Nieuvenhuis, 1991; Picarelli et al., 1995), increase in the thickness of the shearing zone or rate of viscous deformation causing increase in the level of stress (Picarelli & Russo, 2004).

In the following analysis, the landslide velocity is interpreted using an effective stress approach. Changes in velocity are hypothesised to be directly proportional to changes in lateral and vertical stresses ascribed to the generation of positive or negative excess pore water pressures due to compression and dilation, respectively. Velocity is modelled as a linear function of excess effective shear stress, changing pore water pressures during movement and a Coulomb-viscous friction model using critical state parameters and a constant viscosity (van Asch, 2005). Due to low hydraulic conductivity, the excess pore water pressures within the soil cannot readily dissipate, and a non-steady state situation develops temporarily within the slope, leading to acceleration of the landslide.

Figure 15 shows the measured and simulated velocity for five periods of rising and falling groundwater table at the BV16 location, at a depth of 4 m, and indicates the geomechanical

parameters used in the analysis. The model has been calibrated on the hydrological peak and velocity pattern of Spring 1999. Calibration has been carried out on the dynamic viscosity by fixing all the other parameters constant for year 1999, and the model has then been applied to the other four periods (2000-2003). The simulations indicate that the velocity pattern can be reproduced rather well, if a different dynamic viscosity is used for the rising and falling limbs (Fig. 15). An increase of a factor 10 of the dynamic viscosity has to be introduced in the falling limb to fit to the observed data, which could be attributed to changes in effective stresses that affect either soil cohesion or soil viscosity. With this assumption, the model is able to simulate the annual displacement value of the landslide rather well (Fig. 16). The model reacts sharply to the November 1999 peak of pore water pressure with an increase in the displacement rate. During the dissipation of pore water pressure in summer (July-October 1999), the model simulates lower velocities than those observed. Further investigations to characterise the stress conditions within the slope, and the soil geomechanical behaviour, are needed to propose a physical interpretation of the mechanism of excess pore pressure development.

In some cases, displacements of several metres are observed during acceleration periods such as in 1999, 2000, 2006 and 2008 (Malet et al., 2005a; van Asch & Malet, 2009). Small volume mudflows have occurred through a combination of heavy and sustained rainfalls, thawing soils and snowmelt, in the upper part of the mudslide (cross sections A & C; Figs. 5 & 8) characterised by steeper slope gradients and higher groundwater levels.

Such types of acceleration have been analysed with the fully coupled hydro-mechanical finite-element model GefDyn, assuming an elasto visco-plastic Hujieux constitutive model (Malet, 2003) and critical state parameters. Starting from a critical slope, with a safety factor $F = 1.2$, (the geometry used is the one depicted in Fig. 17c) and initial pore water pressure of 56 kPa at -7 m in piezometer EP5, the simulation of a pore water pressure increase of +6 kPa over 5 days leads first to incipient deformation and then to a partial acceleration of the soil mass (Fig. 17d; stage A). Consequent undrained loading leads to a second acceleration (Fig. 17d; stage B). This local failure is rapid enough to generate excess pore water pressures, and a temporarily non-steady-state mechanical situation develops causing failure of the secondary scarp of the mudslide (Fig. 17d; stage C).

This simple analysis demonstrates that differential displacements creating compression and extension zones are an important aspect of mudslide development.

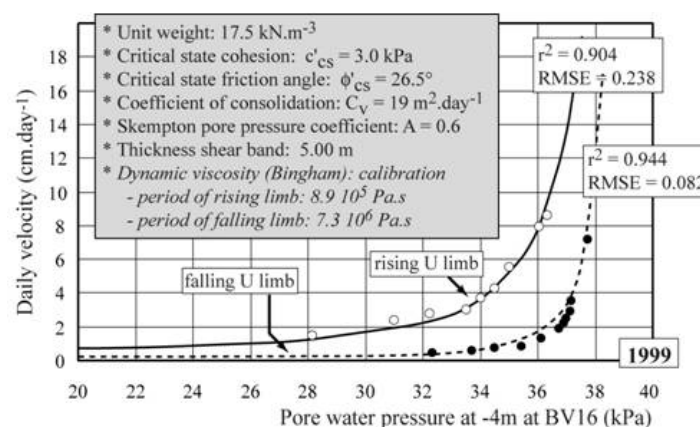


Figure 15a - Observed and simulated hysteresis in the velocity pattern for one period of

acceleration and deceleration (1999) and geomechanical parameter values used in the modelling exercise. The italic lettering indicates calibrated values.

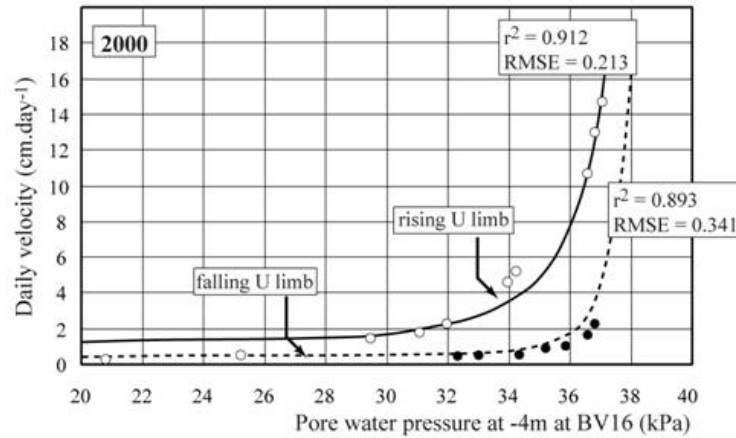


Figure 15b - Observed and simulated hysteresis in the velocity pattern for one acceleration and deceleration period in 2000.

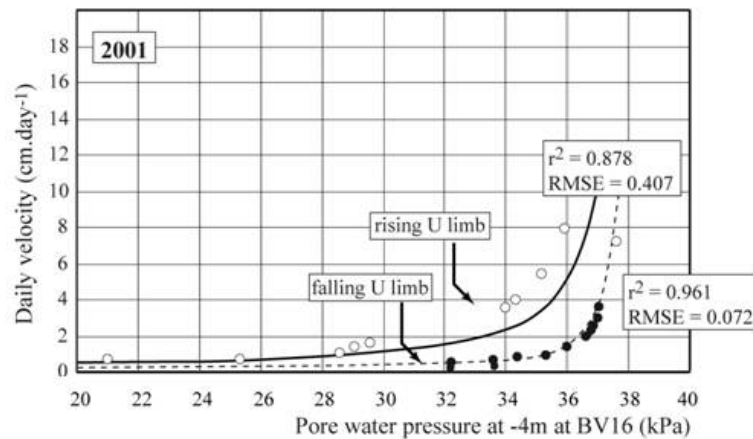


Figure 15c - Observed and simulated hysteresis in the velocity pattern for one acceleration and deceleration period in 2001.

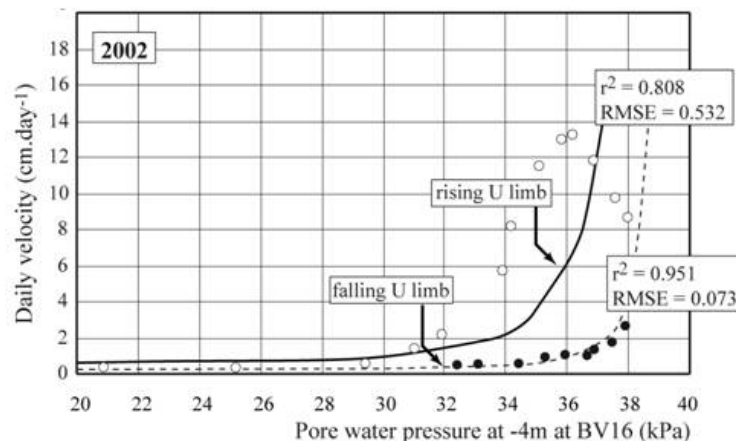


Figure 15d - Observed and simulated hysteresis in the velocity pattern for one acceleration and deceleration period in 2002.

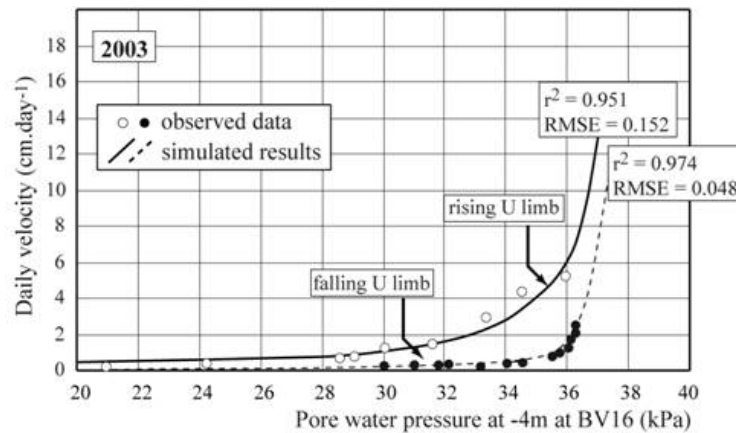


Figure 15e - Observed and simulated hysteresis in the velocity pattern for one acceleration and deceleration period in 2003.

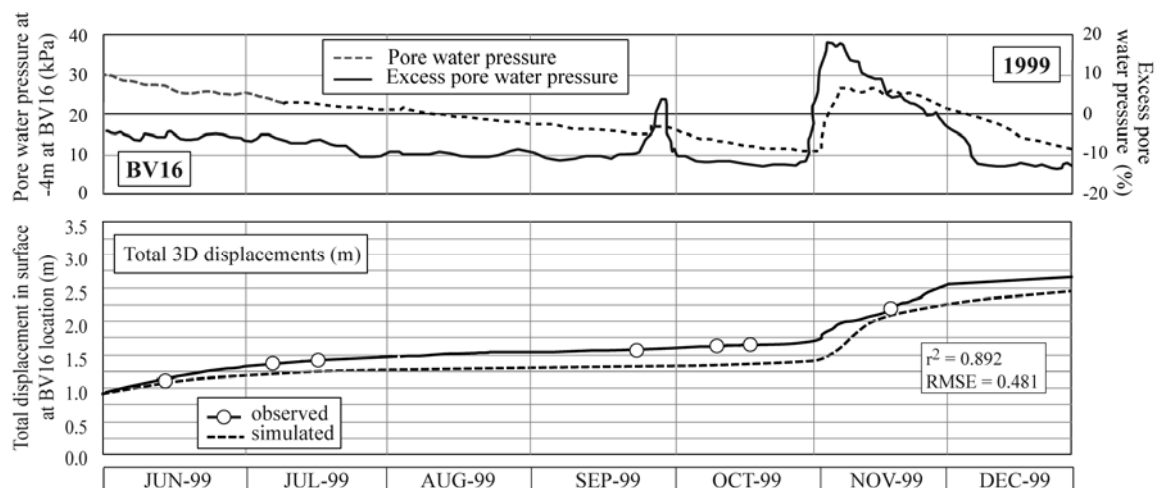


Figure 16 - Observed and simulated displacement of the BV16 benchmark over the period June – December 1999 with a simple rheological model with excess pore water pressure (Malet, 2003).

7. Conclusion

Mudslides are typical landslides in the Callovo-Oxfordian tectonised black marls of the South French Alps. The activity of these mudslides is very longterm, since movement may develop over hundreds of years. Their kinematics are characterised by periods of acceleration (with velocities up to 0.4 m/day) and deceleration, combined with the possibility of triggering rapid mudflows from the landslide mass.

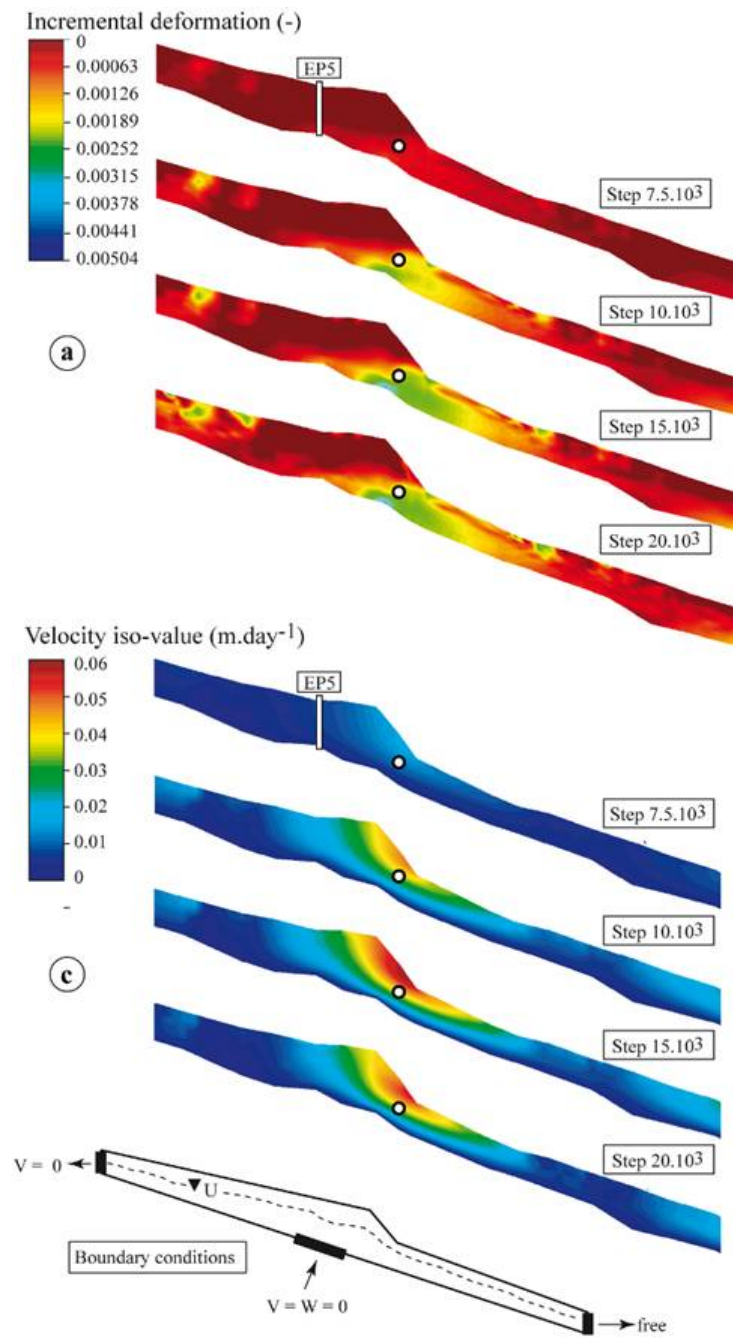
Multi-source observations and theoretical and numerical analysis of the Super-Sauze mudslide point out the significance of shearing of plastic-state material as a major mode of movement, and of the role of pore water pressure in controlling the rate of movement.

Acceleration of the mudslide is governed by thresholds in pore water pressures associated

with seasonal water table changes or to kinematic deformation of the undrained deformable medium. As a consequence, the total stress field is continuously changing due to different mobility patterns within the moving mass. Zones of compression or extension may develop, and excess pore water pressures may arise because of the low hydraulic conductivity of the soil.

A better understanding of the mechanisms controlling the generation of excess pore water pressure is the main challenge in forecasting the possibility of large failures of such types of landslides.

The monitoring of the Super-Sauze mudslide was supported since 1996 by several European Community research projects (TESLEC, NEWTECH, ALARM, MOUNTAIN-RISKS) and French research projects (ACI-MOTE, PNRN-ECLAT, ACI-SAMOA, ACI-GACH2C, ANR-ECOU-PREF, ANR-TRIGGERLAND). All reference and monitoring data are freely available on the OMIV (French Observatory on Landslides) website: <http://eost.u-strasbg.fr/omiv/>



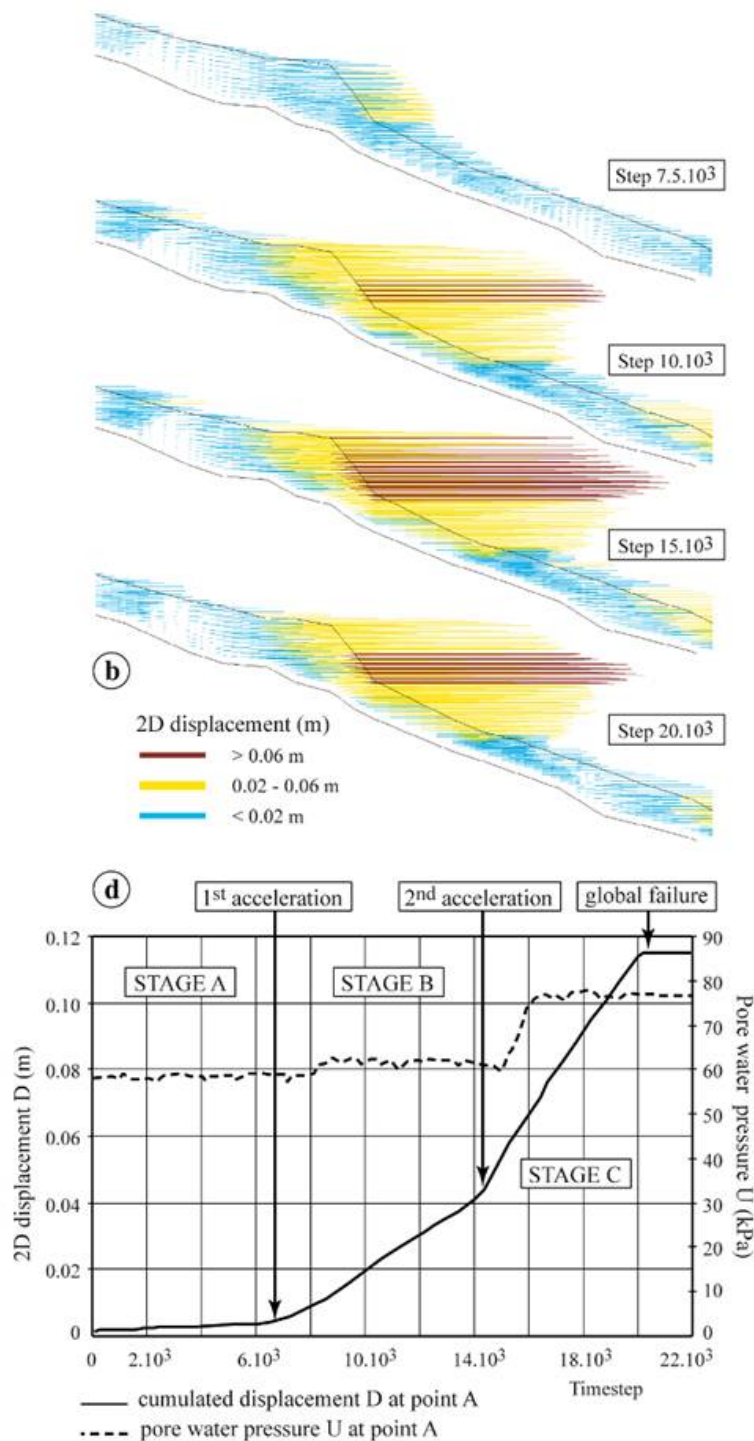


Figure 17 - Geomechanical simulation of an acceleration of the upper part of the mudslide that conducted to an important failure of the secondary scarp. a) Simulated incremental deformation in the direction of the major principal strain axis; b) 2D displacement according to the failure mechanism identified; c) Velocity iso-value according to the failure mechanism identified; d) Pore water pressure and displacement pattern over time.

4.2.2 Synthesis of monitored sites on stiff intact, jointed and highly fissured clays (AMRA)

The hydrological slope response in fine-grained soils depends on the low hydraulic conductivity. In particular, any change in the piezometric regime is delayed, depending on cumulative rainfall over long-lasting lengths of time (usually some months), and is not greatly influenced by short, even intense, rainfalls.

Most case histories concern active movements in stiff clays. Some significant examples are reported below. The cases examined have been differentiated according to these soils: intact clays, jointed clays, highly fissured clays.

1. Intact clays

One of the first well documented examples of weather-induced landslides is the Beltinge earthflow, North Kent, UK (Hutchinson, 1970), which is located on a 30 m high coastal cliff of stiff London Clay subject to marine erosion. The earthflow consists of two parts inclined at 13-18° (flow II A and flow II B, Fig. 18a) that discharge debris in a 65 m long and 20 m wide accumulation zone (flow II of Fig. 18a) inclined at about 7°. The two earthflows have a thickness of 1.0-1.5 m for the upper flow, while the lower one is about 5.0-5.5 m thick. The landslide bodies are bounded by discrete shear surfaces that are slickensided in the direction of movement. The accumulation flow terminates in a tongue, which extends far across the beach (Fig. 18b) during large movements, while it is eroded back to the general line of the cliff foot during periods of small movements.

Figures 19 and 20 report the available climatic and piezometer data. Data of total monthly precipitation (measured) and potential evaporation (calculated) come from two meteorological stations located close to the site. Groundwater conditions have been observed through Casagrande-type piezometers located within as well as outside the landslide body (Fig. 18). In particular, five piezometers (from P4 to P8) have been installed in a line up the cliff outside the mudflow boundaries. Data show that the largest yearly variation in groundwater level (about 2.5 m) is measured by piezometer P5, located in the steeper upper cliff. These readings, which cover a period of almost 3 years, correlate nearly with the histogram showing the difference between monthly total precipitation and the monthly potential evaporation (Fig. 2). Piezometer P6, set between the upper and lower cliffs, shows little variation while the pore-water pressures measured by P8 tend to decrease steadily, probably because of drainage toward the underlying fine sands of the Oldhaven Beds Formation (Fig. 18b). However, the readings of three piezometers installed within the flow II (P9, P10 and P11) show that pore-water regime is different from that in the adjoining cliff. In particular, the pore pressures generally exceed those in the adjoining cliff, sometimes reaching ground level, (piezometer P9, installed in the head of flow II).

Figure 19 reports surface displacements accumulated by flows II and II A, which have been measured at the middle of the flows in a direction normal to assigned lines (line D for flow II and line G for flow II A, Fig. 18a) by means of markers placed along these lines. Such data indicate that a distinction must be drawn between the behaviour of the shallow and relatively steep feeder flow IIA and the deeper, gently inclined accumulation flow II. In fact, the corresponding average inclination is such that the flow II A can be readily triggered by a rise in phreatic groundwater level; in particular, its movements correlate well with the seasonal rise in groundwater pressure of late autumn 1962, reflecting a period of water surplus with

only a short time-lag. However, the movements of accumulation flow II are generally delayed, because they are essentially induced by the load applied by the debris coming from the feeder flows. Because of fast loading and the low soil permeability, this process is responsible for the generation of positive pore-water pressures (Hutchinson and Bhandari, 1971). Such a mechanism could explain the apparently anomalous piezometric readings measured within the accumulation body.

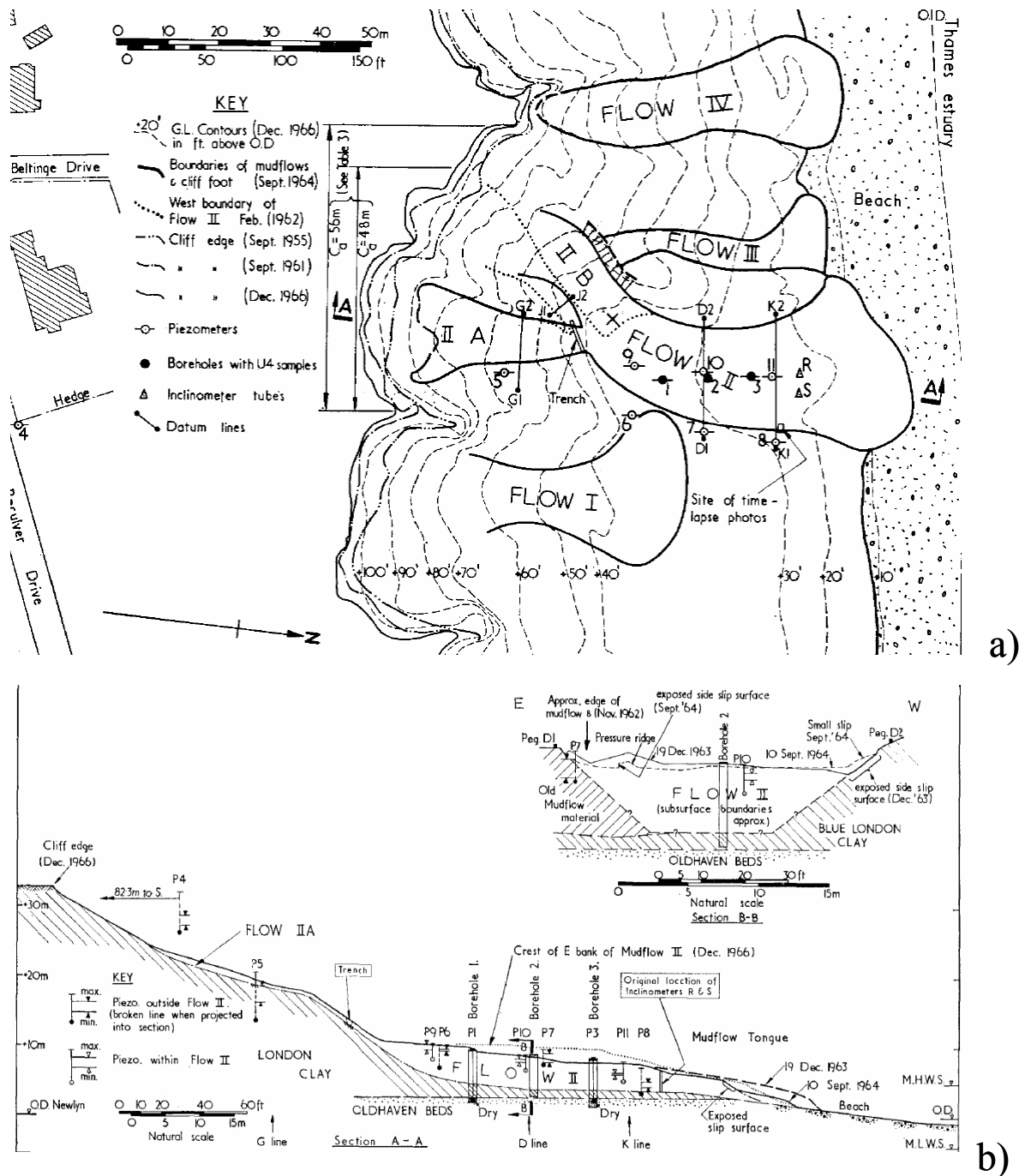


Figure 18 - The Beltinge coastal earthflow: a) plan; b) longitudinal and cross sections (Hutchinson, 1970).

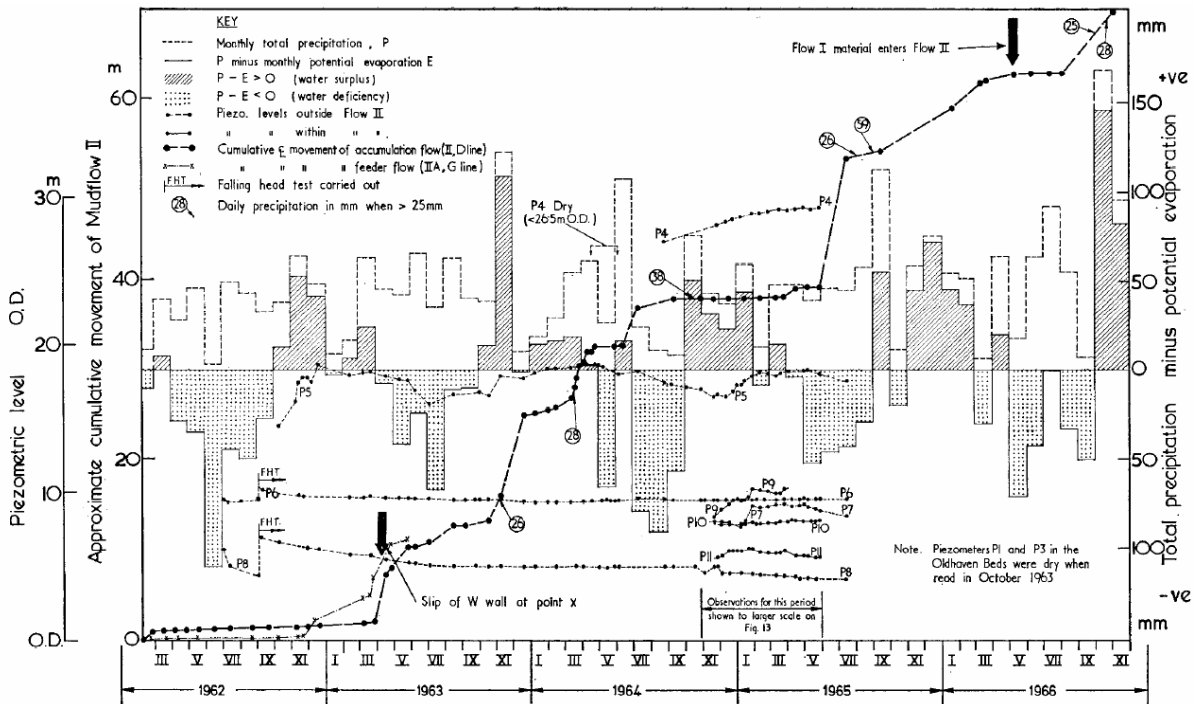


Figure 19 - The Beltinge coastal earthflow: displacements of the accumulation flow II cumulated from February 1962 to November 1966; displacements of the feeder flow II A cumulated from February 1962 to May 1963; piezometric data; climatic data (Hutchinson, 1970).

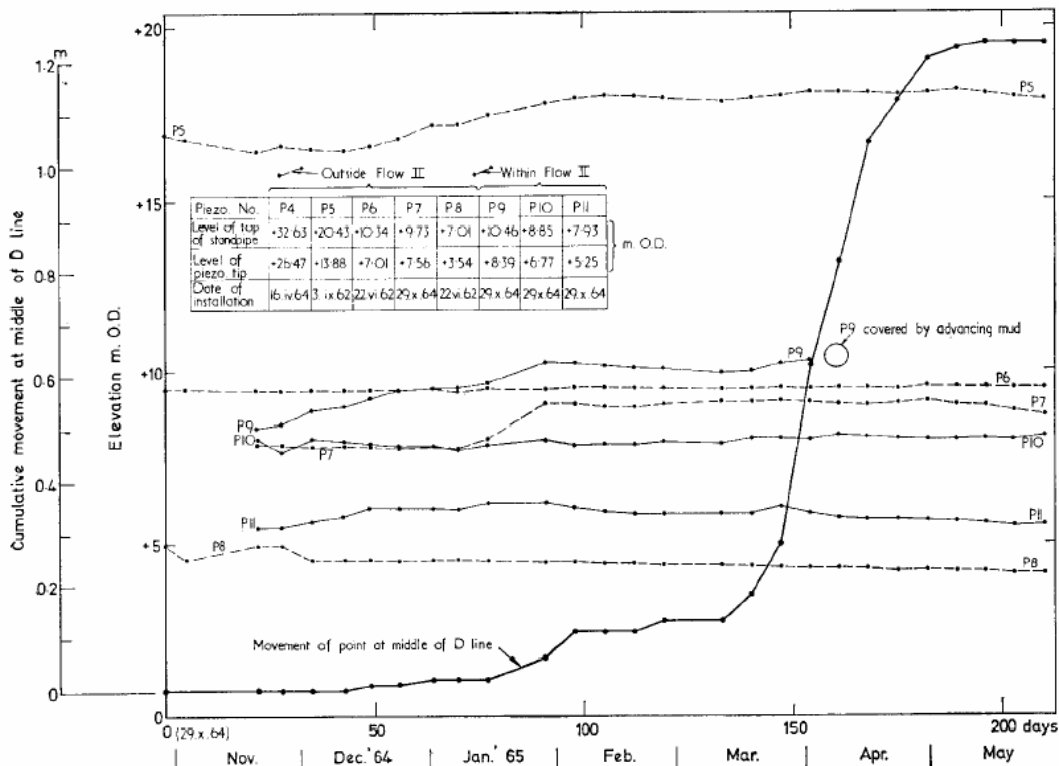


Figure 20 - The Beltinge coastal earthflow: displacements cumulated by the accumulation flow II and piezometric data from November 1964 to May 1965 (Hutchinson, 1970).

Another well documented example (Bertini et al., 1984, 1986) is the active slide along the west side of the St. Martino Stream basin (Abruzzo Region, Central Italy), shaped in Pliocene marine marly clay formations (Fig. 21). The area is located in a temperate zone with Apennine sublittoral Mediterranean features. In particular, the average temperature ranges between 5°C (January) and 24°C (July), while the yearly accumulated rainfall is in between 800 and 1000 mm with two maxima attained in spring and autumn, and two minima attained in summer and winter.

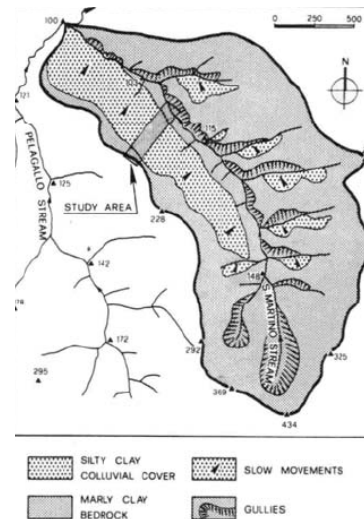


Figure 21 - The St. Martino Stream hydrographic basin (Bertini et al., 1984).

The area was monitored through a pluviometric station, twelve electropneumatic piezometer cells and six inclinometer tubes (Fig. 22a). Available data, which covers a six-year period, reveal that the movements develop along a 9° inclined slope down to a depth of 25 m, involving the weathered part of the parent formation and its colluvial cover (Fig. 22a). Movement is regulated by the pore pressure regime (Fig. 22c,d). In particular, the rate of movement is around 0.35 mm/day when the groundwater surface is less than 3 m deep (Fig. 23). The landslide practically stops if the groundwater level drops below this threshold value. Moreover, the yearly accumulated displacements seem to be affected by the total amount of precipitation during the rainy seasons: in fact, the trend of the piezometric level and of the displacement rate directly follows the rainfall trend (Fig. 22b, c, d).

The Authors suggest that the movement is essentially due to viscous deformation along the slip surface as a combination of both primary and secondary creep. This can justify the different behaviour displayed by the slide during the phases of pore pressure increase and pore pressure decrease: in fact, even under equal pore pressures, the displacement rate is higher during the phases characterized by growing piezometer levels. (Fig. 7). According to the Authors, the decrease in the effective stress during the phase of pore pressure increase causes an increase in the rate of primary creep while the rate of secondary creep decreases; in contrast, in the phase of pore pressure decrease both creep components have the same sign. Further data published in the literature show different behaviours and different interpretations. However, the viscous behaviour of the slip surface is certainly a key point for the analysis of slow slope movements in clay (Corominas et al., 2005; Ledesma et al., 2009).

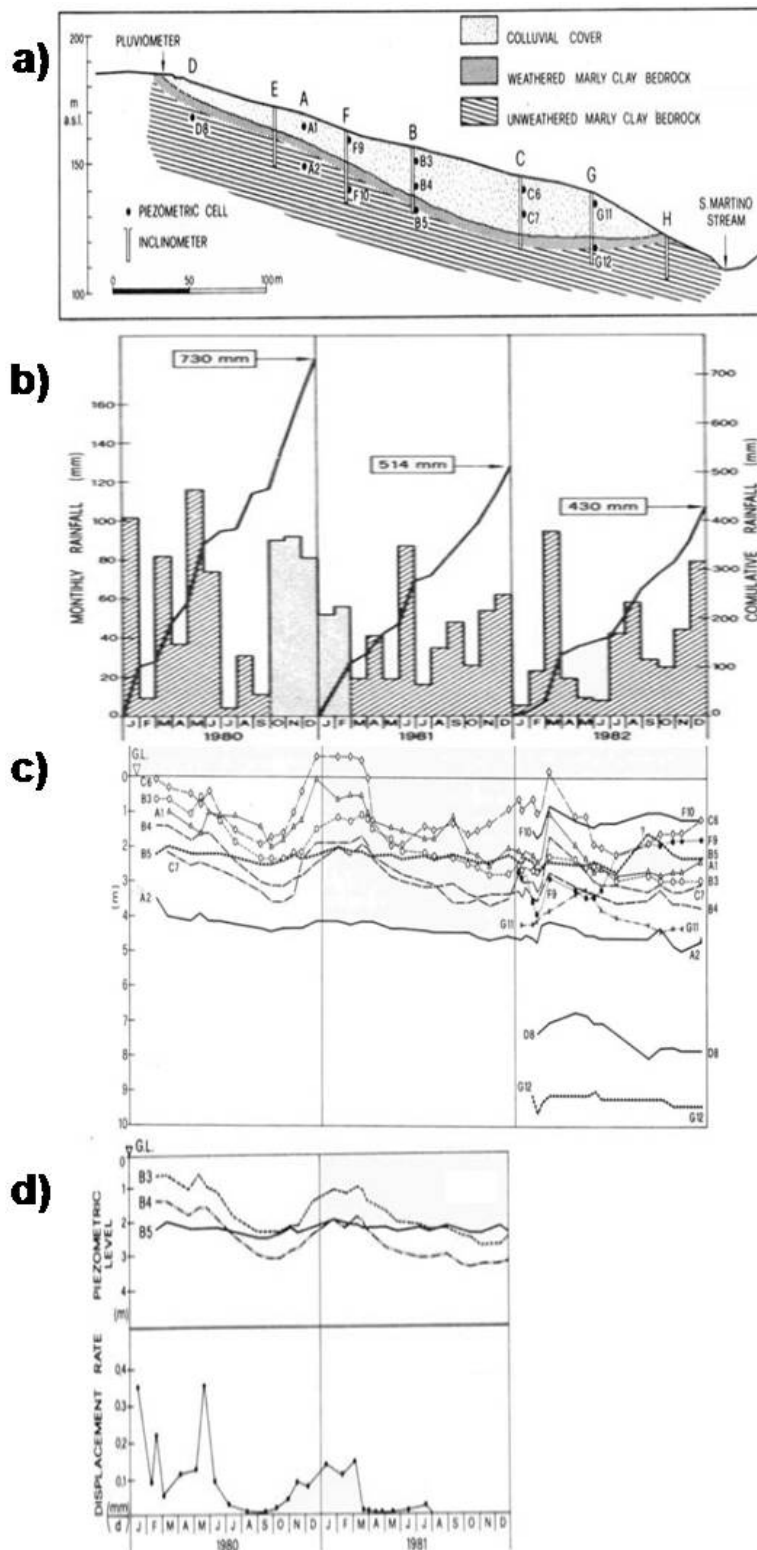


Figure 22 - The St Martino Stream basin slide: a) geological cross section of the valley left side and field instrumentation; b) monthly rainfall and cumulative curves in 1980-1982 (spotted area is the longest period of continuous rainfall); c) piezometric levels; d) piezometric levels vs. time and displacement rate vs. time (Bertini et al., 1984).

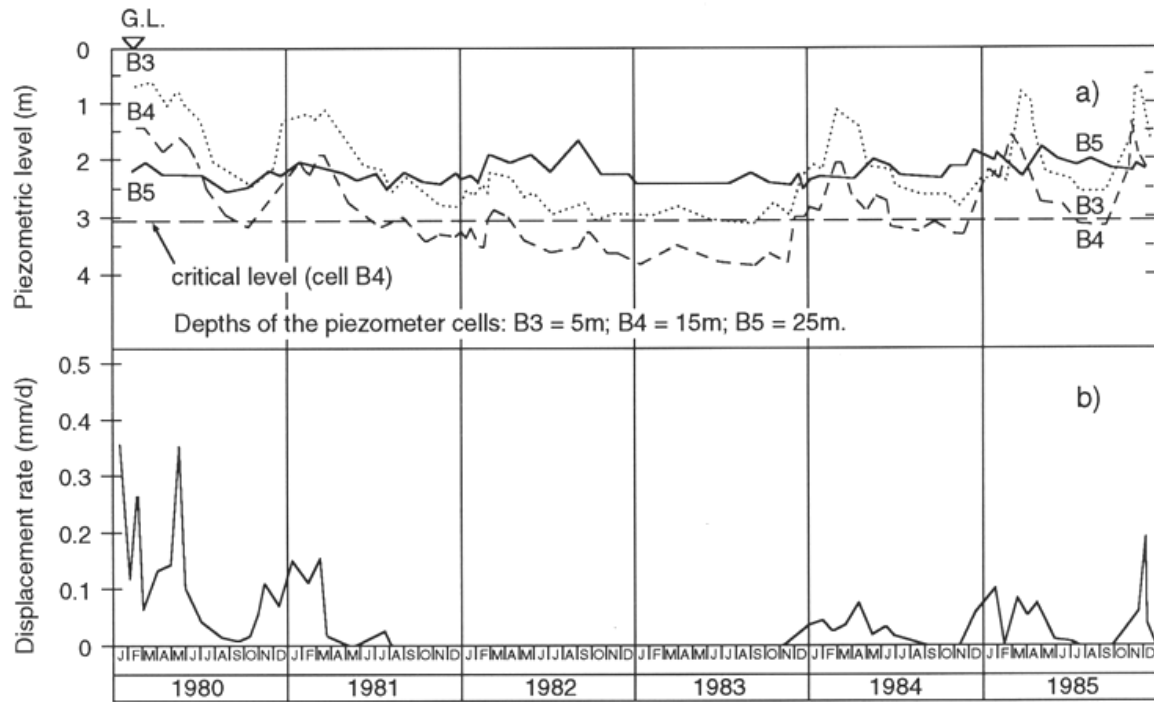


Figure 23 - The St Martino Stream basin slide: pore pressures and displacement rate (Bertini et al., 1986).

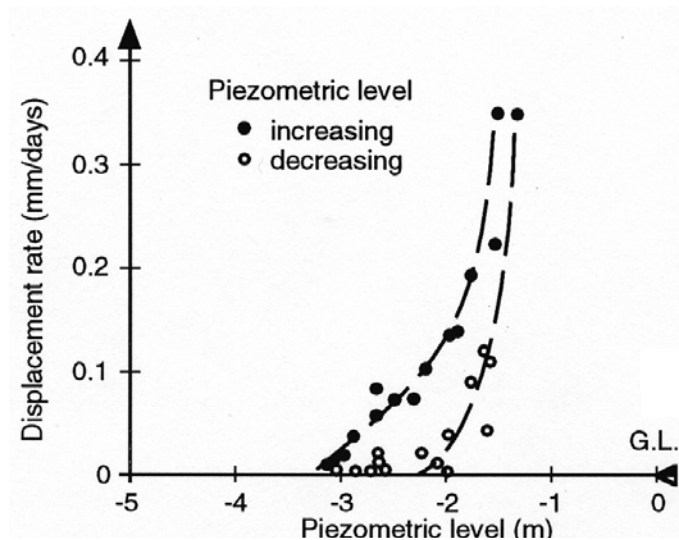


Figure 24 - The St Martino Stream basin slide: groundwater level – displacement rate relationship (Bertini et al., 1986).

Another interesting case that documents the relationship between weather conditions, pore pressures and landslide activity is reported by Tommasi et al. (2006), with reference to a stiff overconsolidated clay slope in the Orvieto town, Central Italy. The town sits on the top of a 50 m thick tuffaceous rock with subvertical cliffs superimposed on ~600 m long and 12° inclined slope formed by a weakly cemented debris layer of fluvio-lacustrine origin (with thickness ranging from 3 to 15 m) covering a Plio-Pleistocene clay formation. Data about the rainfall regime are available from 1920 thanks to a rainfall gauge of the State Hydrographic Survey situated on top of the hill. The average yearly distribution of the two-week rainfall shows that precipitation is concentrated in October and November and has another significant peak in February (Fig. 25). Monitoring carried out since 1982 provides information about the piezometric regime and displacement of the landslide, respectively measured by Casagrande piezometers and inclinometers (Fig. 26). Currently, the northern part of the slope is exposed to shallow translational movements superimposed on deep movements, both essentially parallel to the ground surface. The landslide evolution is characterized by active phases, alternating between deceleration and complete stop, in agreement with the pore pressure regime.

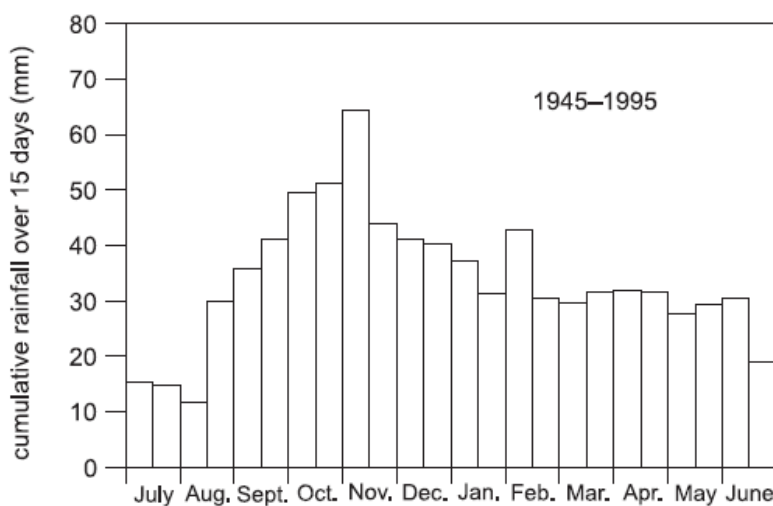


Figure 25 - The Orvieto slide: average two week rainfall distribution measured from 1945 to 1995 (Tommasi et al., 2006).

Shallow movements occur along a slip surface located at the contact between the debris cover and the parent formation, with a maximum depth of about 10 m (surface δ in Fig. 27) and a maximum rate of some tens of cm per year (Fig. 28). In particular, rainfalls cause relatively fast changes of pore pressure in the most permeable shallow materials; shallow movements are then characterized by rather a rapid response to rainfall (cumulative rainfall over up to 60 days).

Deep displacements develop along failure surfaces within the overconsolidated clays to a depth of 33 m (surface α in Fig. 27), with maximum velocities of some tens of mm per year (Fig. 29). Deep movement rates are again characterized by both annual and multi-annual variations that are well correlated to pore pressure and rainfall regimes; in particular,

reactivations occur after long-lasting rainfall periods (cumulative rainfall over up to 180 days) characterized by a sharp excess with respect to the average rainfall regime.

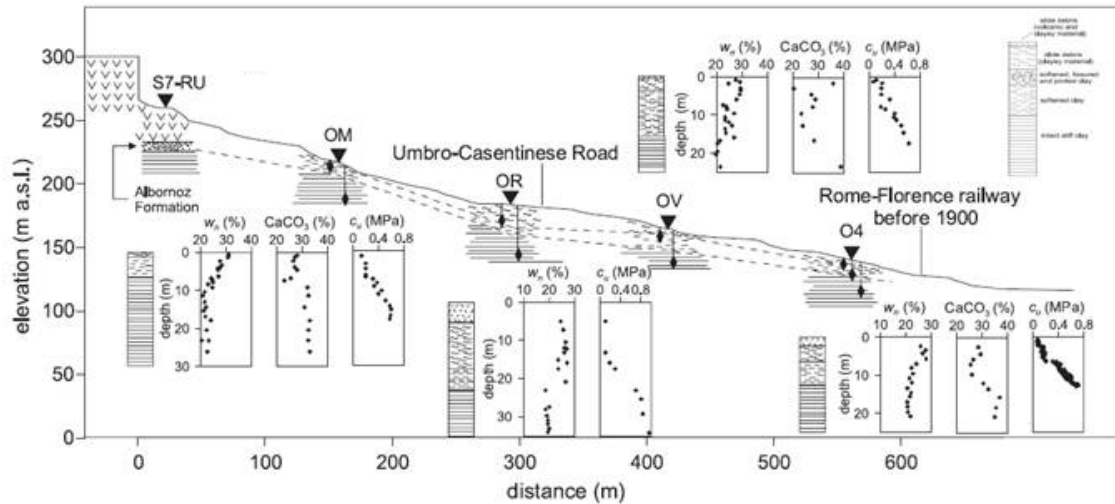


Figure 26 - The Orvietto slide: geotechnical section of the slope (Tommasi et al., 2006).

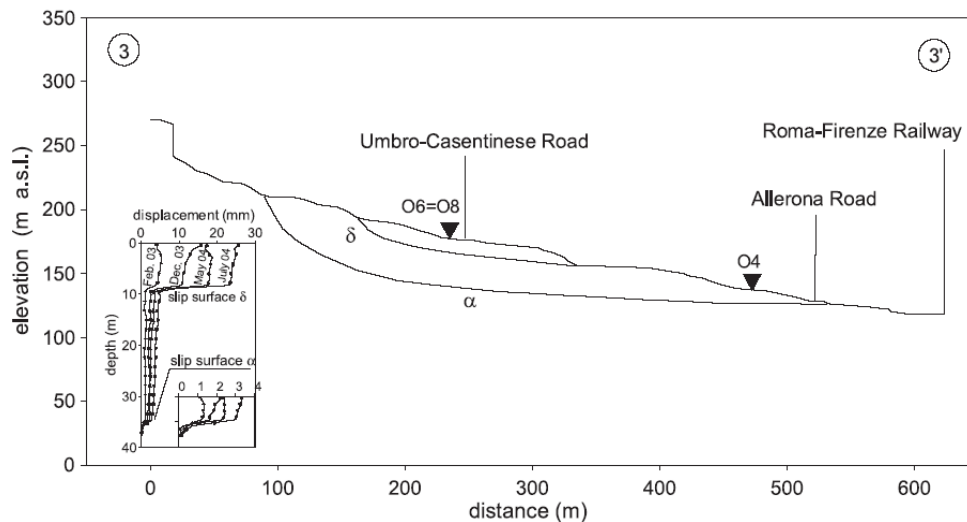


Figure 27 - Detected shallow and deep displacements (Tommasi et al., 2006).

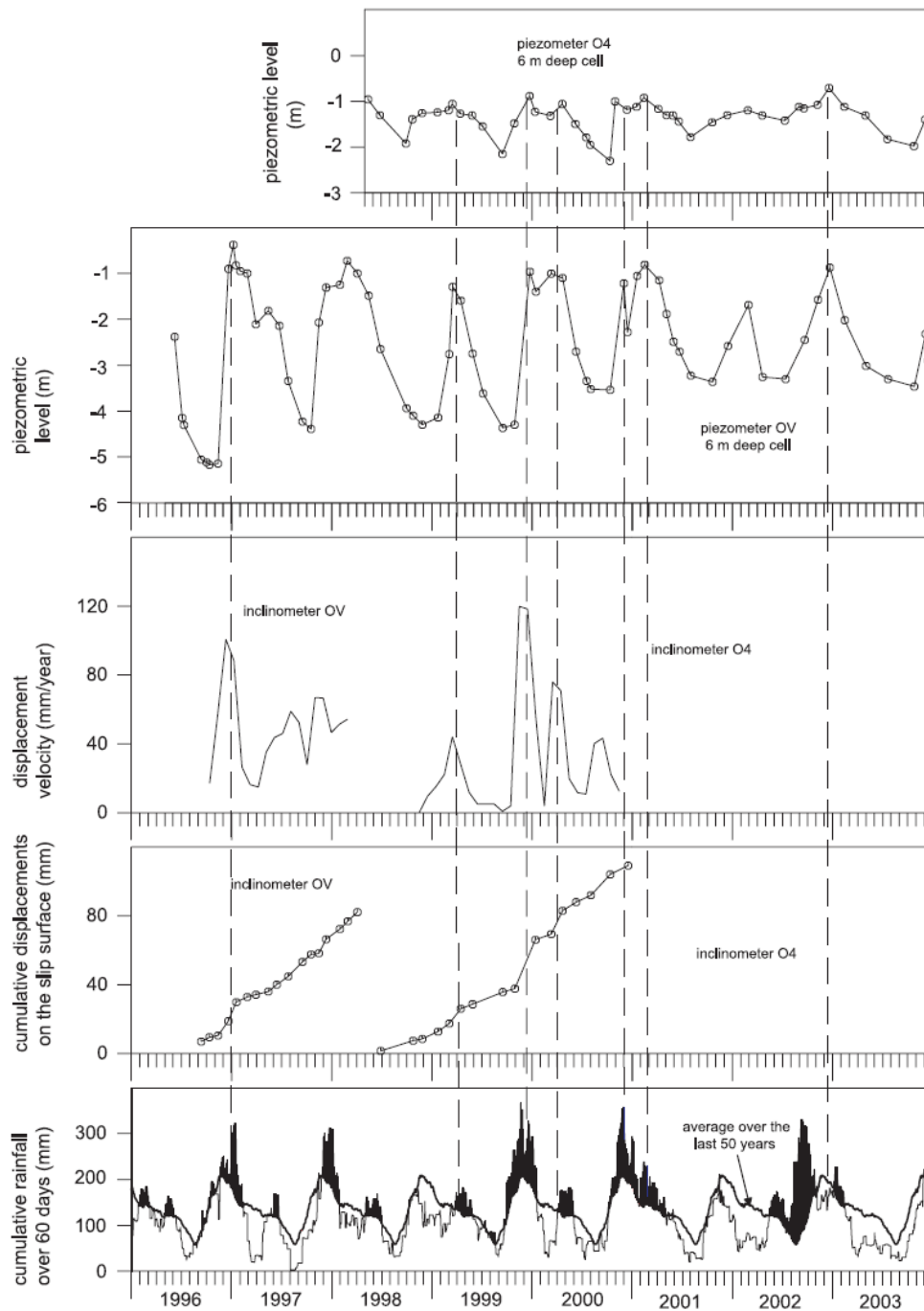


Figure 28 - Rainfall regime, piezometer levels and shallow displacements (Tommasi et al., 2006).

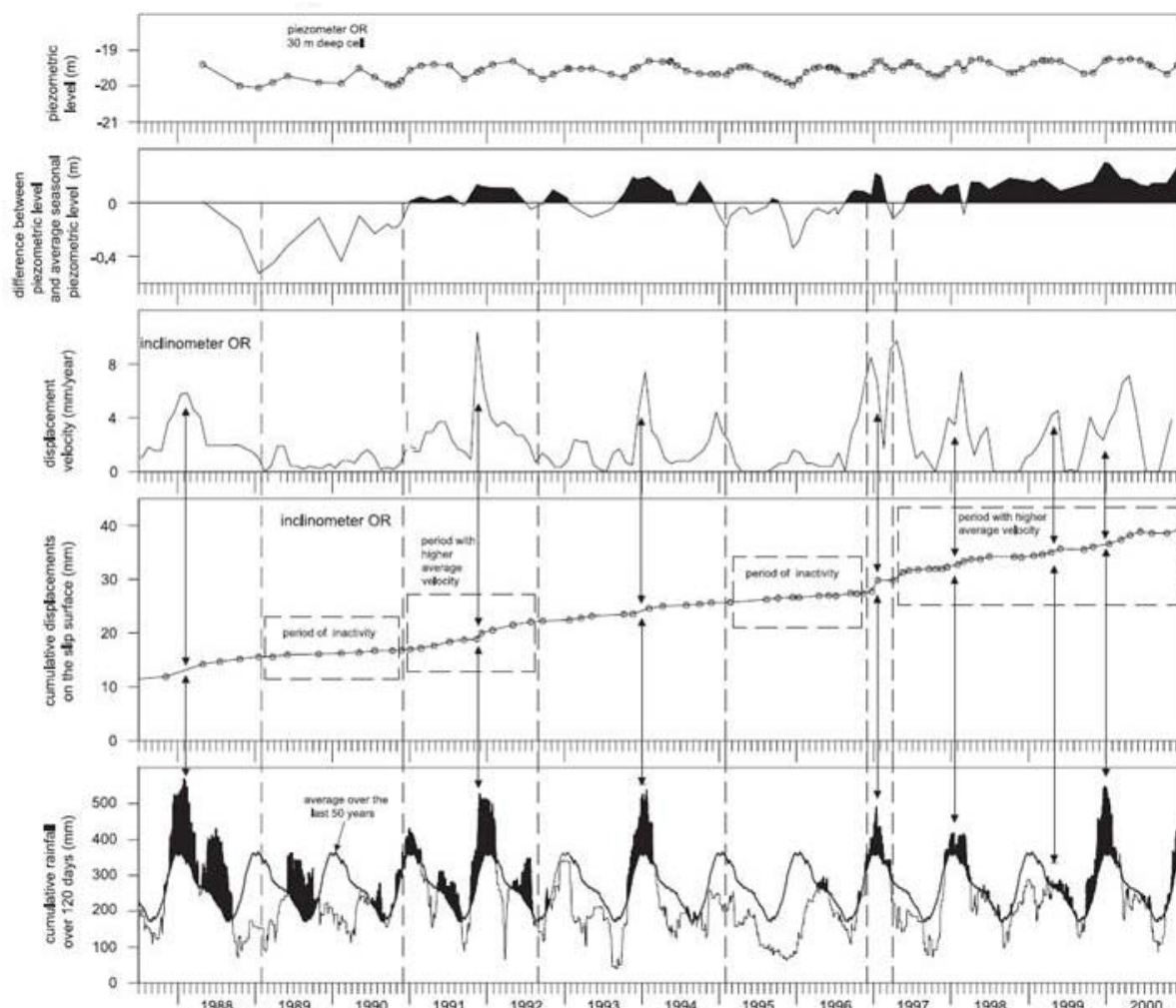


Figure 29 - Rainfall regime, piezometer levels and deep displacements (Tommasi et al., 2006).

2. Jointed clays

The term “jointed clays” usually refers to stiff overconsolidated soils that are crossed by different types of macro-discontinuities such as joints, bedding planes or faults. Some examples can be found in Italy, along the Adriatic coast and in Tuscany.

Esu and Calabresi (1969) analyze a slide, which occurred in August 1968, involving a 25 m high and 45° inclined cut slope excavated in the open coal mine of the Santa Barbara Formation, Upper Valdarno basin, Tuscany Region. The deposit is a Pliocene lacustrine soil, made up of stiff overconsolidated clays crossed by two sets of about one-metre spaced discontinuities, bedding surfaces and vertical joints, and by a fault that subdivided the clay mass into blocks (Fig. 30). The bedding planes were inclined of 10° in the opposite direction with respect to the cut, while the joints direction was parallel to that of the cut. The fault was inclined of 60° in the same direction as the cut.

The results of some direct shear tests performed by Calabresi and Manfredini (1973) show that the strength of the intact clay is much higher than that of the discontinuities. In particular, the intact matrix and the jointed matrix present the same friction angle, but the first one

presents a high cohesion that disappears along joints. Again, the shear strength along fault surfaces is equal to the residual one measured on the intact clay.

Figure 13 reports a schematic view of the landslide evolution, which occurred after the end of the excavation that was completed on August 13th, 1968. A heavy rainfall on August 16th induced movements of the order of some centimetres as a result of the sliding of intact blocks along the discontinuities. The displacements continued for a few metres, accompanied by the opening of discontinuities and the breakdown of the mobilised soil into smaller blocks. The volume of the landslide body increased and the soil below the toe of the cut was affected too.

Esu and Calabresi (1969) carried out a simplified stability analysis based on the limit equilibrium method, assuming a failure mechanism characterised by the slipping of two blocks (EFH and LNMP in Fig. 30) along three discontinuities: a fault, a vertical joint and a bedding surface. According to the analysis, if water had been absent within the discontinuities, the equilibrium conditions would have been granted. The Authors point out that even small cleft pressures in the opened discontinuities could have been responsible for triggering the slide.

In order to understand the role of cleft pressures on the mechanical response of the cut, D'Elia et al. (1998) performed a numerical simulation of the movement using two different models. While the first model (Fig. 31) reproduces the scheme considered by Esu and Calabresi (1969), the second model (Fig. 32) considers the fault and a set of vertical joints and bedding planes, thus simulating a more realistic situation. In both cases, the blocks consist of deformable materials: their geotechnical parameters come from laboratory tests (Esu and Calabresi, 1969; Bertuccioli, 1995). The Authors refer to Calabresi and Manfredini (1973) for the mechanical characteristics of the discontinuities. The geotechnical parameters adopted in the analyses are reported in Table 1.

First analyses assume the absence of water in the discontinuities. Then, a water flow developing along the network of discontinuities, even above the toe of the cut, has been taken into account as an effect of heavy rainfall. In the first model, the water flow has been reproduced by applying a water pressure equivalent to a height of 10 cm of water on the lower and upper banks (Fig. 33). In the second model, the hydraulic condition has been reproduced by considering a hydrostatic distribution of the water pressure on the vertical boundaries of the grid with a water level reaching the ground surface (Fig. 32).

The results were revealed to be very sensitive to both the adopted model and the hydraulic condition. In the first case, the maximum displacement calculated by the first and the second models are respectively equal to 3 cm and 40 cm, while they attain 88 cm and 400 cm respectively if the presence of water in the discontinuities is taken into account. Regardless of the model, the displacements did not affect the area upslope of the fault, thus confirming that the mechanism of rupture is strongly governed by this. Significant differences have been found regarding the zone located below the toe of the cut that is subjected to slip only in the second analysis: the deformed mesh displays a very similar configuration to that effectively observed in situ at the end of the movement (Fig. 34).

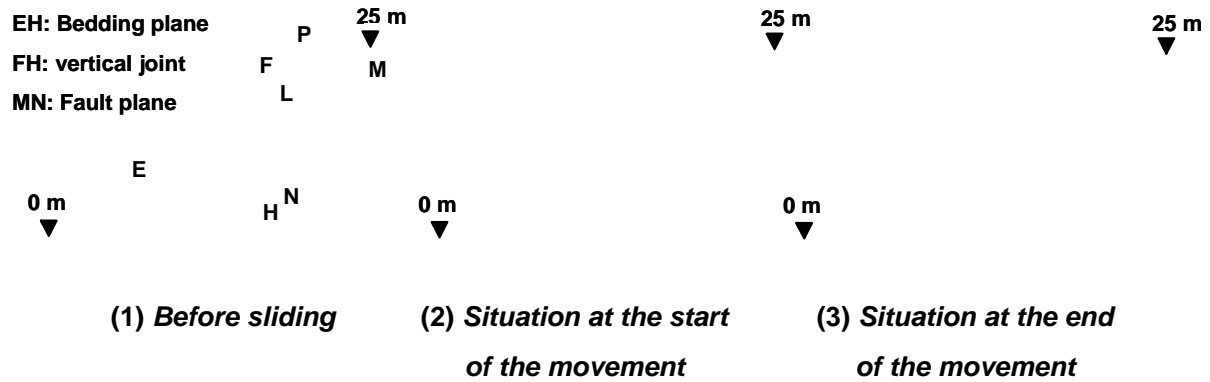


Figure 30 - Plan and section of the slide occurred on August 1968 in the Santa Barbara open pit mine (Esu and Calabresi, 1969).

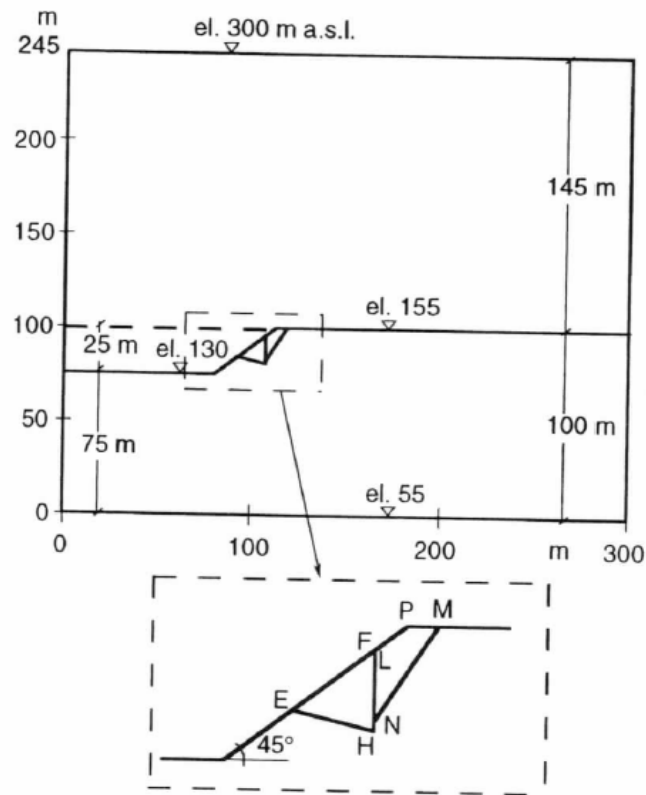


Figure 31 - First model used to simulate the slide occurred on August 1968 in the Santa Barbara open pit mine (D'Elia et al., 1998).

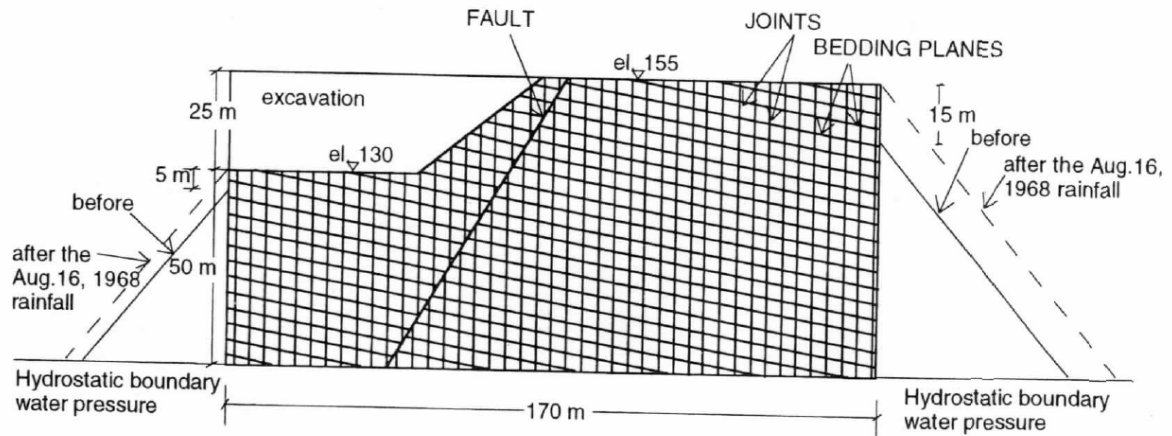


Figure 3. Model 2: block mesh with hydraulic boundary conditions.

Figure 32 - Second model used to simulate the slide occurred on August 1968 in the Santa Barbara open pit mine (D'Elia et al., 1998).

	Block material	Bedding surfaces	Joints	Fault
Model 1	$\rho=1760 \text{ kg/m}^3$ $K=650 \text{ MPa}$ $G=300 \text{ MPa}$ $\phi'=16^\circ$ $c'=150 \text{ kPa}$	$k_n=1400 \text{ MPa/m}$ $k_s=700 \text{ MPa/m}$ $\phi'=16^\circ$ $c'=0$	$k_n=1400 \text{ MPa/m}$ $k_s=700 \text{ MPa/m}$ $\phi'=16^\circ$ $c'=0$	$k_n=1400 \text{ MPa/m}$ $k_s=700 \text{ MPa/m}$ $\phi'=11^\circ$ $c'=0$
Model 2	$\rho=1760 \text{ kg/m}^3$ $K=650 \text{ MPa}$ $G=300 \text{ MPa}$ $\phi'=16^\circ$ $c'=150 \text{ kPa}$	$k_n=1400 \text{ MPa/m}$ $k_s=700 \text{ MPa/m}$ $\phi'=16^\circ$ $c'=0$	$k_n=1400 \text{ MPa/m}$ $k_s=700 \text{ MPa/m}$ $\phi'=19^\circ$ $c'=0$	$k_n=1400 \text{ MPa/m}$ $k_s=700 \text{ MPa/m}$ $\phi'=11^\circ$ $c'=0$

ρ : density

ϕ' : shear angle

G: shear modulus

k_n : discontinuity normal stiffness

c' : cohesion

K: bulk modulus

k_s : discontinuity shear stiffness

Table 1 – Santa Barbara case: geotechnical properties considered in the analyses (D’Elia et al.,1998).

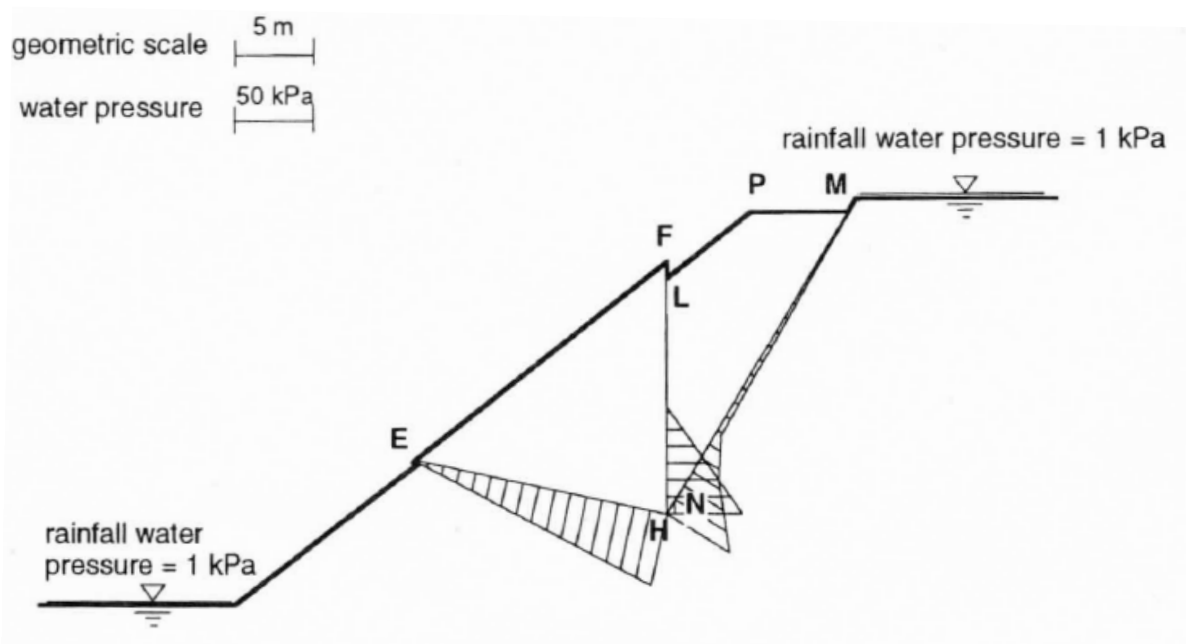


Figure 33 - Santa Barbara case: results from first model. Block displacements and final water pressure in the discontinuities after rainfall occurred on August 16, 1968 (D’Elia et al., 1998).

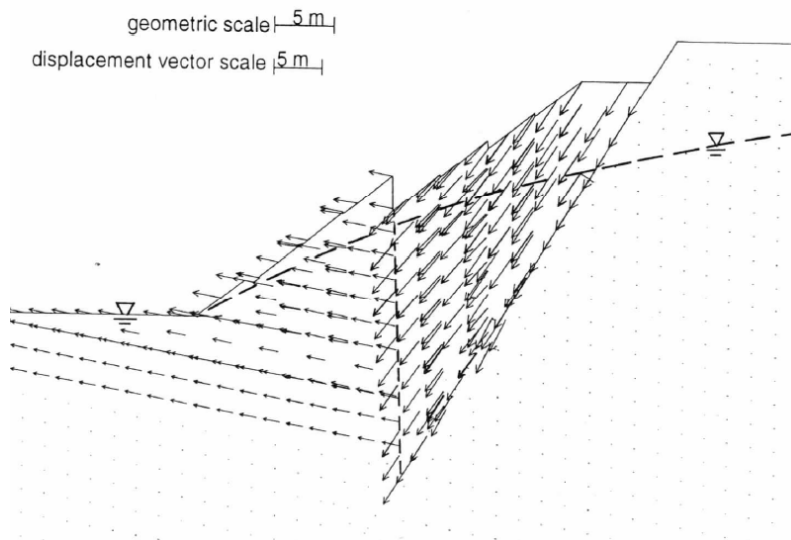


Figure 34 - Santa Barbara case: results from second model. Block displacements and water level in the discontinuities at the end of movement (D’Elia et al., 1998).

The failure mechanism recognised in Santa Barbara clay shows many similarities to that proposed by Henkel (1967) to explain planar slides triggered by rainfall. Such a mechanism (Fig. 35a) considers a planar layer resting on bedrock parallel to the ground surface. The lateral downslope boundary of the upper layer is represented by a vertical cut. A vertical fracture located at a distance x from the cut is assumed to be filled by rain water. Figure 35b shows that the stability condition is a function of location of cracks; in fact, assuming that the contact between the two layers is cohesionless, the friction angle ϕ' necessary for stability increases as the distance x decreases.

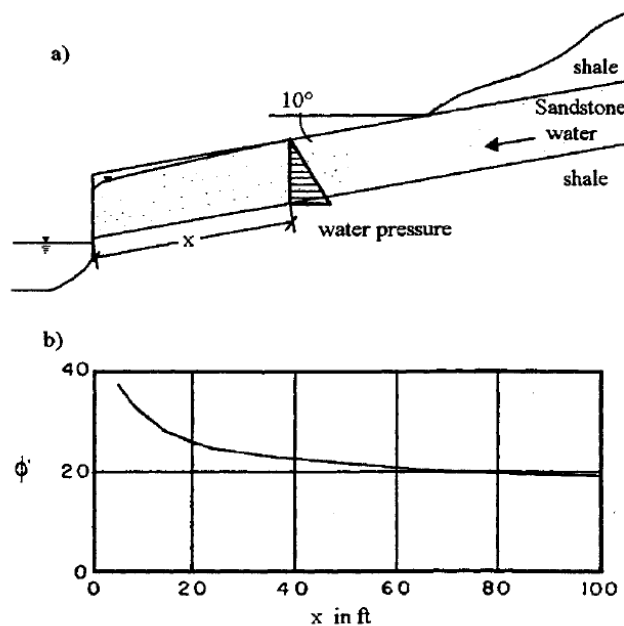


Figure 35 - Mechanism of planar failure induced by cleft pressures: a) reference scheme; b) friction angle ϕ' required for stability (after Henkel, 1967).

Such cracks are often the result of pre-failure deformations. The possible role of pre-failure deformations is suggested by the case history of the Melfi landslide, Southern Italy, reactivated by cutting of the toe of a slope in flysch (Picarelli and Viggiani, 1988). Because of the high residual friction angle of the soil, the only possible explanation of the movement was the effect of cleft pressures within some vertical tension cracks normal to the direction of movement observed some tens of metres from the toe.

The Vallcebre landslide, Eastern Pyrenees, Spain (Fig. 36), is another similar case (Corominas et al., 2005). The landslide has been active for several centuries, involving shale, gypsum and claystone layers moving over a thick limestone bed. It is 1200 m long and 600 m wide and covers an area of 0.8 km² crossed by superficial shear surfaces and tension cracks, which represent preferential drainage pathways to rainfall infiltration. Three distinct units have been recognized. In particular, the lower unit has been monitored since 1996 using conventional surveying and photogrammetry, differential GPS, boreholes equipped with inclinometers, wire extensometers and piezometers. The displacements never stop and are characterized by velocities that are close to zero only during dry seasons (Fig. 37). Piezometers set in tension zones (as S5) measure rather small changes in groundwater levels (ranging between 0.5 and 2 m) and a fast drainage if compared to the piezometers located elsewhere (for example S2, S4 and S11), which experience changes of groundwater level up to 5 m and a slower rate of pore water decrease.

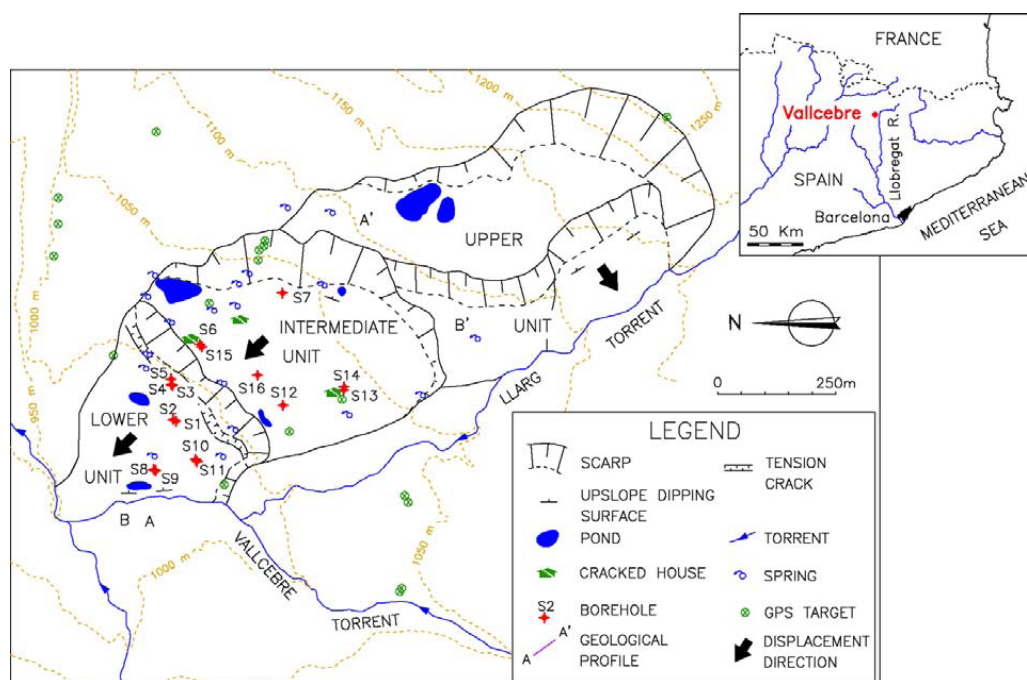


Figure 36 - Plan view of the Vallcebre landslide, Spain (Corominas et al., 2005).

3. Highly fissured clays

Several earthflows in highly-fissured plastic clays and clay shales spread in the Southern Apennines, Italy, have been investigated through site and laboratory investigations,

monitoring and numerical modelling. Such research provides useful data for the understanding and the analysis of triggering in highly fissured clays.

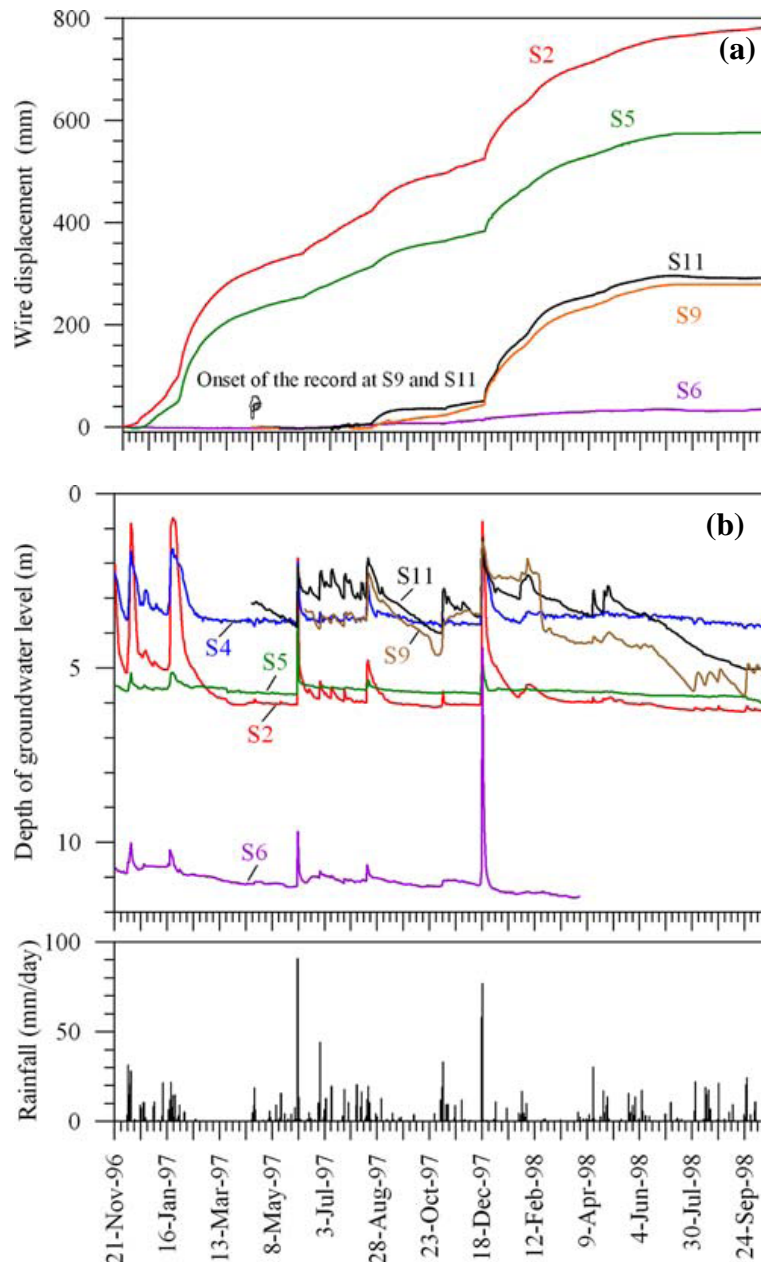


Figure 37 - Vallcebre landslide: a) wire displacements measured at boreholes S-2, S-5, S6, S9 and S-11; b) piezometric levels measured at boreholes S2, S4, S5, S6, S9 and S11 (Corominas et al., 2005).

Triggering generally develops according to a slide style, i.e. along a well defined slip surface; the flow-like style is revealed after failure (Picarelli, 2000). In contrast with slides that move as stiff bodies, earthflows display internal deformations similar to those of viscous liquids. As a consequence, deformation of the entire landslide body seems to predominate in some periods of landslide activity over concentrated shear displacements at the base.

Most of the sites investigated are concentrated in the high Basento valley (Fig. 38): Brindisi di Montagna (Cotecchia et al., 1984; 1986), Masseria Marino (Guerriero, 1995; Picarelli et al., 1995; Giusti et al., 1996; Pellegrino et al., 2000; Comegna et al., 2004; Comegna, 2005; Picarelli et al., 2005; Comegna et al., 2007, Comegna and Picarelli, 2008), Masseria De Nicola (Guerriero, 1995; Giusti et al., 1996; Pellegrino et al., 2004a) and Acqua di Luca (Giusti et al., 1996; Pellegrino et al., 2004a). All earthflows have been instrumented with piezometers installed both in the landslide body and in the stable formation below or around it.



Figure 38 - Position of four earthflows that are ongoing in Basento Valley, Southern Italy: 1 - Brindisi di Montagna; 2 - Masseria Marino; 3 - Masseria De Nicola; 4 - Acqua di Luca (Picarelli et al., 2005).

Figure 39 shows the seasonal fluctuations of the water level in the extremely slowly flowing Acqua di Luca over a period lasting more than 10 years (Pellegrino et al., 2004b). Typically, the pore pressure attains its peak value in the period December-April, then gently decreases, reaching a minimum between October and December. In the dry season between May and November, even intense rainfalls do not produce significant increases in pore pressures, probably because of evapotranspiration and the lower permeability of the shallowest unsaturated soil layers.

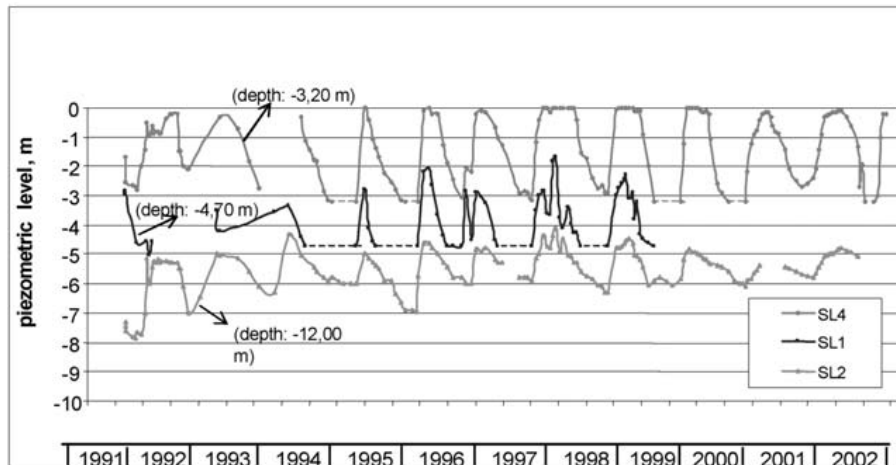


Figure 39 - Piezometric levels measured in the Acqua di Luca earthflow (Pellegrino et al., 2004b).

As with many other landslides in clay, earthflows located in the Basento Valley are active for many tens of years (Iaccarino et al., 1995) but their evolution can display sudden changes of both geomorphological and kinematic features. Where the strength mobilised along the shear zone is at, or near, the residual value, the landslide may be cyclically reactivated by pore pressure fluctuations, thus the movements tend to be strongly seasonal. Figure 40 reports the evolution of the displacement rate of Masseria Marino, Masseria De Nicola and Acqua di Luca earthflows, showing that peaks due to landslide acceleration are followed by a slow decrease in the displacement rate. In the long term, this may drop to a few millimetres per year.

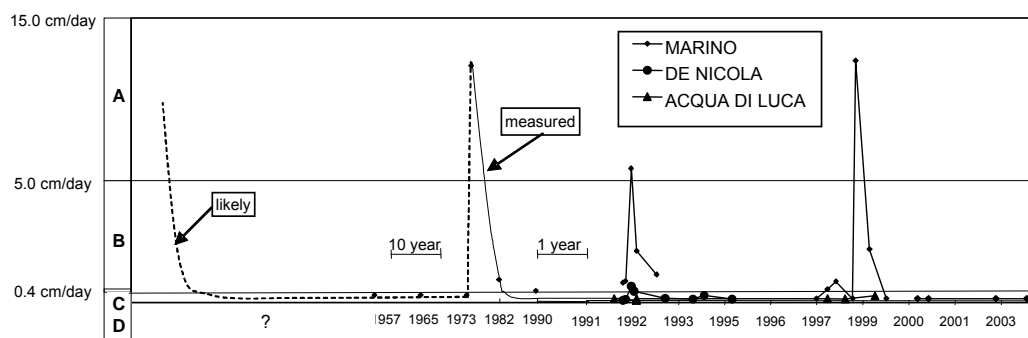


Figure 40 - The displacement rate of three earthflows in the Basento valley, Southern Italy (Picarelli et al., 2005).

Monitoring suggests that movement essentially develops through alternating stages of undrained–drained deformation (Comegna et al., 2007). Undrained conditions are established as a consequence of the non-uniform state of stress and strain induced by landslide mobilisation (or reactivation) combined with the typical properties of soils involved in earthflows, that feature both a low permeability and a contractive behaviour associated with a high degree of softening. Such undrained conditions give rise to the highest velocities: during

such phases, internal strain prevails over displacement concentrated along the slip surface, thus the landslide displays a marked flow-style.

Figure 41 summarises the behaviour of the Masseria Marino earthflow investigated from the middle of 1991 to the end of 1993. Water levels measured with Casagrande piezometers in the zone between the depletion area and the upper part of the main track show quite irregular changes over short periods of time (Fig. 41b). However, as displacement accelerates (Fig. 41c), the water level rises above the ground surface as a likely effect of induced excess pore pressures. It is worth noting that the investigated zone was clearly subjected to some compression, as revealed by topographic measurements (Fig. 41a). Using data provided by a rainfall gauge installed on the slope and accounting for the permeability measured by in situ tests, Comegna et al. (2004) set up some numerical analyses aimed at reproducing the pore water fluctuations caused by rainwater infiltration in active and non-active portions of the Masseria Marino earthflow. The consequent results show a good agreement between measured and calculated values in non-active parts (Fig. 42a). However, the adopted model is not able to reproduce the pore-water pressures measured in active zones (Fig. 42b), where excess pore-water pressures develop as a consequence of the undrained conditions provoked by the landslide mobilisation. The subsequent dissipation of excess pore pressures is associated with the decrease of the displacement rate and the changing pattern of slope movements, which turns from a flow to a slide style, being predominantly featured by movements along a well defined slip surface located at the base of the landslide.

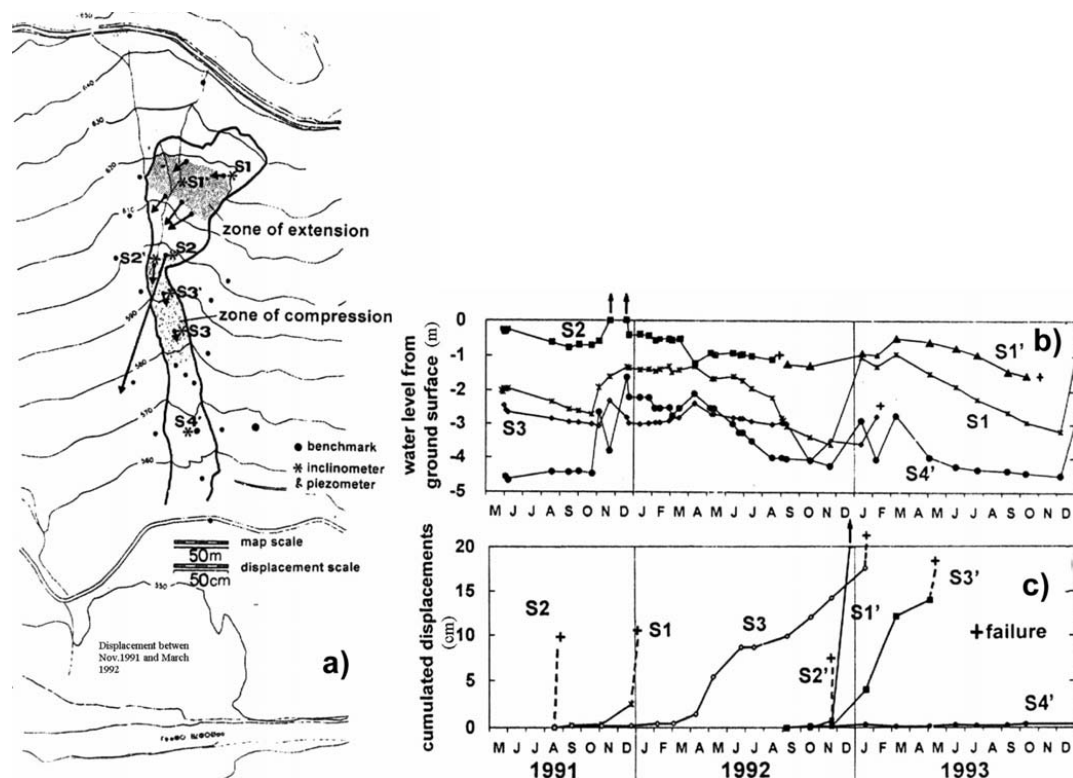


Figure 41 - Displacements and water levels measured in the Masseria Marino earthflow in the period 1991–1993 (from Giusti et al. 1996): (a) plan of the landslide and superficial displacements; (b) water levels measured at some Casagrande piezometers; (c) evolution with time of horizontal displacements.

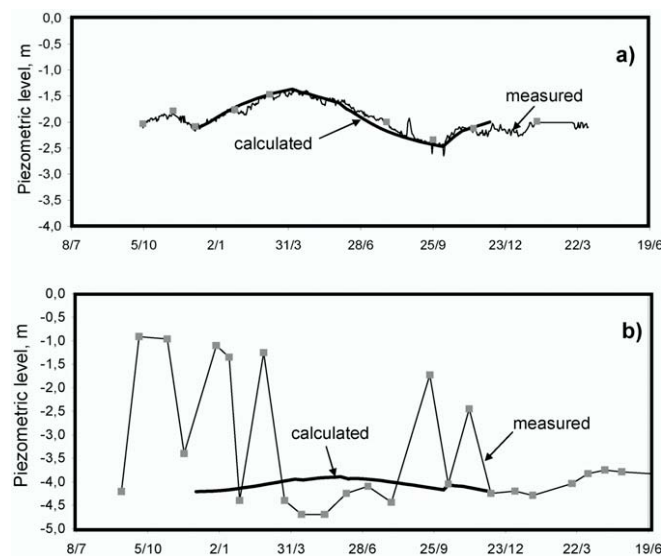


Figure 42 - Comparison between measured and calculated groundwater levels in a non-active a) and in an active part (b) of the Masseria Marino earthflow (from Comegna et al., 2004).

Further information is provided by the monitoring of the Torrente Miscano earthflow (Picarelli et al., 1999), carried out between 1993 and 1999 (Fig. 43). In that period, the area was subjected to moderate rainfall, mainly concentrated in the time interval November to April, with a maximum monthly height of about 250 mm and a maximum accumulated annual height of 788 mm (Fig. 43c). Figure 26d reports the groundwater level depth measured between March, 1993 and April, 1999, by some Casagrande piezometers installed within the landslide body. The pore pressure fluctuations follow a seasonal trend with peak values measured between January and March, and minimum values measured between October and January. During wet seasons, the time lag between rainfalls and groundwater recharge is very short, while the groundwater level declines very slowly in dry seasons and does not show any significant response to isolated, although very intense, rainfall events. Both the maximum groundwater level (very close to the ground surface) and the minimum level (that reaches a depth between 2.0 and 2.5 m) seem to be strongly affected by the amount of rain: for instance, the peak value is higher at the beginning of 1994 and 1996 than in 1995, which follows a dryer period. Figure 43e shows the annual accumulated displacements measured by the inclinometers next to the ground surface. These show large variations along the slope and with time, ranging between about 0.5 and 8 cm/year, so the landslide may be classified as slow to extremely slow. The variability of displacements with space suggests that the landslide body experiences internal deformation, thus its behaviour depends on the local induced strain field. The variability with time essentially depends on the pore pressure regime, in turn affected by the volume of rain. The influence of rainfall is clearly evidenced by Figure 43e that shows a significant increase of the landslide activity systematically following a rainy period: the high displacement rate in the first months of 1994 and 1996, for instance, is clearly related to the preceding cumulated rainfalls. In particular, the inclinometer I3, which is the only working since 1993, shows that slope mobility practically stops every year between May and September as an immediate response to the pore pressure decline (Fig. 43d, f), while it restarts during the wet season. In particular, the earthflow is characterised by

a threshold groundwater level, ranging between 1 and 1.5 m (Fig. 43d), above which movements are cyclically triggered: Figure 44 shows that the relationship between the depth of the groundwater table and the displacement rate is highly non-linear.

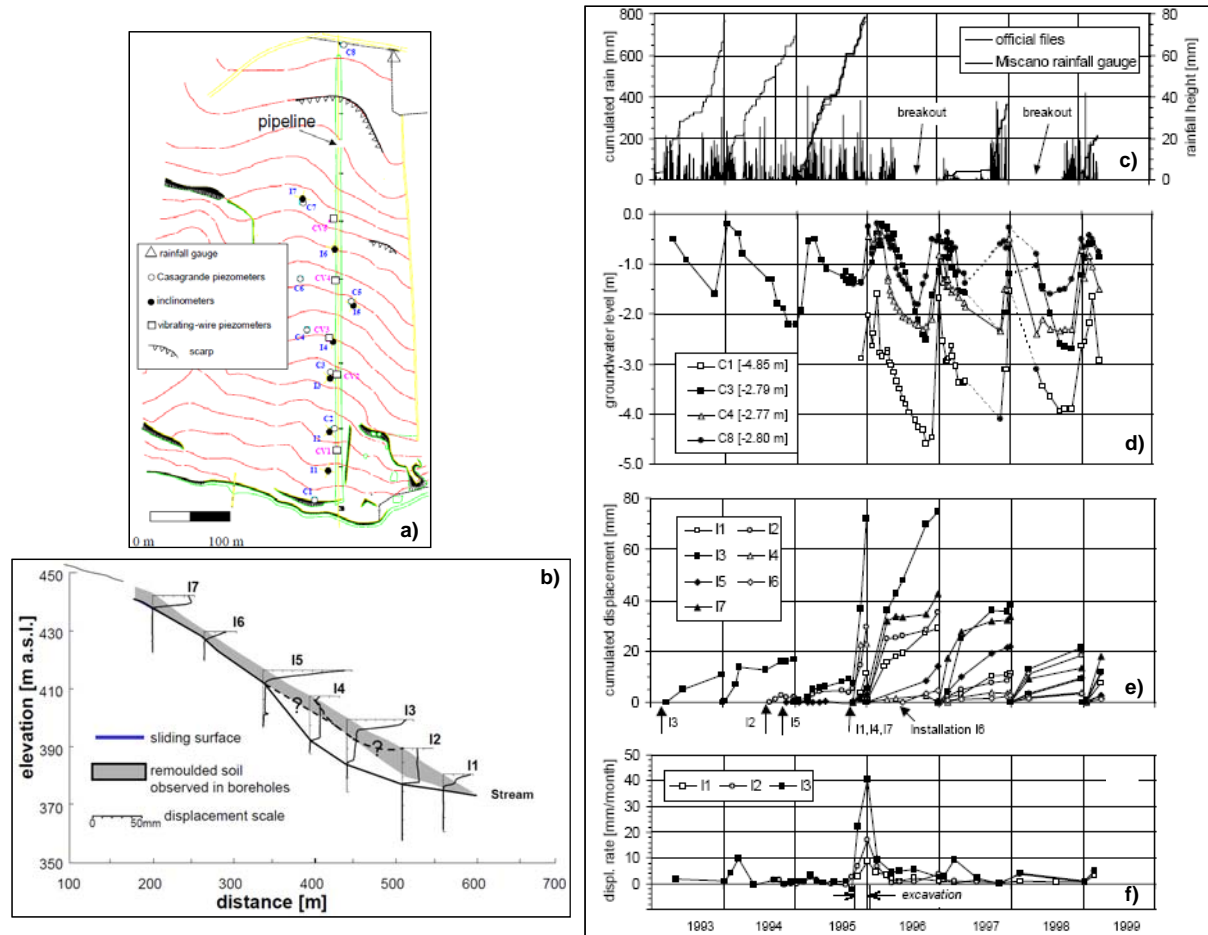


Figure 43 - Torrente Miscano earthflow, Southern Italy: a) instrumentation location; b) landslide body detected by inclinometers; d, e, f) cumulated rainfall, water levels and cumulated displacements (after Picarelli et al., 1999).

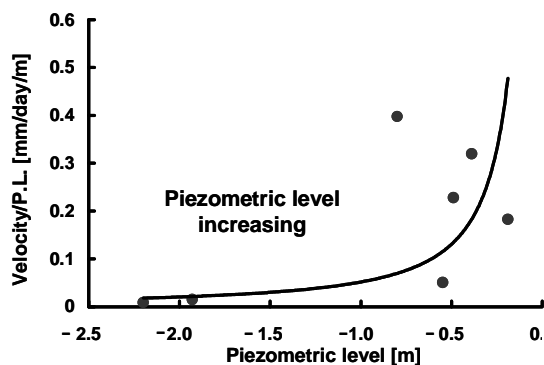


Figure 44 - T. Miscano earthflow, Central Italy: groundwater level – displacement rate relationship (Picarelli and Russo, 2004).

4.3 SYNTHESIS OF MONITORED SITES ON THE SPECIFIC CASE OF PYROCLASTIC SOILS (UNISA)

1. Introduction

Soil suction is one of the most important physical variables governing the behaviour of unsaturated soil slopes. It is responsible not only for the mechanical response of the slope, but also for transfer of water (i.e. infiltration, evaporation and transpiration) and energy between the atmosphere and the soil, through the slope surface. Therefore, it is crucial for geotechnical engineers to understand the mechanisms that control soil suction variations induced by changes in boundary conditions due to human and/or natural actions. Appropriate modelling of the soil suction regime is required for the prediction of slope behaviour. The above statement is of particular relevance when geotechnical analyses are oriented to the assessment of slope stability conditions following infiltration of rain water, in order to predict the onset of shallow slope failure.

A significant example is represented by an area of about 3000 km² in the Campania Region (Southern Italy) where limestone and tuffaceous slopes are diffusely covered by unsaturated pyroclastic soils. These soils were originated from the explosive phases of the Campi Flegrei and Somma-Vesuvius volcanic activity and they are frequently affected by landslides of the flow-type triggered by critical rainfall events (Cascini, 2004). Among recent destructive landslides of the flow-type, one of the most calamitous occurred on May 1998 and caused 159 casualties and serious damage in four towns (Bracigliano, Quindici, Sarno and Siano), located at the toe of the so-called “Pizzo d’Alvano” limestone relief (Fig. 1).

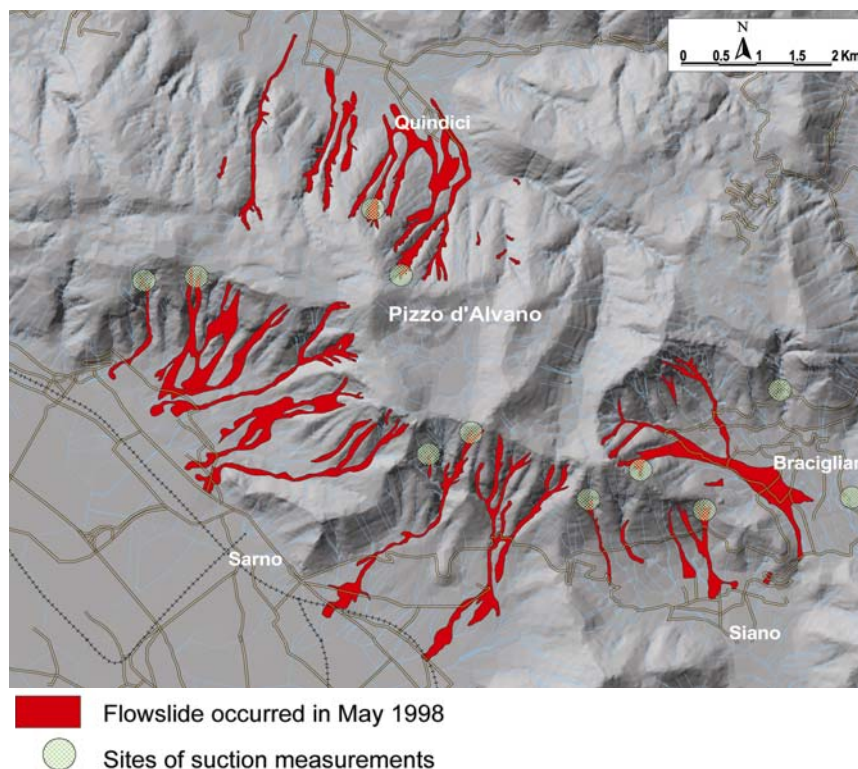


Figure 1 - Landslides of the flow-type occurred in May 1998 and sites of soil suction

measurements.

The relevant extension of the territory (about 60 km²) affected by the 1998 event, pointed out the necessity to set up a wide interdisciplinary research programme to investigate the geological factors (Cascini et al., 2000), the mechanical soil properties (Bilotta et al., 2005) and the triggering mechanisms (Cascini et al., 2008) of the landslides that occurred.

In-situ and laboratory investigations were performed in order to acquire detailed data on the stratigraphy, the mechanical properties of pyroclastic soils, both in saturated and unsaturated conditions, and the soil suction regime during dry and wet seasons.

As for the topographic conditions, Cascini & Sorbino (2003) indicate average slope angle varying from 35 to 41 degrees and soil thickness ranging from 0.5 m to 5.0 m. The typical stratigraphic conditions of the landslide source areas on mountain slopes within the territories of the towns of Bracigliano, Quindici, Sarno and Siano are illustrated in Figure 2. The slopes within the territory of Bracigliano show quite a homogeneous stratigraphy compared to those located in the territories of the other towns, due to a complete absence of pumice layers that in other slopes, and particularly at the Sarno site, are present at different depths among the ashy layers (Fig. 2).

Moreover, physical and mechanical properties of the pyroclastic soils were obtained through a laboratory research programme on undisturbed and remoulded samples collected at the investigation sites. This consisted of various tests on undisturbed samples aimed at investigating the physical properties, as well as the shear strength and hydraulic properties of the pyroclastic soils, both in saturated and unsaturated conditions. Hydraulic properties of the ashy soils in saturated conditions were investigated by means of conventional permeameter tests while, in the unsaturated conditions, three different laboratory equipments were utilised, i.e. Suction Controlled Oedometer, Volumetric Pressure Plate Extractor and Richards Pressure Plate. A detailed description of the methodologies and the experimental procedures as well as the main laboratory results obtained is presented by Sorbino & Foresta (2002) and Bilotta et al. (2005).

Bracigliano

Quindici

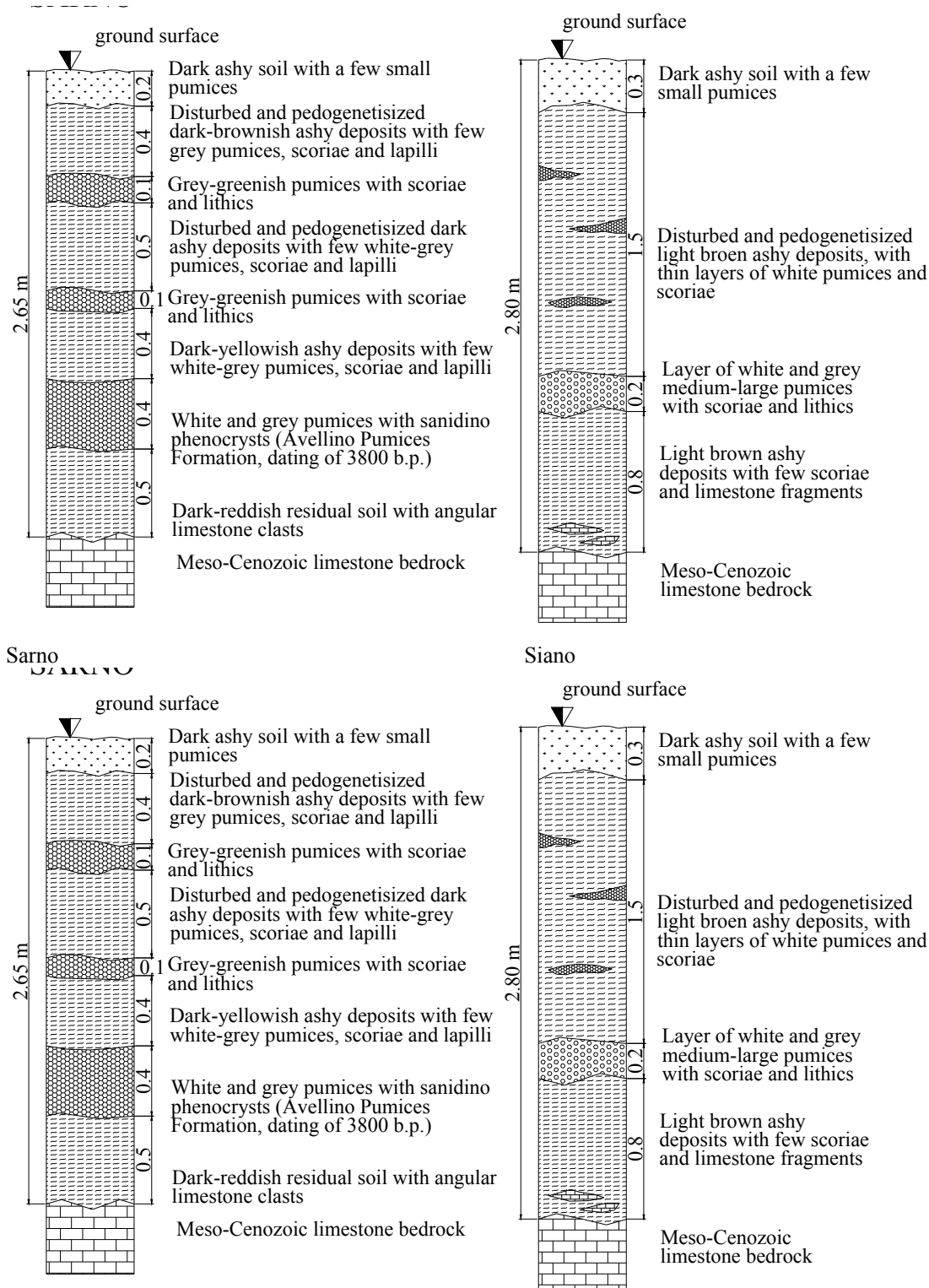


Figure 2 - Typical stratigraphic sections of the investigation sites.

2. Soil Suction Measurements

In order to obtain relevant information on the soil suction regime, in-situ measurements have been performed since November 1999 using “Quick-Draw portable tensiometers” and “Jetfill” in-place tensiometers (Cascini & Sorbino, 2003). The investigated sites were mostly situated in the Pizzo d’Alvano area, especially at medium-high slope levels (Fig. 1).

All the data collected in Figure 3, over the period November 1999 – May 2002 (about 3000 measurements) are reported together with the daily rainfall recorded in the same period from rain-gauges installed in August 1998 on the Pizzo d’Alvano slopes.

As can be readily observed, the suction data show a significant scattering which is, of course, related to the different sites and depths, where measurements were performed. However, the data also show that suction values never exceeded 65 kPa regardless of the measurement site, the depth and the rainfall regime.

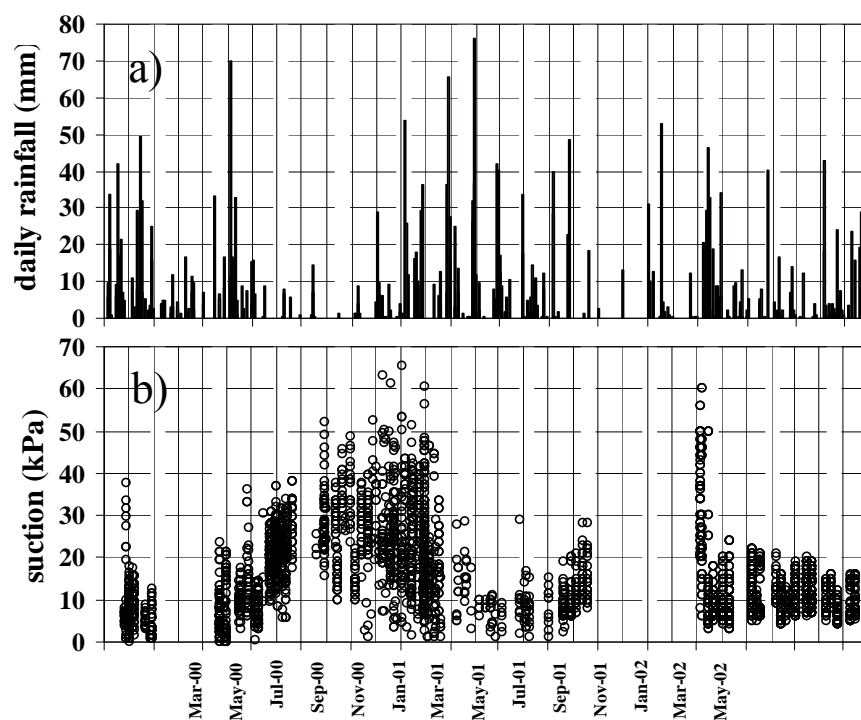


Figure 3 - a) daily rainfall; b) suction data collected at the investigation sites.

In order to verify if the data collected during the three observation periods were representative of all the landslide source areas of the Pizzo d’Alvano massif, a preliminary analysis was carried out for the period ranging from March 2000 to February 2001, during which measurements were available at each investigation site, with negligible exceptions.

Referring to the daily average values recorded during this period at each site, Cascini & Sorbino (2003) observe that suction behaviour seems strongly affected by local factors such as evapotranspiration rate, stratigraphic conditions, etc. (Blight, 1997; Leroueil, 2001), especially in August and September. This seems also to hold true for average values calculated for bi-weekly intervals, while monthly average values appear to be steadier than the previous one. In particular, in the April-July and October-December (Fig. 4) periods, at depths up to 1.0 m, monthly average suction values vary in a range not exceeding 15 kPa. Their variation appears to increase in the dry season (July – September), when the maximum

scatter is slightly less than 20 kPa. In the same period, a tendency towards faster saturation is observable on the slopes facing Sarno, probably due to the presence of many pumice layers (Fig. 2). A similar trend can be observed at depths greater than 1.0 m (Fig. 4), where differences in suction values are generally higher than at lower depths. However, the suction time trend at these lower depths is not monotonic, as it attains two different relative maximum values, one in the summer, the other in early autumn.

Data scattering is reduced to a minimum when the monthly average refers to suction data collected at the same depths, independently of the measurement site (Fig. 5). The maximum difference, taking the different behaviour of the Sarno site in the period from August to September into account, is not greater than 10 kPa, both for depths lower than 1.0 m (Fig. 5a) and for depths greater than 1.0 m (Fig. 5b).

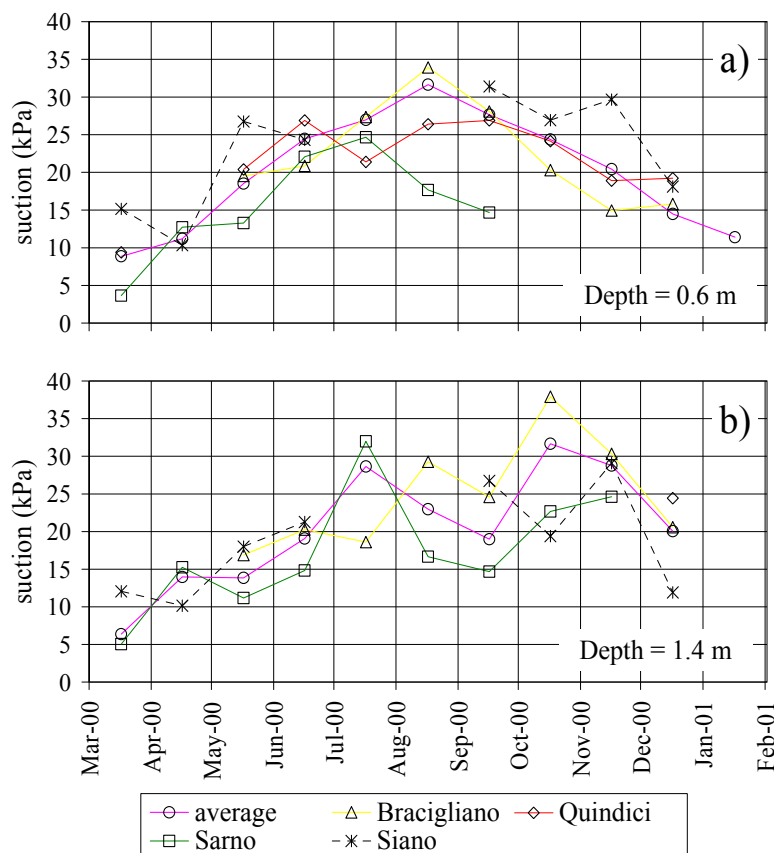


Figure 4 - Typical monthly average suction values, a) at depths lower than 1.0 m and b) at depths higher than 1.0 m (from Cascini & Sorbino, 2003).

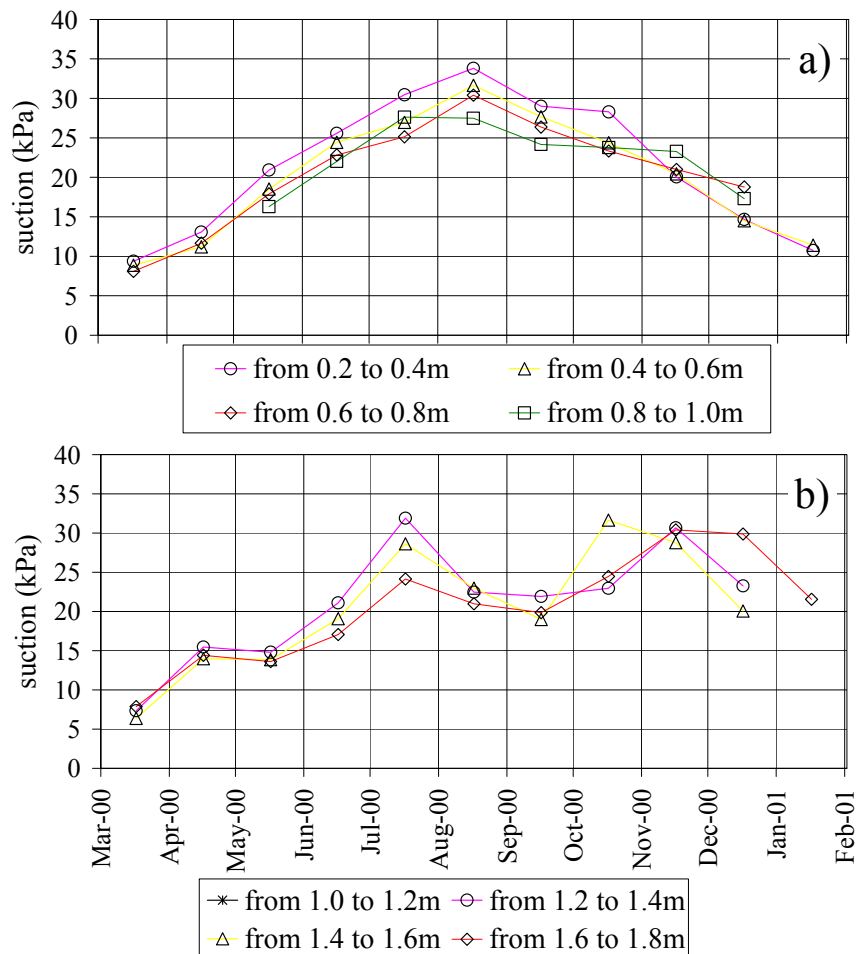


Figure 5 - Monthly average of suction values collected at all the investigated sites, a) at depths lower than 1.0 m and b) at depths ranging from 1.0 m to 1.8 m (from Cascini & Sorbino, 2003).

These analyses indicate that monthly average suction values, distinguished by depth, but not by site, calculated during the second and third observation periods can be considered typical of all the investigation sites. Monthly average suction values calculated over the whole observation period have hence been plotted taking into account only the depth at which each measurement was taken (Fig. 6). The monthly values for depths lower than 1.0 m (Fig. 6a) show an analogous trend, as do those for depths higher than 1.0 m (Fig. 6b). Moreover, the monthly suction regimen appears strongly related to rainfall for depths lower than 1.0 m (Fig. 6a).

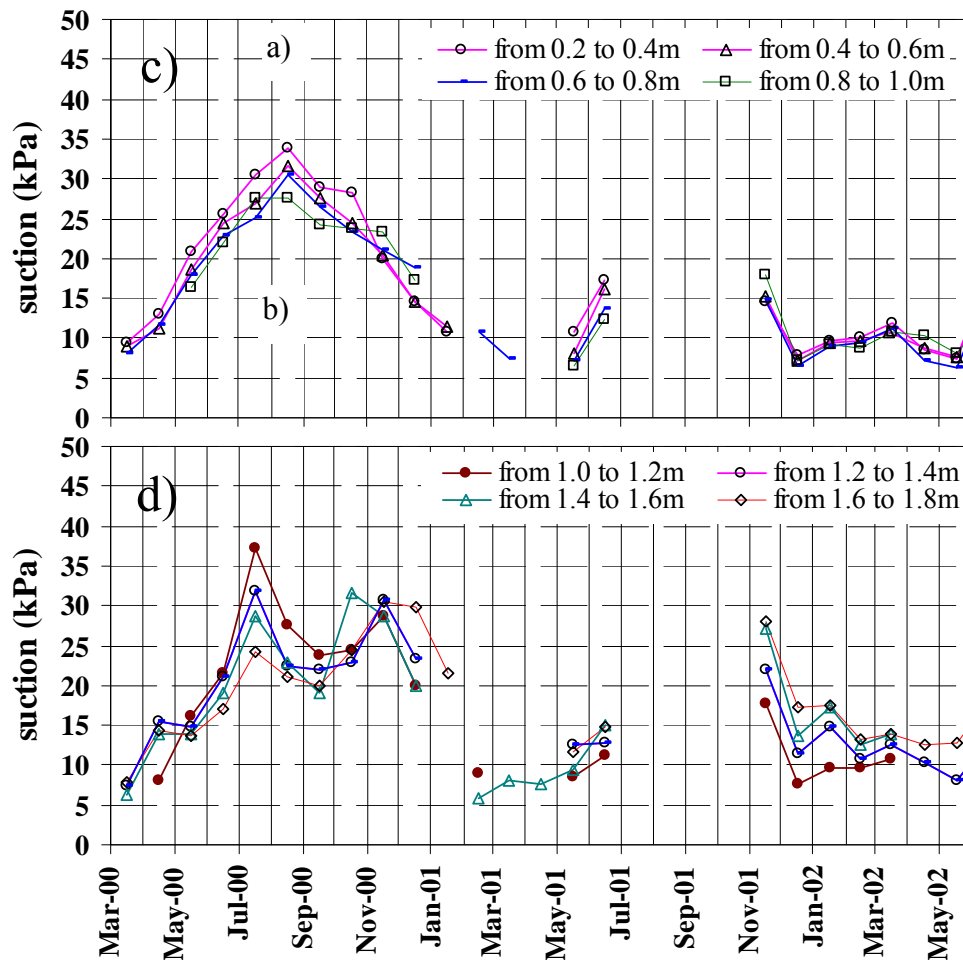


Figure 6 - a) monthly average suction at depths lower than 1.0 m; b) monthly average suction at depths ranging from 1.0 m to 1.8m (from Cascini & Sorbino, 2003).

These results invited two different analyses, one to ascertain relationships, if any, between monthly suction values and rainfall, the other to highlight suction regimen behaviour in time and in space.

Figure 7 shows monthly average suction values for all depths lower than 1.0 m compared with the moving average of daily rainfall over two and three-month periods. The suction values seem to agree with the moving average of daily rainfall over a three-month period. In particular, in spite of variations in the rainfall regimen during the observation period, the increase of suction at the beginning of dry periods (March – June) seems to be related to a moving average of daily rainfall over a three-month period not exceeding 4.0 mm. The same holds true for the beginning of the wet season (November – January), when the three-month period moving average above which suction decreases seems to be equal to about 2.0 mm (Fig. 7). As for suction behaviour regimen, it can be observed (Fig. 7) that, on a yearly scale, the time suction trend is quite similar during months when continuous measurements are available (e.g. November-December and May-June). Hence, it seems appropriate to analyse soil suction measurements on a monthly basis, independently of the year in which the measurements were taken. Monthly suction averages for each investigation site and at various depths (z) up to 1.6 m are plotted (Fig. 8) together with the “mean line” representing average soil suction values for the same depths at all the investigation sites.

Figure 8 shows that, for depths between ground surface and 1.0 m, monthly suction values attain their lowest value of 10 kPa in the January-March period at all the investigation sites. At lower depths, this period progressively decreases and seems to coincide with the month of April when, however, suction values do not differ significantly from 10 kPa. Despite the lack of significant data, this value seems to be the same at depths between 1.8 m to 4.2 m, as shown in Figure 9.

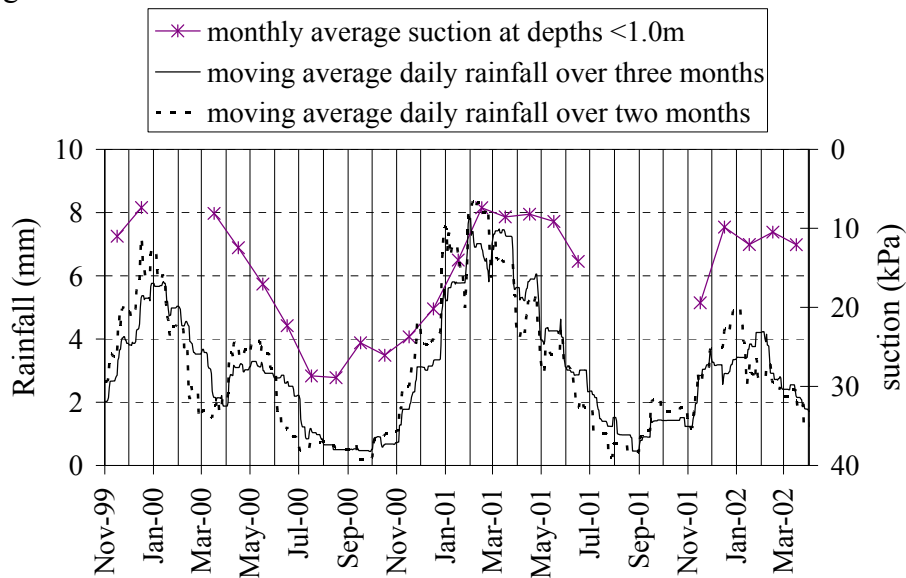


Figure 7 - Comparison among monthly average suction values at depths lower than 1.0 m and the moving average daily rainfall over a two-month and three-month period (from Cascini & Sorbino, 2003).

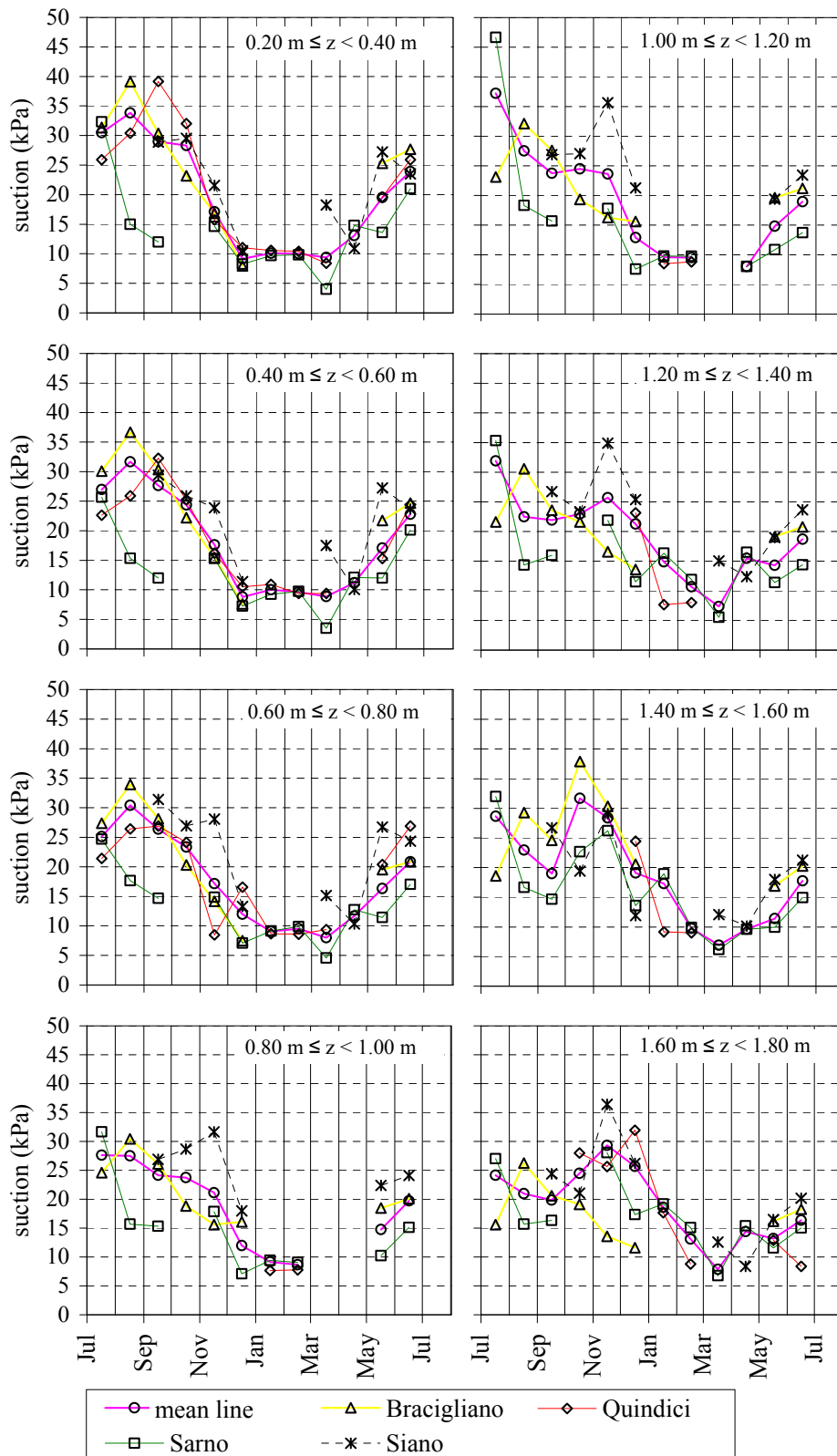


Figure 8 - Soil suction monthly average at various depth (z) from the ground surface at the four investigation sites (from Cascini & Sorbino, 2003).

Also in this case, the Sarno site differs from the others, since it shows a more rapid decrease in suction values, especially at the end of summer and the beginning of autumn. Nevertheless, it is interesting to note that, in December and during the winter, monthly average suction values are equal to 10 kPa in all locations.

In conclusion, the foregoing analyses show that the monthly suction regimen all over the Pizzo d'Alvano massif seems to follow a regular trend during the wet season. The total head distributions with depth, obtained from the average soil suction values of Figure 8, are plotted in Figure 10 to illustrate this better. The figure shows that the unsaturated flow, during the wet season, is directed downward and is characterised, for depths between the ground surface and 1.0 m, by hydraulic gradients always very close to 1. Hydraulic gradients in the same period and at lower depths appear to be quite high initially, and progressively decrease with time, reflecting the advance of the wetting front (Fig. 10). Due to higher temperatures and sun radiation during the dry season (April – August), suction increases. Hydraulic gradients seem to show variations in fluid flow direction at depths up to 0.6 m owing to evaporation phenomena (Fig. 10).

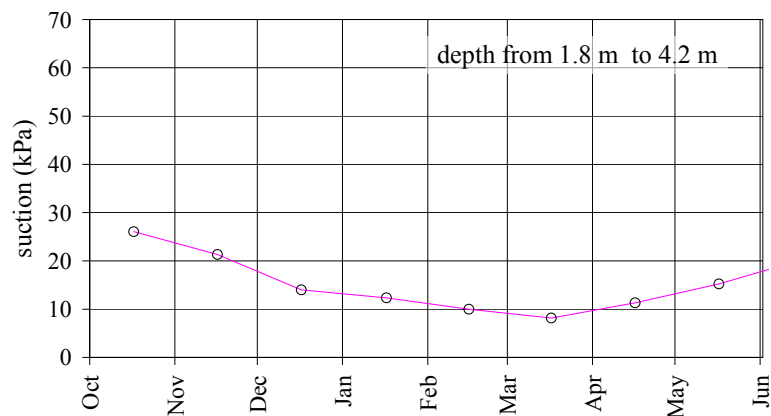


Figure 9 - Monthly average suction values at depths ranging from 1.8 m to 4.2 m (from Cascini & Sorbino, 2003).

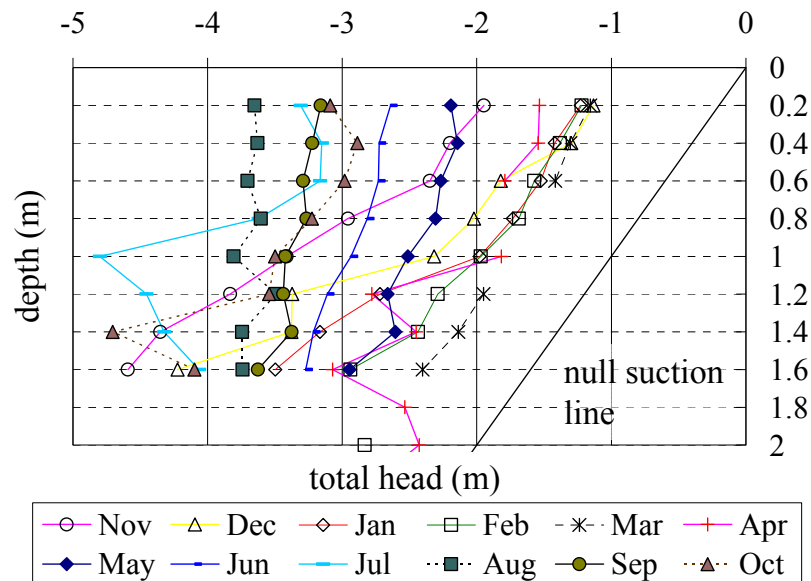


Figure 10 - Monthly total head versus depth distribution (from Cascini & Sorbino, 2003).

3. Numerical modelling of soil suction measurements

The above characteristics of the suction regime all over the area led to a numerical analysis being conducted to investigate the role played by the main physical variables in controlling the suction regime, and to provide an understanding of the in-situ suction measurements.

Suction modelling has been carried out by Sorbino (2005) for the period March 2000 – May 2002 for the simple scheme of an infinite slope, characterised by a slope gradient of 30° and a total thickness of 4.5 m, values that can be considered representative of the flowslide triggering areas of the Pizzo d'Alvano slopes. In order to take different stratigraphic conditions of the pyroclastic cover into account, a number of arrangements for ashy and pumice soil layers have been considered. The slope cross sections analysed (schemes 1 – 8), together with the different thicknesses assumed for pumice and ashy layers, are illustrated in Figure 27.

Seepage analyses were performed using the commercial finite element software SEEP/W (Geo Slope Int. Ltd. 1998) by analysing the two-dimensional transient flow regime both under saturated and unsaturated conditions once the hydraulic properties of the soil, the initial and boundary conditions are provided. Hydraulic properties have been selected for all schemes, from those that were experimentally determined (Table 1, Fig. 17 in section 1.1.3), assuming the soil layers are homogenous and isotropic.

A uniform distribution of soil suction has been adopted as the initial condition, with values equal to 10 and 15 kPa across the pyroclastic cover, in agreement with the back-analyses performed by Cascini et al. (2003). With reference to boundary conditions, the bottom of the slope has been assumed impervious, while two different flux conditions have been adopted at the ground surface. In the first one, a boundary flux equal to the daily rainfall intensity has been considered while, in the second one, the effect of the daily evapotranspiration has been also taken into account.

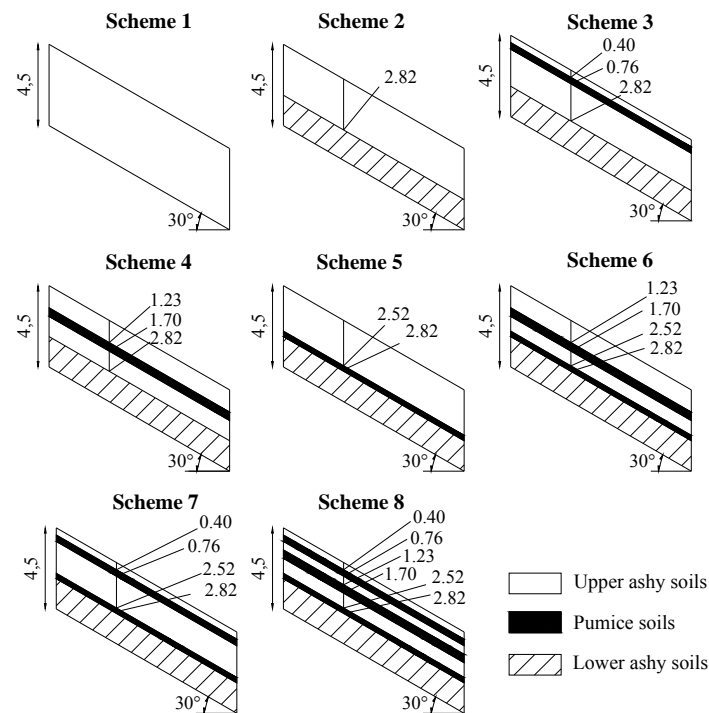


Figure 11 - Slope cross sections adopted in the numerical analyses (numbers specify the depths in metres).

Table 1 - Properties of the soil layers in Figure 11.

Soil properties		Upper ash soil layer	Pumice soil layer	Lower ash soil layer
Dry unit weight	γ_d	7.30 kN/m ³	6.20 kN/m ³	9.10 kN/m ³
Saturated unit weight	γ_{sat}	13.10 kN/m ³	13.10 kN/m ³	15.70 kN/m ³
Porosity	n	0.58	0.69	0.66
Saturated hydraulic conductivity	k_{sat}	10.0 ⁻⁵ m/s	7.50 10 ⁻⁵ m/s	10.0 ⁻⁶ m/s

To this end, the estimation of evapotranspiration rates have been carried out following the procedure suggested by Tarantino et al. (2002), which is based on a comparison between the potential evapotranspiration (E_p) (i.e. the maximum evaporation rate in the case of water availability) and the water limiting evapotranspiration (E_{lim}), which is related to the capacity of the soil to transmit water to the atmosphere. The value of daily evaporation rates for the definition of the flux boundary used in the numerical analyses was fixed equal to the lowest value between E_p and E_{lim} . A detailed description of the procedures used in the case under study for the evaluation of E_p and E_{lim} is reported in Lambiasi (2004). Estimation of E_p was carried out by adopting Thornthwaite's empirical equation (Thornthwaite, 1954) and using air temperatures recorded in the neighbouring sites of Pizzo d'Alvano relief, while E_{lim} was estimated via the steady state flow solution proposed by Gardner (1958), considering the saturated and unsaturated hydraulic properties of the soils shown in Figure 17, section 1.1.3. The computed monthly average suction values are compared in Figure 12 with the measured

ones. Quite a good simulation of in-situ suction is attained only during rainy periods (i.e. Jan. '01, May '01, Dec. '01-May '02) at depths lower than 1.0 m. Computed suction values for the other periods, and for all the depths, systematically underestimate in-situ suctions with differences that, especially in dry periods, increase up to about 20 kPa.

Monthly average in-situ suctions are compared with the computed values in Figure 13, by taking evapotranspiration into account. A satisfactory simulation of the suction regime both in dry and wet periods is attained at depths lower than 1.0 m. Simulation is only effective at higher depths in wet periods, while it fails to interpret the in-situ suction regime in dry periods. A more effective role on the measured suction values at these depths can probably be played by further aspects not considered in the present analysis, such as the presence of discontinuous ashy and pumice layers and additional boundary conditions provided by limestone bedrock acting at the bottom of the pyroclastic slope.

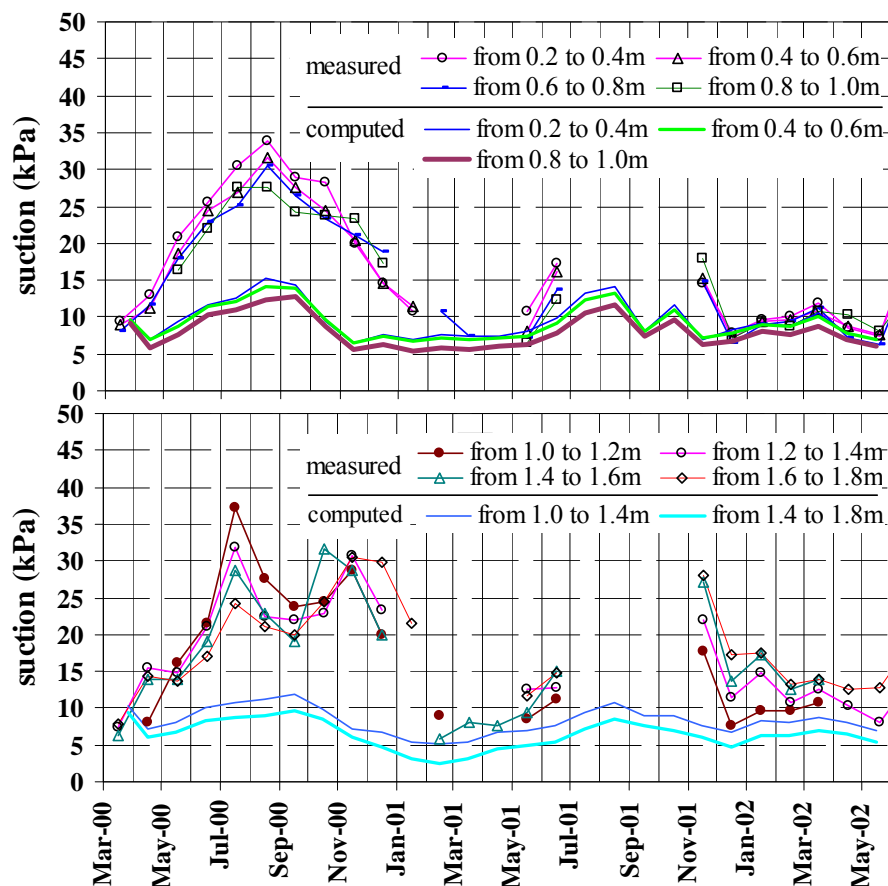


Figure 12 - Comparison between monthly average of computed suction values (without evapotranspiration) and measured values (from Sorbino, 2005).

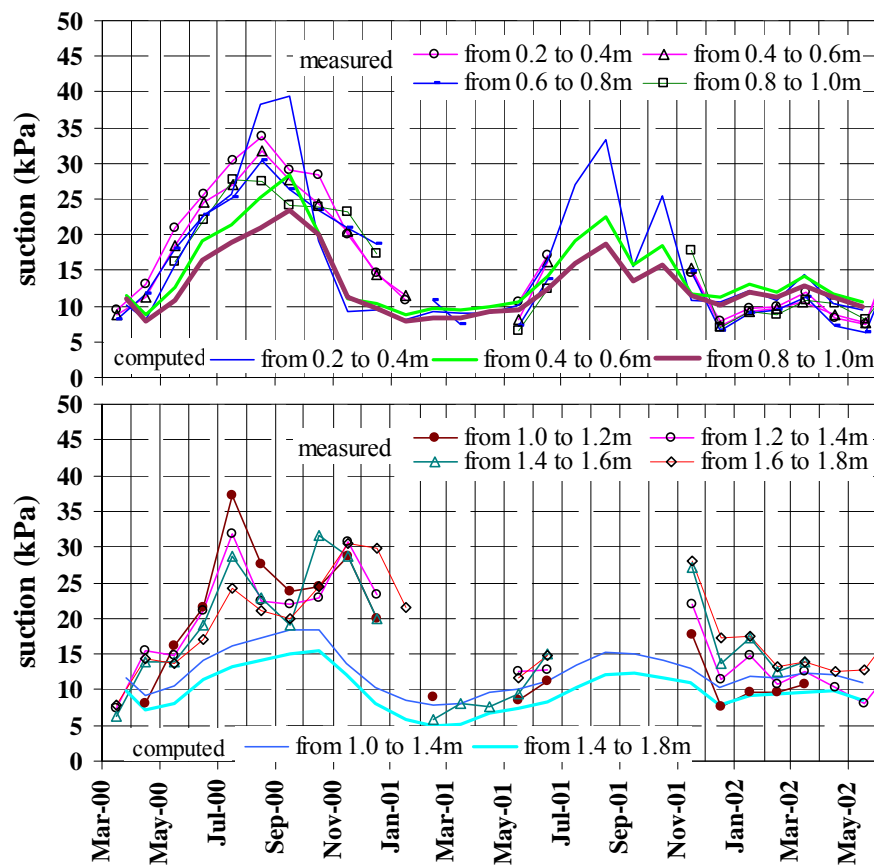


Figure 13 - Comparison between monthly average of computed suction values with evapotranspiration and measured values (from Sorbino, 2005).

4.3.1 Hydrological response of instrumented slopes in pyroclastic soils (AMRA)

Most of the Campania region is covered by unsaturated pyroclastic deposits generated by different volcanic centres (Fig. 14). The best known of these are the Phlaegrean Fields, West of Naples, and the Somma-Vesuvius, East of Naples, both still active inside the Campanian Volcanic Zone (Picarelli et al., 2006). In many cases, such granular soils pose severe geotechnical problems, primarily through rapid landslides triggered by precipitation.

The area subjected to landslides can be divided into three main zones, presenting different geomorphologic features:

- A) the Western Apennine zone, located along the N-NE dispersion direction from the Vesuvius volcano (Partenio, Avella, Sarno Mountains);
- B) the Lattari Mountains located along the S-SE dispersion direction from the Vesuvius volcano;
- C) the Phlegrean Fields volcanic district.

The bedrock in zone A consists of highly fractured Mesozoic-Cenozoic limestones, while the cover is essentially constituted of air-fall deposits. The basal formation in the Sorrento Peninsula also consists of Mesozoic-Cenozoic limestones, which are locally covered by

flysch on the northern slopes (Civita et al., 1975). Even in this case, the covers consist of alternating layers of air-fall ash and highly vesiculated pumice fragments. The thickness of the cover varies from site to site, depending on the distance from the volcanic centre and the average inclination of the slope, but it is rarely higher than 6 m.

The geomorphologic context of the Phlegrean Fields volcanic district is more complex. The pyroclastic soils have been deposited by air-fall, flows or surges and cover the Neapolitan Yellow Tuff formation, which is only locally fractured. The thickness of the cover ranges from about 20 m in proximal areas, to about 4 m, in distal outcrops (Picarelli et al., 2006).

Some monitored sites in these areas, indicated by stars in Fig. 14, have been investigated during the last ten years. The next sections are devoted to the main results of monitoring at these sites.

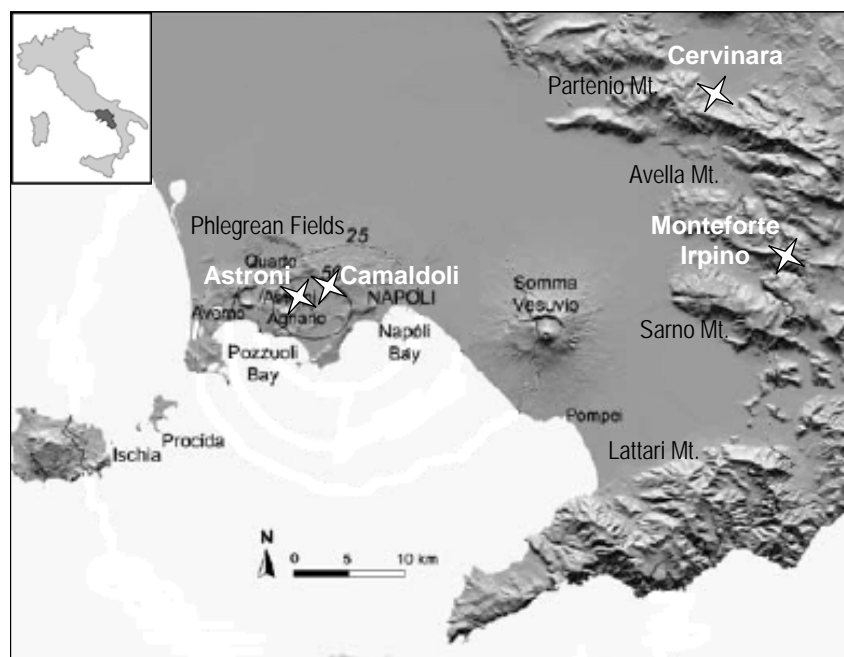


Figure 14 - Map of the instrumented slopes, as shown by a star, in pyroclastic soils.

1. Cervinara site

In December 1999, a number of landslides were triggered during a storm in an area of about 3.8 km² surrounding the town of Cervinara, at the toe of the Partenio Massif, about 50 km from Naples (Fig. 14): one of these landslides (A in Fig. 17) converted into a flowslide and reached the town, located about 2.5 km downslope, causing heavy damage to buildings and the loss of human lives. The monitored site of Cervinara, instrumented two years after, is located just beside the flowslide, at an altitude of 650 masl.

This area presents the typical features of the Mediterranean climate, which is quite variable due to the interaction between the two climatologic areas of Piana Campana and the Apennine Chain. A rain-gauge, installed a few kilometres from the instrumented slope (S. Martino Valle Caudina gauge managed by S.I.M.N. Agency, and after 2002 by the Civil Protection), has provided data since 1964: the yearly rainfall ranges from a minimum of 564 mm, in 1992, and a maximum of 2330 mm, in 1985. The maximum daily precipitation displays a great variability, ranging from 32 mm, in 1992, and 180 mm, in 1968 (Fig. 15a). The mean monthly

precipitation (Fig. 15b) is typical of the Mediterranean regime, being characterised by rainy autumns and winters and by dry summers, with a mean annual precipitation of 1300 mm.

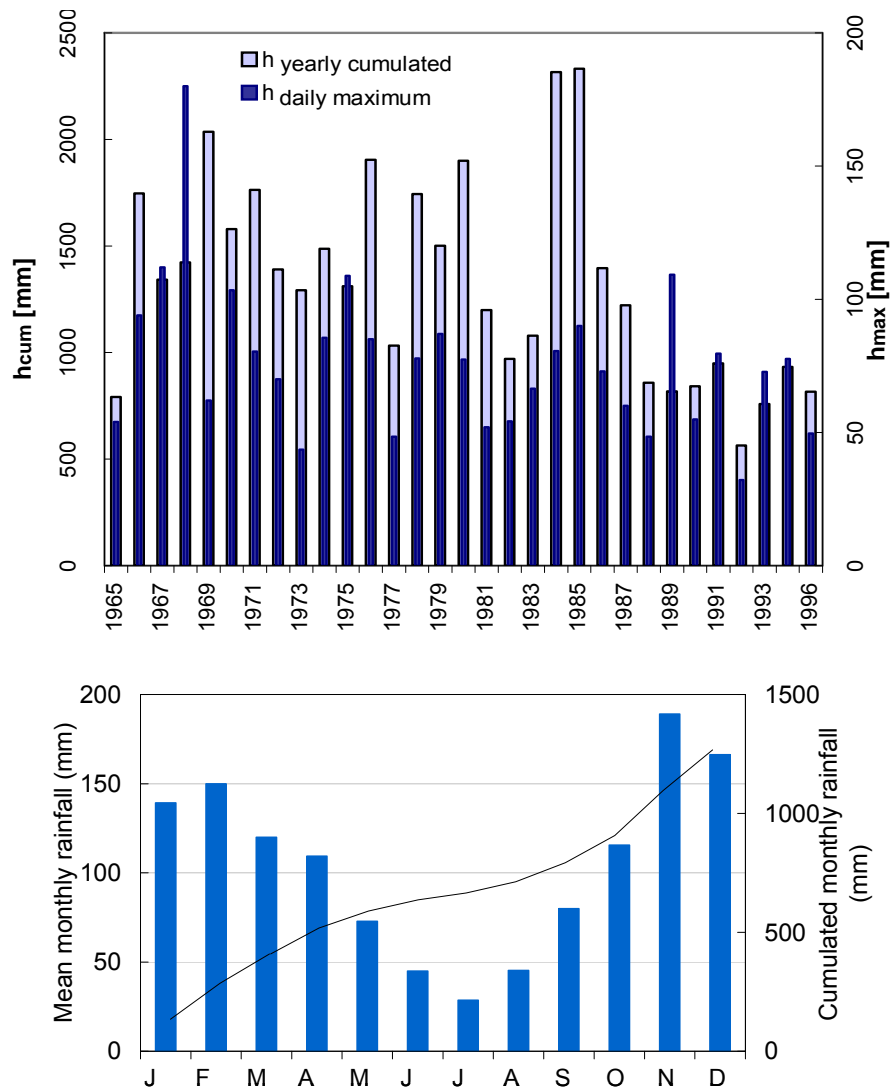


Figure 15 - Rainfall height recorded at Cervinara site in the last three decades of the XXI century: a) yearly cumulative and daily maximum rainfall; b) mean monthly and cumulative mean monthly rainfall.

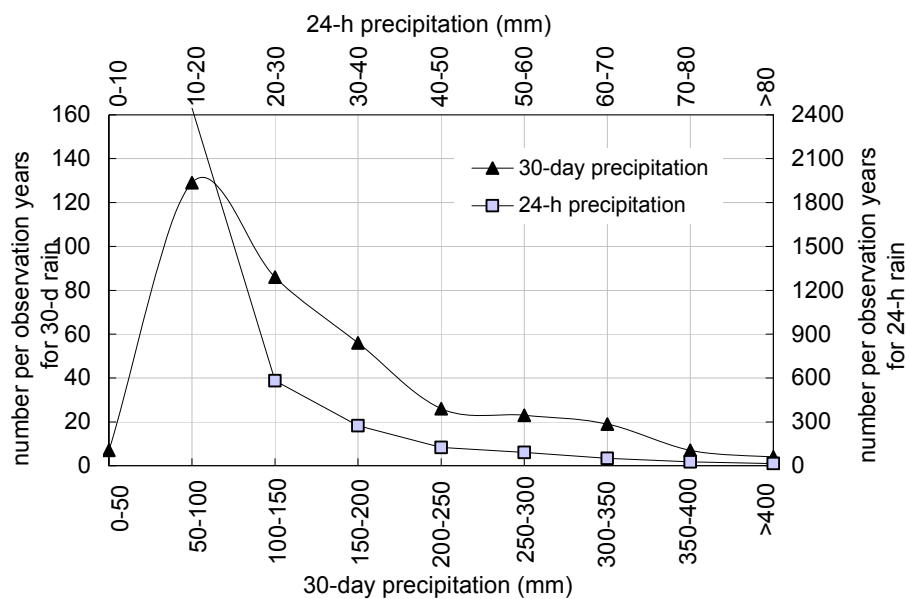


Figure 16 - Probability density functions of 24-h precipitation and 30-day precipitation (modified after Damiano, 2010).

Since the key factor in landslide triggering in pyroclastic soils is the cumulated antecedent precipitation (assumed as the 30-day cumulated rainfall) and the last 24-h rain, a comparison in terms of probability density functions of monthly rain and daily rain has been reported in Fig. 16, for the years under observation. The most recurrent values of 30 days cumulative precipitation fall between 100 mm and 200 mm: however also periods with values from 250 mm and 400 mm are not negligible since such values have been measured about 48 times in 30 years. Fortunately, values of intense daily rainfall (> 80 mm) seldom occur.

Data about air temperature are not available for this site but readings in localities nearby indicate a mean summer temperature of 20°C and a mean winter temperature of about 10°C. No information is available about snow depth, since no snow-gauges are installed. However the snow does not assume a significant value in this area.

The instrumented slope has an average inclination of 40° and is covered by chestnut trees. From the middle part of the slope downwards, a series of cuts and paths locally modify the natural morphology. The average thickness of the pyroclastic cover at the main scarp is about 2.4 m. From top to bottom, under a top soil formed of remoulded volcanic ash (about 60 cm thick), the following layers have been identified (Olivares & Picarelli, 2003): i) an upper layer 20 cm thick of coarse pumices (A); ii) a 100 cm thick layer of volcanic ash (B); iii) a horizon (20 cm) of fine pumices mixed with ash (C); iv) a bottom layer (40 cm) of weathered ash (D) directly covering the fractured calcareous bedrock. The total thickness of the cover moving downward due to the presence of colluvium. A simplified soil profile is shown in Fig. 17.

A detailed description of the physical and mechanical properties of the different materials is reported in section 1.1.1.

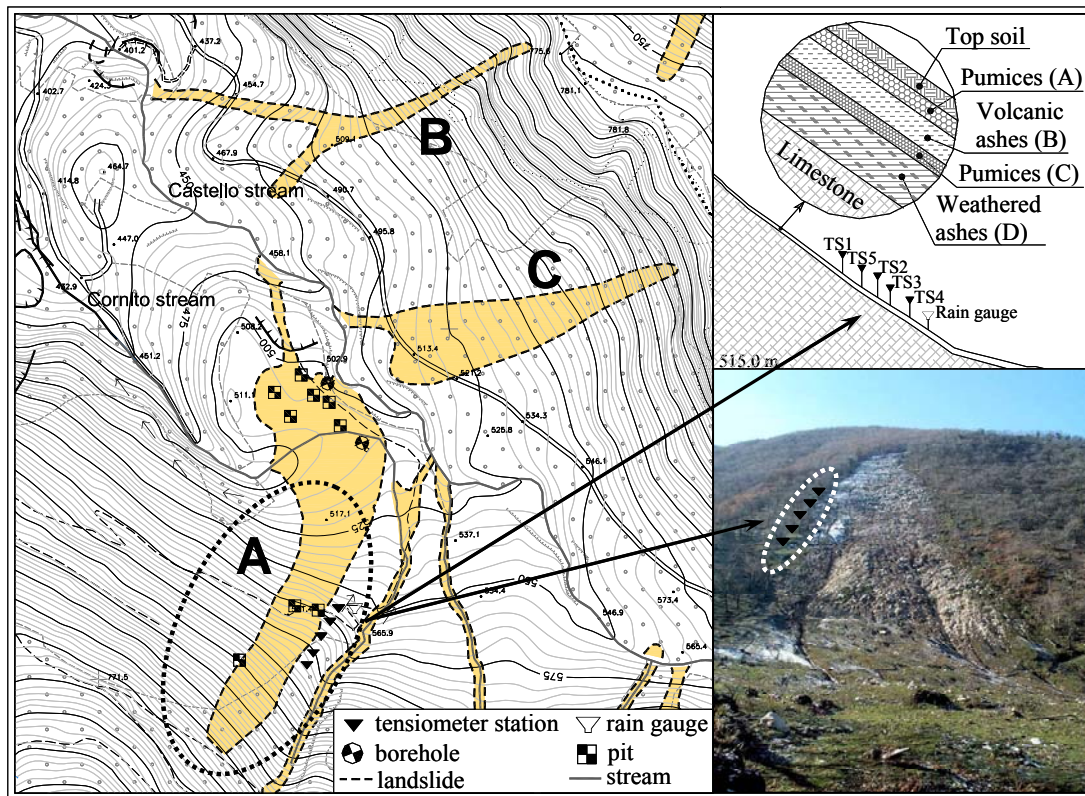


Figure 17 - Cervinara site: plan-view and schematic cross-section (from Damiano & Olivares, 2010).

At the beginning of 2002, the slope was instrumented with several tensiometers and a rainfall gauge (Olivares et al., 2002). The equipment consists of a tipping-bucket rain gauge, with a sensitivity of 0.2 mm, and of five tensiometer stations: at each station, standard jet-fill tensiometers, equipped with a Bourdon manometer, were installed at different depths, within the top soil and the ash layers (B and D). Suction measurements were performed every 7-10 days.

Results of monitoring are illustrated in Figures 18 and 19 which show daily and cumulated rainfall (Figs. 18a, 19a) and mean suction recorded at different depths (Figs. 18b, 19b), respectively from November, 2001, to November, 2005, and from January, 2006, to April, 2007. During the winter season, suction drops to low values, ranging between 2 kPa in the top soil, and about 15 kPa at higher depth; during the dry season, it increases up to some tens of kPa with a peak in September 2003 and August 2006, when the devices installed at a depth of 60 cm report a value close to 80 kPa. Similar high values were not attained during summer, 2002, due to anomalous rainfalls characterised by a total summer rain (550 mm) equal to almost half the annual precipitation (Olivares et al., 2002).

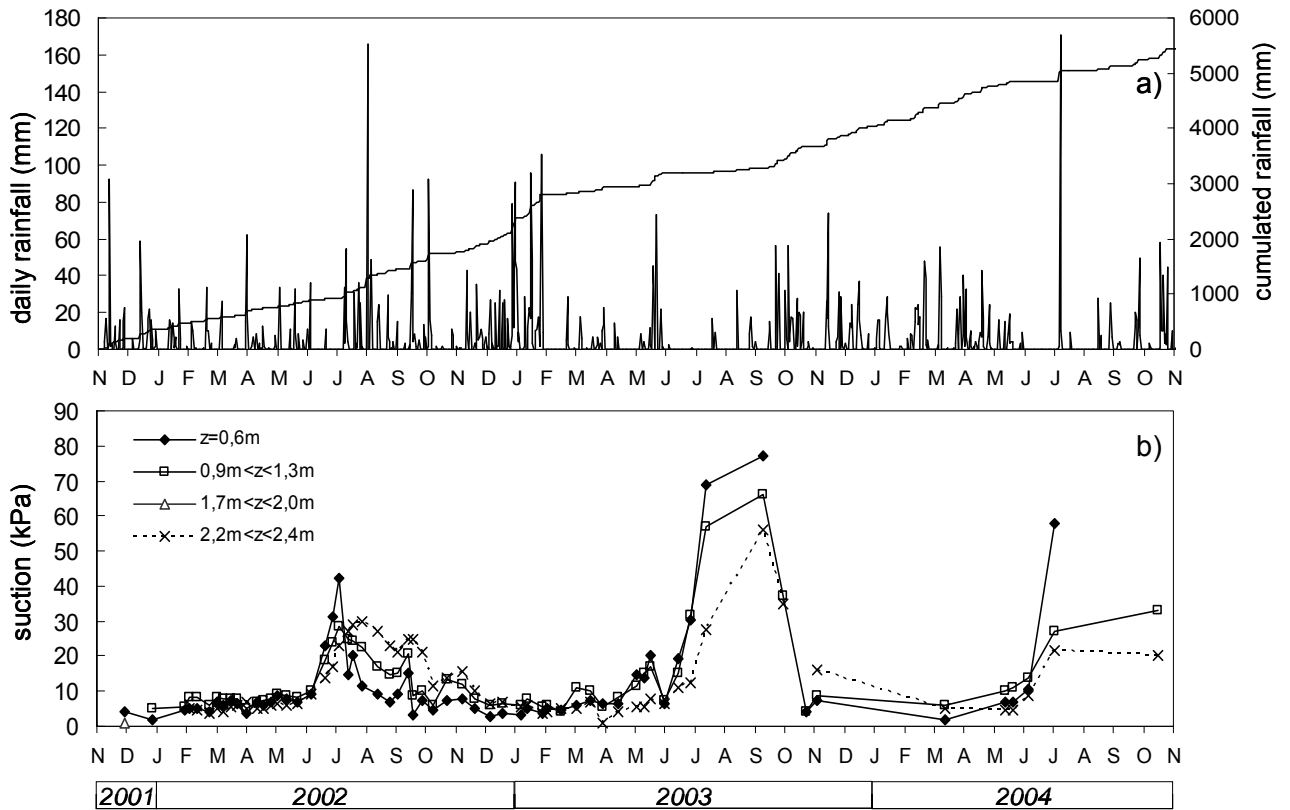


Figure 18 - a) Rainfall and b) mean suction readings during years 2002, 2003, 2004.

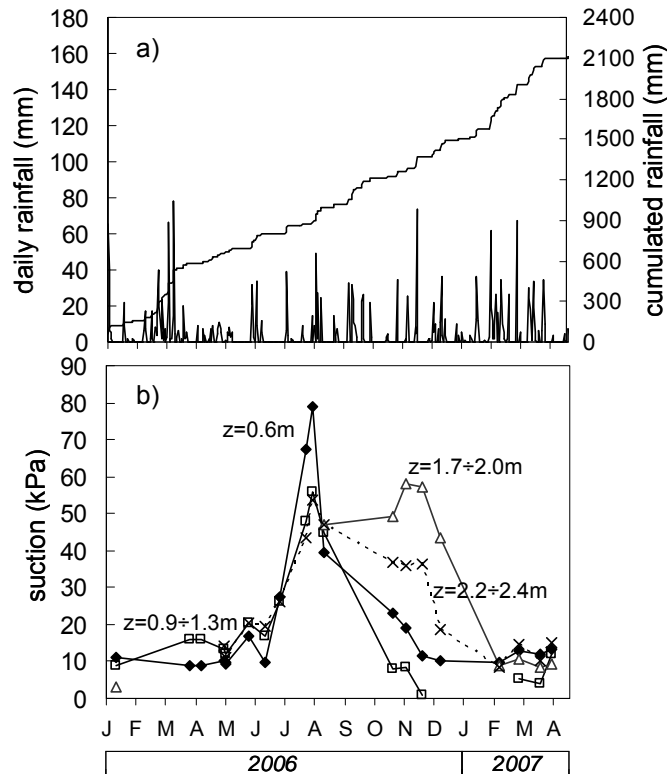


Figure 19. a) Rainfall and b) mean suction readings from January, 2006, to April, 2007.

A comparison of the suction trend within the three ash layers (top soil up to a depth of 0.6 m, B layer from 0.9 m to 2.0 m and D layer between 2.2 m and 2.4 m), shows that, in response to rainfall, suction decreases quicker in the shallowest layers, while it maintains a higher value in the deep layers. In the period between June 25th, and July 10th, 2002, suction increased up to three times throughout the depth, but a 15 kPa reduction occurred only in the upper layer due to the rain of July 25th, with the effects of water infiltration vanishing with depth. Only after the rainfalls of mid August did suction begin to decrease in the deepest layer. This is due to the following reasons: i) the delay of infiltration with depth; ii) the presence of two pumice layers (A and C) that, in some conditions, behave as a screen (Damiano & Olivares, 2010).

Although monitoring was discontinuous from the end of July 2003 till the end of 2004, collected data allows some important aspects of the slope behaviour to be highlighted:

- suction fluctuation is less marked in the deepest layers than in the superficial layers, where the effects of both rain and evapotranspiration immediately affect the pore water regime;
- the maximum value of suction in the deepest layer is lower than that reached in the superficial layers by a percentage of about 30%;
- the highest value of suction is reached in the deepest layer during autumn, but starting from February, it assumes the smallest value: an inversion of suction trend for deepest layers happens during the spring and summer seasons.

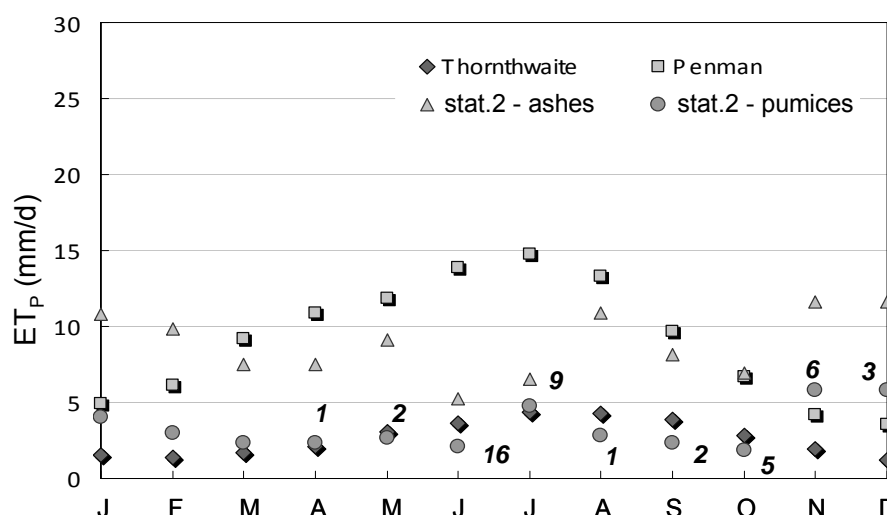


Figure 20 - Assessment of evapotranspiration rate for the Cervinara site.

Figure 20 reports some literature formulae for potential evapotranspiration rates (Penman, 1958; Thornthwaite, 1948), which are compared with data evaluated from suction readings. The assessment has been done under the assumption of isothermic conditions, considering suction readings in the year 2002 across the pumice layer (A) (from 0.6m to 0.9m) during dry periods, and computing the water flux toward the ground surface by the Richards equation for seepage in unsaturated soil. Since the pumice layer A is not present at all locations, the analysis has been carried out using both the values of unsaturated conductivity of volcanic ashes (indicated by triangles in Fig. 20) and of pumices (circles in Fig. 20) (for values of conductivity see section 1.1.1). In the diagram figures indicate the number of sunny days prior to the assessment.

A first remark is that Penman's formula overestimates the ET rate, especially during summer. In contrast, Thornthwaite's formula seems to match the experimental data better, even if it underestimates the value for winter months. However, a minimum value for the evaporatranspiration rate of about 2mm/d can be used as a boundary condition during dry periods. It is worth noting that such rates have been evaluated at depths of 0.6 m and 0.9 m, thus the flux rate at the interface ground-atmosphere could be higher.

2. Monteforte Irpino site

The test site is located along a slope of the Avella Mountains, about 40 km from the Somma-Vesuvius volcano, at an altitude ranging between 600 m and 680 masl. The average slope angle is 25°-30°, with maximum values of 40°. The number of known landslides occurred in the area in the recent past is five, but a number of ancient accumulation zones have been recognized, demonstrating the landslide susceptibility in the area (Evangelista et al., 2008). The climate is quite similar to that of Cervinara, due to the similar position and altitude of the two experimental sites.

The stratigraphic succession has been thoroughly investigated through pits and boreholes. It consists of eight main layers parallel to the ground surface, of volcanic ash and pumices presenting a total thickness of about 6 m. The following layers can be recognised from top to bottom: 1) topsoil; 2) weathered and humified ash soil; 3) pumices from the Avellino eruption (3.7 ky b.p.); 4) paleosoil consisting of weathered volcanic ash; 5) pumices from the Ottaviano eruption (8.0 ky b.p.); 6) paleosoil consisting of weathered volcanic ash; 7) volcanic sand; 8) highly weathered fine-grained ash. While the layers from the Ottaviano eruption are found throughout the investigated area, those from the Avellino eruption and the underlying paleosoil are absent in areas with slope angles higher than 35°. Therefore, continuity of the highly weathered ash at the bottom of the pyroclastic cover is not assured (Evangelista et al., 2008).

The properties of Monteforte Irpino soils are quite similar to those of Cervinara soils since they were formed by the same volcanic eruptions and the same depositional mechanisms (Picarelli et al., 2006). Detailed information can be found in section 1.1.1.

The instrumented slope covers an area of 230 m² in a coppiced chestnut wood, where 26 instrumented vertical sections are present, forming regular square meshes of 4 m x 4 m (Fig. 8). Each section has been instrumented with four or six tensiometers (jet-fill type) installed within the three ash layers (superficial, intermediate, deep), three or five TDR probes near the tensiometers, and a Casagrande piezometer located at the base of deepest ash layer, just above the highly fissured bedrock. These latter devices remained constantly empty (Papa et al., 2010).

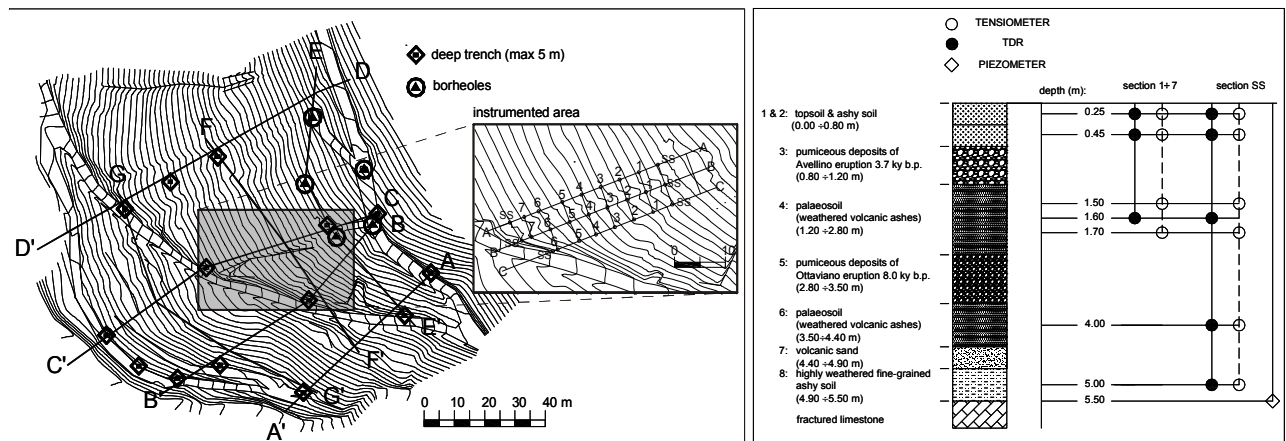


Figure 21 - Detail of the Monteforte Irpino field site (modified after Evangelista et al., 2008).

The mean value of suction at each depth during the period November 2006-March 2009 is reported in Figure 22: suction readings from the deepest devices are available only from July 2008 when the installation was completed. A clear delay between the suction values measured in the superficial, intermediate and deep layers was observed. In fact, even if minimum values of a few kPa are faintly recorded at the different depths, the maximum values reaches 65 kPa in the upper layer, 50 kPa in the intermediate one and only 20 kPa in depth (Papa et al., 2010). Moreover, tensiometers in the top soil seem to respond to singular rainfall events, even if the corresponding suction variations are relatively small compared to the seasonal trend (Evangelista et al., 2008). Conversely, the suction in the intermediate part of the cover follows a trend that is unaffected by individual rainfall events, reaching a maximum in the month of November (both in 2007 and 2008). Finally, suction in the deepest ashy layer seems to follow a delayed trend, reaching a maximum during the month of December. The greater the depth, the lower is the seasonal variation.

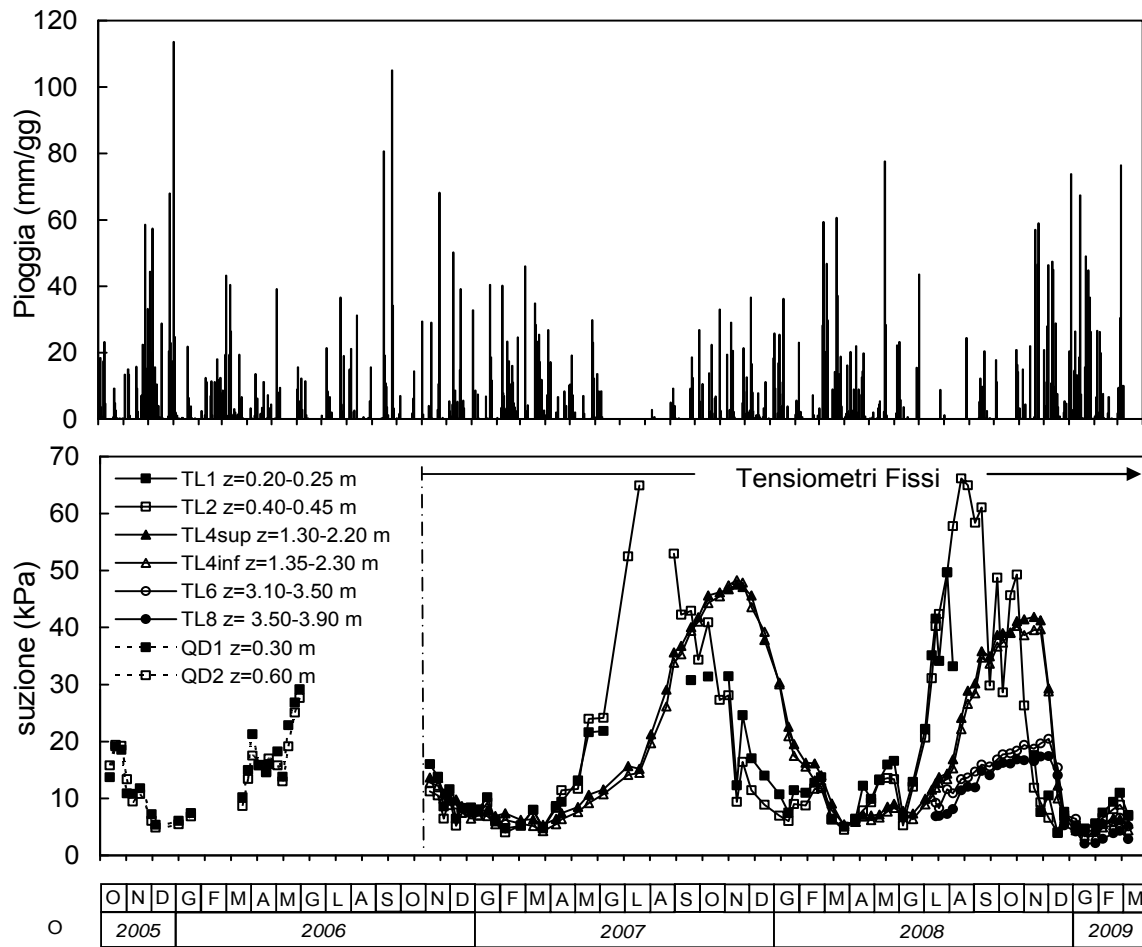


Figure 22 - Rainfall and suction measurements at Monteforte Irpino site (from Papa et al., 2010).

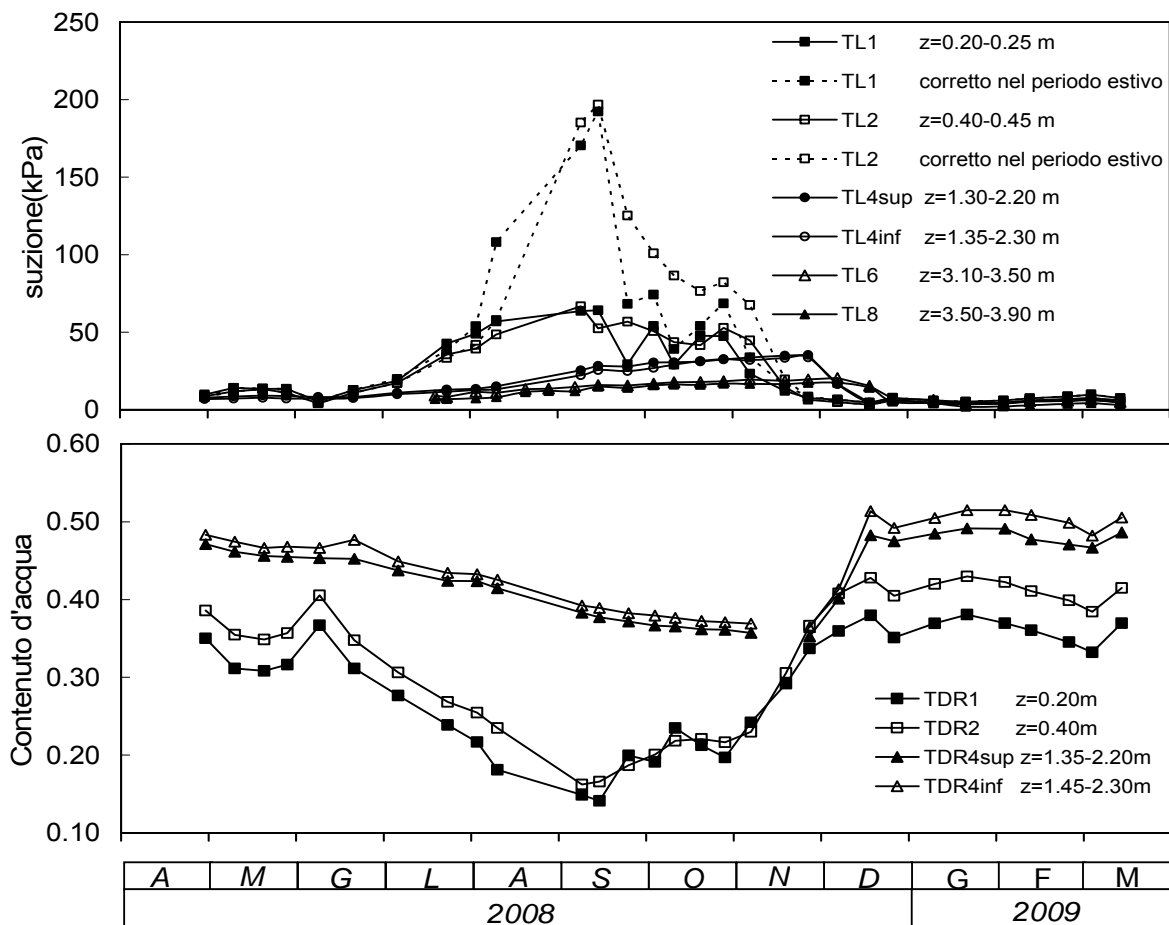


Figure 23 - Water content readings at Monteforte Irpino site (from Papa et al., 2010).

Measurements of soil water content, available from April 2008, are illustrated in Figure 23, which reports the mean values within the topsoil (soil 1) at a depth of 0.2 m, the superficial weathered ashy layer (soil 2) at 0.4 m, and the intermediate weathered ash (soil 4) at depths of 1.4 m and 2.2 m. The measured values are in good agreement with suction: they confirm that the upper layers are subjected to greater excursions, depending on rainfall and evapotranspiration, while the water content is always higher at greater depths than in the upper layers, but is not directly influenced by single rainfall event.

The total flux of water filtrating vertically into the upper and intermediate ashy layers has been estimated based on both monitoring and laboratory data (hydraulic conductivity); the data are shown in Figure 24. The results testify that continuous infiltration occurs in the superficial and intermediate part of the soil cover during fall, winter and early spring, whereas evaporation is predominant during late spring and summer. By comparing the mean cumulative flux across the superficial soil layers 1 and 2, and the intermediate soil layer 4 with the cumulative rainfall height, it is evident that only about 50% of rain infiltrates in the upper layers, while the water moving to the intermediate layer is still less (Papa et al., 2010). Moreover, the suction measurements have been used to reconstruct the direction of flow vectors in the plane of the central longitudinal section BB'. As an example, Figure 25 shows the direction of flow with reference to data taken on December 3 2008: flow vectors are almost vertical and directed downwards, suggesting that the water circulation is essentially due to a one-dimensional process during the wet season.

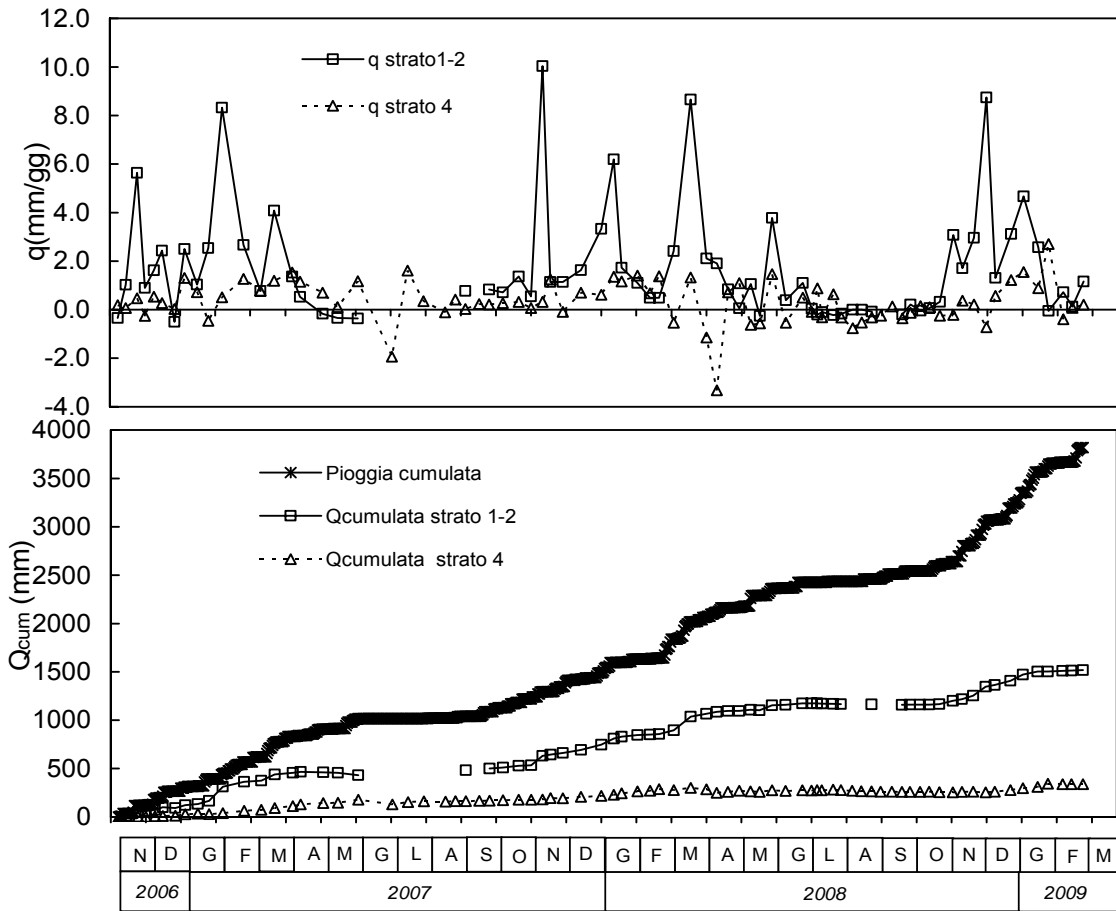


Figure 24 - Estimation of vertical flux along the central cross-section of the Monteforte Irpino site (from Papa et al., 2010).

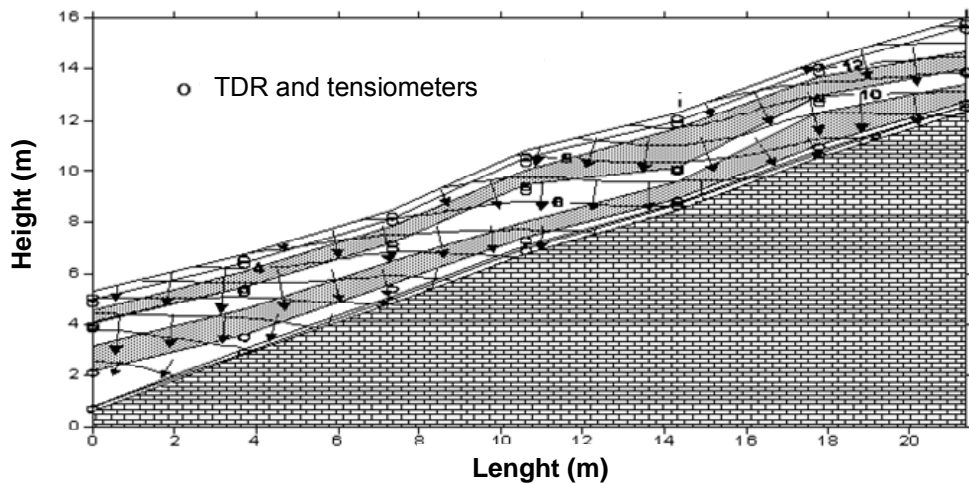


Figure 25 - Estimation of flow vectors along the central cross-section B-B' of the Monteforte Irpino site (from Papa et al., 2010).

3. Sites at the Phlegrean Fields

Some monitoring sites are located in the Phlegrean Fields, in the Eastern neighbourhood of Naples (Evangelista & Scotto di Santolo, 2010).

The distribution of rainfall is qualitatively similar to that observed at the other sites (Fig. 26a). However, a lower mean annual precipitation of about 300 mm has to be expected for this area. 93 rapid rainfall-induced landslides have been recognised during the years from 1986 to 2005 (Fig. 26b). Comparing the diagram in Figure 26a with that in Figure 26b, it is worth noting that landslides did not occur during the months with most rainfall (October-November-December), but mainly in January, after the heavy autumnal rainfalls. This showed that antecedent rainfall (30-60gg) plays a dominant role as a predisposing factor.

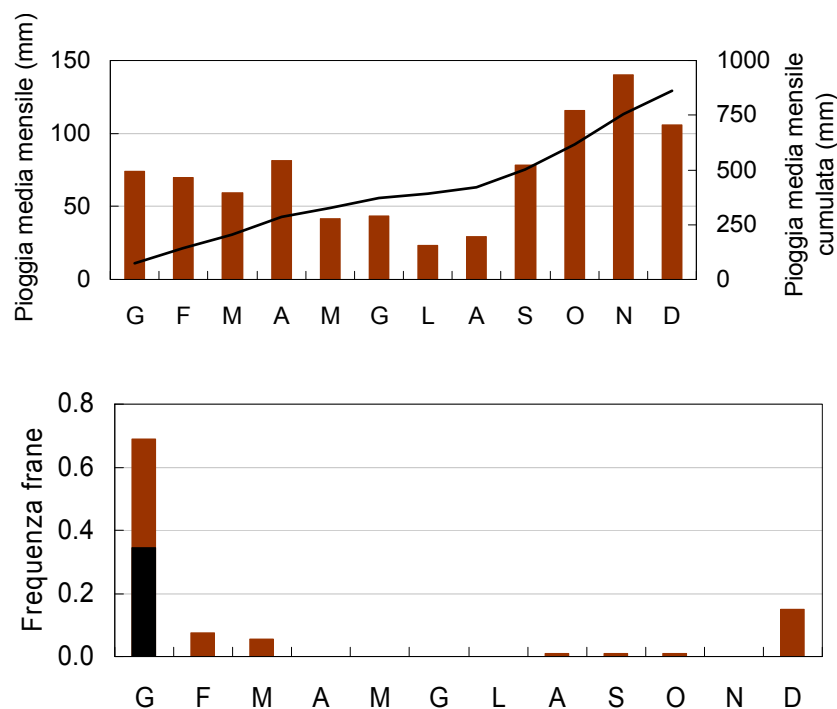


Figure 26 - a) Mean monthly and cumulative mean monthly rainfall; b) distribution of landslides during years 1986-2005 (from Evangelista & Scotto di Santolo, 2010).

Pyroclastic deposits in this area present significant local differences (Fig. 27). In particular, they contain both lithified and unlithified facies, related to eruptive and emplacement conditions, and the pyroclastic materials younger than 15 ky (Intracaldera Phlegrean pyroclastic Deposits, IPD) in the monitored sites in particular (red dots in Fig. 27) outcrop above the Neapolitan Yellow Tuff formation. In general, IPD consists of a sequence of fine to coarse unsaturated ashes with intercalated pumice layers, with thicknesses ranging from metres to tens of metres (Evangelista & Scotto di Santolo, 2001).

The materials range from sandy silt to well graded silty sand, and finally to sandy gravel: the clay fraction is usually less than 10%, while the sandy fraction is less than 40%. This variability is related to the origin of the material, constituted by hydromagmatic eruption-style fall, flow and surge deposits (Picarelli et al., 2006). In general, these soils are characterised by porosity lower than that of air-fall soils present at the other monitored sites: in fact, the highest porosity is about 64%, but values of about 47% have also been found. An investigation about the main properties of these soils is reported in section 1.1.1.

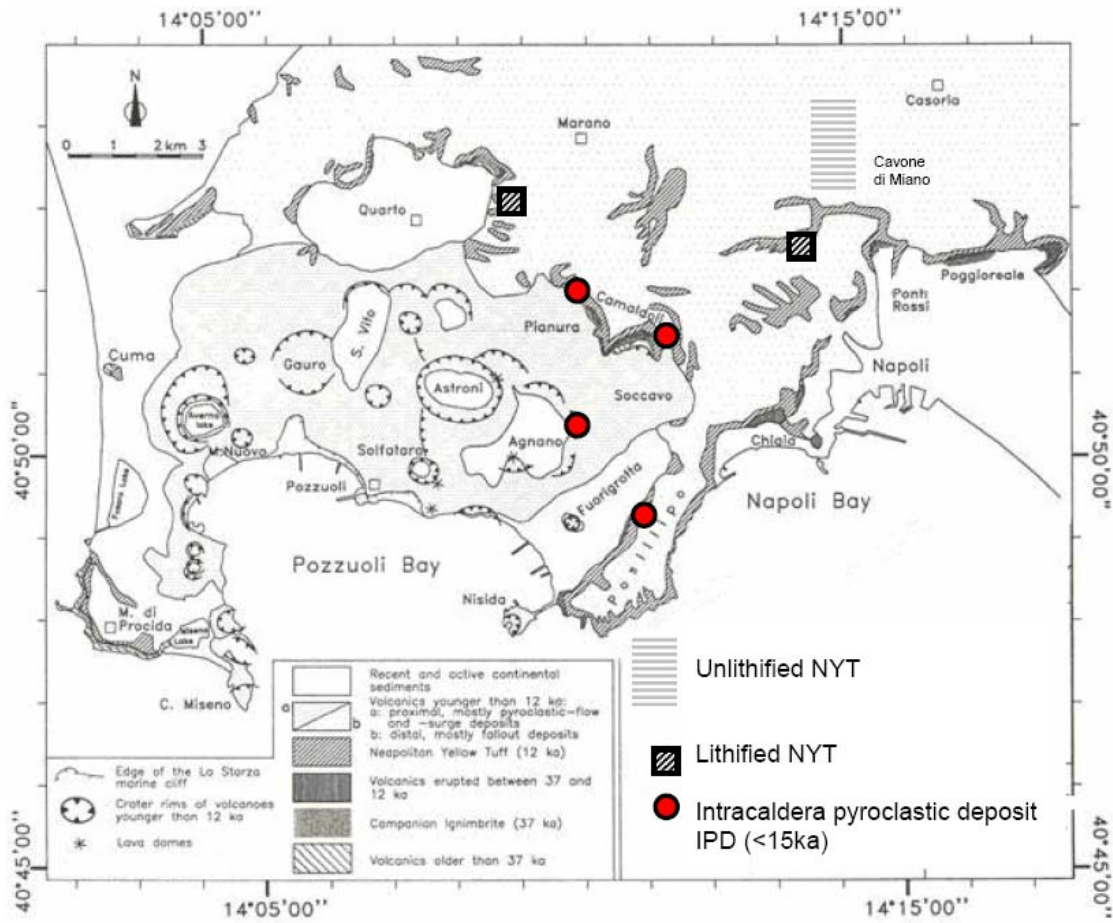


Figure 27 - Geological map of the Phlegrean Fields and in the investigated area (Picarelli et al., 2006).

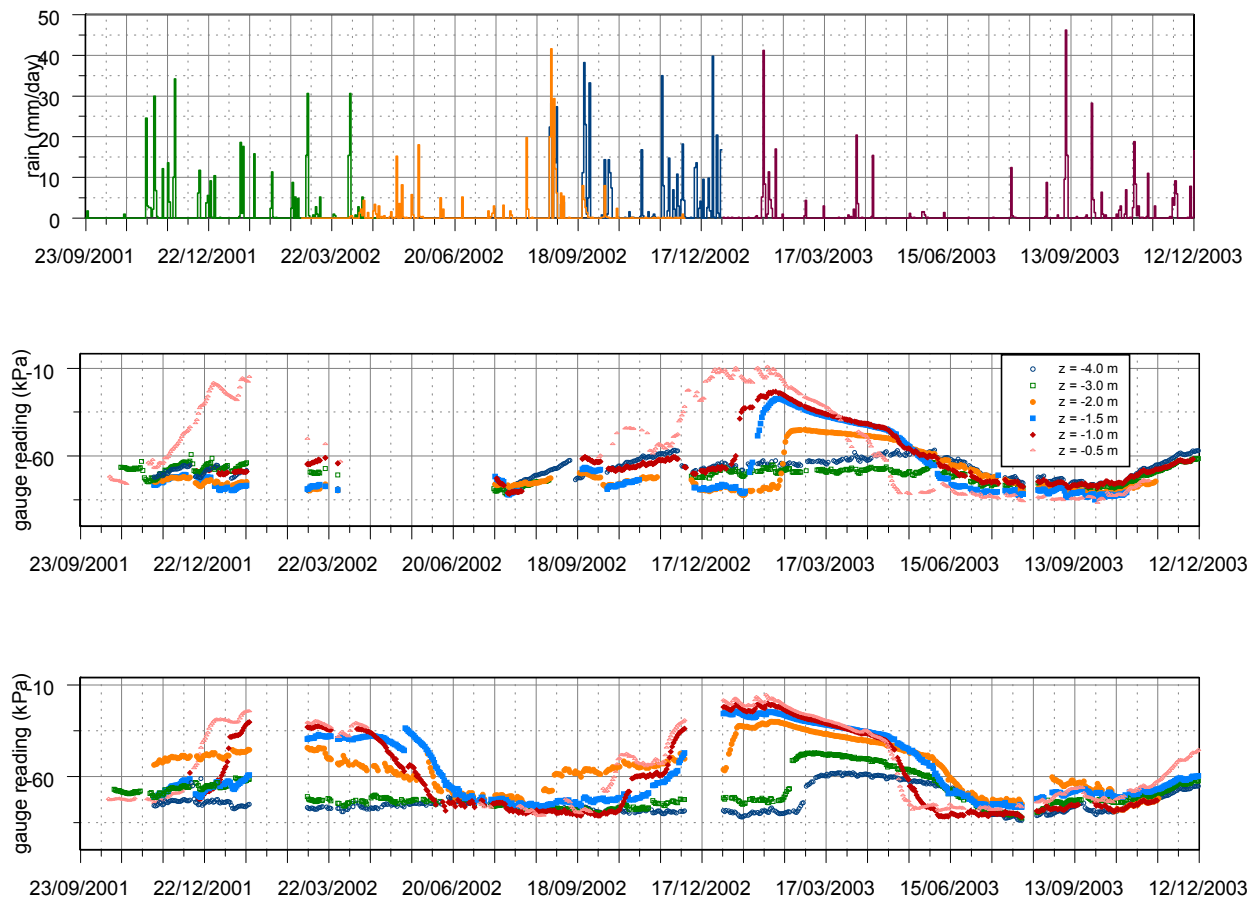


Figure 28 - Camaldoli site: a) daily rainfall height and b) mean daily gauge readings at two stations (from Evangelista & Scotto di Santolo, 2010).

The monitored sites have been instrumented with rain-gauges, tensiometers located at depths between 0.5 m and 4 m, and TDR probes at depths of 0.5 m and 1.0 m. All devices have been equipped with electronic transducers monitored via GSM modem. Data was collected from 2000 to 2005 with continuous readings are available for the period 2001-2003. Daily rain, and mean daily suction values, at two stations located along the Camaldoli hill are reported in Figure 28. As in the other cases, suction in the first metre of soil is deeply related to rainfall whereas the effects of infiltration at greater depths require a longer period of time to take place. Therefore, the greater the depth, the lower the amount of seasonal excursions are: in particular, suction in the superficial layer (0.5 m-1.0 m), which ranges between few kPa and 80 kPa, while it fluctuates between 10 kPa and 40 kPa at depths (3.0 m-4.0 m). Similar consideration can be taken for the Astroni site (Fig. 29), where values of suction during the period December, 2007 – July, 2008 have been collected (Evangelista & Scotto di Santolo, 2010).

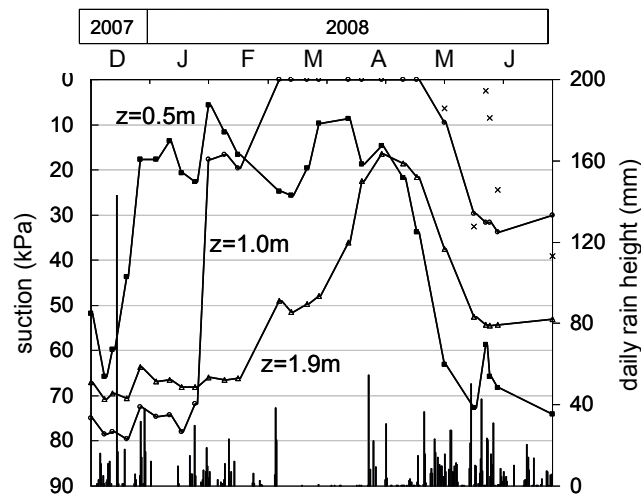


Figure 29 - Astroni site: daily rain height and suction at different depths (from Evangelista & Scotto di Santolo, 2010).

4.4 SYNTHESIS

Long-term monitoring of natural slopes is an indispensable tool for the analysis of landslide processes. The availability of continuous data on displacements and pore pressures enables more adequate numerical hydro-mechanical modelling to be conducted, in conjunction with advanced laboratory testing of soils. This may lead to the achievement of greater insight into the mechanisms governing the behaviour of landslides and prediction of ongoing behaviour.

The preceding chapter has presented long-term monitoring carried out on four field sites consisting of coarse-grained material (Tössegg, Gruben, Rüdlingen and La Frasse), on eleven sites consisting of fine-grained material (Super-Sauze, Beltinge, St. Martino, Orvieto, Santa Barbara case, Vallcebre, Brindisi di Montagna, Masseria Marino, Masseria De Nicola, Acqua di Luca, Torente Miscano) and on six site examples for pyroclastic soils (Bracigliano, Quindici, Sarno, Siano, Cervinara, Monteforte Irpino).

The measurement of water contents and pore water pressures at the grass covered slope (Tössegg) with an average inclination of 27° and with a less permeable layer (clayey sand) overlying a more permeable one (weathered sandstone, silty sand) have revealed a seasonal two-phase soil moisture behaviour of the slope with a typical summer and a typical winter character. Whereas in winter, the upper clayey sand layer was saturated with suctions approaching zero, suctions exceeded about 80 kPa in summer. It is assumed that suction plays an important role for slope stability in most of the slopes consisting of weathered sandstone in that area. This observation corresponds to the tests sites of Gruben, when the 42° slope failed, and Rüdlingen. To reach unstable conditions in coarse-grained soils and moraines on a slope slightly less steep than the critical state friction angle requires large changes in the water content and a flow regime.

The La Frasse landslide mainly consists of decomposed flysch (sandstone and clay schists). Geologists and geotechnical engineers have performed many surface and subsurface

investigations with the goal of understanding the governing mechanisms driving the slope movement. The field data, comprising subsurface measurements of displacements and pore water pressures, and surface measurements of displacements, rainfall and the activity of springs, were essential for the evaluation of the efficiency of possible drainage galleries designed to erase peak responses in pore water pressures in the unstable soil mass.

Long-term monitoring of the Super-Sauze landslide in reworked black marls, a fine-grained material, has shown that acceleration of the mudslide is governed by thresholds in pore water pressures associated with seasonal water table changes or with kinematic deformation of the undrained deformable medium. Two models, a hydrological model and a simplified hydro-mechanical approach, have been developed, calibrated and validated on the basis of the monitoring data.

By means of fine-grained slope examples on intact clays (Beltinge, St. Martino, Orvieto), jointed clays (cut slope in the Santa Barbara open pit mine, Vallcebre) and on highly fissured clays (Brindisi di Montagna, Masseria Marino, Masseria De Nicola, Acqua di Luca, Torente Miscano) it has been demonstrated that the hydrological slope response in fine-grained soils depends on the extent of the low hydraulic conductivity. Any change in the piezometric regime is delayed, depending on cumulative rainfall over long-lasting lengths of time and is not greatly influenced by short, intense rainfalls. Another key point for the analysis of slow slope movements in clay is the viscous behaviour of the slip surface as suggested in the active side of the St. Martino Stream basin.

The Beltinge earthflow consists of two parts inclined at 13-18° that discharge debris to an accumulation zone inclined at about 7°. The movements of the accumulation flow are generally delayed, because they are essentially induced by the load applied by the debris coming from the feeder flows. Fast loading, and the low soil permeability leading to the generation of positive pore-water pressures could explain the apparently anomalous piezometric readings measured within the accumulation body.

Heavy rainfall induced movements of the order of some centimetres as a result of the sliding of intact blocks along the discontinuities in the jointed, overconsolidated clay slope example in the Santa Barbara open pit mine. It is assumed that small cleft pressures in the opened discontinuities could have been responsible for triggering the slide.

As with many other landslides in clay the monitoring of the earthflows in highly-fissured plastic clays and clay shales show that movements tend to be strongly seasonal. It is stated that, where the strength mobilised along the shear zone is at, or near, the residual value, the landslide may be cyclically reactivated by pore pressure fluctuations.

Soil suction is one of the most important physical variables governing the behaviour of unsaturated soil slopes and is of particular relevance when geotechnical analyses are oriented to the assessment of slope stability conditions following infiltration of rain water, in order to predict the onset of shallow slope failure in pyroclastic soils. Therefore the monitoring of the slope examples in pyroclastic soils (Bracigliano, Quindici, Sarno, Siano, Cervinara, Monteforte Irpino) focuses on parameters that control soil suction variations induced by changes in boundary conditions. Monitoring provides data for appropriate modelling of the soil suction regime in order to predict the slope behaviour.

5 CONCLUSION (ETHZ, CNRS)

The mechanisms that initiate and that control landslides have to be studied in order to assess the slope response to precipitation and to validate prediction models. In this deliverable it is shown how those mechanisms are investigated through site and laboratory investigations, monitoring and numerical modelling in coarse-grained material, typically sands and in fine-grained materials, clayey soils, with the specific case of pyroclastics.

On the basis of data from long-term monitoring, as presented in chapter 4, and from soil mechanical experiments, chapter 2, numerical models can be developed, calibrated and validated. More adequate numerical hydro-mechanical modelling may lead to the achievement of greater insight into the mechanisms governing the behaviour of the large landslide, but it is also required for the prediction of the ongoing slope behaviour.

Even if the reproduction of landslide processes at a greatly reduced scale, by means of flume and centrifuge tests, is widely acknowledged not to be fully representative of full-scale behaviour due to the difference in stress levels between model and landslide, it can potentially create well documented, highly-instrumented case-studies of slope behavior. In these tests, the material properties, initial state, and boundary conditions are all well defined and it is less expensive than e.g. in-situ tests, that are presented in chapter 3.

6 BIBLIOGRAPHY

Chapter 2

- AGI. 1977. Some Italian experiences on the mechanical characterization of structurally complex formations. *Proc. 4th Int. Congr. Soc. Rock Mech.*, Montreux, 1: 827-846.
- Alonso, E.E. & Pinyol, N.M. 2008 Unsaturated soil mechanics in earth and rockfill dam engineering. In: Toll et al. (eds) *Unsaturated Soils: Advances in Geo-Engineering*. Taylor & Francis Group, London: 3-32.
- Anderson, S.A., Sitar, N. 1995. Analysis of rainfall-induced debris flow. *Journal of Geotechnical Engineering*, ASCE 121 (7): 544– 552.
- Aversa, S., Evangelista, A., Leroueil, S., Picarelli, L. 1993. Some aspects of the mechanical behaviour of “structured” soils and soft rocks. *Proc. Int. Symp. The Geotechnical Engineering of Hard Soils – Soft Rocks, Athens*, 1: 359-366. Balkema, Rotterdam.
- Bilotta, E., Pellegrino, A., Picarelli, L. 1985. *Geotechnical properties and slope stability in structurally complex clay soils*. Chapter 3: Physical and mechanical properties. Golden Jubilee Volume, A.G.I.: 195-214
- Bilotta, E., Cascini, L., Foresta, V., Sorbino, G. 2005. Geotechnical characterization of pyroclastic soils involved in huge flowslides. *Geotechnical and Geological Engineering*, 23: 365 – 402.
- Bilotta E., Foresta V., Migliaro G. 2006. Suction Controlled Laboratory Tests on Undisturbed Pyroclastic Soil: Stiffnesses and Volumetric Deformations. *Proc. of 4th Intern. Conf. on Unsaturated Soils (UNSAT 2006)*. Carefree, Aprile 2-6 2006, (AZ – Arizona). ASCE 849-860.
- Bishop, A.W., Little, A.L. 1967. The influence of the size and orientation of the sample on the apparent strength of the London Clay at Maldon, Essex. *Proc. Geotechnical Conf., Oslo*, 1: 89-96.
- Brand, E.W. 1981. Some thoughts on rainfall induced slope failures. *Proceedings of 10th International Conference on Soil Mechanics and Foundation Engineering*: 373–376.
- Brenner, R.P., Tam, H.K., Brand, E.W. 1985. Field stress path simulation of rain-induced slope failure. *Proceedings of 11th International Conference on Soil Mechanics and Foundation Engineering*, 2: 373– 376.
- Brooks R. H., Corey A.T. 1964. Hydraulic properties of porous media. *Hydrology Paper N.3*, Colorado State Univ., Fort Collins, Colorado.
- Burland, J.B. 1990. On the compressibility and shear strength of natural clays. *Géotechnique*, 40, 3: 329-378.
- Caruso M., Tarantino A. 2004. A shearbox for testing unsaturated soils at medium to high degrees of saturation. *Géotechnique* 54(4): 281-284.
- Casagrande, A. 1971. On liquefaction phenomenon. *Géotechnique* 21(3), 197– 202.
- Casagrande A. Boston J. 1936. Characteristics of Cohesionless Soils Affecting the Stability of Slopes and Earth Fills. *Soc. of Civ. Engrs.*, 23(1): 13-32.
- Cascini L., Cuomo S., Pastor M., Sorbino G. 2010. Modelling of rainfall-induced shallow landslides of the flow-type. *ASCE's Journal of Geotechnical and Geoenvironmental Engineering*, 136 (1): 85-98.
- Cascini L., Guida D., Nocera N., Romanzi G., Sorbino G. 2000. A preliminary model for the landslides of May 1998 in Campania Region. In: *Proc 2nd Int. Symposium on Geotechnics of Hard Soil-Soft Rock, Napoli*. Balkema, 3: 1623 – 1649.
- Casini F., Jommi C., Springman S.M. 2010. A laboratory investigation on an undisturbed silty sand from a slope prone to landsliding. *Granular matter* 12(3): 303-316.
- Casini F., Minder P., Springman S.M. 2010b. Shear strength of an unsaturated silty sand. *5th Intern. Conference Unsaturated Soils*, Barcelona, Spain 6-8 September.
- Castro, G. 1969. *Liquefaction of sands*. PhD Thesis, Harvard University, Cambridge, MA.
- Castro, G., Poulos, S.J. 1977. Factors affecting liquefaction and cyclic mobility. *Journal of the Geotechnical Engineering Division*, ASCE 103: 501–516.
- Chandler, R.J. 1984. Recent european experience of landslides in over-consolidated clays and soft rocks. *Proc. IV Int. Symp. on Landslides, Toronto*, 1: 61-81.
- Chu J, Leroueil S, Leong WK. 2003. Unstable behaviour of sand and its implication for slope stability. *Canadian Geotechnical Journal* 40:873–885.
- Crosta G., Frattini P. 2008. Rainfall-induced landslides and debris flows. *Hydrological Processes*: 22(4): 473 – 566.
- Damiano E. and Olivares L. 2010. The role of infiltration processes in steep slope stability of pyroclastic granular soils: laboratory and numerical investigation. *Natural Hazards*, 52: 329–350.
- Damiano E., 2004. *Meccanismi d'innesco di collate di fango in terreni piroclastici*. PhD Thesis, Seconda Università di Napoli.
- de Campos T.M.P. and Carrillo C.W. 1995. Direct shear testing on an unsaturated soil from Rio de Janeiro, *Proc. of 1st International Conference on Unsaturated Soils*, 1: 31-38.
- D'Elia, B., Picarelli, L., Leroueil, S., Vaunat, J. 1998. Geotechnical characterisation of slope movements in structurally complex clay soils and stiff jointed clays. *Rivista Italiana di Geotecnica*, 32: 5-47.
- Eckersley, J.D., 1990. Instrumented laboratory flowslides. *Géotechnique*, 40 (3): 489– 502.
- Escario V. and Saez J. 1986 The shear strength of partially saturated soils, *Géotechnique*, 36(3): 453-456.
- Esu, F. 1966. Short-term stability of slopes in unweathered jointed clay. *Géotechnique*, 16(4): 321-328.

- Evangelista A., Nicotera M.V., Papa R., Urciuoli G. 2008. Field investigation on triggering mechanisms of fast landslides in unsaturated pyroclastic soils. In: *Unsaturated Soils: Advances in Geo-Engineering. 1st European Conference on Unsaturated soil. Durham, UK. 2-4 July 2008* LONDON: Taylor & Francis Group plv (UK): 909-915.
- Fannin, R.J., Eliadorani, A., Wilkinson, J.M.T. 2005. Shear strength of cohesionless soils at low stress. *Géotechnique* 55(6): 3-10.
- Fell R., Hungr O., Leroueil S. & Riemer W. 2000. Keynote Lecture - Geotechnical engineering of the stability of natural slopes, and cuts and fills in soil. *GeoEng November 2000* 1: 21-120. Technomic Publishing, Lancaster.
- Fredlund, D.G., Xing, A. & Huang, S. 1994. Predicting the permeability function for unsaturated soils using the soil-water characteristic curve. *Can. Geotech. J.* 31:533-546.
- Fredlund D.G., Morgenstern N.R. and Widger R.A. 1978 The shear strength of unsaturated soils, *Canadian Geotechnical Journal*, 15: 313-321.
- Gan J.K-M., Fredlund D.G. and Rahardjo H. 1988. Determination of the shear strength parameters of an unsaturated soil using the direct shear test, *Canadian Geotechnical Journal*, 25: 500-510.
- Gardner W.R. 1958. Some steady state solutions of the un-saturated moisture flow equation with application to evaporation from water table. *Soil Sci.*, 85(4): 228-232.
- Garnier J, Gaudin C, Springman SM, Culligan PJ, Goodings D, Konig D, Kutter B, Phillips R, Randolph R, Thorel L. 2007. Catalogue of scaling laws and similitude questions in geotechnical centrifuge modelling. *Int J Phys Model Geotechn* 8(3): 1–23
- Geotechnical Engineering Office. 1999. Slope No. 11NW-B/FR61, Beacon Hill Radar Airport Station, Final Laboratory Testing Report, Geotechnical Engineering Office, Civil Engineering Department, The Government of the HKSAR
- Gerolymos N, Vardoulakis I, Gazetas G. 2007. A thermo-poro-viscoplastic shear band model for triggering and evolution of catastrophic landslides. *Soils and Foundations*; 47(1):11–25.
- Gerolymos N 2010. Numerical modeling of seismic triggering, evolution, and deposition of rapid landslides: Application to Higashi–Takezawa (2004). *International Journal for Numerical and Analytical Methods in Geomechanics*; 34:383–407
- Goodings, D.J. 1984. “Relationships for modelling water effects in geotechnical models”. Proceedings. Application of Centrifuge Modelling to Geotechnical Design. University of Manchester: 1-23
- Hird, H.H., Hassona, F.A.K. 1990. Some factors affecting the liquefaction and flow of saturated sands in laboratory tests. *Engineering Geology* 28: 149– 170.
- Hungr O. 2004. Flow slides and flows in granular soils. In Proc. of the Int. Workshop “Flows 2003 - Occurrence and Mechanisms of Flows in Natural Slopes and Earthfill”, Sorrento, Patron Ed.
- Ishihara, K. 1993. Liquefaction and flow failure during earthquakes. *Géotechnique* 43(3): 349– 451.
- Iverson, R.M., LaHusen, R.G. 1989. Dynamic pore-pressure fluctuations in rapidly shearing granular materials. *Science* 246: 796– 799.
- Iverson, R.M. 1997. The physics of debris flows. *Reviews of Geophysics* 35(3): 245– 296.
- Iverson, R.M., Reid, M.E., LaHusen, R.G., 1997. Debris-flow mobilization from landslides. *Annual Review of Earth and Planetary Sciences* 25: 85–138.
- Iverson R.M. 2000. Landslide triggering by rain infiltration. *Water Resources Research* 36(7): 1897- 1910.
- Iverson, R.M., Reid, M.E., Iverson, N.R., LaHusen, R.G., Logan, M., Mann, J.E., Brien, D.L., 2000. Acute sensitivity of landslide rates to initial soil porosity. *Science* 290: 513– 516.
- Jessberger, H.L. & Güttler, U. 1988. Geotechnische Grosszentrifuge in Bochum - Modellversuche im erhöhten Schwerfeld Geotechnik, Heft 2
- Jotisankasa A., Mairaing W. 2010. Suction-Monitored Direct Shear Testing of Residual Soils from Landslide-Prone Areas. *J. Geotech. Eng. ASCE* 136(3): 533–537.
- Kimura, T., Takemura, J., Suemasa, N., and Hiro-oka, A. 1991. “Failure of fills due to rainfall.” Centrifuge 91, H.-Y. Ko, ed., Balkema, Rotterdam, The Netherlands: 509–516.
- Knill, J.L., Lumb, P., Mackey, S., Mello, V.F.B., Morgenstern, N.R., and Richards, B.G. 1976. Report of the independent review panel on fill slopes. Government of Hong Kong, hong Kong.
- Kramer, K.L. 1988. Triggering of liquefaction flow slides in coastal soil deposits. *Engineering Geology* 26: 17– 31.
- Kubota, T. 1997. *An experimental study on mechanism of liquified landslides*. MS thesis, Nagoya university, Japan.
- Kunze R. J., Uehara G., Graham K. 1968. Factors important in the calculation of hydraulic conductivity. *Proc. Soil Sci. Soc. Amer.*, 32: 760-765.
- Lade P. V. 1993. Initiation of static instability in the submarine Nerlerk berm. *Can Geotech. J.* 30:895-904.
- Lampitiello, S. 2004. *Resistenza non drenata e suscettività alla liquefazione di ceneri vulcaniche della Regione Campania*. PhD Thesis, Seconda Università di Napoli
- Leroueil, S., Guerriero, G., Picarelli, L., Saihi, F. 1997. Large deformation shear strength of two types of structured soils. *Proc. Int. Symp. on Deformation and Progressive Failure in Geomechanics*, A. Asaoka, T. Adachi and F. Oka eds, Nagoya, 217-222.
- Leroueil, S., Vaughan, P.R. 1990. The general and congruent effects of structure in natural soils and weak rocks. *Géotechnique*, 40(3): 467-488.
- Leroueil S. 2001. Natural slopes and cuts: movement and failure mechanisms. *Geotechnique* 51(3): 197-243.
- Leroueil S. 2004. Geotechnics of slopes before failure. Land-slides: Evaluation and Stabilization, Lacerda, Ehrlich, Fon-toura & Sayao (eds), 1: 863-884.

- Le, T.T., Delage, P., Cui, Y.J., Tang, A.M., Lima, A., Romero, E., Gens, A. & Li, X.L. 2008. Water retention properties of Boom clay: A comparison between different experimental techniques. In: Toll et al. (eds) *Unsaturated Soils: Advances in Geo-Engineering*. Taylor & Francis Group, London: 229-334.
- Lings M. L., Dietz M. S. 2004. An improved direct shear apparatus for sand. *Géotechnique* 54(4): 245–256.
- Lo, K.Y. 1970. The operational strength of fissured clays. *Géotechnique*, 20(1): 57-74.
- Lourenço, S. D. N., K. Sassa, and H. Fukuoka. 2006. Failure process and hydrologic response of a two layer physical model: Implications for rainfall-induced landslides, *Geomorphology*, 73: 115–130.
- Major, J.J., Iverson, R.M. 1999. Debris-flow deposition: effects of pore-fluid pressure and friction concentrated at flow margins. *Geological Society of America Bulletin* 111 (10): 1424– 1434.
- Maquaire, O., Malet, J-P, Remaître, A., Locat, J., Klotz, S. & Guillon, J. 2003. Instability conditions of marly hillslopes: towards landsliding or gullying? The case of the Barcelonnette basin, South East France. *Engineering Geology* 70(1-2):109-130.
- Malet, J-P. 2003. *Les glissements de type écoulement dans les marnes noires des Alpes du Sud. Morphologie, fonctionnement et modélisation hydromécanique*. PhD Thesis in Earth Sciences, Université Louis Pasteur, Strasbourg.
- Malet, J-P, Remaître, A., Maquaire, O., Durand, Y., Etchevers, P., Guyomarch, G., Déqué, M. & van Beek, L.P.H. 2007. Assessing the influence of climate change on the activity of landslides in the Ubaye Valley. In: *Proceedings International Conference on Landslides and Climate change - Challenges and Solutions*, Wiley, London
- Marsland, A., Butler, M.E. 1967. Strength measurements in stiff fissured Barton Clay from Fawley (Hampshire). *Proc. Geotechnical Conf., Oslo*, 1: 139-145.
- Melinda F., Rahardjo H., Han K.K., Leong E.C. Shear Strength of Compacted Soil under Infiltration Condition *J. Geotech. Eng. ASCE* 130(8): 807–817.
- Meschyan, S.R. & Petrosyan, T.L. 2005. Water seepage in clay soils with large dimensions of specimens and small head gradients. *Soil Mechanics and Foundation Engineering* 30(1):8-10.
- Migliaro G. 2008. *Il legame costitutivo nei terreni piroclastici per la modellazione di scavi in ambiente urbanizzato ed influenza della parziale saturazione*. Ph.D. Thesis (in Italian) University of Salerno.
- Morgenstern, N.R. 1977. Slopes and excavations in heavily overconsolidated clays. *Proc. 9th ICSMFE, Tokyo*, 2: 567-581.
- Moriwaki, H., Inokuchi, T., Hattajji, T., Sassa, K., Ochiai, H. and Wang, G. 2004. Failure processes in a full-scale landslide experiment using a rainfall simulator. *Landslides*, 1:277–288.
- Murray, E.J., Jones, R.H. & Rix, D.W. 1997. Relative Importance of Factors Influencing the Permeability of Clay Soils. In: Yong RN and Thomas HR (eds) *Geoenvironmental engineering, Contaminated ground: fate of pollutants and remediation*, Thomas Telford, London: 229-239.
- Ng CWW, Fung WT, Cheuk CY, Zhang L. 2004. Influence of stress ratio and stress path on behaviour of loose decomposed granite. *ASCE Journal of Geotechnical and Geoenvironmental Engineering* 130(1):36–44.
- Oberg A.-L. and Salfors G. 1997. Determination of shear strength parameters of unsaturated silts and sands based on the water retention curve, *Geotechnical Testing Journal*, 20(1): 40-48.
- Olivares L., Damiano E., Greco R., Zeni L., Picarelli L., Minardo A., Guida A., Bernini R., 2009. An instrumented flume to investigate the mechanics of rainfall-induced landslides in unsaturated granular soils. *ASTM Geotechnical Testing Journal* 32(2): 1–11.
- Olivares L. and Damiano E., 2007. Postfailure mechanics of landslides: laboratory investigation of flowslides in pyroclastic soils. *Journal of geotechnical and geoenvironmental engineering*, ASCE, 133(1): 51-62.
- Olivares, L., Picarelli, L. 2003a. Shallow landslides triggered by intense rainfalls on natural slopes covered by loose unsaturated pyroclastic soils. *Géotechnique* 53(2) : 283–287.
- Olivares L., Picarelli L., 2003b. Shallow flowslides triggered by intense rainfalls on natural slopes covered by loose unsaturated pyroclastic soils. *Géotechnique*, 52(2).
- Olivares L. 2001. Static liquefaction: an hypothesis for explaining transition from slide to flows in pyroclastic soils. *TC11 Landslide conf. on Transition from slide to flow – Mechanisms and remedial measures. Trabzon, Turkey*.
- Oloo, S.Y. and Fredlund, D.G. 1996. A method for determination of σ^b for statically compacted soils, *Canadian Geotechnical Journal*, 33: 272-280.
- Olson, S.M., Stark, T.D., Walton, W.H., and Castro, G. 2000. Static liquefaction flow failure of the north dike of Wachusett dam. *Journal of Geotechnical and Geoenvironmental Engineering*, ASCE, 126(12): 1184–1193.
- Papa R., Evangelista A., Nicotera M.V. and Urciuoli G., 2008. Mechanical properties of unsaturated pyroclastic soils affected by fast landslide phenomena. In: *Unsaturated Soils: Advances in Geo-Engineering. 1st European Conference on Unsaturated soil*. Durham, UK. 2-4 July 2008. (pp. 917-923). LONDON: Taylor & Francis Group plv (UK).
- Pellegrino, A. 1967. Proprietà fisico-meccaniche dei terreni vulcanici del Napoletano. *Proc. of VIII Convegno Italiano di Geotecnica, Cagliari*, 3: 113–146.
- Peroni, N., Fratolocchi, E. & Tarantino, A. 2006. Water permeability of unsaturated compacted kaolin. In: Schanz T. (eds) *Unsaturated Soils: Experimental Studies I*, Springer: 45-57.
- Petley, D. N., Petley, D. J., Bulmer, M. H. & Carey, J. 2005. Development of progressive landslide failure in cohesive materials. *Geology* 33(3):201-204.
- Picarelli, L. 1986. Caratterizzazione geotecnica dei terreni strutturalmente complessi nei problemi di stabilità dei pendii. *Proc. 16th Conv. Italiano di Geotecnica*, 3: 155-169.

- Picarelli L. 2009. Conoscere per prevedere (dall'equilibrio limite alla meccanica dei pendii). *Arrigo Croce Lecture, Rivista Italiana di Geotecnica*, n. 4, 12-68.
- Picarelli L., Di Maio C. 2010. Deterioration of stiff clays and clay shales. In: *Weathering as a Predisposing Factor to Slope Movements*, D. Calcaterra and M. Parise eds., Geological Society of London
- Picarelli, L., Di Maio, C., Olivares, L., Urciuoli, G. 1998. Properties and behaviour of tectonised clay shales in Italy. *Proc. 2nd Int. Symp. The Geotechnics of Hard Soils – Soft Rocks, Naples*, 3: 1211-1241. Balkema, Rotterdam.
- Picarelli, L., Olivares, L., Di Maio, C., Silvestri, F., Di Nocera, S., Urciuoli, G. 2002. Structure, properties and mechanical behaviour of the highly plastic intensely fissured Bisaccia Clay Shale. *Proc. Int. Symp. on Characterisation and Engineering Properties of Natural Soils. Singapore*, 2: 947-962.
- Picarelli L., Olivares L., Comegna L., Damiano E., 2008. Mechanical aspects of flow-like movements in granular and fine-grained soils. *Rock mechanics and rock engineering* 41(1):179-197.
- Picarelli L., Evangelista A., Rolandi G., Paone A., Nicotera M.V., Olivares L., Scotto di Santolo A., Lampitiello S., Rolandi M. 2006. Mechanical properties of pyroclastic soils in Campania Region. *Proc. 2nd int. work. on Characterization and Engineering Properties of Natural Soils*, Singapore, 3: 2331-2383.
- Rassam D.W. and Williams D.J. 1999. A relationship describing the shear strength of unsaturated soils, *Canadian Geotechnical Journal*, 36: 363-368.
- Reynolds, O. 1886. Dilatancy, *Nature* 33 :429-430.
- Romero, E., Gens, A. & Lloret, A. 1999 Water permeability, water retention and microstructure of unsaturated compacted Boom clay. *Engineering Geology* 54:117-127.
- Roscoe, K.H. & Burland, J.B. 1968. On the generalized stress-strain behavior of wet clay. *Engineering Plasticity*, Cambridge: 535-609.
- Roscoe, K.H. & Poorooshasb, H.B. A theoretical and experimental study of strains in triaxial tests on normally consolidated clays. *Geotechnique* 13(1):12-38.
- Roscoe, K.H., Schofield, A.N. & Thurairajah, A. 1963. Yielding of clays in state wetter than critical. *Géotechnique* 13(3):211-240
- Sassa, K. 1972. Analysis on slope stability: I. Mainly on the basis of the indoor experiments using the standard sand produced in Toyoura, Japan. *Journal of the Japan Society of Erosion Control Engineering* 25 (2): 5 –17 (in Japanese with English abstract).
- Sassa, K. 1974. Analysis on slope stability: II. Mainly on the basis of the indoor experiments using the standard sand produced in Toyoura, Japan. *Journal of the Japan Society of Erosion Control Engineering* 26 (3): 8 –19 (in Japanese with English abstract).
- Sassa, K., Takei, A. 1977. Consider vertical subsidence in slope unstabilization: I. Stress fall phenomenon and bearing power of the sides. *Journal of Japan Landslide Society* 14(2): 19–26 (in Japanese with English abstract).
- Sassa, K. 1984. The mechanism starting liquefied landslides and debris flows. *Proceedings of 4th International Symposium on Landslides, Toronto, Canada*, 2: 349–354.
- Sassa, K. 1996. Prediction of earthquake induced landslides. Special Lecture of 7th International Symposium on Landslides, *Landslides* 1: 115–132.
- Sassa, K. 1998a. Recent urban landslide disasters in Japan and their mechanisms. *Proc. 2nd International Conference on Environmental Management, "Environmental Management"*, vol. 1: 47– 58.
- Sassa, K. 1998b. Mechanisms of landslide triggered debris flow. In: Sassa, K. (Ed.), “*Environmental Forest Science*”. *Proceedings of IUFRO Div. 8 Conference. Kluwer Academic Publishing, Kyoto*: 471– 490.
- Schofield A. N., Wroth C. P, *Critical State Soil Mechanics*, (McGraw-Hill, New York, 1968).
- Sidle, R.C., Swanston, D.N. 1982. Analysis of a small debris slide in coastal Alaska. *Canadian Geotechnical Journal* 19: 167– 174.
- Sitar, N., Anderson, S.A., Johnson, K.A. 1992. Conditions leading to the initiation of rainfall-induced debris flows. *Geotech. Eng. Div. Specialty Conf.: Stability and Perf. of Slopes and Embankments— II*. ASCE, New York, NY: 834–839.
- Skempton, A.W., Schuster, R.L., Petley, D.J. 1969. Joints and fissures in the London Clay at Wraybury and Edgware. *Géotechnique*, 19: 205-217.
- Sladen J.A., D'Hollander R.D. and Krahn J. (1985). The liquefaction of sands, a collapse surface approach. *Canadian Geotechnical Journal* 22: 564–578.
- Sorbino, G., Foresta, V. 2002. Unsaturated hydraulic characteristics of pyroclastic soils. In: *Proc. 3rd International Conference on Unsaturated Soils, Recife (Brasil)*. Balkema, 1: 405 – 410.
- Sorbino G., Sica C., Cascini L. 2010. Susceptibility analysis of shallow landslides source areas using physically based models. *Natural Hazards*, 53: 313–332.
- Sorbino G., Migliaro G. and Foresta V. 2010. Laboratory investigations on static liquefaction potential of pyroclastic soils involved in rainfall-induced landslides of the flow-type. In: *Proc. 5th International Conference on Unsaturated Soils, Barcellona (Spain)*. Balkema, in press.
- Sorbino G. and Foresta V. (in prep.). A new Unsaturated Direct Simple Shear Apparatus.
- Spence, K.J., Guymmer, I. 1997. Small-scale laboratory flowslides. *Géotechnique* 47 (5): 915–932.
- Spickermann, A., Malet, J.-P. & van Asch Th.W.J. 2009. Failure modes and mechanisms in cohesive slopes: theoretical and numerical analysis of field and laboratory-triggered events. In: *Proceedings of the 1st Italian Workshop on Landslides Rainfall-Induced Landslides*, Naples, Italy, 103-110.

- Spickermann, A., Malet, J.-P., van Asch Th.W.J. & Schanz, T. in prep. Analysis of hydrological triggered clayey landslides by small scale experiments.
- Springman, S.M., Jommi, C., Teyssere, P. 2003. Instability on moraine slopes induced by loss suction: a case history. *Géotechnique* 53(1): 3–10.
- Take WA, Bolton MD. 2002. An atmospheric chamber for the investigation of the effect of seasonal moisture changes on clay slopes, *Proceedings of the International Conference on Physical Modelling in Geotechnics—ICPMG_02*: 765–770
- Take, W.A., Bolton, M.D., Wong, P.C.P. & Yeung, F. J. 2004. Evaluation of landslide triggering mechanisms in model fill slopes. *Landslides*, 1: 173–184.
- Taylor RN. 1995. Centrifuges in modelling: principles and scale effects. *Geotechnical Centrifuge Technology*
- Terribile, F., Basile, A., De Mascellis, R., di Gennaro, A., Mele, G. & Vingiani, S. 2000. I suoli delle aree di crisi di Quindici e Sarno: proprietà e comportamenti in relazioni ai fenomeni franosi. *Quaderni di Geologia Applicata*, 7-1: 59-79.
- Terzaghi, K. 1950. Mechanism of landslides. In: Paige, S. (Ed.), *Application of Geology to Engineering Practice* (Berkey Volume). Geological Society of America, New York: 83– 123.
- Thu T.M., Rahardjo H., Leong E.C. 2006. Shear Strength and Pore-Water Pressure Characteristics during Constant Water Content Triaxial Tests. *J. Geotech. Eng. ASCE*: 132 (3).
- Urciuoli, G. 1992. *Rigonfiamento di un'argilla di alta plasticità e modellazione dei fenomeni erosivi del colle di Bisaccia*. PhD Thesis, Università di Napoli Federico II.
- Urciuoli, G. 1994. Permeabilità di argilliti a scaglie. *Proc. Conf. on "Il ruolo dei fluidi nei problemi di Ingegneria Geotecnica"*, Mondovì, 1: 185-204.
- Vanapalli S.K., Fredlund D.G., Pufahl D.E. and Clifton A.W. 1996. Model for the prediction of shear strength with respect to soil suction, *Canadian Geotechnical Journal*, 33, 379-392.
- Vanapalli S.K. Fredlund D.G. and Pufahl D.E. 1999. The influence of soil structure and stress history on the soil-water characteristics of a compacted till, *Géotechnique*, 49(2), 143-159.
- Van Genuchten M. Th. 1980. A closed-form equation for predicting the hydraulic conductivity of unsaturated soil. *Soil Sci. Soc. Am. J.*, 44: 615-628.
- Walker, B.F., Blong, R.J., McGregor, J.P. 1987. Landslide classification, geomorphology and site investigations. *Soil Slope Instability and Stabilisation*, 1-52. Balkema, Rotterdam.
- Wang, G., Sassa, K. 2001. Factors affecting rainfall-induced flowslides in laboratory flume tests. *Géotechnique* 51 (7): 587–599.
- Wang G, Sassa K. 2003. Pore-pressure generation and movement of rainfall-induced landslides: effects of grain size and fine-particle content. *Eng Geol* 69:109–125.
- White DJ, Take WA, Bolton MD. 2003. Soil deformation measurement using particle image velocimetry (PIV) and photogrammetry, *Géotechnique* 53:619–631.
- Whitham A.G. and Sparks R.S. (1986). Pumice. *Bullettin of Volcanology*, 48, 209 – 223.
- Yeung, F.J. 2002. *Modelling of the behaviour of saprolitic slopes under severe rainfall*. MPhil Dissertation: University of Cambridge.
- Zhu J.H., Anderson S.A. 1998. Determination of shear strength of Hawaiian residual soil subjected to rainfall-induced landslides. *Géotechnique* 48(1): 73-82.

Chapter 3

- Askarnejad, A., Casini, F., Kienzler, P., Springman, S.M., 2010. Comparison of the in situ and laboratory water retention curves for a silty sand. *5th Intern. Conf. of unsaturated soils*, 6-8 September 2010, Barcelona, Spain.
- Casini, F., Jommi, C., Springman, S.M., 2010a. A laboratory investigation on an undisturbed silty sand from a slope prone to landsliding. *Granular Matter*, 12 (DOI: 10.1007/s10035-010-0182-y).
- Casini, F., Minder, P., Springman, S.M., 2010b. Shear Strength of an unsaturated silty sand. *5th Intern. Conf. of unsaturated soils*, 6-8 September 2010, Barcelona, Spain.
- Cortona, L. 2000. *Laboratory and Field Investigations on morainic soils*. Institute of Geotechnics, Zurich & Politecnico di Torino, Diploma project.
- Fischer, C., López, J.; Springman, S.M. 2003. Remediation of an eroded steep slope in weathered sandstone after a major rainstorm. *International Conference on Landslides*, Hong Kong,: 878-883.
- Haeberli, W. 1992, Zur Stabilität von Moränenseen in hochalpinen Gletschergebieten, *Wasser-Energie-Luft* 84: 361-364.
- Haeberli, W., Kääb, A., Teyssere, P. 1996, Entwicklung und Sanierung eines Thermokarst - See am Gruben – Blockgletscher (Wallis), *Forschungsberichte, Geographisches Institut Universität Freiburg*, Schweiz, 8:155-168.
- Keller, G.V. & Frischknecht, F.C. 1966. *Electrical methods in geophysical prospecting*. Pergamon Press: Oxford; 517..
- Kienzler P.M., Naef F. 2008. Subsurface storm flow formation at different hillslopes and implications for the "old water paradox". *Hydrological Processes*, 22(1): 104-116.
- Loke, M.H. 2006. RES2DINV ver. 3.55, Rapid 2D resistivity & IP inversion using the least-squares method. Software Manual; 139.
- Rings, J. & Hauk, C. 2009. Reliability of resistivity quantification for shallow subsurface water processes. *Journal of Applied Geophysics* 68: 404-416.
- Schwarz, M., Rickli, C. 2008. Characterisation of the vegetation cover at the test site of Ruedlingen. Internal GEOLEP CCES-TRAMM report.

- Springman, S. M. & Teyssere, P. 2001. Artificially induced rainfall instabilities on moraine slopes. *Proceedings of the international conference on landslides* (eds M. Kühne et al.), pp. 209–223. Essen: VGE.
- Springman, S. M., Jommi, C., Teyssere, P. 2003. Instability on moraine slopes induced by loss suction: a case history. *Géotechnique*, 53(1): 3-10.
- Springman, S.M., Kienzler, P., Casini, F., Askarnejad, A. 2009. Landslide triggering experiment in a steep forested slope in Switzerland. In: *17th Int. Conf. on Soil Mechanics & Geotech. Eng.*, 5-9 october, Alexandria.
- Tacher, L., Locher, D. 2008. Geological Characterization of the Buchberg field site (Ruedlingen). Internal TRAMM report.
- Teyssere, P., Cortona, L., Springman, S. 2000. Water retention in a steep moraine slope during periods of heavy rain, *Unsaturated Soils for Asia*, Singapore, 831-836.
- Travelletti, J., Sailhac, P., Malet, J.-P., Grandjean, G., Ponton, J. in press. Observation and monitoring of water infiltration in weathered and reworked clay shale with electrical resistivity tomography. *Hydrological Processes* (accepted, in press).
- Vonder Mühl, D., Haeblerli, W., Klingele, E. 1996, Geophysikalische Untersuchungen zur Struktur und Stabilität eines Moränendammes am Grubengletscher (Wallis), Interpraevent, S. 123-132.

Chapter 4

- Askarnejad, A. 2009. A method to locate the slip surface and measuring subsurface deformations in slopes. *4th Intern. Young Geotechnical Engineers' Conference*, Alexandria, Egypt: 171-174.
- Askarnejad, A., Casini, F., Kienzler, P., Springman, S.M., 2010. Comparison of the in situ and laboratory water retention curves for a silty sand. *5th international conference of unsaturated soils*, 6-8 September 2010, Barcelona, Spain.
- Bertini, T., Cugusi, F., Délia, B., Rossi-Doria, M. 1986. Lenti movimenti di versante nell'Abruzzo Adriatico: criteri di stabilizzazione. *Proc. 16th Convegno Nazionale di Geotecnica*, Bologna, Associazione Geotecnica Italiana, Roma: 91-100.
- Bertini T., Cugusi F., D'Elia B., Rossi Doria M. 1984. Climatic conditions and slow movements of colluvial covers in Central Italy. *Proc IV Int. Symp. on Landslides*, Toronto, 1: 367-376.
- Bertuccioli P. 1995. *Deformabilità di un'argilla sovraconsolidata con discontinuità*. PhD Thesis, Consortium of Università di Roma La Sapienza, Università di Napoli Federico II, Seconda Università di Napoli.
- Bilotta, E. Cascini, L. Foresta, V. Sorbino, G. 2005. Geotechnical characterization of pyroclastic soils involved in huge flowslides. *Journal of Geological and Geotechnical Engineering*.
- Bilotta, E. Foresta, V. 2002. On the measured shear strength of some pyroclastic soils of Sarno mountains. *Proc. 3rd Int. Conf. on Unsaturated Soils, Recife* (2): 495-500.
- Blight G.E. 1997. 37th Rankine Lecture: Interaction between the atmosphere and the Earth. *Géotechnique* 47(4): 715-766.
- Calabresi, G., Manfredini, G. 1973. Shear strength characteristics of the jointed clay of S. Barbara. *Géotechnique*, 23: 233-244.
- Cascini, L. 2004. The flowslides of May 1998 in the Campania Region, Italy: The Scientific Emergency Management. *Rivista Italiana di Geotecnica* (2): 11-44.
- Cascini L., Cuomo S., Guida D. 2008. Typical source areas of May 1998 flow-like mass movements in the Campania region, Southern Italy. *Engineering Geology*, 96: 107-125.
- Cascini, L. Guida, D. Nocera, N. Romanzi, G. Sorbino, G. 2000. A preliminary model for the landslides of May 1998 in Campania Region. *Geotechnics of Hard Soil-Soft Rock; Proc. 2nd Int. Symp., Naples 12-14 Oct. '98*(3): 1623-1649.
- Cascini, L. Sorbino, G. 2003. The contribution of soil suction measurements to the analysis of flowslides triggering. *IWFloWS Proc. intern. Symp., Sorrento 14-16 May '03*: 77-85.
- Cascini, L. Sorbino, G. Cuomo, S. 2003. Modelling flowslide triggering in pyroclastic soils. *Fast Slope Movements; Proc. of Int. Conf., Naples May 12-13, 2003*: 93-100.
- Casini, F., Jommi, C., Springman, S.M. 2010a. A laboratory investigation on an undisturbed silty sand from a slope prone to landsliding. *Granular Matter* 12 (DOI: 10.1007/s10035-010-0182-y).
- Casini, F., Minder, P., Springman, S.M., 2010b. Shear Strength of an unsaturated silty sand. *5th international conference of unsaturated soils*, 6-8 September 2010, Barcelona, Spain.
- Civita M., de Riso R., Lucini P., Nota d'Elogio E., 1975. Studio delle condizioni di stabilità dei terreni della penisola Sorrentina (Campania). *Geologia Applicata e Idrogeologia*, Bari, X(I): 129-188
- Comegna L. 2005. *Considerazioni sulla meccanica delle colate in argilla*. PhD Thesis, Consortium of Università di Roma La Sapienza, Università di Napoli Federico II, Seconda Università di Napoli. Available on-line at the web-site <http://padis.uniroma1.it>.
- Comegna L., Picarelli L. 2008. Anisotropy of a shear zone. *Géotechnique*, 58 (9): 737-742.
- Comegna L., Picarelli L., Urciuoli G. 2004. The role of pore pressures on the mechanics of mudslides. In: Lacerda, W. (ed), *Proceedings of the 9th International Symposium on Landslides, Rio de Janeiro*, 2: 1183-1188, Pub: Balkema, Rotterdam.
- Comegna L., Picarelli L., Urciuoli G. 2007. The mechanics of mudslides as a cyclic undrained-drained process. *Landslides – Journal of the International Consortium on Landslides*, 4 (3): 217-232.
- Commend S., Geiser F., Tacher L. 2004. 3D numerical modeling of a landslide in Switzerland. In *Proceedings of the International Symposium on Numerical Models in Geomechanics NUMOG IX*, Ottawa: 595-601.
- Corominas J., Moya J., Ledesma A., Lloret A., Gili J.A. 2005. Prediction of ground displacements and velocities from groundwater level changes at the Vallcebre landslide (Eastern Pyrenees, Spain). *Landslides*, 2: 83-96.

- Cotecchia V., Del Prete M., Federico A., Fenelli G.B., Pellegrino, A., Picarelli, L. 1984. Some observations on a typical mudslide in a highly tectonized formation in Southern Apennines. In: *Proceedings of the 4th International Symposium on Landslides, Toronto*, 2: 39-44.
- Cotecchia V., Del Prete M., Federico A., Fenelli G.B., Pellegrino, A., Picarelli, L. 1986. Studio di una colata attiva in formazioni strutturalmente complesse presso Brindisi di Montagna Scalo (PZ). In: *Proceedings of the 14th Convegno Italiano di Geotecnica, Bologna*, 1: 253-264.
- Damiano E., 2010. Technical Report "A study on climatologic aspects for forecasting of shallow landslides in pyroclastic soils due to climatic change".
- Damiano E., Olivares L., 2010. The role of infiltration processes in steep slopes stability of pyroclastic granular soils: laboratory and numerical investigation. *NATURAL HAZARDS, Journal of the Inter. Society for the Prevention and Mitigation of Natural Hazard*, 52(2):329-350.
- D'Elia B., Esu F., Bertuccioli P. 1998. Displacements and stability of a cut in a hard jointed clay. *Proc. 2nd Int. Symp. The Geotechnics of Hard Soils - Soft Rocks*, Napoli, A. Evangelista, L. Picarelli Eds., Balkema, Rotterdam, 2: 1067-1074.
- De Montety, V., Marc, V., Emblanch, C., Malet, J.-P., Bertrand, C., Maquaire, O., Bogaard, T.A. 2007. Identifying the origin of groundwater and flow processes in complex landslides affecting black marls: Insights from a hydrochemical survey. *Earth Surface Processes and Landforms*, 32(1): 32-48.
- DUTI - Détection et Utilisation des Terrains Instables 1986. Le glissement de Cergnat – La Frasse, Projet EPFL.
- Esu F., Calabresi G. 1969. Slope stability in an overconsolidated caly. *Proc. VII ISSMFE, Mexico City*, 2: 555-563.
- Evangelista A., Scotto di Santolo A., 2001. Mechanical behaviour of unsaturated pyroclastic soil. In: *Proc. Landslides: Causes, Impacts and Countermeasures, Davos-Switzerland*, June, 2001.
- Evangelista A., Nicotera M.V., Papa R., Urciuoli G., 2008. Field investigation on triggering mechanisms of fast landslides in unsaturated pyroclastic soils. In: *Unsaturated Soils: Advances in Geo-Engineering. 1st European Conference on Unsaturated soil*. Durham, UK. 2-4 July 2008. (pp. 909-915). LONDON: Taylor & Francis Group plv (UK).
- Evangelista A., Scotto di Santolo A., 2010. Regime della suzione nelle coltri piroclastiche della città di Napoli. In: *Proc. First Italian Workshop on Landslides - Rainfall-induced landslides: mechanisms, monitoring techniques and nowcasting models for early warning systems*. Naples, 8-10 June, 2009, Vol.2. In press.
- Fischer, C., López, J.; Springman, S.M. 2003. Remediation of an eroded steep slope in weathered sandstone after a major rainstorm. *International Conference on Landslides, Hong Kong*: 878-883.
- Flageollet, J.-C., Malet, J.-P., Maquaire, O. 2000. The 3-D structure of the Super-Sauze earthflow (Alpes-de-Haute-Provence, France): a first stage towards modelling its behaviour. *Physics and Chemistry of the Earth, Part B*, 25(9): 785-791.
- Flageollet, J.-C., Malet, J.-P., Maquaire, O., Schmutz, M. 2004. Chapter 14. Integrated investigations on landslides: example of the Super-Sauze earthflow. In Casale, R., Margottini, C. (Eds): *Natural Disasters and Sustainable Development*, Springer-Verlag, Berlin, 213-238.
- Friedel, S., Thielen, A. & Springman, S.M. 2006. Investigation of a slope en-dangered by rainfall-induced landslides using 3D resistivity tomography and geotechnical testing. *Journal of Applied Geophysics*, 60(2): 100-114.
- Gardner, W.R. 1958. Some steady-state solutions of the unsaturated moisture flow equation with application to evaporation from a water table. *Soil Science* (85): 228-232.
- Geo-Slope Int. Ltd. 1998. SEEP/W User's guide. Version 4. Calgary, Alberta, Canada.
- Giusti, G., Iacarina, G., Pellegrino, A., Russo, C., Urciloi, G. Picarelli, L. 1996. Kinematic features of earthflows in Southern Apennines, Italy. In Senneset, K. (Ed): *Proc. 7th Int. Symp. on Landslides*, Trondheim, Norway, Balkema, Rotterdam, 1: 457-462.
- Grandjean, G., Malet, J.-P., Bitri, A., Méric, O. 2007. Geophysical data fusion by fuzzy logic for imaging the mechanical behaviour of mudslides. *Bulletin de la Societe Géologique de France*, 178 (2): 127-136.
- Guerrero G. 1995. *Modellazione sperimentale del comportamento meccanico dei terreni in colata*. PhD Thesis, Università di Napoli Federico II.
- Henkel D.J. 1967. Local geology and the stability of natural slopes. *Journal of the Soil Mechanics and Foundations Division, ASCE*: 437-450.
- Hutchinson J.N. 1970. A coastal mudflow on the London Clay cliffs at Beltinge, Kent. *Géotechnique*, 20: 412-438.
- Hutchinson J.N., Bhandari R.K. 1971. Undrained loading, a fundamental mechanism of mudflows and other mass movements. *Géotechnique*, 21: 353-358.
- Iaccarino G., Peduto F., Pellegrino A., Picarelli L. 1995. Principal features of earthflows in part of Southern Apennine. *Proceed. of the 11th European Conference on Soil Mechanics and Foundation Engineering, Copenhagen*, 4: 354-359.
- Laloui L., Tacher L., Moreni M., Bonnard C. 2004. Hydro-mechanical modeling of crises of large landslides : application to the La Frasse Landslide. *Proc. 9th Int. Symp. on Landslides*, Rio de Janeiro, Ed. Balkema: 1103-1110.
- Lambiasi, A. 2004. Modellazione del regime delle pressioni neutre negative nelle coltri piroclastiche della Regione Campania. *MSc Thesis, University of Salerno, Italy*.
- Ledesma, A., Corominas, J., González, D.A., Ferrari, A. 2009. Modelling slow moving landslides controlled by rainfall. In *Proceedings of the 1st Italian Workshop on Landslides*, June 8 – 10, 2009. Naples, Italy.
- Leroueil S. 2001. 39th Rankine Lecture: Natural slopes and cuts: movement and failure mechanisms. *Géotechnique* 51(3): 197-243.

- Lugeon M., Patschoud E., Rothpletz F. 1922. Rapport d'expertise sur le glissement des Frasses, Etat de Vaud, Département des Travaux Publics, Service des Routes.
- Malet, J.-P. 2003. *Les glissements de type écoulement dans les marnes noires des Alpes du Sud. Morphologie, fonctionnement et modélisation hydro-mécanique*. PhD Thesis in Earth Sciences, Université Louis Pasteur, Strasbourg.
- Malet, J.-P., Laigle, D., Remaître, A., Maquaire, O. 2005a. Triggering conditions and mobility of debris flows associated to complex earthflows. *Geomorphology*, 66(1-4): 215-235.
- Malet, J.-P., Maquaire, O. 2003. Hydrological behaviour of earthflows developed in clay-shales: investigation, concept and modelling. In Picarelli, L. (Ed). *The Occurrence and Mechanisms of Flows in Natural Slopes and Earthfills*, Sorrento, Italy, Patrone Editore, Bologna: 175-193.
- Malet, J.-P., Maquaire, O., Calais, E. 2002. The use of Global Positioning System for the continuous monitoring of landslides. Application to the Super-Sauze earthflow (Alpes-de-Haute-Provence, France). *Geomorphology*, 43: 33-54.
- Malet, J.-P., van Asch, Th.W.J., van Beek, L.P.H., Maquaire, O. 2005b. Forecasting the behaviour of complex landslides with a spatially distributed hydrological model. *Natural Hazards and Earth System Science*, 5(1):71-85.
- Manetti L., Steinmann G. 2007. 3DeMoN ROBOVEC – Integration of a new measuring instrument in an existing generic remote monitoring platform. *FMGM 2007: Seventh International Symposium on Field Measurements in Geomechanics*, ASCE.
- Maquaire, O., Flageollet, J.-C., Malet, J.-P., Schmutz, M., Weber, D., Klotz, S., Albouy, Y., Descloîtres, M., Dietrich, M., Guérin, R., et Schott, J.-J. 2001. Une approche multidisciplinaire pour la connaissance d'un glissement-coulée dans les marnes noires du Callovien-Oxfordien (Super-Sauze, Alpes-de-Haute-Provence, France). *Revue Française de Géotechnique*, 95/96: 15-31.
- Méric, O., Garambois, S., Malet, J.-P., Cadet, H., Guéguen, P., Jongmans, D. 2007. Seismic noise-based methods for soft-rock landslide characterization, *Bulletin de la Société Géologique de France* 178(2): 137-148.
- NCG-EPFL : Association technique Norbert, De Cèrenville Géotechnique & EPFL pour l'étude du glissement de La Frasse. 2004. Glissement de La Frasse, modélisation et étude de faisabilité.
- Nieuwenhuis, J.D. 1991. *The lifetime of a landslide*. Balkema, Rotterdam.
- Noverraz F., Bonnard Ch. 1990. Technical note on the visit of the La Frasse landslide. In: Proceedings of the Vth International Symposium on Landslides, Lausanne, Balkema, volume 3: 1549-1554.
- Olivares L., Picarelli L., Andreozzi L., Avorio B., Damiano E., Lampitiello S., 2002. Scenari di pericolosità di frana in terreni sciolti di natura piroclastica. In Proc. XXI Convegno Nazionale di Geotecnica L'Aquila: Opere Geotecniche in Ambiente Urbano, 11-13 Settembre 2002; Patron Editore – Bologna; 1:173-182.
- Olivares L., Picarelli L., 2003. Shallow flowslides triggered by intense rainfalls on natural slopes covered by loose unsaturated pyroclastic soils. *Géotechnique*, 52 (2).
- Papa R., Pirone M., Nicotera M.V., Urciuoli G. 2010. Meccanismi di innesco di colate di fango in piroclastiti parzialmente sature. In: *Proc. First Italian Workshop on Landslides - Rainfall-induced landslides: mechanisms, monitoring techniques and nowcasting models for early warning systems*. Naples, 8-10 June, 2009, Vol.2. In press.
- Pellegrino, A. 1967. Proprietà fisico-meccaniche dei terreni vulcanici del napoletano. *Proc. 8th Italian Geotechnical Congress, Cagliari* (3): 113-145.
- Pellegrino A., Ramondini M., Russo C., Urciuoli G. 2000. Kinematic features of earthflows in Southern Apennines. In: Bromhead, E.N., Dixon, N., Ibsen, M.L. (eds), *Proceedings of the 8th International Symposium on Landslides, Cardiff*, 2: 1195-2002. Thomas Telford, London
- Pellegrino A., Ramondini M., Urciuoli G. 2004a. Interplay between the morphology and mechanics of mudslides: field experiences from southern Italy In: Lacerda, W. (ed), *Proceedings of the 9th International Symposium on Landslides, Rio de Janeiro*, 2: 1403-1409, Balkema, Rotterdam.
- Pellegrino A., Ramondini M., Urciuoli G. 2004b. Regime delle pressioni neutre in un pendio in Argille Varicolori stabilizzato con drenaggi. In: Picarelli, L. (ed), *Proceedings International Workshop Living with Landslides. Effects on Structures and Urban Settlements. Strategies for Risk Reduction, Anacapri*, October, 2003.
- Penman H.L., 1958. Natural evapotranspiration from open water, bare soil and grass. *Proc. Roy. Soc., London*, ser. A.193: 120-145.
- Picarelli, L., Evangelista, A., Rolandi, G., Paone, A., Nicotera, M.V., Olivares, L., Scotto di Santolo, A., Lampitiello S., Rolandi M., 2007. Mechanical properties of pyroclastic soils in Campania Region. In: *Proc. Int. Workshop on Characterization & Engineering Properties of Natural Soils*, December 2006, Taylor & Francis Group plc: London: 2331-2383.
- Picarelli, L., Russo, C. 2004. Remarks on the mechanics of slow active landslides and the interaction with man-made works. In Lacerda, W. (Ed): *Proc. 9th Int. Symp. on Landslides, Rio de Janeiro, Brazil*, Balkema, Rotterdam, 2: 1141-1176.
- Picarelli, L., Russo, C., Urcioli, G. 1995. Modelling earthflow movement based on experiences. *Proc. 11th European Conference on Soil Mechanics and Foundation Engineering*, Copenhagen, Denmark, Danish Geotechnical Society, Copenhagen, 6: 157-162.
- Picarelli L. 2000. Mechanisms and rates of slope movements in fine grained soils. In: *Proceedings of the International Conference on Geotechnical and Geological Engineering, GEOENG2000, Melbourne*: 1618-1670.
- Picarelli L., Russo C., Mandolini A. 1999. Long-term movements of an earthflow in tectonized clay shales. In: Yagi, N., Yamagami, T., Jiang, J.C. (eds), *Proceedings of the International Symposium on Slope Stability Engineering: Geotechnical and Geo-environmental aspects, Matsuyama*, 2: 1151-1158. Balkema, Rotterdam.

- Picarelli L., Urciuoli G., Ramondini M., Comegna L. 2005. Main features of mudslides in tectonized highly fissured clay shales. *Landslides – Journal of the International Consortium on Landslides* 12, 2 (1), April 2005: 15-30.
- Picarelli L., Viggiani C. 1988. A landslide in a structurally complex formation. *Proc. of the 5th Int. Symp. On Landslides, Lausanne, July*, 1: 289-297.
- Planchat J. 2009. La Frasse landslide (CH): analysis of the hydro-mechanical behavior of the instability and of the associated risks. *Master Thesis in Civil Engineering, Ecole Polytechnique Fédérale de Lausanne, Lausanne*, 124 pages.
- Planchat J., Bonnard Ch., Peron H., Laloui L. 2009. After 10'000 years of movement, is the La Frasse landslide stabilized ? Numerical modeling of the crises of a large landslide and of its mitigation measures. In E. Alonso, J. Corominas, and M. Hürlimann, editors, *proceedings of the VII Simposio Nacional sobre Taludes y Laderas Inestables*, volume 1, pages 95-126, Barcelona, 2009. CIMNE.
- Rippa, F., Picarelli, L. 1977. Some considerations on index properties of southern Italy shales. *Proc. Int. Symp. on the Geotechnics of Structurally Complex Formations*, Capri, Italy, Associazione Geotecnica Italiana, Roma: 401-406.
- Schmutz, M., Albouy, Y., Guérin, R., Maquaire, O., Vassal, J., Schott, J.-J., Descloîtres, M. 2001. Joint electrical and time domain electromagnetism (TDEM) data inversion applied to the Super-Sauze earthflow (France) *Surveys in Geophysics*, 21(4): 371-390.
- Sorbino, G. Foresta, V. 2002. Unsaturated hydraulic characteristics of pyroclastic soils. *Proc. 3rd Int. Conf. on Unsaturated Soils, Recife*, (1): 405-410.
- Sorbino, G. 2005. Numerical modelling of soil suction measurements in pyroclastic soils.” *Int. Symp. Advanced Experimental Unsaturated Soil and Mechanics*: 541-547.
- Springman, S.M., Kienzler, P., Casini, F., Askarnejad, A. 2009. Landslide triggering experiment in a steep forested slope in Switzerland. In: *17th Int. Conf. on Soil Mechanics & Geotech. Eng.*, 5-9 october, Alexandria.
- Springman, S. M., Teyssie, P. 2001. Artificially induced rainfall instabilities on moraine slopes. Proceedings of the international conference on landslides (eds M. Kühne et al.), pp. 209-223. Essen: VGE.
- Springman, S. M., Jommi, C., Teyssie, P. 2003. Instability on moraine slopes induced by loss suction: a case history. *Géotechnique*, 53(1), 3-10.
- SWISS GEO TESTING LTD. Géothermie et Géomécanique 2009. Continuous measurements of surface displacements at the La Frasse landslide. Nax, VS, Switzerland.
- Tacher L., Bonnard Ch., Laloui L., Parriaux A. 2005. Modelling the behaviour of a large landslide with respect to hydrogeological and geomechanical parameter heterogeneity. *Landslides* 2: 3-24.
- Tarantino, A. Mongiovi, L. Mc Dougall, L.R. 2002. Analysis of hydrological effects of vegetation on slope stability. *Proc. 3rd Int. Conf. on Unsaturated Soils, Recife* (2): 749-754.
- Thielen, A., Springman, S.M. 2010. A long term field study for the investigation of rainfall induced landslides. Submitted to *Géotechnique*.
- Thielen, A., Friedel, S., Plötze, M. & Springman, S.M. 2005. Combined approach for site investigation in terms of the analysis of rainfall induced landslides. Proceedings of the 16th International Conference on Soil Mechanics and Geotechnical Engineering, Osaka, Japan.
- Thielen, A. & Springman, S.M. 2005. First results of a monitoring experiment for the analysis of rainfall induced landslides. Proceedings of the International Symposium on Advanced Experimental Unsaturated Soil Mechanics - EXPERUS 2005, Trento, Italy.
- Thornthwaite C. W., 1948. An approach toward a rational classification of climate. *Trans. Am. Geophys. Union*, 27(1).
- Thornthwaite, C. W. 1954. A re-examination of the concept and measurement of potential transpiration. In *The measurement of potential evapo-transpiration* (ed. J. R. Mather), 200-209.
- Teyssie, P., Cortona, L., Springman, S. 2000. Water retention in a steep moraine slope during periods of heavy rain, *Unsaturated Soils for Asia*, Singapore: 831-836.
- Travelletti, J., Oppikofer, T., Delacourt, C., Malet, J.-P., Jaboyedoff, M. 2008. Monitoring landslides displacements during a controlled rain experiment using a long-range terrestrial laser scanning (TLS). *The International Archives of the Photogrammetry, Remote Sensing and Spatial Information Sciences*. XXXVII. Part B5: 485-490.
- Thielen, A. 2007. Einfluss der Bodensättigung auf die Stabilität von Hängen, Diss-Nr. 17303. ETH Zurich, Zurich, <http://e-collection.ethbib.ethz.ch/>.
- Tommasi P., Pellegrini P., Boldini D., Ribacchi R. 2006. Influence of rainfall regime on hydraulic conditions and movement rates in the overconsolidated clayey slope of the Orvieto hill (central Italy), *Canadian Geotechnical Journal*, 43: 70-86.
- van Asch, Th.W.J. 2005. Modelling the hysteresis in the velocity pattern of slow-moving earthflows: the role of excess pore pressure. *Earth Surface Processes and Landforms*, 30: 403-411.
- van Asch, Th.W.J. and Malet, J.-P. 2009. Flow-type failures in fine-grained soils: an important aspect in landslide hazard analysis. *Natural Hazards and Earth System Science*, 9: 1703-1711.
- Weber, D., Herrmann, A. 2000. Reconstitution de l'évolution géomorphologique de versants instables par photogrammétrie numérique : l'exemple du glissement de terrain de Super-Sauze (Alpes-de-Haute-Provence, France). *Bulletin de la Société Géologique de France*, 171: 637-648.